Multi-variant experimental and numerical analysis of selected design and energetic aspects of parabolic trough collectors

BARTOSZ STANEK

Supervisors:
Łukasz Bartela
Daniel Węcel

Doctoral Thesis in Environmental Engineering, Mining and Energy
Silesian University of Technology
Gliwice, Poland, 2023

Author:
Bartosz Stanek, MSc
Silesian University of Technology
Joint Doctoral School
e-mail: bartosz.stanek@polsl.pl

Supervisor:
Łukasz Bartela, PhD with habilitation
Associate Professor at the Silesian University of Technology
Faculty of Energy and Environmental Engineering
Department of Power Engineering and Turbomachinery
Konarskiego 18, 44-100 Gliwice, Poland
e-mail: lukasz.bartela@polsl.pl

Co-Supervisor:
Daniel Węcel, PhD
Assistant Professor at the Silesian University of Technology
Faculty of Energy and Environmental Engineering
Department of Power Engineering and Turbomachinery
Konarskiego 18, 44-100 Gliwice, Poland
e-mail: daniel.wecel@polsl.pl

Polish title:

Wielowariantowa analiza eksperymentalno-obliczeniowa wybranych zagadnień konstrukcyjnych i energetycznych dla technologii parabolicznych koncentratorów promieniowania słonecznego

“The greatest threat to our planet is the belief that someone else will save it.”
Robert Swan

- - -

dedicated to Natalia …

Acknowledgments

I would like to express my sincere gratitude to my supervisor, Prof. Łukasz Bartela, for his invaluable support, guidance and endless fruitful discussions. I am deeply grateful for all your devoted time, valuable advice and extreme commitment to my doctoral research.

I gratefully acknowledge the enormous contribution and support from my co-supervisor Dr Daniel Węcel, especially for his substantial help and knowledge sharing in connection with experimental research. I really appreciate the valuable advice you gave me and the many hours of discussion while working together in the laboratory.

At this point, I would also like to acknowledge the people I had the opportunity to work with over the years. I am very grateful for the company and friendship of Jakub Ochmann, with whom I shared not only the office but also all my worries and celebrated successes. Thank you for your help and support with my research. Sincere thanks go to Wojciech Uchman and Michał Jurczyk for our friendship, for countless coffees together and for invaluable advice. I am glad that I had the opportunity to work with Prof. Anna Skorek-Osikowska, Daria Katla, Katarzyna Janusz-Szymańska and Iwona Adamczewska. Thank you all for sharing all the successes and difficulties we experienced during the implementation of many projects.

My particular gratitude goes to Prof. Sebastian Rulik, for his dedication, enormous help and support in the construction of the test stand. Thank you for all the knowledge you have shared with me.

I would like to acknowledge the huge contribution of Dr Wujun Wang from KTH Royal Institute of Technology (Stockholm, Sweden), who was my supervisor during my three-month internship at this excellent research institution. Thank you for taking me into your care, for all your guidance and also for showing me this right direction.

I would like to express my sincere gratitude to Mr Sylwester Adamski, founder of the Heliograf company, for the great knowledge he has shared with me during our meetings and discussions and, above all, for his invaluable help in acquiring the main

components of the solar simulator. Without his help, experimental studies might not have been possible.

This doctoral thesis was carried within the framework of the European Social Fund programme “Power for Student, Staff, Science”, Interdisciplinary doctoral studies no. POWR.03.05.00-00-Z305, which I would like to gratefully acknowledge.

I would like to also acknowledge the support of the National Science Centre, Poland. Financial assistance was provided by grant no. 2018/29/B/ST8/02406 under the framework of OPUS15 PTC Solar Project. As part of this project, certain studies and the experimental test stand could be developed.

Above all, my deepest gratitude goes to my loved family and friends. I am extremely grateful for the care, the opportunities and the right direction you have shown me, thanks to you I am in this place.

Finally, my deep sincere goes to my beloved fiancée, Natalia. I am really grateful for her constant support, particularly in difficult times, her encouragement, her sacrifice and her patience, which I truly appreciate.

B. Stanek

Contents

Abstract

Increasing the share of renewable energy generation in the total energy mix is crucial to reduce environmentally harmful gas emissions and strengthening energy security by becoming less dependent on fossil fuels, which are often the subject of international policy. In the field of useful forms of energy, low and high-temperature heat has the highest demand. One of the most efficient and environmentally friendly methods of obtaining useful heat is to absorb and convert solar energy using a collector infrastructure or solar concentrators.

Parabolic trough collectors (PTCs) are a mature technology primarily used to generate electricity by indirect heat extraction at a temperature of approximately 400 °C, most favourably in large installations located in areas with very high annual insolation. These installations were often characterised by a large aperture of parabolic mirrors, i.e. around 5 - 7 metres, an external diameter of the absorbers of 70 mm and a total solar loop length of up to several hundred metres. A system of solar loops connected in parallel forms a solar plant with a capacity of several hundred MW. The ongoing development of industrial installations around the world has triggered a need to develop solutions that can partially cover the heat demand in the temperature range up to around 250 °C, using the potential of renewable energy. Parabolic trough collectors with reduced dimensions, specially adapted to medium-temperature heat generation, are the most suitable solution.

Despite the maturity of the technologies utilising concentrated radiation, modifications to the geometry of absorbers and concentrators adapted to operate at lower temperature-level, have created new opportunities for intensifying heat absorption methods and reducing the cost of individual system components.

The overall aim of the dissertation was to identify the heat transfer processes occurring in a parabolic trough collector, to determine methods for intensifying heat collection and reducing the capital investment of the selected components, and to demonstrate the potential for applying these methods to specific installations. The dissertation is based on the author's four selected scientific publications, and the scope of the research itself can be classified under two main aspects that were developed in the two stages of the accomplished work.

In the first stage of the work, a test installation was comprehensively designed and constructed, whose desired functionality enabled experimental tests to be carried out for various absorbers in a parabolic solar concentrator system. To ensure stable and repeatable experimental analysis conditions, the test stand with solar radiation simulator was developed and the modelling and optimisation process is presented in the first paper (*International Journal of Energy Research, publ. Wiley & Sons*). This article presents the results of optical-energy analyses that were carried out using the Monte Carlo ray tracing method. In this research, the most optimal type of light source, metal halide discharge lamps, and the geometry of the paraboloidal reflectors were determined, along with their optimal arrangement in relation to each other and to the radiation concentrator. Through optical analysis, losses due to partial radiation scattering and the potential heat flux delivered to the outer surface of the linear absorber were estimated. Based on the results obtained, the author of this dissertation comprehensively designed and constructed a test stand and carried out a series of experimental tests for different types of absorbers and methods of intensifying heat collection. The research results obtained have been presented in many conference presentations, mainly of international scope, including at conferences organised abroad. In this dissertation, the test stand and the validation of the developed mathematical models describing the heat transfer in the absorber are presented in the second article (*Energies publ. MDPI*).

In the second stage of the study, analyses were carried out to determine the application potential of methods to intensify heat absorption by thermal fluid circulating through the absorber in a parabolic trough system. Increasing installation efficiency through the sequential use of turbulent flow inserts (twisted tapes) was analysed within the scope of the second article (*Energies publ. MDPI*). Three types of inserts with a twisted ratio (*Tr*) of 1, 2 and 4 were evaluated in an installation operating in the temperature range 60 - 250 °C and with thermal fluid, mass flows of 0.15 kg/s, 0.225 kg/s and 0.3 kg/s, i.e. at parameters consistent with installations producing heat for industrial applications. As part of the study, the hydraulic and heat transfer parameters were evaluated. For the cases studied, it was determined that of the three inserts analysed, the highest energy benefit, for fluid temperatures up to 190 °C, could be obtained for *Tr* of 1. Above this temperature, an insert of *Tr* equal to 2 is more optimal. However, it should be emphasised that each of the inserts used in the case study, led to an intensification of heat absorption by the thermal fluid. In the case of the 90-metre installation analysed, the average efficiency improvement was found to be 0.27%. The analysis demonstrated that the parabolic trough collector efficiency increment, where heat intensification inserts

were used, depended on their arrangement in the solar loop, the assumptions for the operation of the system and the atmospheric conditions.

Within the framework of the studies, a series of investigations into the potential application of non-selective absorber coatings were carried out, where the possibility of applying a Pyromark coating to the external surface of the absorber was demonstrated as an example. The analysis presented in the third article (*Applied Energy – publ. Elsevier*), aimed to provide a strategy for the use of extremely low-cost non-selective coatings, which are characterised by a high energy absorption ratio, but also by a high surface emissivity. The author of this dissertation has proposed a novel approach to apply these coatings only in the initial segments of the solar system, where the temperature of the heat transfer fluid, which collects heat from the internal surface of the absorber, is low enough that the higher radiation losses due to increased emissivity are overcompensated by the higher surface absorptivity in comparison to the reference cases. The analysis demonstrated that such a solution can only be applied at low concentration ratios and is strictly dependent on flow parameters and atmospheric conditions. The proposed sequential absorber arrangement enables a reduction in capital investment, as the application process for the non-selective coating is based on only one-step spray technology. The analysis showed that for an absorber with an external diameter of 33.4 mm, the price of a Pyromark coating would be 1.34 $/m.

The third article presents the mathematical model developed for heat transfer in a parabolic trough collector, which enabled studies to be carried out on the applicability of coatings. A new assumption applied in the mathematical model developed was to consider separately the heat delivered to the absorber surface through concentrated and non-concentrated radiation. The reason for applying this approach is because of the significantly higher proportion of unconcentrated radiation for low-aperture PTC installations than for the previously analysed wide-aperture installations. The applied detailed analytical method used in the developed mathematical model was intended to increase the analysis accuracy of the heat absorption process in low-concentration PTC installations.

The last part of the analysis deals with issues related to the tracking system, i.e. the integral part of the solar concentrator by which a mirror or mirror array continuously focuses direct sunlight onto the absorber surface. The accuracy with which the radiation is focused on the surface of the absorber is closely related to the quality of the installation, as well as the operating procedures used for the mechanism enabling the tracking movement. This aspect is also connected to the investment cost, as well as the energy consumption of tracking mechanisms.

The analyses performed enabled the assessment of the impact of the concentrator alignment deviation in comparison with perfect tracking on PTC efficiency. In the fourth article (*Renewable Energy – publ. Elsevier*), a series of numerical studies were carried out to determine the effect of tracking systems deviation on the optical and thermodynamic efficiency of low-concentration parabolic trough collectors. The analysis considered a concentrator geometry consistent with the previously mentioned radiation simulator bench. A series of analyses were also performed for the case that included no vacuum cover around the linear absorber. The results of the analyses carried out showed that the maximum deviation, which does not affect the reduction in energy input to the absorber surface, is 1.75°. It has also been demonstrated that such a deviation from the optimum position results in a more non-uniform distribution of heat flux on the absorbers surface. The curves which describe the heat flux distribution on the surface of the absorber that were obtained during the analyses can be used in future to carry out CFD analyses which will accurately demonstrate the effect of this non-uniform behaviour on the parabolic trough collector efficiency.

Streszczenie

Zwiększenie udziału energii ze źródeł odnawialnych w całkowitym miksie energetycznym jest kluczowe dla redukcji emisji gazów oddziałujących negatywnie na środowisko oraz zwiększenia bezpieczeństwa energetycznego poprzez uniezależnienie się od paliw kopalnych, będących często przedmiotem polityki międzynarodowej. W obszarze użytkowych form energii, największym zapotrzebowaniem charakteryzuje się nisko oraz wysokotemperaturowe ciepło. Jednym z najbardziej wydajnych i przyjaznych dla środowiska sposobem pozyskiwania ciepła użytkowego jest zaabsorbowanie oraz przetworzenie energii słonecznej przy użyciu infrastruktury kolektorów lub koncentratorów słonecznych.

Paraboliczne koncentratory promieniowania słonecznego (PTC), to dojrzała technologia dotychczas w głównej mierze wykorzystywana do produkcji energii elektrycznej, poprzez pośrednie pozyskiwanie ciepła przy temperaturze około 400 °C, najkorzystniej w dużych instalacjach zlokalizowanych w obszarach o bardzo wysokim rocznym nasłonecznieniu. Instalacje te charakteryzowały się często dużą aperturą zwierciadeł parabolicznych, tj. około 5 – 7 metrów, zewnętrzną średnicą absorberów 70 mm oraz całkowitą długością pętli solarnej wynoszącą nawet kilkaset metrów. Układ równolegle połączonych pętli solarnych tworzyć może instalację solarną o mocy cieplnej rzędu kilkuset MW. Ciągły rozwój instalacji przemysłowych na świecie spowodował konieczność poszukiwania rozwiązań mogących zaspokoić część zapotrzebowania na ciepło w zakresie temperaturowym do około 250 °C, wykorzystując potencjał energii odnawialnej. Rozwiązaniem idealnie, wpasowującym się w te założenia, są paraboliczne koncentratory promieniowania słonecznego o zredukowanych wymiarach, dostosowanych specjalnie do wytwarzania ciepła średniotemperaturowego.

Pomimo dojrzałości technologii wykorzystującej proces koncentracji promieniowania, zmiany w geometrii absorberów oraz koncentratorów charakteryzujących się niższymi wartościami koncentracji, niż miało to miejsce w przypadku systemów wysokotemperaturowych, otworzyły nowe możliwości zastosowania metod intensyfikacji absorbcji ciepła przez płyn termalny oraz redukcji kosztów poszczególnych elementów instalacji.

Ogół prac zrealizowanych na potrzeby niniejszej rozprawy doktorskiej miał na celu identyfikację procesów wymiany ciepła zachodzących w parabolicznym koncentratorze promieniowania słonecznego, określenie metod intensyfikacji odbioru ciepła oraz redukcji nakładów inwestycyjnych wybranych elementów, a także wykazanie potencjału zaaplikowania tych metod dla poszczególnych instalacji. Rozprawa doktorska bazuje na czterech wybranych publikacjach naukowych autora, a sam zakres realizowanych badań można sklasyfikować w ramach dwóch głównych zagadnień, jakie były rozwijane w dwóch etapach zrealizowanych prac.

W pierwszym etapie prac kompleksowo zaprojektowano oraz skonstruowano instalację badawczą, której oczekiwana funkcjonalność umożliwiła przeprowadzenie badań eksperymentalnych dla różnych absorberów w układzie parabolicznego koncentratora promieniowania słonecznego. W celu zagwarantowania stabilnych i powtarzalnych warunków analizy eksperymentalnej, w stanowisku badawczym zdecydowano się na użycie symulatora promieniowania słonecznego, którego proces modelowania oraz optymalizacji przedstawiono w artykule pierwszym (*International Journal of Energy Research wyd. Wiley & Sons*). W tym artykule przedstawiono rezultaty z serii analiz optyczno-energetycznych, jakie przeprowadzono przy wykorzystaniu metody Monte Carlo. W tych badaniach określono najbardziej optymalny rodzaj źródeł światła, jakim są wyładowcze lampy metalohalogenowe oraz geometrię odbłyśników paraboloidalnych wraz z ich optymalną aranżacją względem siebie oraz względem koncentratora promieniowania. Poprzez analizę optyczną oszacowano straty wynikające z częściowego rozproszenia promieniowania oraz potencjalną moc doprowadzoną do zewnętrznej powierzchni absorbera liniowego. Na podstawie uzyskanych wyników autor tej dysertacji kompleksowo zaprojektował oraz skonstruował stanowisko badawcze oraz przeprowadził serię badań eksperymentalnych dla różnego typu absorberów oraz metod intensyfikacji odbioru ciepła. Uzyskane rezultaty badań przedstawiane były w ramach wielu wystąpień konferencyjnych, głównie o zasięgu międzynarodowym, w tym na konferencjach zagranicznych. W tej rozprawie stanowisko badawcze oraz walidację opracowanych modeli matematycznych opisujących przepływ ciepła w absorberze przedstawiono w artykule drugim (*Energies wyd. MDPI*).

W drugim etapie prac przeprowadzono analizy, które miały na celu określenie potencjału aplikacji metod intensyfikacji odbioru ciepła przez płyn solarny przepływający przez absorber w układzie parabolicznego koncentratora promieniowania słonecznego. Zwiększenie wydajności instalacji poprzez sekwencyjne zastosowanie wkładek turbulizujących przepływ (twisted tapes) przeanalizowano w ramach drugiego artykułu (*Energies wyd. MDPI*).

Ewaluacji podlegały trzy rodzaje wkładek o zmiennym skoku, (twisted ratio – *Tr*) równym 1, 2 oraz 4, zastosowanych w instalacji pracującej w zakresie temperaturowym 60 – 250 °C i przepływie masowym płynu termalnego 0,15 kg/s, 0,225 kg/s oraz 0,3 kg/s, czyli przy parametrach zgodnych z instalacjami produkującymi ciepło do zastosowań przemysłowych. W ramach badań określono parametry hydrauliczne po stronie czynnika odbierającego ciepło oraz te związane z przepływem ciepła w instalacji. Dla badanych przypadków określono, że spośród trzech analizowanych wkładek, największą korzyść energetyczną, dla temperatur czynnika do 190 °C, można uzyskać dla *Tr* równego 1. Powyżej tej temperatury, optymalne jest zastosowanie wkładki o *Tr* równym 2. Należy jednak podkreślić, że każda z zastosowanych wkładek w analizowanym przykładzie, prowadziła do intensyfikacji odbioru ciepła przez płyn termalny. W analizie wykazano, że przyrost wydajności instalacji parabolicznych koncentratorów promieniowania słonecznego, gdzie użyto wkładek intensyfikujących odbiór ciepła, zależny jest od ich aranżacji w pętli solarnej, założeń dla pracy instalacji oraz warunków atmosferycznych. W analizowanym przypadku instalacji o długości 90 metrów wykazano, że średni przyrost sprawności wyniósł 0,27%.

W ramach analiz przeprowadzono serię badań nad potencjałem zastosowania nieselektywnych powłok absorpcyjnych, gdzie jako przykład przedstawiono możliwość aplikacji powłoki Pyromark na zewnętrznej powierzchni absorbera. Przedstawiona w artykule trzecim (*Applied Energy – wyd. Elsevier*) analiza, miała na celu przedstawienie strategii wykorzystania niezwykle tanich powłok nieselektywnych, które charakteryzują się wysokim stopniem pochłaniania energii, ale z drugiej strony również wysoką emisyjnością powierzchni. Autor tej dysertacji zaproponował nowatorskie rozwiązanie polegające na aplikacji tych powłok jedynie w początkowych segmentach instalacji solarnej, gdzie temperatura płynu termalnego, odbierającego ciepło od wewnętrznej powierzchni absorbera, jest na tyle niska, że wyższe straty radiacyjne wynikające ze zwiększonej emisyjności, są rekompensowane z naddatkiem poprzez wyższą absorpcyjność powierzchni względem przypadków referencyjnych. W analizie wykazano, że takie rozwiązanie może zostać zaaplikowane jedynie przy niskim stopniu koncentracji i jest ono ściśle zależne od parametrów przypływu oraz warunków atmosferycznych. Zaproponowany sekwencyjny układ absorberów umożliwia redukcję nakładów inwestycyjnych, ponieważ proces aplikacji nieselektywnej powłoki bazuje jedynie na jednoetapowej technologii natryskowej. W analizie wykazano, że dla absorbera o zewnętrznej średnicy 33,4 mm, cena powłoki Pyromark wyniesie 1,34 $/mb.

W artykule trzecim przedstawiono opracowany model matematyczny przepływu ciepła w parabolicznym koncentratorze promieniowania słonecznego, który

umożliwił przeprowadzenie badań nad możliwością aplikacji powłok. Nowym założeniem zaaplikowanym w opracowanym modelu matematycznym było osobne rozpatrywanie ciepła doprowadzonego do powierzchni absorbera poprzez promieniowanie skoncentrowane oraz nieskoncentrowane. Wynika to ze znacznie wyższego udziału promieniowania nieskoncentrowanego dla instalacji PTC o niskim stopniu koncentracji, niż dla uprzednio analizowanych instalacji o bardzo szerokiej aperturze. Zastosowane uszczegółowienie metody analitycznej wykorzystanej w opracowanym modelu matematycznym miało na celu zwiększenie dokładności wyników analizy procesu absorpcji ciepła w instalacjach PTC o niskim stopniu koncentracji.

Ostatnia część analizy dotyczyła zagadnień związanych z systemem nadążnym, a więc integralnej części koncentratora promieniowania słonecznego, dzięki któremu zwierciadło lub układ zwierciadeł w sposób ciągły skupia bezpośrednie promienie słoneczne na powierzchni absorbera. Dokładność z jaką promieniowanie jest skupiane na powierzchni absorbera jest ściśle związana z jakością wykonania instalacji, jak również z zastosowanymi procedurami pracy mechanizmu umożliwiającego ruch nadążny, co jest też związane z wielkością nakładów inwestycyjnych, jak również energochłonnością tych mechanizmów. Wykonane analizy umożliwiły ocenę wpływu odchylenia ustawienia koncentratora w stosunku do ustawienia optymalnego na sprawność instalacji. W artykule czwartym (*Renewable Energy – wyd. Elsevier*), przeprowadzono serię badań numerycznych mających na celu określenie wpływ błędu układów nadążnych na sprawność optyczną oraz termodynamiczną parabolicznych koncentratorów promieniowania o niskim stopniu koncentracji. W analizie rozważano geometrię koncentratora zgodną ze wcześniej wspomnianym stanowiskiem z symulatorem promieniowania. Wykonano również serię analiz dla przypadku, który uwzględniał brak zastosowania osłony próżniowej wokół absorbera liniowego. Wyniki przeprowadzonych analiz wykazały, że maksymalne odchylenie, które nie wpływa na redukcję ilości energii doprowadzanej do powierzchni absorbera, wynosi 1,75°. Dowiedziono również, że takie odchylenie od pozycji optymalnej powoduje bardziej niejednorodny rozkład promieniowania na jego powierzchni. Przebiegi charakterystyk promieniowania na powierzchni absorbera, jakie uzyskano podczas prowadzonych analiz, mogą w przyszłości posłużyć do wykonania analiz CFD, które dokładnie wykażą wpływ tego niejednomiernego rozkładu na efektywność pracy instalacji.

List of publications

The presented thesis consists of 4 monothematic papers listed below. The full texts of this publications can be found in the Appendices chapter. The papers are referred by the Roman numerals through the thesis.

I. Ł. Bartela, **B. Stanek***, D. Węcel, A. Skorek-Osikowska, *A solar simulator numerical modeling for heat absorption phenomenon research in a parabolic trough collector*, International Journal of Energy Research, Vol. 46, 2021, (**IF**$_{2021}$=**4.672**)

II. **B. Stanek**, J. Ochmann, D. Węcel, Ł. Bartela*, *Study of twisted tape inserts segmental application in low-concentrated solar parabolic trough collectors*, Energies, Vol. 16, 2023, (**IF**$_{2022\text{-}2023}$=**3.252**)

III. **B. Stanek***, W. Wang, Ł. Bartela, *A potential solution in reducing the parabolic trough based solar industrial process heat system cost by partially replacing absorbers coatings with non-selective ones in initial loop sections*, Applied Energy, Vol. 331, 2023, (**IF**$_{2022\text{-}2023}$=**11.446**)

IV. **B. Stanek***, D. Węcel, Ł. Bartela, S. Rulik, *Solar tracker error impact on linear absorbers efficiency in parabolic trough collector – Optical and thermodynamic study*, Renewable Energy, Vol. 196, 2022, (**IF**$_{2022}$=**8.634**)

*corresponding author

The author's contribution for each paper was following:

I. **Bartosz Stanek's contribution** was to plan and design the experimental test station, develop a numerical model for ray tracing analysis, carry out a calculation campaign, analyse results, estimate the cost of the solar simulator, prepare and submit the manuscript. According to the author's statement, Bartosz Stanek's contribution was equal to **55 %**.

II. **Bartosz Stanek's contribution** was to prepare the scope of the numerical and experimental analysis, comprehensively design, construct and assemble the experimental test stand, develop the experimental methodology, manufacture twisted tape inserts, execute experimental tests and validate numerical models, perform ray tracing analysis, formulate boundary conditions for CFD analysis, conduct long term analysis, analyse results,

prepare the manuscript. According to the author's statement, Bartosz Stanek's contribution was equal to **65 %**.

III. **Bartosz Stanek's contribution** was to formulate research assumptions and methodology, develop a mathematical model of heat transfer, conduct a calculation campaign, analyse the results, prepare and submit the manuscript. According to the author's statement, Bartosz Stanek's contribution was equal to **80 %**.

IV. **Bartosz Stanek's contribution** was to prepare scope and assumptions for optical and thermodynamic analysis, develop Ray Tracing numerical models, conduct a calculation campaign, analyse the results, prepare and submit the manuscript. According to the author's statement, Bartosz Stanek's contribution was equal to **65 %**.

Supplementary publications

The author of this thesis is the co-author of 3 research papers related to parabolic trough collectors. These papers are listed below.

1. **B. Stanek**, K. Grzywnowicz, Ł. Bartela, D. Węcel, W. Uchman, *A system analysis of hybrid solar PTC-CPV absorber operation*, Renewable Energy, Vol. 174, 2021, (**IF_{2021}=8.634**)
2. **B. Stanek**, Ł. Bartela, D. Węcel, S. Rulik, *An experimental study on parabolic trough collector in simulated conditions by metal-halide solar radiation simulator*, Archives of Thermodynamics, Vol. 43, 2022, (**IF_{2022}=0.92**)
3. K. Grzywnowicz, Ł. Bartela, L. Remiorz, **B. Stanek**, *Enhancement of Convective Heat Transfer in a Parabolic Trough Collector Using Vibrations—an Introductory Numerical Analysis*, Journal of Power Technologies, Vol. 100, 2020

The author of this thesis is the co-author of 17 conference papers and presentations related to parabolic trough collectors. The papers are listed below. The presenter is underlined.

1. **B. Stanek**, Ł. Bartela, D. Węcel, *Heat absorption intensification methods in linear absorber - the experimental study in simulated solar conditions*, Proceedings of the 17th Conference on Sustainable Development of Energy, Water and Environment Systems (SDEWES22). Paphos, Cyprus, 6-10.11.2022
2. Ł. Bartela, **B. Stanek**, D. Węcel, J. Ochmann, *Electricity Production and Storage System Using Parabolic Trough Solar Collectors and trans critical CO_2 Brayton Cycle*, Proceedings of the 17th Conference on Sustainable Development of Energy, Water and Environment Systems (SDEWES22). Paphos, Cyprus, 6-10.11.2022
3. D. Węcel, Ł. Bartela, **B. Stanek**, A. Skorek-Osikowska, *An experimental study of a parabolic trough solar concentrator with two-axis tracking system operating under Poland climatic conditions*, Proceedings of the 17th Conference on Sustainable Development of Energy, Water and Environment Systems (SDEWES22). Paphos, Cyprus, 6-10.11.2022

4. **B. Stanek**, W. Wang, Ł. Bartela, D. Węcel, *Potential of using Pyromark as an absorber coating in low-temperature solar installation sections – A case study for heat industrial application and parabolic trough collectors*, Proceedings of the 7th International Conference Contemporary Problems of Thermal Engineering : Towards sustainable & decarbonized energy system (CPOTE22). Warsaw, Poland, 20-23.09.2022
5. **B. Stanek**, Ł. Bartela, D. Węcel, S. Rulik, *An experimental study on parabolic trough collector in simulated conditions by metal-halide solar radiation simulator*, Book of abstracts, XV Research and Development in Power Engineering Conference (RDPE21). Warsaw, Poland, 30.11-3.12 2021
6. D. Węcel, **B. Stanek**, Ł. Bartela, *Operation analysis of parabolic trough solar collector*, Book of abstracts, XV Research and Development in Power Engineering Conference (RDPE21). Warsaw, Poland, 30.11-3.12 2021
7. Ł. Bartela, **B. Stanek**, A. Skorek-Osikowska, *Hybrydowe systemy produkcji ciepła i chłodu wykorzystujące koncentratory promieniowania słonecznego*. II Seminarium Nowoczesne Ciepło - chłód, ciepło odpadowe, magazyny ciepła, Poznań 5-6.10.2021
8. **B. Stanek**, Ł. Bartela, *Numerical and experimental study on 10 kWe metal-halide solar simulator for parabolic-trough collector testing*, Proceedings of the 34th International Conference on Efficiency, Cost, Optimization, Simulation and Environmental Impact of Energy Systems (ECOS21). Taormina, Italy, 28.06-02.07.2021
9. K. Grzywnowicz, **B. Stanek**, Ł. Bartela, *Increasing the efficiency of the parabolic trough collector under variable solar irradiance by internal flow turbulization - a numerical study*, Proceedings of the 34th International Conference on Efficiency, Cost, Optimization, Simulation and Environmental Impact of Energy Systems (ECOS21). Taormina, Italy, 28.06-02.07.2021
10. **B. Stanek**, Ł. Bartela, D. Węcel, A. Skorek-Osikowska, *Research on Spatial Non-Uniformity of Power Distribution for Solar Radiation Simulation*, Book of abstracts, 12th International Exergy, Energy and Environment Symposium (IEEES-12), Hamad Bin Khalifa University, Qatar, 20-24.12.2020
11. **B. Stanek**, K. Grzywnowicz, Ł. Bartela, D. Węcel, W. Uchman, *A system analysis of hybrid solar PTC-CPV absorber operation*, Book of abstracts, 15th Conference on Sustainable Development of Energy, Water and Environment Systems (SDEWES20), Cologne, Germany, 01-05.09.2020
12. K. Grzywnowicz, G. Wiciak, L. Remiorz, K. Janusz-Szymańska, Ł. Bartela, **B. Stanek**, Wpływ zastosowania turbulizatora przeciwprądowego na wzrost uzysków energetycznych z instalacji kolektora słonecznego: badania

numeryczne, 59 Sympozjon "Modelowanie w Mechanice" 2020, Ustroń, 22-26.02.2020

13. K. Grzywnowicz, Ł. Bartela, L. Remiorz, **B. Stanek**, *Modeling of influence of vibration on intensification of heat transfer within the absorber of the vacuum solar collector*, Book of abstracts, XV Research and Development in Power Engineering Conference (RDPE21). Warsaw, Poland, 03 – 06.12.2019
14. **B. Stanek**, Ł. Bartela, D. Węcel, G. Wiciak, M. Jurczyk, *Koncepcja stanowiska do badań porównawczych absorberów w układzie parabolicznego koncentratora promieniowania*, Book of abstracts, XV Research and Development in Power Engineering Conference (RDPE21). Warsaw, Poland, 03 – 06.12.2019
15. D. Węcel, **B. Stanek**, Ł. Bartela, *Współpraca krzemowego ogniwa fotowoltaicznego z parabolicznym koncentratorem promieniowania słonecznego*, Book of abstracts, XV Research and Development in Power Engineering Conference (RDPE21). Warsaw, Poland, 03 – 06.12.2019
16. Ł. Bartela, L. Remiorz, **B. Stanek**, K. Grzywnowicz, *Kierunki intensyfikacji przepływu ciepła w absorberze parabolicznego koncentratora promieniowania słonecznego,* Zarządzanie Energią i Teleinformatyką, Rynek Gazu, Rynek Ciepła, Nałęczów 17-19.06.2019
17. Ł. Bartela, **B. Stanek**, D. Węcel, *Analysis of production of useful forms of Energy using a solar parabolic trough collectors*, Proceedings of the 32nd International Conference on Efficiency, Cost, Optimization, Simulation and Environmental Impact of Energy Systems (ECOS19). Wrocław, Poland, 23-28.06.2019

Other topic publications

The author of this thesis has been working on energy storage topics in addition to solar energy research during his doctoral studies, which is worth emphasising. The research resulted in the publication of the following series of articles, of which Bartosz Stanek is a co-author.

1. K. Rusin, J. Ochmann, Ł. Bartela, S. Rulik, **B. Stanek**, M. Jurczyk, S. Waniczek, *Influence of geometrical dimensions and particle diameter on exergy performance of packed-bed thermal energy storage*, Energy, Vol. 260, 2022, (**IF**$_{2022}$=**8.857**)
2. **B. Stanek**, J. Ochmann, Ł. Bartela, M. Brzuszkiewicz, S. Rulik, S. Waniczek, *Isobaric tanks system for carbon dioxide energy storage – The performance analysis*, Journal of Energy Storage, Vol. 52, 2022, (**IF**$_{2022}$=**8.907**)
3. J. Ochmann, Ł. Bartela, K. Rusin, M. Jurczyk, **B. Stanek**, S. Rulik, S. Waniczek, *Experimental studies of packed-bed Thermal Energy Storage system performance*, Journal of Power Technologies, Vol. 102, 2022
4. Ł. Bartela, A. Skorek-Osikowska, S. Dykas, **B. Stanek**, *Thermodynamic and economic assessment of compressed carbon dioxide energy storage systems using a post-mining underground infrastructure*, Energy Conversion and Management, Vol. 241, 2021, (**IF**$_{2021}$=**11.533**)

Nomenclature

Abbreviations		
ALD	atomic layer deposition	-
BRDF	bidirectional reflectance distribution function	-
CFD	computational fluid dynamics	-
CSP	concentrated solar power	-
CVD	chemical vapor deposition	-
HMI	metal-halide	-
LCR	local concentration ratio	-
MCRT	Monte Carlo Ray Tracing	-
PET-G	polyethylene terephthalate glycol	-
PTC	parabolic trough collector	-
PVD	physical vapor deposition	-
SHIP	solar heat for industrial process	-
Subscripts		
abs	absorber	-
ap	aperture	-
B	beam (direct)	-
c	glass envelope	-
CSP	concentrated solar power	-
d	dirt	-
e	external	-
el	reference electricity production	-
i	internal	-
in	inlet	-
loss	energy losses	-
m	mirror	-
opt	optical	-
out	outlet	-
r	receiver	-
ref	reflectance	-
s	solar	-

sh	shadowing	-
SP	non-concentrated solar energy	-
track	tracking	-
u	useful	-
Roman symbols		
A	area	m²
C	concentration ratio	-
cp	specific heat	J/(kg K)
d	diameter	m
G	irradiance	W/m²
H	twisted length	m
IAM	incidence angle modifier	-
L	length	m
$\dot{m}$	mass flow rate	kg/s
Q	heat flux	W
T	temperature	°C
Tr	twisted ratio	-
W	width	m
W_p	required pumping power	W
Greek symbols		
α	absorptivity	-
ε	emissivity	-
η	efficiency	-
θ	incidence angle	°
τ	transmittance	-

Chapter 1

Introduction

1.1 Background

In 2022, the global CO_2 emissions from energy combustion and industrial processes were reported at 36.8 Gt [1]. The biggest sectoral increment was observed from electricity and heat generation, whose emissions were up to 261 Mt. Global emissions, especially from coal-fired electricity and heat generation grew by 2.1%, where Asian emerging economies played a major role.

According to International Energy Agency (IEA), despite the increment in CO_2 emissions, the strong development of renewable energy sources has slightly limited the growth in emissions from coal-fired power stations [1]. Moreover, the global energy crisis, driven by Russia's invasion of Ukraine, created unprecedented momentum for renewables. Power installations based on renewable energy, are politically independent, only their potential differs in various locations around the world. According to Renewables 2022 report by IEA [2], because of the political situation, renewable capacity expansion in the next five years will be much faster than what was expected last year. The use of modern renewable heat is projected to increase by almost one-third over the period 2022-2027, boosting the modern use of renewables in heat from 11.4% to 14% in 2027 [2].

Solar power, as a major source of clean energy, offers great potential for heat production [3,4]. The global yield of solar energy from all installed solar systems in 2020 corresponds to a saving of 43.8 million tonnes of oil and 141.3 million tonnes of CO_2, which highlights the significant contribution of this technology to reducing global greenhouse gas emissions [2,5]. According to IEA reports [6], in many regions of the world, there is sufficient potential to further increase the generation capacity of variable renewable energy sources. Concentrated radiation technologies have great potential for use, e.g. for the production of heat utilizes in industrial processes.

1.2 Design of parabolic trough collector

Parabolic trough collector (PTC) is one of the solar thermal technologies based on the concentration process, that is the multiplication of solar radiation on the receiver surface through a system of highly reflective surfaces in the shape of a parabola [7]. Direct solar radiation, through parabolic mirror (or mirrors), is concentrated on the external surface of a linear absorber located at its focal point. The absorber consists of a tubular pipe made of steel, coated on the external surface with a selective coating designed to absorb heat flux. Selective character indicates that the coating is characterised by high absorptivity and low emissivity to reduce radiation losses [8,9]. The absorber is usually situated inside a highly transmissive glass envelope, allowing low pressure close to the vacuum to be maintained. The glass envelope and the absorber pipe are connected by special brackets, which are capable of expanding and shrinking to reduce material stress and avoid cracking the glass envelope as well as unsealing the low-pressure area. A parabolic trough collector scheme is illustrated in Figure 1.1.

The entire absorber along with the glass envelope and mounts is called the receiver. The radiation multiplication process in concentrated solar power (CSP) technologies, is enabled by the use of solar trackers that continuously follow the sun to use direct radiation [10]. Parabolic concentrators along with receivers are connected in series to form a solar loop. Solar loops connected in parallel are defined as solar field.

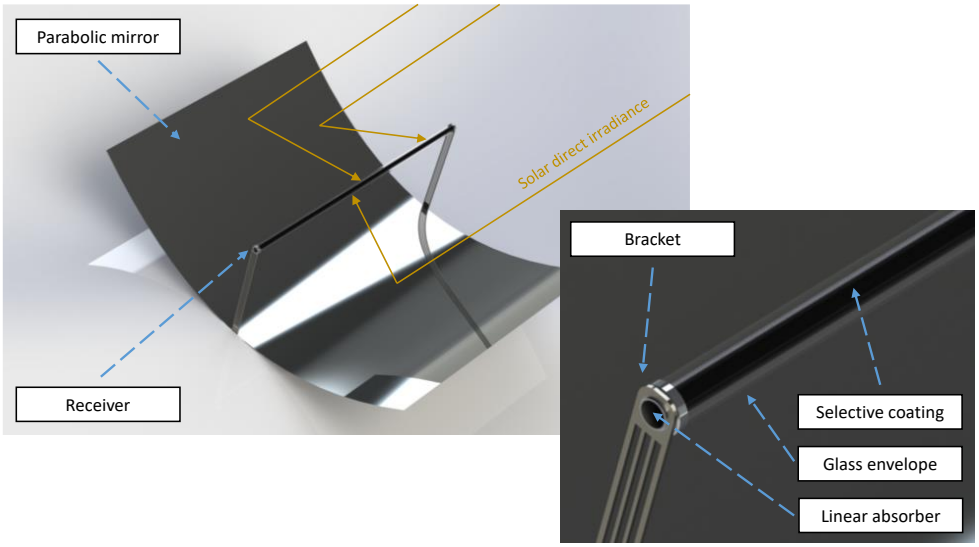

Figure 1.1. Parabolic trough collector

Originally, parabolic trough collectors were used for large solar power plants to produce steam and then, by expanding it in a turbine, to produce electricity [11,12]. The desired temperature of heat transfer fluid, which was used to absorb heat from the internal wall of the absorber, at the outlet of the solar loop was 393 °C, assuming an inlet temperature of 293 °C. These temperatures could be reached with a high concentration ratio defined as [11]:

$$C = \frac{W_{\mathrm{ap}}}{\pi \cdot d_{\mathrm{abs,e}}}, \tag{1.1}$$

where W_{ap} is aperture width and $d_{\mathrm{abs,e}}$ is external absorber diameter. Installations commonly used receivers such as the PTR 70 or UVAC manufactured by Schott, Solel, Siemens and Rioglass, with an internal absorber diameter of 66 mm [13–15]. In full-scale PTC, parabolic collectors were typically used in EuroTrough (ET-150) technology with an aperture width of 5.77 m and UltimateTrough with an aperture of 7.51 m [12,16,17]. The concentration ratio for ET-150 and PTR 70 according to equation (1.1) was 26.2.

Technology evolutions have contributed to the development of more compact and reduced-concentration solutions, to adapt this technology to lower-temperature heat demands [18,19]. The potential of such facilities is mainly used for industrial applications as a supplementary heat source, as presented in a later section of this thesis. The design and operating principle of the installation are similar to the reference, full-scale technology, with certain differences.

The first aspect is the smaller concentration ratio. Usually, for low-concentrated parabolic trough collectors, the aperture of the parabolic mirror is a maximum of 3 metres. One example is Inventive Power, whose products PowerTrough 110 and PowerTrough 250 have apertures of 1.1 m and 2.5 m respectively [20,21]. The PolyTrough concept is defined by an aperture of 1.8 m and the Absolicon T160 is a 1 m width collector [22,23]. The outer diameter of the absorbers used in low-concentrated parabolic trough collectors is accordingly smaller than in the full-scale previously mentioned receivers. The characteristic range is 33.4 - 38 mm.

Unlike full-scale PTCs, low-concentrated installations can be placed both at ground level and on the roofs of buildings, expanding their area of application. Moreover, the temperature and design flow is significantly lower than in full-scale installations, which opens multiple paths in the application of alternative, previously unconsidered materials with parameters that increase PTC loop efficiency or reduce capital expenditure. It is therefore necessary to search for new methods of

intensifying heat absorption or adapting existing methods to the new operating parameters.

1.3 Operational installations

1.3.1 Full scale CSP

Installations utilising direct solar irradiance can be divided into parabolic trough collectors, solar power towers, linear Fresnel reflectors, dish/engine concentrators while the two most significant are parabolic trough collectors and power towers [24]. The International Energy Agency program SolarPACES, reports the total capacity of CSP projects of 6314 MW operational and 1161 MW under construction [25,26].

As previously mentioned, parabolic trough collectors have mainly been and still are used in full-scale solar power plants, where electricity is produced. Currently, 79 operational PTC-based power plants with a total capacity of 4737.2 MW can be listed [26,27]. The three largest installations based on linear concentration technology are located in the United States of America and are as follows: Mojave Solar Project (280 MW, California), Solana Generating Station (250 MW, Arizona) and Genesis Solar Energy Project (250 MW, California) [28–30]. Until 2014, the largest PTC-based installation was the US SEGS I-IX project, which was the largest and also the oldest PTC power plant (353.8 MW) [31]. SEGS consisted of the nine installations constructed since 1984, as shown in Figure 1.2. Currently, only SEGS IX is still operational, the rest facilities are decommissioned [32].

The largest annual increase in capacity at PTC installations was recorded from 2011 to 2014 when power plants were established in Spain, mainly 50 MW nominal capacity units. Currently, Spain has the largest installed capacity of PTC-based solar installations. Forty-five operational power plants are characterised by a total capacity of 3306.7 MW which accounts for 69.8 % of the total share of PTC-based solar full-scale power plants [26]. The largest planned parabolic trough collectors-based power plant named Noor Energy 1 will consist of 3 segments, each with a capacity of 200 MW (in total 600 MW) and will be located in the United Arab Emirates [33]. In addition to the 3 PTC segments, a solar power tower (100 MW) and a PV panels field (250 MW) are planned to construct. Since 2014, a significant increase in the capacity of installations based on power towers is noticeable. New full-scale PTCs are also being created, but in significantly lower numbers than in previous years.

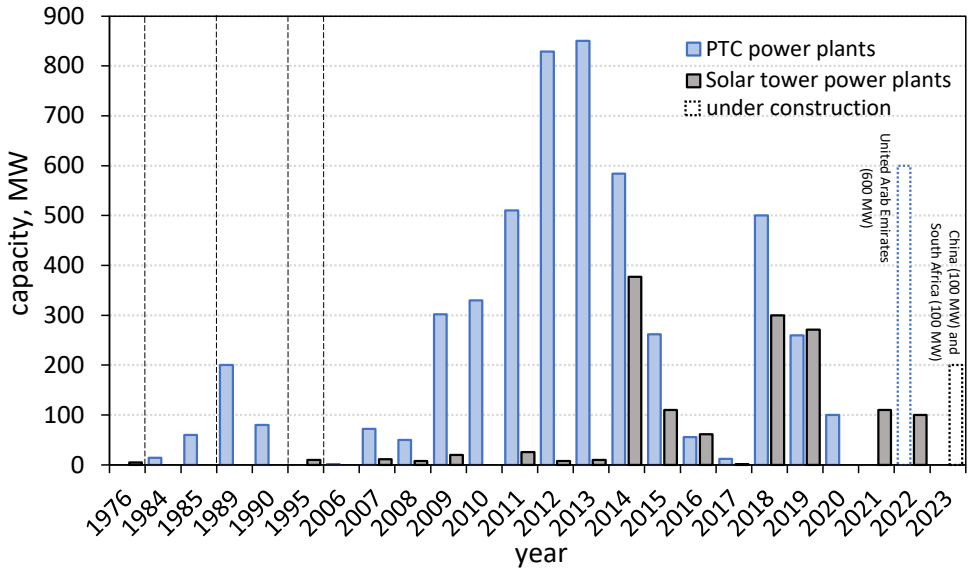

Figure 1.2. Concentration based full scale solar power plants capacity increment in specific years, based on [26,27]

1.3.2 Low-concentrated installations

Compared to full-scale PTC power plants, the list of low-concentrated PTC-based facilities cannot be considered fully comprehensive due to the lack of mandatory reporting on these types of facilities, so the quantities described below may deviate slightly from the current state of facilities. In the author's opinion, however, the summary presented in this chapter seems to be complete in presenting the state of development of these systems and also details the areas in which the potential of CSP is currently being exploited and can be developed in the future.

The data presented is based on the solar heat systems for industrial processes (SHIP) database operated by AEE INTEC in Austria and information obtained from the realisations of individual manufacturers [34]. By the end of 2020, at least 891 SHIP, with a total collector area of 1.12 million m^2, have been installed all over the world to meet various industrial process heat requirements [35]. However, these statistics apply to all types of solar thermal installations producing heat of any energy potential.

Installations based on low-concentrated parabolic trough collectors are presented along with full-scale PTC-based and power tower-based power plants in Figure 1.3. It should be emphasised that SHIP installations operate as a supplementary heat source to reduce emissions, by partially covering the heat demand for industrial

processes. Unlike power plants, they do not generate electricity but only heat at a particular temperature potential, so the data for solar fields, define them by specifying the maximum thermal output that the plant can generate.

The Figure 1.3 shows the locations of 54 SHIP PTC-based facilities. The current largest installation generating heat for industrial processes is located in Miraah Oman and is characterised by a maximum thermal capacity of 1.021 MW_{th}, with a solar field covering an area of almost 2 km^2 [36]. Steam produced is used for thermal enhanced oil recovery to extract heavy and viscous oil at the Amal oilfield. An authentic feature of this installation is the solar field covers to protect the parabolic mirrors against desert dust. It is the only heavily deviated SHIP installation with such a high thermal output. The second largest installation reported is located in China with a maximum thermal output of 1050 kW_{th}.

Excluding the Oman installation, the average maximum thermal capacity of the other 53 installations shown is 145 kW_{th}. The highest concentration of SHIP installations is in Mexico, where 31 installations can be listed with a total maximum thermal output of 3598 kW_{th}, as a result of the high popularisation and continuous development of the technology, as well as the energy potential available in the area [37].

It is also important to highlight the deployment of PTC-based SHIP in other locations, primarily those with lower energy potential [38]. Despite the much lower average annual insolation, it is possible to list three PTC SHIPs in Switzerland, two in Germany, and even in Sweden, which works as heat-generating installations for industrial applications as well as demonstration installations [39–42].

Based on the available data for Europe, only two SHIP installations operate in Spain, two in Greece and one in Portugal. Comparing this data to the locations of full-scale CSP-based power plants, the unexploited potential that exists in these well-insulated locations is visible. Europe, which is characterised by a highly developed industry, has a huge heat demand, which can be partially covered by a low-concentrated parabolic trough collector, as described in detail in the next chapter. However, to expand this technology, it is necessary to develop methods of intensifying heat collection to increase efficiency and also methods to reduce costs so that low-concentrated PTC can compete with other thermal generation technologies.

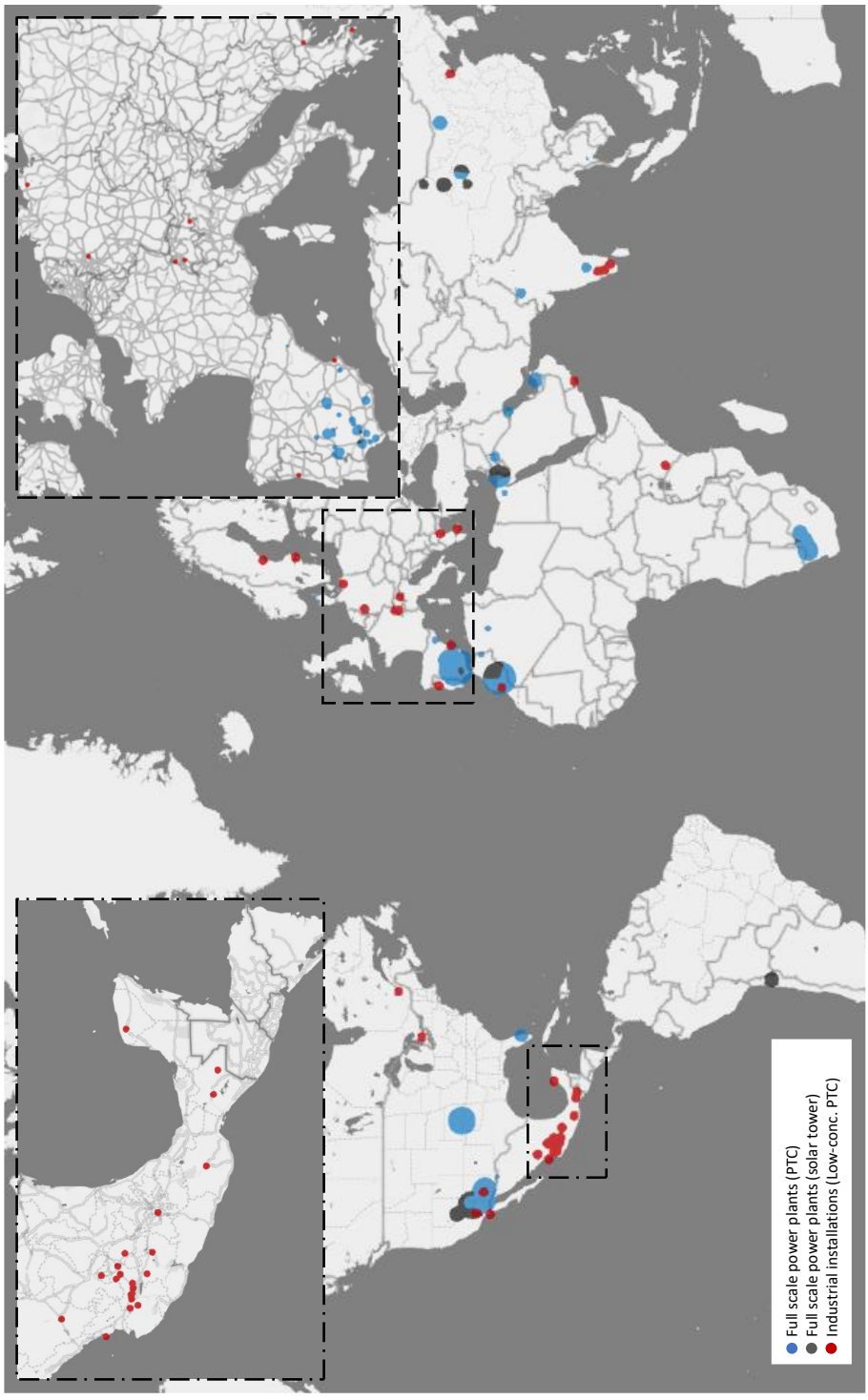

Figure 1.3. Solar installations using concentrated radiation technology, based on [26,34]

1.4 Potential applications

In 2019, the final energy consumption was reported as 418 EJ, by the International Energy Agency [43]. According to International Energy Agency (IEA) and International Renewable Energy Agency (IRENA) reports, over 32% of final energy is consumed by the industry sector, where 74% is in the form of heat and 26 % is in the form of electricity [4,44]. Figure 1.4 highlights that the industry sector has the highest share of energy consumption, compared to other sectors [45]. Heat supply, which contributed more than 40% of energy-related global CO_2 emissions in 2020, remains mainly dependent on fossil fuels, and renewable energies account for less than a quarter. Therefore, the crucial step toward achieving a low-carbon production system is integrating renewable energy into the industrial process heat sector. As shown in Figure 1.4, the heat demand can be divided into 3 temperature levels where the heat up to 400 °C is 52%. This part of the heat can be partly covered by low-concentrated parabolic trough collectors. As Kumar et al. [45] and Kalogirou [46] indicated, low-concentrated parabolic trough collectors, are well suited to operate in the range of 60 - 300 °C, which can be used to produce steam, used in many industrial applications. Depending on the concentration ratio, the analysed technology can be used for sterilization, drying, bleaching, washing and pasteurization. The industry type the low-concentrated parabolic trough collectors can be used is broad, for example, dairy, paper and textile industry, chemical industry (soaps and synthetic rubber production), oil refinery plastics and brewery.

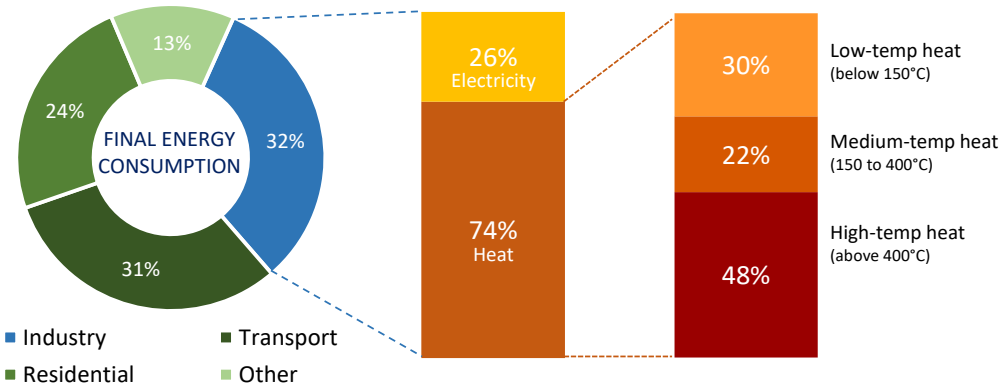

Figure 1.4 Final energy consumption and its classification by type and temperature level based on [45,47]

1.5 Selected heat absorption enhancement methods in PTC

The development of methods to intensify the heat collection in the absorber in the solar technology considered in this thesis is one way of increasing the efficiency of the installation. The efficiency of the parabolic trough collector can be generally represented as Eq. (1.2) [48]:

$$\eta = \frac{Q_{\mathrm{u}}}{Q_{\mathrm{s}}}, \tag{1.2}$$

where Q_u is heat absorbed by thermal fluid and Q_s is solar energy which reaches PTC installation. Total solar energy received by a PTC installation is defined as Eq. (1.3) [49]:

$$Q_{\mathrm{s}} = A_{\mathrm{ap}} \cdot G_{\mathrm{B}}\,, \tag{1.3}$$

where A_{ap} is aperture surface area, and G_B is direct solar irradiance. The heat collected by the thermal fluid, can be calculated from the following Eq. (1.4) [50]:

$$Q_{\mathrm{u}} = \dot{m} \cdot c_{\mathrm{p}} \cdot (T_{\mathrm{out}} - T_{\mathrm{in}}), \tag{1.4}$$

where $\dot{m}$ is the mass flow, c_p is the specific heat of the working fluid, T_{out} is the outlet temperature of the working fluid, T_{in} is the inlet temperature of the working fluid.

Increasing the temperature at the outlet from the absorber, directly influences the increase in efficiency of PTC. This can be achieved by using methods inside and outside the absorber.

1.5.1 Inserts application

A frequently researched method to increase heat collection inside the absorber is the use of different types of inserts. Research is being conducted on: fins, porous inserts, wire coils, rings, cylinders/rods and twisted tapes [51]. Overall, the use of inserts increases the thermal efficiency of parabolic trough collectors and increases the pressure drop across the absorbers. The most challenging aspect is proving to be the use of different types of inserts inside the absorber and optimising their positioning taking all parameters into account. According to Allam et al. [51], fin inserts achieve optimum thermal and hydraulic performance. Bellos et al. [52,53] also demonstrated that finned inserts showed the highest average efficiency

increase, which was 0.7% for the vacuum tube and 1.3% for the tube without a glass envelope and vacuum layer. However, the challenge is found to be the cost of manufacturing such an absorber, where instead of a traditional mass-produced tube, the appropriate components have to be specially produced, which significantly increases the required production time and requires the use of supplementary equipment. When looking at the bigger picture, in this case, the required process can be much more energy-demanding than the benefits of increased heat collection.

Twisted tapes, which are characterised by a relatively simple and rapid manufacturing process, can provide an opportunity. What's more, twisted tapes are widely used in industry, so their lower price can be just as important an advantage as the increase in efficiency. Varun et al. [54] demonstrated a high research interest in twisted tape inserts for various flow regimes and configurations. Conventional twisted tapes as well as wire coil twisted tapes, double twisted tapes or perforated twisted tapes were analysed in [55–58]. Most studies reported in the literature on the subject, use several simplifications that introduce a significant error when examining their application in linear absorbers.

The most frequent simplification in numerical studies is to assume a uniform heat flux distribution around the circumference of the absorber or to specify a uniform wall temperature, which completely incorrectly represents the heat flow in the absorber, as well as the effect of twisted tape on its efficiency. The great majority of publications related to linear absorbers are related to full-scale PTCs, for example with a PTR70, LS-2 or UVAC absorber, where the boundary conditions are substantially different from those of a low-concentration parabolic trough, so the correlations provided in these studies do not apply to the case being considered, which are low concentrated parabolic trough collectors. Moreover, there remains a deficit of reports in the literature on the application of this type of solution for solar loops, showing the actual impact of the inserts on solar plant operation. Therefore, additional investigations are required to identify and optimise twisted tapes in low-concentrated parabolic trough collectors.

1.5.2 Absorber coatings consideration

The external surface of the absorbers is covered with a selective coating, which is characterised by high absorptivity and low emissivity, thus reducing radiation losses. The procedure for applying the selective coating to the absorber surface usually requires high costs due to the multi-stage processes involved [8]. Methods for producing spectrally selective coatings include dip coating, spin coating, laser sintering, chemical vapour deposition (CVD), atomic layer deposition (ALD), physical vapour deposition (PVD), electroless plating, electroplating and lithography [59].

The most widely used method of fabricating selective coatings, by which many types of coatings can be obtained, is PVD [60]. Ordinarily, the process is based on the application of multiple layers, semiconductor-metal tandems or cermet, which requires a significant amount of time and an expensive manufacturing facility [8,59]. Solel, which is a cermet-based coating, reports an absorptivity of 0.96 and an emissivity of 0.07-0.17 for temperatures ranging from 100-400 °C [9]. The coating used in PTR70, also reports a high absorptivity of 0.957 [14].

Improving the efficiency of a parabolic collector can be achieved by using coatings in various configurations. Yang et al. [61] proposed an absorber with two different coatings on the concentrating and natural radiation absorbing side. The results indicated an improvement in receiver efficiency from 64.7% to 68.1%. A cascade arrangement of absorbers with different selective coatings was also considered [62]. Zhao et al. [63] presented a strategy to increase efficiency by cascading multiple selective coatings based on their emissivity characteristics. The results showed a 29.3% reduction in heat loss and a 4.3% increase in thermal efficiency at a temperature range of 290-550 °C. However, all of these analyses were carried out for large-scale solar power plants with high concentration ratios and thermal fluid temperature levels.

The high prices of coatings were not reduced in this analysis, as still any coatings considered had to be applied by multilayer methods. An opportunity to reduce investment costs may be the use of cost-effective absorptive coatings, the application process of which is extremely cheap compared to solar selective coatings. An example is the most commonly used high-temperature Pyromark solar absorber coating in power towers, which achieves extremely high absorption of up to 96.5 % [64,65]. However, the disadvantage of these coatings is their high emissivity. Therefore, the development potential of these coatings only occurs in the preliminary section of absorber loops, where the temperature of the heat transfer fluid is relatively low.

1.5.3 Solar tracking requirement

As previously mentioned, concentrators mainly utilise direct radiation, so solar tracking is required to achieve high-efficiency values. As an optical system, the PTC is characterised by several parameters that can negatively affect its operation. These optical errors are due to the design, fabrication of the reflector and absorber and errors in the solar tracking system.

Assuming that the parabolic reflector and absorber are fabricated correctly, it is essential to note that during operation, the PTC may deform due to the heating of

the structure and some stresses caused by atmospheric conditions (wind, rain, snow) [66]. The correct alignment of the solar tracker is based on measuring the current position of the sun or based on the solar calendar data. Both methods can lead to some errors [67,68].

Ongoing research is being conducted to improve the precision of positioning systems. Wu et al. [69] implemented a two-axis tracker with an inclinometer for automatic positioning with open-loop GPS tracking. Fuentes-Morales et al. [70] and Lee et al. [10] underlined the importance of control algorithms to improve tracking systems. Valentin et al. [71] studied the impact of wind on solar trackers. Research is also being conducted to increase the optical efficiency of the PTC. Kaluba et al. [72] introduced a hot mirror coating on the absorber glass to reduce energy losses. Dahlioui et al. [73] developed an anti-soiling coating on solar mirrors that increased their clarity.

Operational faults can be reduced but not eliminated, so investigations are usually limited to determining the sensitivity of the PTC to errors from the point of view of optical efficiency, local concentration ratio (LCR) and heat loss in the PTC absorber [74]. However, these are primarily analyses performed for commercial-sized installations, which are the most frequently used in full-scale solar power plants. Each scale of geometry must be considered individually in the solar tracking aspect. Since there is still a lack of information in the literature on the different types of defects and requirements for solar trackers for low-concentration geometries, more research needs to be conducted to fill this gap.

1.6 Motivation and objectives

As demonstrated in the literature review, low-concentration parabolic trough collectors are highly versatile systems that, when properly designed and parameterised to suit the characteristics of a particular industry sector, can cover a significant proportion of the heat demand at different desired temperature levels. Despite the maturity of the concentration technology and the many studies related to full-scale PTC, the different, reduced geometry and thermodynamic parameters offer the potential for the application of new solutions and materials that will both increase the efficiency of the technology and reduce the price of the selected components, which may influence the spread of this type of solar installation even in areas with lower average annual insolation. This could lead to an increasing share of renewables in the total energy mix, resulting in lower emissions and higher

independence from fossil fuels. The materials used in the concentrators are simple to manufacture and later recycle, so this type of device has an additional positive impact on the environment relative to other solar energy technologies. It is essential, to search for areas and solutions that can intensify the heat absorption of parabolic trough collectors and enable comparative studies of these devices under stable and repeatable solar conditions. Therefore, this thesis aims to investigate different types of heat intensification on the inner and outer sides of absorbers in parabolic trough collectors and to examine their impact on entire solar loop installations.

The scientific problems discussed in this thesis are related to three selected elements of parabolic trough collectors, however, with comprehensive consideration of the entire technology: heat extraction enhancement inside the absorber through the use of inserts in a suitable arrangement, heat absorption intensification through using highly absorptive non-selective coating, and analysis of the influence of the crucial element in PTC such as the active solar tracker on the efficiency of the heat concentration and absorption process.

The following research activities were formulated to reach the objectives of this thesis:

- comprehensive design and construction of a solar radiation simulator test stand, enabling tests to be carried out on different types of absorbers, under stable and repeatable conditions,
- identification of processes and development of a mathematical model for heat transfer in a parabolic trough collector,
- conducting a series of experimental analyses to validate the developed models,
- investigating the impact of twisted tapes located inside a linear absorber and their arrangement in a solar loop to maximise the efficiency of a parabolic trough collector,
- investigating the effect of different types of highly absorbing coatings on the outer surface of the absorber and their segmental application along the length of the solar loop,
- development of a numerical optical parabolic concentrator model and performance of a series of analyses to identify the impact of tracking error on PTC efficiency.

1.7 Scope of the thesis

The doctoral thesis consists of 6 following chapters.

Chapter 1 is this chapter.

Chapter 2 is devoted to a description of the test bench modelling required for experimental research on parabolic trough collectors and the process of heat absorption by heat transfer fluid in tubular absorbers. Due to the varying natural atmospheric conditions over time, to investigate linear absorbers under constant and repeatable conditions, the author of this thesis designed and then comprehensively constructed a stand based on a solar radiation simulator enabling the simulation of near-natural radiation not dependent on the time of year or day. A series of numerical analyses were carried out using the Monte Carlo Ray Tracing Method to determine the most suitable type of light source, the optimum geometry of the parabolic cross-section reflectors and their arrangement against the parabolic trough collector. The study considered the desired spectrum of the simulated radiation analysis, its scattering and non-uniformity and how these factors affect the radiation concentration process. This part of the thesis also identifies the estimated cost of the radiation simulator, detailing specific components, which was missing in the literature on the subject. The results of performed analyses were crucial in further work, which was a comprehensive construction of the test stand by the author of this thesis.

Chapter 3 presents the results of an analysis aimed at intensifying heat extraction inside the linear absorber using twisted tape inserts, segmentally positioned in different sections of the solar loop. A low-concentrated ratio installation was considered, which could be used as an additional heat source for industrial applications. The study was conducted using a CFD model and a two-dimensional mathematical heat transfer model. The mathematical model of heat transfer is described in detail in the next chapter. The calculations were validated with experimental results, carried out on a developed laboratory station equipped with a solar radiation simulator, which showed high agreement, confirming the validity of using these models. Both temperature increment and pressure drop were validated. This chapter also presents the developed and assembled test bench for absorbers comparative research. In the numerical studies, the non-uniform distribution of concentrated heat flux on the absorber surface, consistent with the real conditions, was applied, which increases the accuracy of the calculations against most models presented in the literature. The results obtained demonstrate the validity of the segmented application of twisted tapes, by considering the additional pressure

losses and the increased demand to cover installation own needs caused by higher circulating pump demand. A long-term analysis of the specified conditions showed the potential to increase the efficiency of the solar facility by approximately 0.27 percentage points.

Chapter 4 is focused on coatings applied on absorber external surfaces to increase the absorptivity and thus the efficiency of the installation. The main objective of the results presented in this chapter was to determine the possibility of replacing the expensive selective coatings typically used in linear absorbers with cost-effective but highly absorptive no-selective coatings in preliminary absorber sections, with maintaining at least the same efficiency level. To determine the potential of such a design, analyses were performed for parabolic trough collectors with different geometries that reflect the varied nature of their application. To perform the assumed analyses, a detailed heat transfer model in parabolic trough collectors was developed, the calculation procedures of which are presented in the study methodology. Furthermore, the model was developed with special consideration for the separation of the heat flux supplied to the absorber surface into a concentrated and natural form. In parabolic trough collectors with a low concentration ratio, this separation significantly increases the accuracy of the results obtained, due to the higher proportion of natural radiation compared to full-scale parabolic trough systems. The results showed that, due to the lower temperature level of heat transfer fluid, a high potential of the non-selective coatings co-application was indicated. Furthermore, the use of a low-cost non-selective coating can provide a significant reduction in the investment cost of the installation and impact the development potential of concentrating solar power systems.

Chapter 5 deals with an aspect of solar tracking. Parabolic trough collectors, which are one of the technologies based on concentrating solar radiation, require continuous solar tracking due to the utilisation of mainly direct irradiance. As an active component, the solar tracker is characterised by a certain degree of positioning accuracy and is exposed to weather conditions, especially wind. Based on a low-concentrated parabolic trough collector geometry, a series of optical and thermodynamic analyses were conducted to determine the maximum positioning deviations of the solar tracker to avoid reducing its efficiency. Ray tracing analysis and heat transfer model was adopted for this purpose. The results are intended to indicate assumptions for the design of low-concentrated parabolic trough tracking devices. The study also compiled results for another way of reducing the cost and weight of the installation, i.e. not using a glass envelope around the absorber pipe. The increased level of non-uniformity of heat flux on the absorber surface was also

discussed, which, because of the tracking error, can cause high-temperature differences on the absorber surface and thus affect its potential damage.

Chapter 6 presents a summary and conclusions.

Chapters 2 to 5 highlight the most significant aspects of Articles I to IV, which are included in the appendix section. Figure 1.5 shows a graphical visualisation of the thesis scope.

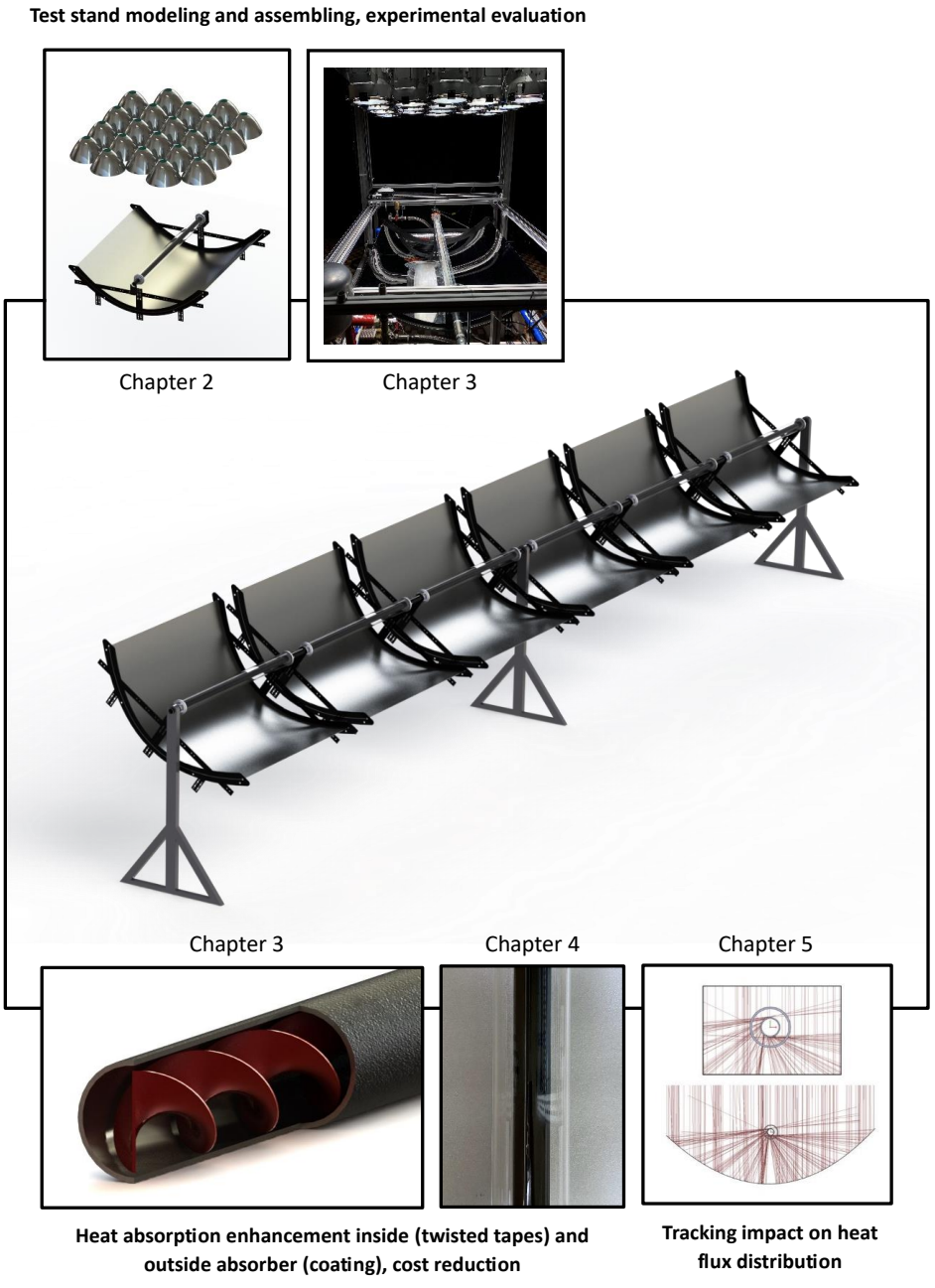

Figure 1.5. Graphical visualisation of the thesis scope

Chapter 2

Modelling of the solar simulator experimental bench for linear absorbers testing - Paper I

Solar radiation simulation is a complex multi-dimensional process that requires the consideration of a whole range of optical, spectral and thermodynamic parameters [75,76]. Depending on the application planned, simulators differ and it is not possible to directly adapt expensive prefabricated solutions. Primarily in solar concentrators, where the desired rays should be as parallel as possible, optical analyses are required to design the entire array of sources along with the optimisation of their positioning, which was part of the first tasks presented in this section of the doctoral thesis.

2.1 Formulation of test bench design assumptions

The considered research stand had to be multipurpose enough to be used mainly for testing parabolic trough collectors but also in the future for testing photovoltaic panels, so the main idea was that the light sources would be arranged on one plane surface and illuminate the target below. Due to the high cost of prefabricated solutions that could not be directly adapted to the planned tests, it was decided to carry out a series of optical-numerical studies to perform a preliminary analysis to check the validity of using different light sources and designing the test bench. The objectives were that the illuminated area had to be a minimum of 1 square metre (1x1 m), the radiation as uniform as possible, the spectrum as similar to solar radiation as possible, and the heat flux provided to the absorber surface corresponding to approximately 1000 W/m^2 direct normal irradiance.

After an examination of the solutions available in stock, the available budget and an in-depth analysis of the literature on the subject, which at the time provided relatively limited suggestions, as well as the market for the individual components, the two most promising cases were selected and the validity of their design was checked using the (MCRT) Monte Carlo Ray Tracing method [77,78]. At that moment, it was decided to study the use of 22 reflectors and metal halides of 200 W or 400 W or 4 xenon lamps with 4 larger reflectors. A visualisation of this solution in the arrangement of the entire test stand with a parabolic trough collector, is shown in Figure 2.1.

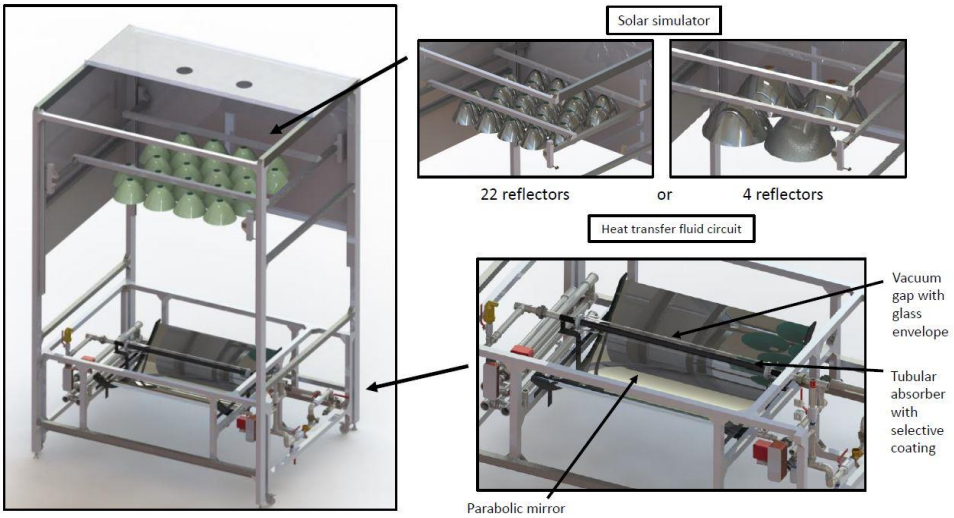

Figure 2.1. The design of the solar simulator for testing parabolic trough collectors [79]

2.2 Limitations of simulated radiation

As mentioned earlier, radiation simulation is a multi-stage process with many defining parameters. In this case, the most challenging aspect was to simulate the radiation in such a form that the simulated rays would be as close to direct radiation paths as possible, i.e. as perpendicular to the illuminated surface, so that they could then reflect off the parabolic mirror at the appropriate angle and reach the absorber external surface. This study required the design of a suitable light source model and its arrangement in the reflector, based on manufacturer and literature data.

The light sources analysed generate radiation through a few millimetre-long arcs between two electrodes, so a light source, even if positioned directly in the focus of

a reflector with a parabola shape, will emit radiation which, when reflected, will not be parallel in its full range, like natural direct radiation. Furthermore, over a large area, emitting irradiance with high uniformity is an extremely challenging process, as it is dependent strictly on the size and arrangement of the reflectors. Therefore, when designing the stand, it was accepted that not all the radiation emitted by the light source would be delivered to the surface of the absorber. Hence the need for sufficient surplus heat flux. Figure 2.2 shows the heat flux distribution for the two cases analysed, from which it can be concluded that the smaller the light sources, the more uniform the radiation will be on the illuminated surface. Limitations due to the specific dimensions of single-ended arc sources, and the production sizes available, as well as the required components for each lamp such as power supply, ballast, sockets and special wires, or parabolic reflectors, and the increased costs as the number of lamps increased, necessitated the identification of an optimum. The optical analysis indicated that the required heat flux delivered to the absorber surface would be appropriate when using case one. Therefore, for that stage of the analysis, it was decided to use 22 floodlights with 400 W metal-halide (HMI) sources [80,81]. Moreover, the estimated cost of 22 reflectors with HMI sources and power supply was approximately 8 000 € lower than for 4 larger reflectors with xenon arc lamps.

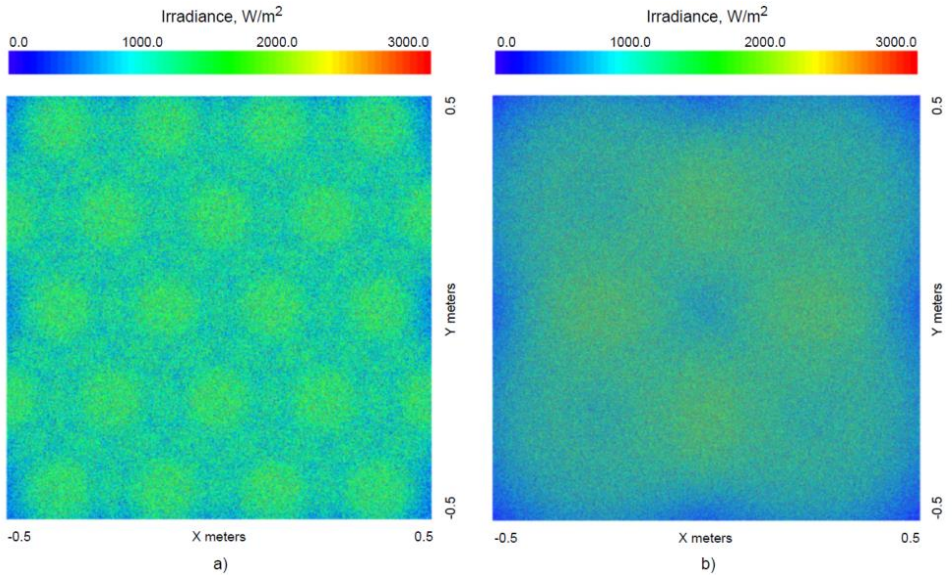

Figure 2.2. Non-uniformity of simulated solar irradiance on analysed illuminated area: a) 22 reflectors case, b) 4 reflectors case

2.3 Conclusions for the next steps

Besides light sources and their positioning, the selection of appropriate power supply, ballast and additional elements was analysed. Due to the lack of information in the literature about these crucial components, Paper I presents an analysis summarising the planned costs associated with the total construction of the simulator installation to fill this gap [79].

Above and beyond this, the mechanical part of the installation was developed, where the stand frame, the system for positioning the light sources relative to the parabolic trough collector was designed. A comprehensive design of the parabolic trough collector was also carried out, taking into account the hydraulic model on the heat transfer fluid side, the parabolic mirror frame and its mounting method, the design of the absorber together with the glass envelope and brackets to maintain low pressure close to vacuum. The work carried out as part of the doctoral thesis also consisted of selecting the appropriate measurement instrumentation for the hydraulic part, including the flow meter, thermocouples and their arrangement, pressure drop meter and, at a later stage, the power and control system as well as data recording. An essential point to consider in the further development of the test bench was to determine a method for measuring the heat flux supplied to the absorber surface and also to establish a method for measuring the absorbers, to obtain repeatable results.

Chapter 3

Heat absorption enhancement inside tubular absorber by using twisted tape inserts - Paper II

The next stage of the research was the comprehensive construction of a test stand, based on the assumptions and results obtained in the previous chapter, which enables the influence of internal and external methods of heat intensification in the tubular absorber to be determined. This part of the study presents a description of the test stand, the experimental procedure and the influence of the applied twisted tapes on the enhancement of heat absorption inside the linear absorber, along with a long-term analysis for which CFD investigation and a mathematical model were used.

3.1 Test stand construction and experimental campaign under simulated solar conditions

The comprehensive assembly of the experimental stand can be divided into many stages, but two main parts were the most demanding: the radiation simulator and the parabolic trough collector.

3.1.1 Installation description

The final stand arrangement consisted of 18 ARRI spotlights, each with an HMI OSRAM source of 575 W configured as shown in Figure 3.1. Because the final light source used is of the same type and series but differs in power and size from previous optical analyses, and the reflectors used were manufactured using different technology, the study was repeated with additional experimental validation of the

heat flux distribution to validate the use of these lamps in the correct configuration [82]. This analysis was presented with an emphasis on the modelling of the light source as presented at one of the scientific conferences in which the author of this thesis participated. However, due to the purely optical character of the article focusing on how the light source should be modelled, this article was not included in the thesis scope, but the results highlight the possibility of using reflectors in this configuration as well.

All tests were performed under solar simulator stable conditions, following verification of the stability of the radiation emitted by the discharge sources, and with the laboratory shaded to neutralise the influence of outdoor conditions. The longer operation of the installation affects the ambient temperature, which, however, was continuously monitored and considered in post-processing analysis, the bench itself required continuous cooling and the heat was removed outside the laboratory. Measurements of heat flux and its distribution were carried out periodically to determine both the energy input to the absorber surface and the changes associated with source degradation. Radiance distribution and evaluation of individual reflectors were carried out using a pyranometer mounted on a 2-axis scanner. When measuring the energy delivered to the outer surface of the absorber, the measurement was carried out with a water-cooled heat flux meter, which scanned the radiation along the length of the absorber and around the absorber circumference, which was referred to as the boundary condition to the mathematical model.

The mounting, on a highly reflective mirror, was designed and manufactured by laser cutting to ensure that the parabolic shape was accurately reproduced. The absorber, covered with a high-absorbing coating, is positioned in the focus of the parabolic mirror and inside the borosilicate glass envelope, with the equipment maintaining a very low surrounding pressure, close to the vacuum. This parameter was monitored continuously during the study. The receiver was developed in such a way that different configurations of the various intensification methods could be studied [83,84].

Temperature increment measurement was carried out using two K-type thermocouple sensors placed inside the absorber at a distance of 1 m from each other, which enabled the temperature increment of heat transfer fluid to be measured accurately. PT100 resistance sensors were used to monitor the temperature in other characteristic points of the installation. The pressure drop measurement was carried out by a pressure drop meter with an adjustable range, which increased the accuracy of the measurements performed. The mass flow was

calculated based on the measurement from the volume flow meter and temperature. The test bench was constructed in such a way that selected segments of the solar loop could be simulated. The inlet temperature of heat transfer fluid could be adjusted by using additional electric heaters before the absorber.

All tests were performed for a steady state, which required sufficient time for thermal stabilisation of the installation. Data recording was carried out continuously to determine the stability of the measurement. The stabilisation time itself (about 5 - 10 minutes depending on the case studied) indicated the validity of using a radiation simulator to test the linear absorbers. In the case of natural radiation, the tests would have been purely statistical because of constantly changed insolation conditions and the influence of wind, which would not have guaranteed reproducible and stable results. The associated measurement uncertainty, in each case, was calculated according to GUM (Guide to the Expression of Uncertainty in Measurement) objectives [85].

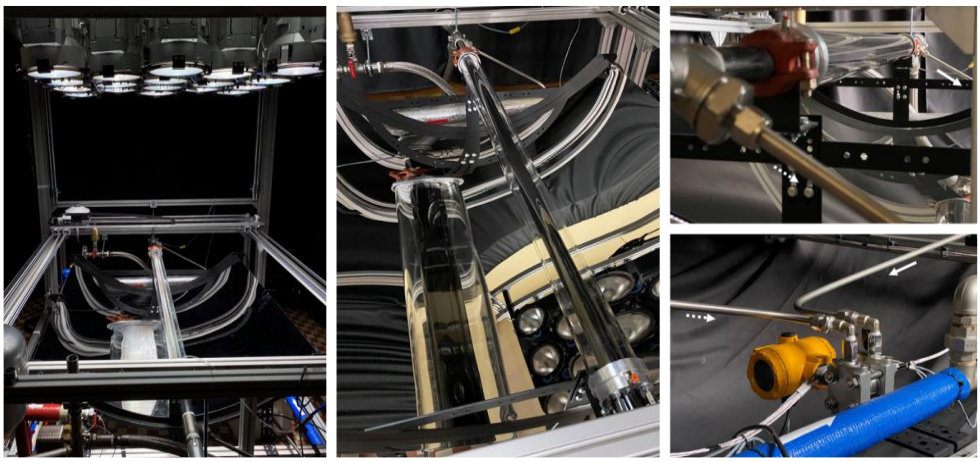

a) b) c)

Figure 3.1. Experimental bench: a) solar simulator and parabolic trough collector, b) linear absorber placed in parabolic trough focal length, c) pressure drop meter and its connections before and after linear absorber

Testing of twisted tapes in the linear absorbers was performed in a similar way to the testing of reference ones. The inserts were fabricated using the fused deposition modelling method, where PET-G was used. Due to this form and implementation of the inserts, the tests were carried out at a lower temperature level.

3.1.2 Limitations of solar loop testing

The performance parameters of the installation should also be highlighted. Because a certain limitation was the area illuminated by the radiation simulator which was due to the cost of the whole device, the tests could be carried out for specific assumptions. Before selecting a suitable heat transfer fluid circulating pump, a preliminary calculation was performed to estimate the temperature increment in the absorber based on the geometry of the installation, the simulated insolation conditions and the type of heat transfer fluid, which in this case and most of the studies analysed was Therminol VP-1 [86]. The objective was to select a parameter range for which the temperature increment is measurable in terms of instrument accuracy. Therefore, studies of the full flow characteristic of reference low-concentrated installations for solar thermal industrial applications were excluded due to the very low-temperature increment in 1 metre of the absorber. Therefore, the tests were performed in a volumetric flow range of approximately 50 – 550 dm^3/h, which provided a measurable temperature increment. The difference in temperature increase between the reference absorber and the twisted tape is within the error limits of the measurement instruments, which limits direct comparisons of the different inserts based on experimental studies but enables validation of the numerical and mathematical models. The experimental tests performed are therefore primarily intended to enable the validation of the models developed and to highlight their feasibility.

3.2 Heat absorption enhancement method

The application of flow-disturbing inserts inside the tubular absorber is one of the known methods of intensifying heat absorption by the heat transfer medium. The study analysed the use of tabulating inserts in a segmented arrangement along the length of the absorber to identify a combination that maximises heat extraction and does not cause excessive pressure drop. Twisted tapes are characterised by a simple structure and potentially the highest chance of use in a solar loop due to their simplicity of application and manufacturing process [87]. The characteristic parameter which describes the twisted tapes is the twisted ratio defined as Eq. (3.1) [88]:

$$Tr = \frac{H}{d_{\mathrm{abs,i}}} \tag{3.1}$$

where *H* is the parameter describing the length of the insert and $d_{abs,i}$ is the inner diameter of the absorber. Both parameters are indicated in Figure 3.2.

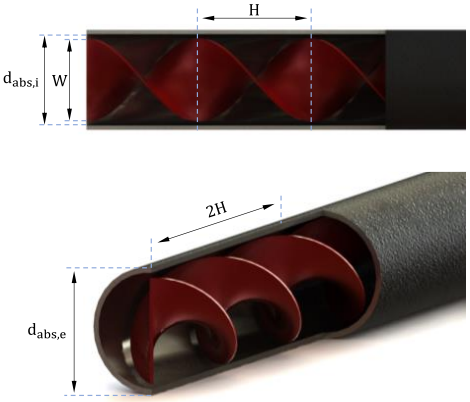

Figure 3.2. Linear absorber with twisted tape insert

The impact of twisted tapes on the installation strictly depends on a variety of parameters, which also limits the possibility of performing a broad multi-parametric analysis. In the research conducted, geometries and parameters similar to those of manufactured solar installations which are based on parabolic trough collectors were assumed and for these assumptions, the validity of their use in the particular sequence was presented.

3.2.1 Heat flux non-uniformity distribution

The parabolic collector causes direct radiation to be reflected and directed towards the linear absorber, which irradiates only one part of the absorber, causing a high temperature gradient, as shown in Figure 3.3 [89].

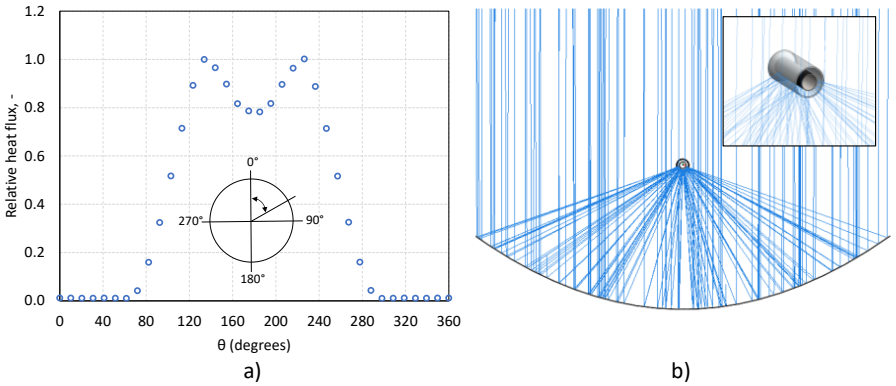

Figure 3.3. Concentrated irradiance on absorber pipe external surface: a) relative heat flux on absorber surface, b) visualization of concentration process in PTC

In the analysis carried out, it was shown that the application of such a distribution to the numerical model is necessary to analyse the heat transfer process properly. Thus, for each geometry of the parabolic trough collector, a series of optical analyses before performing heat flow calculations is required to obtain valid results.

3.3 Swirl flow impact on heat absorption

Twisted tapes applied inside the absorber loop create a swirl flow, which is characterised by intensive mixing of the fluid and detachment of the near-wall layer, thus intensifying heat absorption [90]. The analysis indicates the correlations of how the Nusselt number increases with decreasing twisted ratio. A reduction in the fluid temperature differential around the absorber circumference has also been demonstrated, potentially extending the operating period of the absorbers and reducing the internal thermal stress of the receiver.

3.4 Pressure drop and increasing self-demand

Each element placed inside the linear absorber results in an additional increase in pressure drop, which requires additional power from the circulation pump. Thus, when analysing the intensification of heat extraction inside the absorbers, it is necessary to consider the power required for pumping. These energy needs can be taken into account when determining the efficiency of the parabolic trough collector. The analyses used the definition of efficiency according to the Eq. (3.2) [7,53,91]:

$$\eta_{\mathrm{PTC}} = \frac{Q_{\mathrm{u}} - \dfrac{W_{\mathrm{p}}}{\eta_{\mathrm{el}}}}{Q_{\mathrm{s}}} \tag{3.2}$$

where W_{p} is required pump power, and η_{el} is reference electricity production efficiency. For purposes of this analysis, the value 32.7% was selected [92].

In the results, the maximum range of applicability of the inserts in the solar loop analysed was determined, which maximises the efficiency of the installation. The applied solution was tested by performing a long-term analysis, with varying weather conditions based on the NREL weather database [38].

Chapter 4

No-selective absorber coating segmental application in solar loop - Paper III

The external surface of serially produced linear absorbers is usually coated with a selective coating, which is a coating with high absorptivity and low emissivity [8]. This is a result of adapting regular parabolic trough collectors to their smaller-scale equivalents and preserving this design feature. However, the lower temperature level occurring in the preliminary sections of low-concentrated parabolic trough collectors loop provides the opportunity to apply significantly cheaper coatings, of a non-selective nature but with extremely high absorptivity, a low price and a simpler application process. An analysis of the potential for applying this previously not considered approach to reduce investment costs and, in some cases, increase installation efficiency is presented in this chapter [47]. The tool that enabled this analysis was the developed 2-dimensional heat transfer model, especially for low-concentrated ratio parabolic trough collectors. This study was partially carried out during the author's 3-month visiting research at KTH Royal Institute of Technology in cooperation with KTH solar group scientists.

4.1 Heat transfer model approach

The advanced mathematical model developed includes parameters such as the geometry of the parabolic collector installation, the materials used and their thermodynamic and optical properties, the atmospheric conditions such as solar irradiance, ambient and sky temperature, sun position and wind speed. The effect of the positioning error, mirror and receiver dirt, type of coating, shading and incidence angle modifier is also included in the model.

The heat transfer model in the receiver includes convection between the inner surface of the absorber and the heat transfer fluid, conduction through the absorber pipe, radiation and convection losses between the external surface of the absorber (including coating) and the internal surface of the glass envelope, conduction through the glass envelope, convection and radiation losses from external glass envelope to ambient and sky. Each absorber being analysed can be divided into N sections, as shown in Figure 4.1 so that the accuracy of the results obtained increases and it is possible to apply different parameters to each separate section. For this analysis, the variable parameter was the absorptivity and emissivity of the coating.

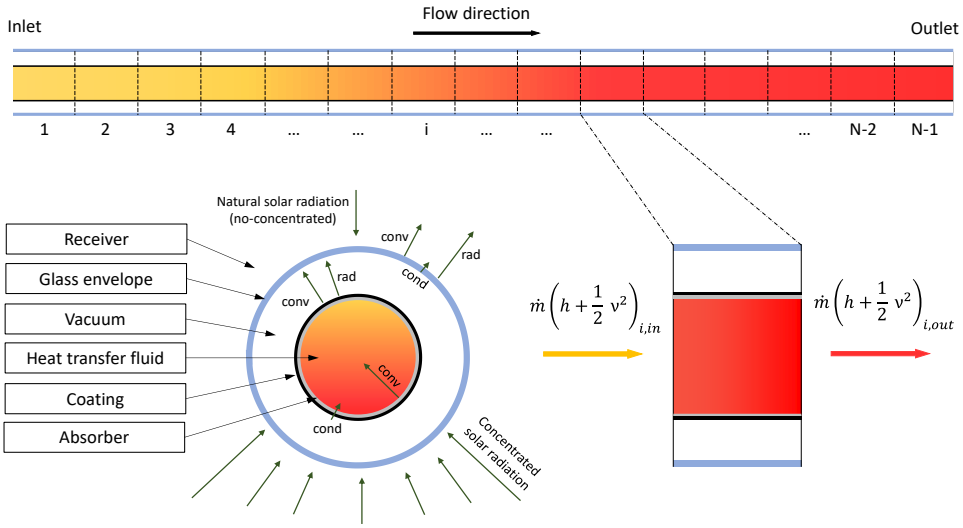

Figure 4.1. Two-dimensional model of heat transfer in PTC receiver

So far, the mathematical models appearing in the literature on the subject do not take into consideration the separation of heat flux into natural radiation and radiation concentrated by a parabolic mirror [93,94]. This assumption is valid in solar power plants, where the aperture of the mirror is up to 7 metres and natural radiation contributes only a minor proportion of the total heat flux at the outer surface of the absorber. In the case of low-concentrated parabolic trough collectors, this parameter should be taken into account, which is the main novelty, increasing the accuracy of the developed model. The heat absorbed by the parabolic trough collector can then be described by Eq. (4.1) [47]:

$$Q_{\mathrm{u}} = (Q_{\mathrm{u,CSP}} + Q_{\mathrm{u,SP}}) - Q_{\mathrm{loss}} \tag{4.1}$$

where $Q_{\mathrm{u,CSP}}$ is the concentrated solar energy, $Q_{\mathrm{u,SP}}$ is the non-concentrated solar energy, Q_{loss} is energy losses.

Heat flux from concentrated solar irradiance including the shadow of the absorber is defined as Eq. (4.2) and heat flux from non-concentrated radiation is presented as Eq. (4.3) [95]:

$$Q_{\mathrm{u,CSP}} = (A_{\mathrm{ap}} - d_{\mathrm{abs,e}} \cdot L) \cdot G_{\mathrm{B}} \cdot \eta_{\mathrm{opt,CSP}} \cdot \cos\theta \cdot IAM, \tag{4.2}$$

$$Q_{\mathrm{u,SP}} = \left(d_{\mathrm{abs,e}} \cdot L\right) \cdot G_{\mathrm{B}} \cdot \eta_{\mathrm{opt,SP}}, \tag{4.3}$$

where A_{ap} is the aperture surface area, $d_{\mathrm{abs,e}}$ is the absorber external diameter, G_{B} is the direct solar irradiance, $\eta_{\mathrm{opt,CSP}}$ is the optical efficiency for concentrated solar power, θ is the incident angle, IAM is the incidence angle modifier, L is absorber length, $\eta_{\mathrm{opt,SP}}$ is the optical efficiency for solar power.
Concentrated and non-concentrated radiation differ in the path from Sun to the absorber surface, so optical efficiency must be considered separately, hence the biggest difference in the proposed model. Two different optical efficiency equations need to be used to calculate total solar power, which are shown as Eq. (4.4) and (4.5) [96]:

$$\eta_{\mathrm{opt,CSP}} = \tau_{\mathrm{c}} \cdot \alpha_{\mathrm{abs}} \cdot \eta_{\mathrm{sh}} \cdot \eta_{\mathrm{track}} \cdot \eta_{\mathrm{ref}} \cdot \eta_{\mathrm{d,m}} \cdot \eta_{\mathrm{d,r}} \tag{4.4}$$

$$\eta_{\mathrm{opt,SP}} = \tau_{\mathrm{c}} \cdot \alpha_{\mathrm{abs}} \cdot \eta_{\mathrm{d,r}} \tag{4.5}$$

where τ_{c} is transmittance of glass envelop, α_{abs} absorptivity, η_{sh} shadowing, η_{track} tracking error, η_{ref} mirror reflectance, $\eta_{\mathrm{d,m}}$ and $\eta_{\mathrm{d,r}}$ dirt on mirror and receiver.

4.1.1 Calculations algorithm

The calculations are performed using the algorithm depicted in Fig. 4.2, consisting of a series of equations described in more detail in the Appendix section. For an assumed section, of a selected length (usually a few to several millimetres), an entire calculation process is carried out generating results of high accuracy. Besides the temperature increment of heat transfer fluid, the temperature of the absorber, glass envelope, losses to ambient, and flow parameters are calculated. The analysis includes the temperature-dependent parameters of the individual medium or component, which determines high-quality and reliable results. This model was validated based on experimental results shared by National Renewable Energy Laboratory [14].

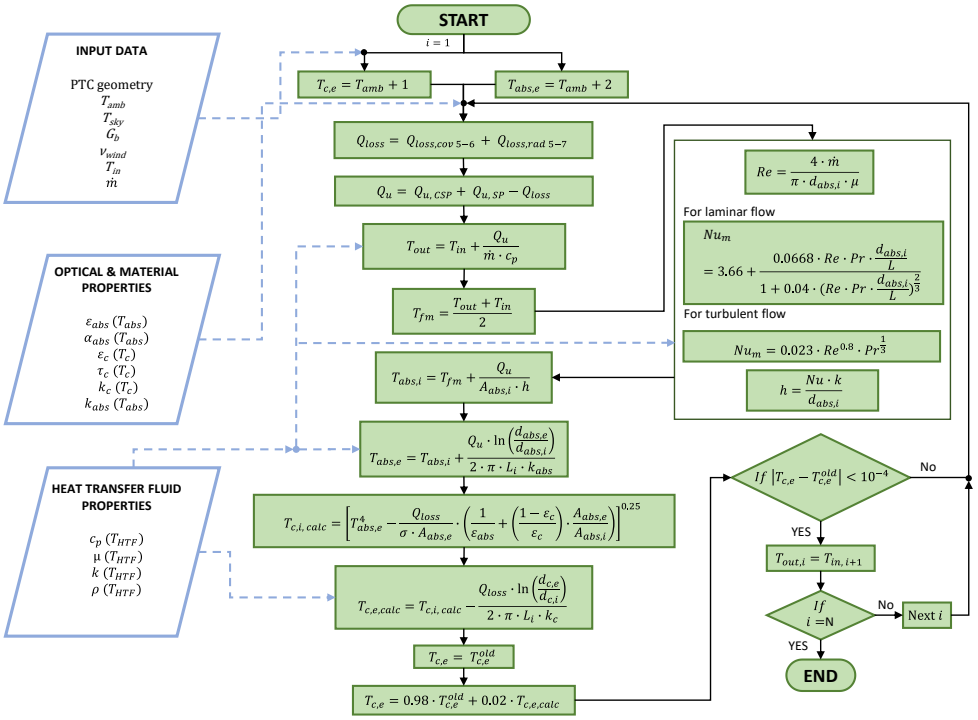

Figure 4.2. Flow chart of the mathematical model [47]

4.2 No-selective coating application

The extremely high absorptivity of some non-selective coatings applied to the external surface of the absorber compensates for the radiation losses resulting from the high emissivity, which is dependent on the temperature of the heat transfer fluid and absorber surface. The optimisation of the use of these coatings is highly dependent on the nature of the flow, type of heat transfer fluid, temperature and concentration ratio. Paper III analyses the application potential of this solution for three PTC geometries with different temperature stages, reflecting possible applications in the solar thermal industrial process and one case reflecting a full-scale power plant. The advantage of non-selective coatings such as the Pyromark analysed is the very simple application method, in this case, it is a spray coating [64]. Compared to the multi-step application process of selective coatings, which requires a series of expensive equipment, the potential for a reduction in investment cost seems significant.

4.3 Selected results discussion

The study analysed both the efficiency of the absorber in its length and the efficiency of the entire solar loop, consisting of several absorbers. The first results showed the potential in the application of a non-selective coating up to a heat transfer fluid temperature range of about 115 °C for a single solar loop length of up to 45 metres. At the same time, the results depended mainly on the reference coating and the type of flow adopted, in accordance with the respective industrial installations. Figure 4.3 shows the results where the inlet temperature to the solar loop was 100 °C and the minimum assumed outlet temperature was 200 °C. The analysis was performed for G_B=800 W/m^2 and three different solar loop lengths consisting of 8, 16 or 24 absorbers. To obtain the minimum desired temperature for the same conditions, the corresponding mass flow had to be adjusted. The application of Pyromark in the preliminary absorber sections initially increases the efficiency of the solar loop, but with too many absorbers, the efficiency decreases below the reference value. Points A and B, respectively, determine the operating points that maximise efficiency and maximise the number of absorbers while maintaining an efficiency higher than the reference value. It was demonstrated that, for the conditions analysed, a low-cost non-selective coating could be used in up to 25%, 50% and 62.5% of the absorbers. The results showed the high application potential of this method at the same time demonstrating its high dependence on work parameters.

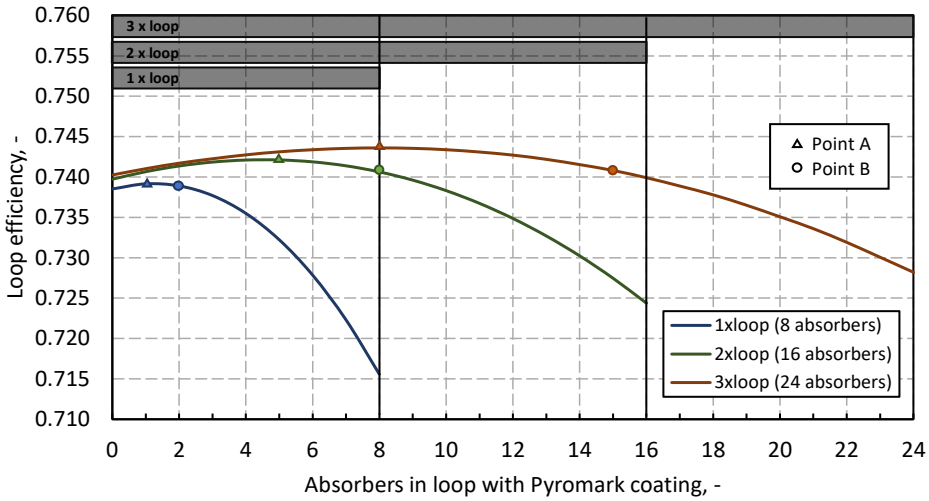

Figure 4.3. Solar loop efficiency as a function of number of absorbers with no-selective coating, results for selected case

Chapter 5

Evaluation of tracking deviation impact on parabolic trough collector efficiency - Paper IV

Since mainly direct solar radiation is utilised in CSP installations, the correct irradiance concentration is a crucial process in achieving high efficiency [97]. Therefore, in this chapter, it was decided to analyse this phenomenon and investigate the impact of the potential error that can occur with a solar tracker which is vulnerable to atmospheric conditions, especially wind [98]. This research aims to answer the following question:

- What is the maximum tracker error that does not affect installation operation?
- What is the positioning effect on the low-concentrated parabolic trough collectors' efficiency?
- How does tracking error affect the radiation distribution on the absorber surface?

5.1 Methodology of numerical modeling

The impact of solar tracking error was investigated using optical-engineering Monte Carlo ray tracing software APEX, which uses a Bidirectional Reflectance Distribution Function (BRDF) to describe the reflected beam behaviour [89]. This method allows the energy accompanying each ray to be tracked and the total flux and distribution to be calculated on the selected surface, in this instance the outer surface of the absorber. The BRDF function describes the form in which the incident light over a surface is scattered [78,99]. This method considers the material properties of

individual parts, including reflectivity, transmissivity and absorptivity. In this study, the radiation source was the sun model, including the solar half angle of 0.27°. The parabolic trough collector geometry was consistent with the experimental test stand and similar to many geometries used in industrial installations [83,100]. Figure 5.1 shows a model of the sun and the PTC installation, which enabled the impact of the tracking error to be investigated by changing the position relative to the reference one (ideal to the sun).

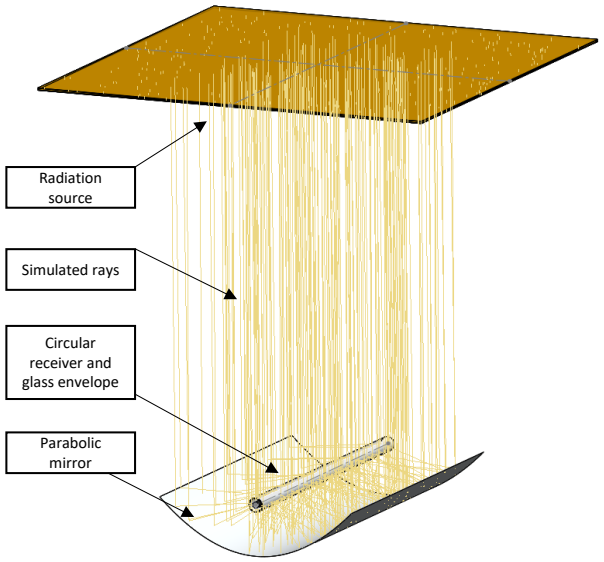

Figure 5.1. Numerical investigation model in optical engineering software

5.2 Tracking deviation effect on optical system

Changing the position of the parabolic mirror relative to the direct solar rays shifts the focus point of the absorber axis, in one direction as can be seen in Figure 5.2. Certain rays are focused unevenly on the surface of the tubular absorber, while others completely miss the surface of the absorber. The selected results graphically visualise path rays that, when reflected from the parabolic mirror, entirely skip the absorber surface for a tracker deviation of 4°. The usual distribution of heat flux on the surface of the absorber generates a non-uniform distribution of radiation, but still, one that has its axis of symmetry. In the studies carried out, it was shown that an error in the position of the tracker generates areas with very high heat flux values.

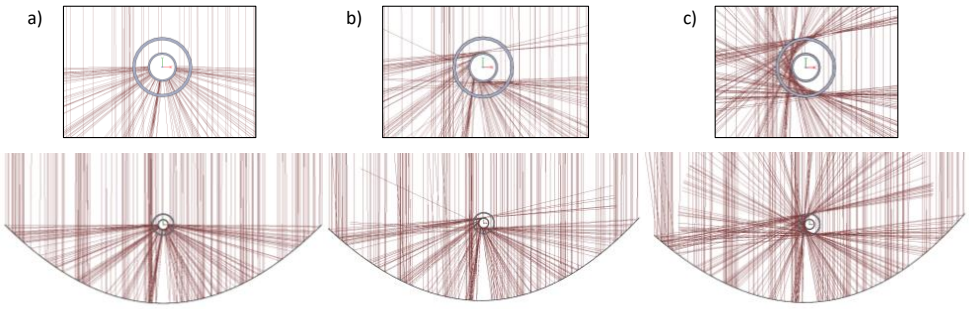

Figure 5.2. Solar radiation path for selected tracker error presented in the cross-section, tracker position deviation: a) 0° (ideal), b) 2°, c) 4°

Example distributions for a 33.7 mm diameter absorber are shown in Figure 5.3, where 5 curves of heat flux can be distinguished. The highest maxima of the radiation distribution occurred for a tracking deviation of 2°. The curve for 4°, highlights the very high loss in the optical system. The results for the higher concentration ratio, where the diameter of the absorber was 29.7 mm, and for the cases without the glass envelope used, are analysed in detail in the Appendix section (Paper IV).

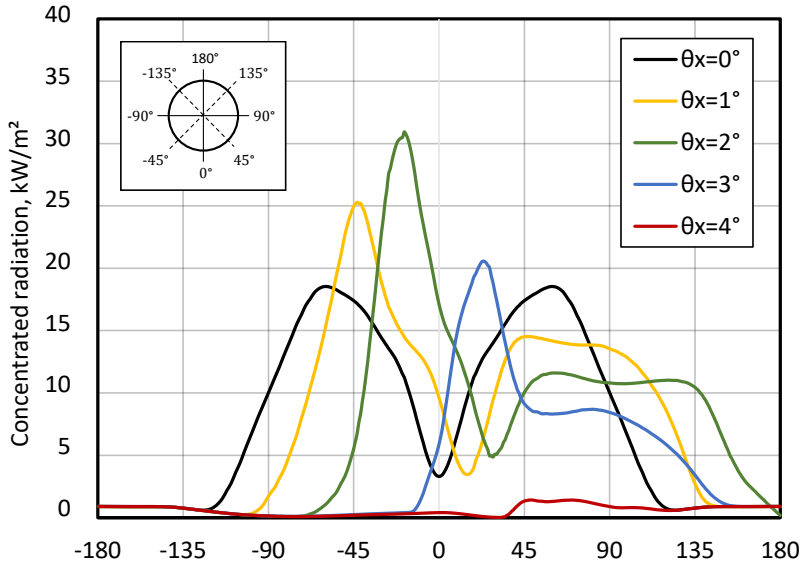

Figure 5.3. Heat flux distribution on the absorber external surface for selected solar tracker error θ_x

5.3 Tracking accuracy impact on heat flux

It is important to emphasise, however, how the tracking error affects the total heat delivered to the outer surface of the absorber. Selected results for different G_B values for the case with a glass envelope (Case 1) and without (Case 2) are shown in Figure 5.4. The study showed that the total heat delivered to the outer surface of the absorber decreases relative to the reference value for an error of more than about 1.75°. Without the consideration of the glass envelope, transmission losses are excluded, so the heat input is higher but, as shown in Paper IV, results in much higher heat loss to the ambient and reduced efficiency.

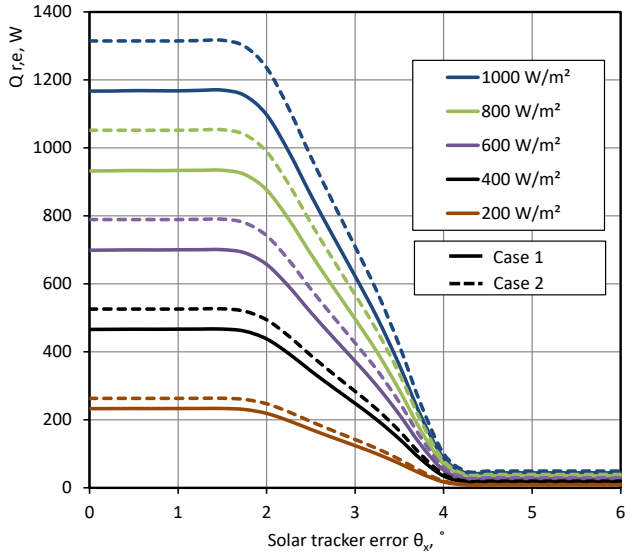

Figure 5.4. Solar heat delivered to the linear absorber including the PTC optical efficiency as a function of solar tracker error for selected cases

Chapter 6

Summary and conclusions

The doctoral dissertation is based on the author's four major monothematic publications in the following journals: Paper I - International Journal of Energy Research (*publ. Wiley & Sons*), Paper II - Energies (*publ. MDPI*), Paper III - Applied Energy (*publ. Elsevier*), Paper IV - Renewable Energy (*publ. Elsevier*).

The main objective of this study was to identify the phenomenon of heat absorption in a parabolic trough collector and to determine methods to intensify heat absorption by analysing selected components of PTC. In the thesis, the primary research interest was placed on parabolic trough collectors with low-concentration ratios, which can produce heat with the potential for use in industrial processes.

Research activities which made the objective of the dissertation possible were the development of a model of heat flow in a linear absorber, the description of this model by a set of mathematical equations, the creation of 2 and 3-dimensional models, and the development of an optical model of the phenomenon of radiation concentration on the external surface of a tubular absorber. Validation of the developed designs was possible by conducting a series of experimental tests on a test stand, where a parabolic trough collector with multiple absorbers was tested using a solar simulator. The experimental test stand created as part of the doctoral study was comprehensively designed and manufactured by the author of this thesis.

The research work on analysing the performance of parabolic trough collectors was initiated by conducting two activities simultaneously. The first involved analysing and in-depth comprehension of the process of radiation concentration on the external surface of the absorber and the phenomenon of absorption of this heat in linear absorbers. The data resulting from this analysis directly influenced the parallel research activity, which was the definition of assumptions and the design of an experimental test stand on the previously mentioned heat absorption phenomenon.

In the paper I included in the dissertation, the process of designing the test bench is presented, which began with the analysis and selection of the light source type, considering the spectrum of radiation as well as the operating characteristics.

The analysis considered, three potential sources: tungsten halogen, metal-halide and xenon arc lamp. In terms of, spectral distribution and the nature of the radiative emission, tungsten halogen was rejected and the potential sources metal-halides and xenon arc lamps were adopted for further consideration. At this stage of the research, considering the assumed illuminated area of at least 1 m^2 and the variety of commercially available HMI and Xenon sources, the use and corresponding arrangement of reflectors with different coatings were considered. Two geometries were selected, one for HMI and one for Xenon, taking into account the assumed geometry of the parabolic concentrator and absorber, as well as possible reflectors and their compatibility with the light sources. The subsequent step, was the modelling of the optical system using the optical-engineering software APEX which is based on Monte Carlo Ray Tracing Method. The analysis revealed that for both cases, a portion of the simulated radiation has a scattered nature, and after reflection from the parabolic mirror did not reach the absorber which highlighted the need to oversize the light sources to achieve sufficient heat flux. It was determined that the best conditions for radiation simulation were achieved for the case where 22 units of 400 W HMI were considered. The analysis concludes that the simulation of optical systems depends on many parameters and each of them affects the nature of the simulated radiation. The use of a higher number of smaller reflectors with metal-halide sources allows for a higher energy stream reflected from the mirror of the concentrator and reaching the absorber tube. At the stage of planning the test stand (2019/2020), the cost of the solar simulator was estimated at around 20 000 euros.

The next stage of the work was the comprehensive construction of a test stand, in which the parabolic trough collector, could be tested under constant and repeatable conditions. This was the most time-consuming phase of the work because it took about 3 years in total. Finally, in the stand 18 HMI 575 W sources of the same series of types as those studied in the optical tests presented in the first part of the study were used. Optical analyses were repeated for higher source power and fewer reflectors and confirmed the feasibility of using this configuration. The experimental stand was divided into 2 parts, a solar radiation simulator and a parabolic trough loop. The incident radiation on the outer surface of the linear absorber corresponded to a natural radiation value of 990 W/m^2. The results of the conducted series of analyses were intended to validate numerical models developed simultaneously, describing the process of heat transfer in parabolic trough collectors. The research was carried out for stabilized conditions, where intensification of heat absorption was considered through, for instance, the effect of coatings on absorber efficiency, as well as the application of various inserts inside the linear absorber on the heat transfer fluid side. Validation results showed high agreement between models and experiments.

At the same time, mathematical models of parabolic trough collectors were developed. The proposed mathematical model was specifically adapted to low-concentrated installations by considering concentrated and non-concentrated radiation separately.

Regarding the analysis of heat absorption by the absorber, one can distinguish the work carried out into ones focused on the inner and outer parts of the linear absorber. Inside the absorber, the focus was on the application of twisted tapes, introducing swirl flow, which results in the intensive mixing of heat transfer fluid inside the tubular absorber, and a more intensive collection of heat from the inner walls of the absorber. Twisted tapes with twisted ratios of 1, 2 and 4 were considered, where the diameter of the absorber was corresponding to the installation to heat industrial process applications. The temperature range of the analyses performed was within the assumptions of heat for industrial processes and was in the range between 60 °C and 250 °C. Analyses demonstrated that each of the considered inserts results in an intensification of heat extraction, an increase in efficiency and a reduction in maximum temperature peaks, which reduces stresses in the installation. For the analyzed results, optimization showed that the most optimal is to use an insert with twisted ratio 1 up to 190 °C of thermal fluid, and twisted ratio 2 for higher temperatures. The results of the numerical analysis were applied to a mathematical model to verify the long-term impact of this arrangement on the PTC facility efficiency. The study was performed for southern Spain location to highlight the applicability of low-concentrated PTC for heat industrial processed in locations with extremely high application potential, highlighted in the introduction section. The analysis was performed at a 1-hour frequency, considering changing weather conditions, for a solar loop of 90 meters. Besides the 12-month analysis for the one year period, results for three selected days were presented. The average increase in the system's efficiency was 0.27%, including pressure losses in the installation and the higher power demanded for its own needs. The studies performed are limited to thermodynamic analyses. The study excluded an evaluation of the cost of twisted tapes and the potentially higher cost of purchasing a pump for circulating fluid, which provides the potential for further research into the application of this method of enhancing heat collection. The analysis was conducted for a specific thermal fluid and PTC geometry. Changing certain parameters can significantly affect the optimal applicability of twisted tapes, so in future work, more extensive analysis may be done.

On the outer side of the absorber, the application of previously unconsidered non-selective coating was examined, which is characterized by high absorptivity but also high emissivity. The Pyromark coating, which was also applied to the absorber in the test stand, was used as an example in the study. The motivation for conducting research on coatings was driven by the relatively high cost of selective coatings, which are applied using multi-step methods, which increases their cost and also,

because of the potential for using non-selective coatings in preliminary sections of absorber loops. The analysis considered multiple concentration ratios and temperatures to provide a preliminary assessment of the feasibility of using this coating for various applications for facilities producing heat for industrial processes. Preliminary analyses indicated the inability to apply the non-selective coating in full-scale installation, which highlights the reason why such a solution was not considered before. The geometries and operating parameters tested, reflected entirely or were very close to industrially used solutions. For the case where the aperture was 1 meter, the analysis showed that non-selective coating can be applied in the whole solar loop. In that case, the low-temperature range of heat transfer fluid 60 - 120 °C was considered. The PTC system with a medium temperature range and a concentration ratio of 17.3 has shown the possibility of optimization for absorbers where the temperature of HTF is up to 115 °C. Changing the connection of 3 parallel solar loops into 1 series increases the possibility of optimizing the number of absorbers. In the best optimal case (800 W/m^2), 15 of the 24 absorbers can be coated with a Pyromark instead of the reference selective coating. The Pyromark coating price for absorbers was estimated as 12.8 $\$/m^2$. In future analyses, it is worth considering other non-selective coatings and demonstrating the potential of their application to reduce investment costs.

In this analysis, case studies were performed for an assumption in which mass flow is adjusted according to the parameters of weather conditions to reach a given temperature level. In future work, which has already been done in part as mentioned in the dissertation, a case can be considered where mass flow is constant and the outlet temperature is dependent on weather conditions. Then an additional heat source can be applied, which reheats the given heat transfer fluid to the desired parameters. The application potential of this solution is broad, which also enables a wide range of future research.

An analysis worth consideration in the future is to use both methods at once: segmented positioning of twisted tapes and segmental applied no-selective coating in an absorber loop.

The last parameter considered in the dissertation was aimed at determining the impact of solar tracker deviation on PTC efficiency. The optical-engineering software used enabled the determination of ray propagation paths and analysis of the illuminated surface, considering the influence of individual optical elements and their properties. The maximum angle deviation of the solar tracker positioning for the tested geometry, not significantly affecting the operation of the linear absorber for a diameter of 33.7 mm was reported as 1.5°, for 21.3 mm was reported as 0.9°. Increasing the concentration factor by reducing the diameter of the absorber was found to increase the system's sensitivity to optical errors. For an absorber diameter of 33.7 mm, a tracking deviation of 3° results in a decrease in the irradiance

concentration factor from 7.36 to 3.92. For the lower absorber diameter, a reduction from 11.81 to 5.4 was calculated for a 2° defect. The maximum tracking deviation for the 33.7 mm and 21.3 mm diameters and the geometry analyzed was 4.5° and 2.7°, respectively. At higher values, solar rays do not focus on the absorber surface at all. In the parabolic collectors analyzed with higher solar tracking deviation, it is possible to observe greater differences in the values of concentrated heat flux reaching the absorber surface, which can cause greater temperature gradients in the absorber and worse heat transfer from the internal absorber wall to the circulating medium, but also cause high stresses in the absorber material. For 1000 W/m^2 and a tracking deviation of 2°, the highest value of focused irradiance for the 33.7 mm absorber, increases from 17.5 kW/m^2 to nearly 32 kW/m^2.

The results emphasize the need for a highly accurate solar tracking system even for low-concentration solar technologies. Potential future work related to the sun-tracking process could be to optimize the shape of the parabolic mirrors and/or to use a second mirror with an optimal geometry that would eliminate such a high sensitivity of the optical system to deviations in the positioning of the tracker, which could also increase the utilization of non-direct and partially diffuse radiation.

In conclusion, the extensive research reported in this thesis presented methods for analysing parabolic trough collectors, primarily with low-concentration ratios, methods for intensifying heat absorption on the inner and outer sides of a linear absorber, as well as optimization of these methods for selected configurations and the importance of the sun position tracking function in the context of the concentration process. The methodology for the comprehensive design of solar radiation simulators that enable the testing of parabolic trough collectors under constant and repeatable conditions is also presented. The author's experience in relation to the design and construction of solar radiation simulators results in current collaboration with researchers from Solar Group in KTH Royal Institute of Technology, where the author of this thesis is applying the gained experience and co-designing a simulator for testing photovoltaic panels. At the beginning of 2023, the dissertation author also began working with a researcher from the University for Continuing Education Krems. As part of this cooperation, preliminary studies of the solar calcination process were carried out on a test stand. The overall experience gained resulted in the author's commitment to analysis related to energy storage, a topic that is complementary to renewable energy production, which in the future may provide a solid basis for further analysis in this direction.

Bibliography

[1] CO2 Emissions in 2022 – Analysis - IEA n.d. https://www.iea.org/reports/co2-emissions-in-2022 (accessed April 3, 2023).

[2] Renewables 2022 – Analysis - IEA n.d. https://www.iea.org/reports/renewables-2022 (accessed April 3, 2023).

[3] Schoeneberger CA, McMillan CA, Kurup P, Akar S, Margolis R, Masanet E. Solar for industrial process heat: A review of technologies, analysis approaches, and potential applications in the United States. Energy 2020;206. https://doi.org/10.1016/J.ENERGY.2020.118083.

[4] Solar Heat for Industry – Solar Payback 2017. https://www.solar-payback.com/wp-content/uploads/2017/07/Solar-Heat-for-Industry-Solar-Payback-April-2017.pdf (accessed June 3, 2022).

[5] Weiss W, Spörk-Dür M. Edition 2022 Global Market Development and Trends 2021 Detailed Market Figures 2020 SOLAR HEAT WORLD WIDE n.d. https://doi.org/10.18777/ieashc-shw-2022-0001.

[6] Electricity Market Report 2023 – Analysis - IEA n.d. https://www.iea.org/reports/electricity-market-report-2023 (accessed April 3, 2023).

[7] Kalogirou SA. Solar Energy Collectors. Solar Energy Engineering, Elsevier; 2014, p. 125–220. https://doi.org/10.1016/B978-0-12-397270-5.00003-0.

[8] Ding Z, Qi C, Wang Y, Tu J, Wang C, Du X. Spectrally selective absorption coatings and their applications: A review. Sustainable Energy Technologies and Assessments 2022;52:102031. https://doi.org/10.1016/J.SETA.2022.102031.

[9] Kennedy CE, Price H. PROGRESS IN DEVELOPMENT OF HIGH-TEMPERATURE SOLAR-SELECTIVE COATING, ISEC2005-76039, 2005.

[10] Lee CY, Chou PC, Chiang CM, Lin CF. Sun Tracking Systems: A Review. Sensors 2009, Vol 9, Pages 3875-3890 2009;9:3875–90. https://doi.org/10.3390/S90503875.

[11] Moya EZ. Parabolic-trough concentrating solar power systems. Concentrating Solar Power Technology, Elsevier; 2021, p. 219–66. https://doi.org/10.1016/B978-0-12-819970-1.00009-8.

[12] Schweitzer A, Schiel W, Birkle M, Nava P, Riffelmann KJ, Wohlfahrt A, et al. ULTIMATE TROUGH® - Fabrication, Erection and Commissioning of the World's Largest Parabolic Trough Collector. Energy Procedia 2014;49:1848–57. https://doi.org/10.1016/J.EGYPRO.2014.03.196.

[13] RIOGLASS PTR® 70-4G - Rioglass n.d. https://old.rioglass.com/rioglass-ptr704g/ (accessed May 1, 2022).

[14] Burkholder F, Kutscher C. Heat Loss Testing of Schott's 2008 PTR70 Parabolic Trough Receiver. 2008.

[15] Bishoyi D, Sudhakar K. Modeling and performance simulation of 100 MW PTC based solar thermal power plant in Udaipur India. Case Studies in Thermal Engineering 2017;10:216–26. https://doi.org/10.1016/J.CSITE.2017.05.005.

[16] Geyer M, Lüpfert E, Osuna R, Esteban A, Schiel W, Schweitzer A, et al. EUROTROUGH-Parabolic Trough Collector Developed for Cost Efficient Solar Power Generation. 11 Th SolarPACES International Symposium on Concentrated Solar Power and Chemical Energy Technologies n.d.

[17] Development of a Low Cost European Parabolic Trough Collector EUROTrough n.d.

[18] Ktistis PK, Agathokleous RA, Kalogirou SA. Experimental performance of a parabolic trough collector system for an industrial process heat application. Energy 2021;215. https://doi.org/10.1016/J.ENERGY.2020.119288.

[19] Tagle-Salazar PD, Nigam KDP, Rivera-Solorio CI. Parabolic trough solar collectors: A general overview of technology, industrial applications, energy market, modeling, and standards. Green Processing and Synthesis 2020;9:595–649. https://doi.org/10.1515/gps-2020-0059.

[20] POWER TROUGH 110® - Inventive Power n.d. https://inventivepower.com.mx/english/power-trough-110/ (accessed May 1, 2022).

[21] POWER TROUGH 250® - Inventive Power n.d. https://inventivepower.com.mx/english/power-trough-250/ (accessed May 1, 2022).

[22] Ibarra M, Rovira A, Alarcón-Padilla DC, Zaragoza G, Blanco J. Performance of a 5 kWe Solar-only Organic Rankine Unit Coupled to a Reverse Osmosis Plant. Energy Procedia 2014;49:2251–60. https://doi.org/10.1016/J.EGYPRO.2014.03.238.

[23] Absolicon T160 Solar collector - Designed to run industrial processes - Absolicon n.d. https://www.absolicon.com/applying-absolicon/ (accessed March 6, 2023).

[24] Fernández AG, Gomez-Vidal J, Oró E, Kruizenga A, Solé A, Cabeza LF. Mainstreaming commercial CSP systems: A technology review. Renew Energy 2019;140:152–76. https://doi.org/10.1016/j.renene.2019.03.049.

[25] CSP Projects Around the World - SolarPACES n.d. https://www.solarpaces.org/csp-technologies/csp-projects-around-the-world/ (accessed March 30, 2023).

[26] Concentrating Solar Power Projects | NREL n.d. https://solarpaces.nrel.gov/ (accessed March 30, 2023).

[27] Thonig R, Lilliestam J. CSP.guru 2022-07-01 2022. https://doi.org/10.5281/ZENODO.7112761.

[28] Mojave Solar Project (Abengoa) | California Energy Commission n.d. https://www.energy.ca.gov/powerplant/solar-thermal/mojave-solar-project-abengoa (accessed April 2, 2023).

[29] SOLANA | Department of Energy n.d. https://www.energy.gov/lpo/solana (accessed April 2, 2023).

[30] GENESIS | Department of Energy n.d. https://www.energy.gov/lpo/genesis (accessed April 2, 2023).

[31] SEGS IX - Harper Dry Lake | California Energy Commission n.d. https://www.energy.ca.gov/powerplant/solar-thermal/segs-ix-harper-dry-lake (accessed April 2, 2023).

[32] U.S. Energy Information Administration - EIA - Independent Statistics and Analysis n.d. https://www.eia.gov/todayinenergy/detail.php?id=49616 (accessed April 2, 2023).

[33] Noor Energy – The largest single-site concentrated solar power plant in the world n.d. http://noorenergy.ae/ (accessed April 2, 2023).

[34] World Map of Solar Thermal Plants | Solar Heat for Industrial Processes (SHIP) Plants Database n.d. http://ship-plants.info/solar-thermal-plants-map?collector_type=5 (accessed June 1, 2022).

[35] Weiss W, Spörk-Dür M. Solar Heat Worldwide 2021, Institute of Sustainable Technologies AEE, Austria n.d. https://www.iea-shc.org/solar-heat-worldwide-2021 (accessed June 3, 2022).

[36] Miraah Solar Thermal Project n.d. https://www.power-technology.com/projects/miraah-solar-thermal-project/ (accessed June 2, 2022).

[37] IMPLEMENTED PROJECTS - Inventive Power n.d. https://inventivepower.com.mx/english/implemented-projects/ (accessed June 2, 2022).

[38] Sengupta M, Xie Y, Lopez A, Habte A, Maclaurin G, Shelby J. The National Solar Radiation Data Base (NSRDB). Renewable and Sustainable Energy Reviews 2018;89:51–60. https://doi.org/10.1016/j.rser.2018.03.003.

[39] T160 Solar collector - Designed to run industrial processes - Absolicon n.d. https://www.absolicon.com/applying-absolicon/ (accessed June 2, 2022).

[40] Minder S. Example of concentrated solar systems (PTC) in the dairy industry in Switzerland n.d. www.nep-solar.com (accessed June 2, 2022).

[41] Häberle A, Krüger D. Concentrating solar technologies for industrial process heat. Concentrating Solar Power Technology: Principles, Developments, and Applications, Elsevier; 2020, p. 659–75. https://doi.org/10.1016/B978-0-12-819970-1.00011-6.

[42] Reflective Surfaces - Solar - Industries - Alanod n.d. https://alanod.com/en/industries/solar/reflective-surfaces (accessed June 2, 2022).

[43] Key World Energy Statistics 2021 – Analysis - IEA n.d. https://www.iea.org/reports/key-world-energy-statistics-2021 (accessed June 23, 2022).

[44] International Renewable Energy Agency. Innovation outlook: Thermal energy storage 2020. www.irena.org.

[45] Kumar L, Hasanuzzaman M, Rahim NA. Global advancement of solar thermal energy technologies for industrial process heat and its future prospects: A review. Energy Convers Manag 2019;195:885–908. https://doi.org/10.1016/J.ENCONMAN.2019.05.081.

[46] Kalogirou SA. Solar thermal collectors and applications. Prog Energy Combust Sci 2004;30:231–95. https://doi.org/10.1016/J.PECS.2004.02.001.

[47] Stanek B, Wang W, Bartela Ł. A potential solution in reducing the parabolic trough based solar industrial process heat system cost by partially replacing absorbers coatings with non-selective ones in initial loop sections. Appl Energy 2023;331:120472. https://doi.org/10.1016/J.APENERGY.2022.120472.

[48] Bellos E, Tzivanidis C. A detailed exergetic analysis of parabolic trough collectors. Energy Convers Manag 2017;149:275–92. https://doi.org/10.1016/J.ENCONMAN.2017.07.035.

[49] Fernández-García A, Zarza E, Valenzuela L, Pérez M. Parabolic-trough solar collectors and their applications. Renewable and Sustainable Energy Reviews 2010;14:1695–721. https://doi.org/10.1016/J.RSER.2010.03.012.

[50] Yilmaz IH, Söylemez MS. Thermo-mathematical modeling of parabolic trough collector. Energy Convers Manag 2014;88:768–84. https://doi.org/10.1016/J.ENCONMAN.2014.09.031.

[51] Allam M, Tawfik M, Bekheit M, El-Negiry E. Heat transfer enhancement in parabolic trough receivers using inserts: A review. Sustainable Energy Technologies and Assessments 2021;48:101671. https://doi.org/10.1016/J.SETA.2021.101671.

[52] Bellos E, Tzivanidis C, Tsimpoukis D. Thermal enhancement of parabolic trough collector with internally finned absorbers. Solar Energy 2017;157:514–31. https://doi.org/10.1016/J.SOLENER.2017.08.067.

[53] Bellos E, Tzivanidis C. Enhancing the Performance of Evacuated and Non-Evacuated Parabolic Trough Collectors Using Twisted Tape Inserts, Perforated Plate Inserts and Internally Finned Absorber. Energies 2018, Vol 11, Page 1129 2018;11:1129. https://doi.org/10.3390/EN11051129.

[54] Varun, Garg MO, Nautiyal H, Khurana S, Shukla MK. Heat transfer augmentation using twisted tape inserts: A review. Renewable and Sustainable Energy Reviews 2016;63:193–225. https://doi.org/10.1016/J.RSER.2016.04.051.

[55] Seemawute P, Eiamsa-ard S. Thermohydraulics of turbulent flow through a round tube by a peripherally-cut twisted tape with an alternate axis. International Communications in Heat and Mass Transfer 2010;37:652–9. https://doi.org/10.1016/J.ICHEATMASSTRANSFER.2010.03.005.

[56] Promvonge P. Thermal augmentation in circular tube with twisted tape and wire coil turbulators. Energy Convers Manag 2008;49:2949–55. https://doi.org/10.1016/J.ENCONMAN.2008.06.022.

[57] Eiamsa-ard S, Thianpong C, Eiamsa-ard P, Promvonge P. Thermal characteristics in a heat exchanger tube fitted with dual twisted tape elements in tandem. International Communications in Heat and Mass Transfer 2010;37:39–46. https://doi.org/10.1016/J.ICHEATMASSTRANSFER.2009.08.010.

[58] Bhuiya MMK, Chowdhury MSU, Saha M, Islam MT. Heat transfer and friction factor characteristics in turbulent flow through a tube fitted with perforated twisted tape inserts. International Communications in Heat and Mass Transfer 2013;46:49–57. https://doi.org/10.1016/J.ICHEATMASSTRANSFER.2013.05.012.

[59] Noč L, Jerman I. Review of the spectrally selective (CSP) absorber coatings, suitable for use in SHIP. Solar Energy Materials and Solar Cells 2022;238. https://doi.org/10.1016/J.SOLMAT.2022.111625.

[60] Weinstein LA, Loomis J, Bhatia B, Bierman DM, Wang EN, Chen G. Concentrating Solar Power. Chem Rev 2015;115:12797–838. https://doi.org/10.1021/ACS.CHEMREV.5B00397/ASSET/IMAGES/LARGE/CR-2015-00397F_0024.JPEG.

[61] Yang H, Wang Q, Huang X, Li J, Pei G. Performance study and comparative analysis of traditional and double-selective-coated parabolic trough receivers. Energy 2018;145:206–16. https://doi.org/10.1016/J.ENERGY.2017.12.126.

[62] Stollo A, Chiarappa T, D'Angelo A, Maccari A, Matino F. LCOE reduction for parabolic trough CSP: Innovative solar receiver with improved performance at medium temperature, 2016, p. 030034. https://doi.org/10.1063/1.4949086.

[63] Zhao K, Jin H, Gai Z, Hong H. A thermal efficiency-enhancing strategy of parabolic trough collector systems by cascadingly applying multiple solar selective-absorbing coatings. Appl Energy 2022;309:118508. https://doi.org/10.1016/J.APENERGY.2021.118508.

[64] Ho CK, Mahoney AR, Ambrosini A, Bencomo M, Hall A, Lambert TN. Characterization of Pyromark 2500 Paint for High-Temperature Solar Receivers. J Sol Energy Eng 2014;136. https://doi.org/10.1115/1.4024031.

[65] PK2500FBLK - TDS - Pyromark Series 2500 TDS - Pyromark Product Image n.d. https://www.datasheetarchive.com/whats_new/d484cb021dbf4938e9c08d1d515c4609.html (accessed August 9, 2022).

[66] Gharat P V., Bhalekar SS, Dalvi VH, Panse S V., Deshmukh SP, Joshi JB. Chronological development of innovations in reflector systems of parabolic trough solar collector (PTC) - A review. Renewable and Sustainable Energy Reviews 2021;145:111002. https://doi.org/10.1016/j.rser.2021.111002.

[67] Sallaberry F, Pujol R, Perers B. Optical Losses Due to Tracking Misaligment on Linear Concentrating Solar Thermal Collectors. Proceedings of EuroSun2016, Freiburg, Germany: International Solar Energy Society; 2016, p. 1–12. https://doi.org/10.18086/eurosun.2016.07.10.

[68] Sallaberry F, Pujol-Nadal R, Larcher M, Rittmann-Frank MH. Direct tracking error characterization on a single-axis solar tracker. Energy Convers Manag 2015;105:1281–90. https://doi.org/10.1016/j.enconman.2015.08.081.

[69] Wu CH, Wang HC, Chang HY. Dual-axis solar tracker with satellite compass and inclinometer for automatic positioning and tracking. Energy for Sustainable Development 2022;66:308–18. https://doi.org/10.1016/J.ESD.2021.12.013.

[70] Fuentes-Morales RF, Diaz-Ponce A, Peña-Cruz MI, Rodrigo PM, Valentín-Coronado LM, Martell-Chavez F, et al. Control algorithms applied to active solar tracking systems: A review. Solar Energy 2020;212:203–19. https://doi.org/10.1016/J.SOLENER.2020.10.071.

[71] Valentín D, Valero C, Egusquiza M, Presas A. Failure investigation of a solar tracker due to wind-induced torsional galloping. Eng Fail Anal 2022;135:106137. https://doi.org/10.1016/J.ENGFAILANAL.2022.106137.

[72] Kaluba VS, Mohamad K, Ferrer P. Experimental and simulated performance of hot mirror coatings in a parabolic trough receiver. Appl Energy 2020;257:114020. https://doi.org/10.1016/J.APENERGY.2019.114020.

[73] Dahlioui D, Wette J, Fernández-García A, Bouzekri H, Azpitarte I. Performance assessment of the anti-soiling coating on solar mirrors soiling in the arid climate of Ouarzazate-Morocco. Solar Energy 2022;241:13–23. https://doi.org/10.1016/J.SOLENER.2022.05.063.

[74] Yang B, Liu S, Zhang R, Yu X. Influence of reflector installation errors on optical-thermal performance of parabolic trough collectors based on a MCRT - FVM coupled model. Renew Energy 2022;185:1006–17. https://doi.org/10.1016/J.RENENE.2021.12.102.

[75] Ekman BM, Brooks G, Akbar Rhamdhani M. Development of high flux solar simulators for solar thermal research. Solar Energy Materials and Solar Cells 2015;141:436–46. https://doi.org/10.1016/J.SOLMAT.2015.06.016.

[76] Sabahi H, Tofigh AA, Kakhki IM, Bungypoor-Fard H. Design, construction and performance test of an efficient large-scale solar simulator for investigation of solar thermal collectors. Sustainable Energy Technologies and Assessments 2016;15:35–41. https://doi.org/10.1016/J.SETA.2016.03.004.

[77] Wang W, Aichmayer L, Garrido J, Laumert B. Development of a Fresnel lens based high-flux solar simulator. Solar Energy 2017;144:436–44. https://doi.org/10.1016/j.solener.2017.01.050.

[78] Martínez-Manuel L, Wang W, Peña-Cruz MI. Optimization of the radiative flux uniformity of a modular solar simulator to improve solar technology qualification testing. Sustainable Energy Technologies and Assessments 2021;47:101372. https://doi.org/10.1016/j.seta.2021.101372.

[79] Bartela Ł, Stanek B, Węcel D, Skorek-Osikowska A. A solar simulator numerical modeling for heat absorption phenomenon research in a parabolic trough collector. Int J Energy Res 2021. https://doi.org/10.1002/er.6585.

[80] Parabolic Reflectors - Optiforms, Inc. n.d. https://www.optiforms.com/electroformed/parabolic-reflectors/ (accessed April 4, 2023).

[81] HMI DIGITAL 575 W | OSRAM PIA n.d. https://www.osram.com/ecat/HMI%20brand%20DIGITAL-HMI%20single-ended-HMI%20brand-Discharge%20lamps-Entertainment-Specialty%20Lighting/com/en/GPS01_3043421/ZMP_4058340/ (accessed April 4, 2023).

[82] Stanek B, Bartela Ł. Numerical and experimental study on 10 kWe metal-halide solar simulator for parabolic-trough collector testing, ECOS 2021 Conference Proceedings.

34th International Conference on Efficiency, Cost, Optimization, Simulation and Environmental Impact of Energy Systems (ECOS21), Taormina: 2021, p. 1198–209.

[83] Stanek B, Bartela Ł, Węcel D, Rulik S. An experimental study on parabolic trough collector in simulated conditions by metal-halide solar radiation simulator. Archives of Thermodynamics 2022;43:47–61. https://doi.org/10.24425/ATHER.2022.143171.

[84] Stanek B, Wang W, Bartela Ł. Potential of using Pyromark as an absorber coating in low-temperature solar installation sections – A case study for heat industrial application and parabolic trough collectors. In: Stanek W, Werle S, Simla T, Patela K, Gładysz P, editors. 7th International Conference on Contemporary Problems of Thermal Engineering: TOWARDS SUSTAINABLE & DECARBONIZED ENERGY SYSTEM, Warsaw: Department of Thermal Technology; 2022, p. 821–31.

[85] JCGM. Evaluation of measurement data-Guide to the expression of uncertainty in measurement Évaluation des données de mesure-Guide pour l'expression de l'incertitude de mesure 2008.

[86] Therminol VP-1 Heat Transfer Fluid | Therminol | Eastman n.d. https://www.therminol.com/product/71093459 (accessed February 1, 2022).

[87] Mwesigye A, Bello-Ochende T, Meyer JP. Heat transfer and entropy generation in a parabolic trough receiver with wall-detached twisted tape inserts. International Journal of Thermal Sciences 2016;99:238–57. https://doi.org/10.1016/J.IJTHERMALSCI.2015.08.015.

[88] Hasanpour A, Farhadi M, Sedighi K. A review study on twisted tape inserts on turbulent flow heat exchangers: The overall enhancement ratio criteria. International Communications in Heat and Mass Transfer 2014;55:53–62. https://doi.org/10.1016/J.ICHEATMASSTRANSFER.2014.04.008.

[89] APEX. 2019. Breault Research Organization, Inc n.d. http://www.breault.com/ (accessed February 3, 2022).

[90] Cabello R, Plesu Popescu AE, Bonet-Ruiz J, Curcó Cantarell D, Llorens J. Heat transfer in pipes with twisted tapes: CFD simulations and validation. Comput Chem Eng 2022;166. https://doi.org/10.1016/J.COMPCHEMENG.2022.107971.

[91] Kalogirou SA. A detailed thermal model of a parabolic trough collector receiver. Energy 2012;48:298–306. https://doi.org/10.1016/J.ENERGY.2012.06.023.

[92] Wirz M, Petit J, Haselbacher A, Steinfeld A. Potential improvements in the optical and thermal efficiencies of parabolic trough concentrators. Solar Energy 2014;107:398–414. https://doi.org/10.1016/J.SOLENER.2014.05.002.

[93] Tzivanidis C, Bellos E, Korres D, Antonopoulos KA, Mitsopoulos G. Thermal and optical efficiency investigation of a parabolic trough collector. Case Studies in Thermal Engineering 2015;6:226–37. https://doi.org/10.1016/j.csite.2015.10.005.

[94] Allam M, Tawfik M, Bekheit M, El-Negiry E. Heat transfer enhancement in parabolic trough receivers using inserts: A review. Sustainable Energy Technologies and Assessments 2021;48:101671. https://doi.org/10.1016/J.SETA.2021.101671.

[95] Mansour K, Boudries R, Dizene R. Optical, 2D thermal modeling and exergy analysis applied for performance prediction of a solar PTC. Solar Energy 2018;174:1169–84. https://doi.org/10.1016/j.solener.2018.09.040.

[96] Kalogirou SA. A detailed thermal model of a parabolic trough collector receiver. Energy 2012;48:298–306. https://doi.org/10.1016/j.energy.2012.06.023.

[97] Alami AH, Olabi AG, Mdallal A, Rezk A, Radwan A, Rahman SMA, et al. Concentrating solar power (CSP) technologies: Status and analysis. International Journal of Thermofluids 2023;18:100340. https://doi.org/10.1016/J.IJFT.2023.100340.

[98] Stanek B, Węcel D, Bartela Ł, Rulik S. Solar tracker error impact on linear absorbers efficiency in parabolic trough collector – Optical and thermodynamic study. Renew Energy 2022;196:598–609. https://doi.org/10.1016/J.RENENE.2022.07.021.

[99] Pompea SM, McCall SH. OPTICAL COATINGS | Optical Black Surfaces. Encyclopedia of Modern Optics, Elsevier; 2005, p. 349–60. https://doi.org/10.1016/B0-12-369395-0/00872-1.

[100] Stanek B, Grzywnowicz K, Bartela Ł, Węcel D, Uchman W. A system analysis of hybrid solar PTC-CPV absorber operation. Renew Energy 2021;174:635–53. https://doi.org/10.1016/j.renene.2021.04.110.

List of figures

Appendices

In this Chapter, the full-text papers that were briefly described in Chapters 2 – 6 are presented. The papers are listed in the following order:

I. Ł. Bartela, B. Stanek, D. Węcel, A. Skorek-Osikowska, *A solar simulator numerical modeling for heat absorption phenomenon research in a parabolic trough collector*, **International Journal of Energy Research**, Volume 46, March 2021, pp. 10074 - 10087

II. B. Stanek, J. Ochmann, D. Węcel, Ł. Bartela, *Study of twisted tape inserts segmental application in low-concentrated solar parabolic trough collectors*, **Energies**, Volume 16, April 2023

III. B. Stanek, W. Wang, Ł. Bartela, *A potential solution in reducing the parabolic trough based solar industrial process heat system cost by partially replacing absorbers coatings with non-selective ones in initial loop sections*, **Applied Energy**, Volume 331, February 2023

IV. B. Stanek, D. Węcel, Ł. Bartela, S. Rulik, *Solar tracker error impact on linear absorbers efficiency in parabolic trough collector – Optical and thermodynamic study*, **Renewable Energy**, Volume 196, August 2022, pp. 598 - 609

Paper I

Received: 31 August 2020 | Revised: 8 February 2021 | Accepted: 14 February 2021

DOI: 10.1002/er.6585

SPECIAL ISSUE RESEARCH ARTICLE

INTERNATIONAL JOURNAL OF ENERGY RESEARCH WILEY

A solar simulator numerical modeling for heat absorption phenomenon research in a parabolic trough collector

Łukasz Bartela | **Bartosz Stanek** | **Daniel Węcel** | **Anna Skorek-Osikowska**

Department of Power Engineering and Turbomachinery, Silesian University of Technology, Gliwice, Poland

Correspondence
Bartosz Stanek, Department of Power Engineering and Turbomachinery, Silesian University of Technology, Konarskiego 18, 44-100 Gliwice, Poland.
Email: bartosz.stanek@polsl.pl

Funding information
National Science Centre, Grant/Award Number: 2018/29/B/ST8/02406

Summary

The development of renewable solar technologies determines the constant need to improve and increase their energy efficiency. Determination of solar systems performance characteristics must take place under given conditions set by proper standards. Due to unstable weather conditions, including temperature and solar radiation, it is necessary to simulate the laboratory conditions' radiation. For these purposes, so-called solar radiation simulators are being constructed. This article presents the results of solar simulator modeling for parabolic trough collectors testing. A new approach presented here proposes to use reflectors placed parallel on one plane to simulate both, total radiation and direct radiation used in parabolic concentrator tests. The methodology adopted from the normative approach for evaluating the quality of the simulator is presented. The methodology used for solar radiation simulators was modified to test concentrators in constant, repeatable conditions. The analysis was carried out not only to assess the energy distribution on the plane area but also to assess the energy reaching the tubular absorber external surface. The optical engineering ray tracing software, based on Monte Carlo Method, was used for the analysis. A selection of appropriate light sources, quantity, type, and arrangement of reflectors and their coatings was carried out. Metal-halides and xenon arc lamps were considered as sources. The distribution of radiation intensity on the analyzed surface was determined for two cases, 22 reflectors and 4 reflectors. The analyzed area was 1 square meter. The evaluation index has been defined to determine the quality of the energy distribution. The influence of the simulator distance on the amount of energy reaching the absorber surface was also analyzed. An estimation of the required financial outlays for analyzed constructions of the simulator was performed. Research has shown that in terms of maintaining the energy field's homogeneity and the price for the entire radiation simulator, it is more reasonable to construct a simulator consisting of 22 reflectors. The construction of such a simulator seems to meet the assumptions required for the correct operation of the radiation simulator.

Novelty statement

Paper's novelty is the methodology to identify and evaluate solar radiation simulators to simulate heat radiation for parabolic trough collectors. The

paper specifies the evaluation index and the way of its interpretation, which determines the radiation distribution on the simulated surface, which is crucial in this issue. In a better and more accurate way, this factor assesses the energy field in terms of quality. Modifying the normative measurement approach of solar radiation on a flat surface, we propose the analysis of concentrated radiation by performing optical analyses using software which are based on the Monte-Carlo method. The location of light sources on the plane surface is a new approach for PTC testing.

KEYWORDS

energy distribution, irradiance, parabolic trough collectors, solar energy, solar simulator

1 | INTRODUCTION

Currently, solar energy is gaining importance even in those countries where solar conditions for many decades have been preventing from satisfactory results of conducted investment analyses. The main premise is the increasingly argued need to reduce fossil fuel consumption in energy production, of which combustion is responsible for the emission of harmful substances, including greenhouse gas emissions. Various support mechanisms, often defined at central government levels, contribute to the promotion of green technologies. Unlike wind power, which is also very popular, solar energy is characterized by more proper correlation of time characteristics: generation potential and energy demand occurring in the countries power systems.[1]

The literature on the subject is dominated by issues related to the search for more and more efficient solutions in photovoltaic solar cell technology. The development of this technology, mainly in the last two decades,[2] was accompanied by an increase in the energy efficiency of PV panels and a decrease in the cost of their production. These contributed to the popularization of technology, mainly in the area of distributed energy systems. Solar cell technology is responsible for highest dynamics of solar power capacity growth in the segment of all renewable sources.[3] Among European countries, Germany and Spain have been implementing solar systems most dynamically.[4]

Simultaneously and independently of the world's research in the field of development of PV technology, research on the development of solar concentrators technologies is also carried out.[5-9] The research profile is often directed at obtaining high-temperature heat that can be used in the energy sector. The research on concentrators is propelled by the progressing popularization of ORC technology, Stirling engines, absorption heat pumps, or absorption refrigeration devices.[10-12] Concentrated radiation is also proposed as an energy source in thermochemical processes, where concentrated radiation is the energy source for the pyrolysis process[13] or the thermolysis process.[14] In the last two decades, the highest number of projects dealing with systems with solar radiation concentrators have been launched in Europe, with research institutes from Spain being the most active. Radiation concentrators are increasingly being considered as part of non-energy production systems, where heat is used for drying, sterilization, distillation, and pasteurization purposes.[15]

The development of solar radiation simulators accompanies research on solar technologies. Such devices enable to plan tests regardless the time of the day, season, or current weather conditions. Research carried out at a given location can be profiled to simulate solar conditions at any geographical location. The functionality of solar simulators goes beyond energy technology research. Radiation simulators are used in the field of material research, as well as research on biological and physicochemical processes.

Currently, the market offer of solar simulator manufacturers is flexibly addressed to the user's individual needs. Such needs are considered at the design stage and allow cost minimization by limiting the simulator's functionality. The group of significant features defining such functionality is standardized. The most often features that are considered are spectral matching, spatial nonuniformity, and temporal stability. Construction costs are also determined by the dimensions of the illuminated surface (or degree of concentration) and the expected system automation degree. Despite the extensive market offer, many research units decide to design and make simulators on their own. The simulator's design process is accompanied by a cognitive aspect that could be an inspiration for solar research directions. A measurable effect may also be reduction of the cost of the simulator.

Many publications devoted to the problems of simulator optimization can be found in the subject literature. Assessment criteria are often standardized or go beyond

standards, considering the specifics of the research objectives and the available budget. Due to the popularity of photovoltaic cell research,[16,17] a broad group of simulators is designed to illuminate surface of the test stand homogeneously. It is crucial to obtain high stability and proper radiation spectrum, simulating the natural solar radiation. Sabahi et al[18] analyzed the simulator based on 12 metal-halide lamps, half of which are 1 kW lamps, while the other half are 2 kW lamps. The working area of the test stand is up to 7.56 m^2. Effective regulation of radiation intensity can be made by changing the distance of radiation sources from the work surface of the test stand due to the highly diffuse nature of radiation. An even more extensive field of the working area, 17.46 m^2, has a simulator analyzed by Meng et al.[19] One hundred eighty-eight metal-halide lamps were used in the simulator. Radiation intensity regulation in the range from 150 to 1100 W/m^2 can be implemented using a variable number of lamps turned on and by changing the lamp-to-area distance.

A large group of simulators is a solution that enables concentrating rays on the working plane. An example is the simulator analyzed by Ekman et al.[20] The simulator uses seven metal-halide lamps, each with an electric power of 6 kW, installed in paraboloid reflectors. Point-focused radiation allows reaching temperature up to 2000°C. In Reference 21, Boubalt et al analyze a radiation simulator with an electric power of 7.2 kW, using four ellipsoidal reflectors. The simulator is used to test the materials used to build radiation concentrators. The concentrator's simple construction allows obtaining the low financial costs required for the construction of the simulator, in this case, $ 2.38 per radiative watt. A similar structure, but enabling a much higher concentration coefficient, was implemented by Li et al.[22] The simulator uses 18 point-focused mirrors and can be used to study thermochemical processes.

Planning simulators to test parabolic or paraboloid concentrators is a big challenge. In these cases, the criterion considering the angle of incidence of rays on the illuminated plane is highly essential. Jin et al[23] analyzed a simulator system for universal applications. The use of seven xenon lamps, an optical integrator, and a collimating lens of radiation in the optical system allows the simulator to obtain both concentrated radiation and similar to solar radiation. A simulator with compatible characteristics may be the large area solar illuminator (LASI) unit offered by Sciencetech Inc.[24] The modular design allows for combining individual units into large systems, enabling uniform illumination of a square area of 0.25 m^2. The optical system uses one xenon lamp with 1.6 kW electrical power in the module.

Okuhara et al[25] propose a different approach to planning simulators to enable the study of absorption processes in the absorber system linearly located in the focal parabolic mirror. In the case of the test stand, 20 optical systems using reflectors with 5 kW xenon lamps, a spherical lens, and a Fresnel lens, allowing a linear concentration of radiation, were used. Another narrow focus of the solar simulator is analyzed by Pernpeinter et al.[26] In this case, the radiation sources are six metal-halide lamps, which are symmetrically arranged in a linear oval reflector, where the tested absorber is also located. Linear simulators analyzed by Onkuhar et al[25] and Pernpeinter et al[26] can be efficient solutions for absorber testing. Undoubtedly, however, they are not universal simulators.

The literature on the subject focuses mainly on the study on parabolic trough collectors in natural solar radiation. To determine the impact of individual elements of the system on its operation, stable and repeatable measurement conditions are necessary, which is difficult to obtain in, for example, Polish climatic conditions. Hence, there is a need to construct a solar radiation simulator. Only a few research installations are presented in the literature use simulators to test absorbers, but these are expensive devices which are focused only on the simulation of concentrated radiation for a given type of technology. Thus, the solutions that are cheaper but not significantly inferior in quality to simulated radiation are sought.

So far, simulators in which light sources were placed on one plane were used only for aging tests or tests of solar installations using total radiation, for example, solar collectors or PV installations. Here, the authors propose to use such a simulator in a versatile way, both for testing the installations using total radiation and direct radiation, which is a novelty. Modifying the normative measurement approach of solar radiation on a flat surface, we propose the analysis of concentrated radiation by performing optical analyses using APEX software which are based on the Monte Carlo method. The location of light sources is a new approach for parabolic trough collector (PTC) testing. This way of evaluating radiation simulators aims to demonstrate the feasibility of constructing such units using a method that makes the solution cheaper and therefore more available for other researchers.

This article presents the simulator's concept and the path for determining the characteristics of the essential elements of the simulator (reflectors, radiation sources). The simulator is planned to be used in tests profiled on testing prototype absorbers, of which, numerical optimization leads to the intensification of heat absorption by thermal oil. For this purpose, turbulization inserts, a vibrating element, and thermal oil recirculation are used. The requirements for the planned simulator are as follows:

- The square surface area in the simulator's working plane should be 1 m^2;
- The total concentrated radiation power that reaches the absorber surface located in the focal parabolic

mirror should reach 800 W, which corresponds to DNI of about 1000 W/m^2;
- The radiation intensity distribution in the simulator's working plane should be as homogeneous as possible;
- The spectrum measured in the simulator's working plane should be as close as possible to the spectrum specific to solar radiation;
- The total cost of the simulator should not exceed 20 000 €.

2 | METHODS

This article presents the description of the assessment methodology and the results of numerical modeling of solar radiation simulator for parabolic trough collectors testing. The purpose of the numerical analysis is to select the appropriate set of elements for the construction of the radiation simulator. The article aims to preliminary analyze the simulator quality and the costs associated with its construction. The analysis is divided into three sections, as shown in Figure 1. The first section, input data, concerns the light source in terms of its radiation spectrum, type, and size. This section is also analyzing parabolic reflectors and their coatings. In the second section, numerical modeling is performed, in which, according to the normative approach, the analysis of radiation distribution on a flat surface above the parabolic mirror is performed. The analysis is performed based on equations defined by the standards and according to the proposed evaluation index. Then, the radiation energy analysis reaching the absorber surface was made. The last stage of modeling concerns investment cost balance.

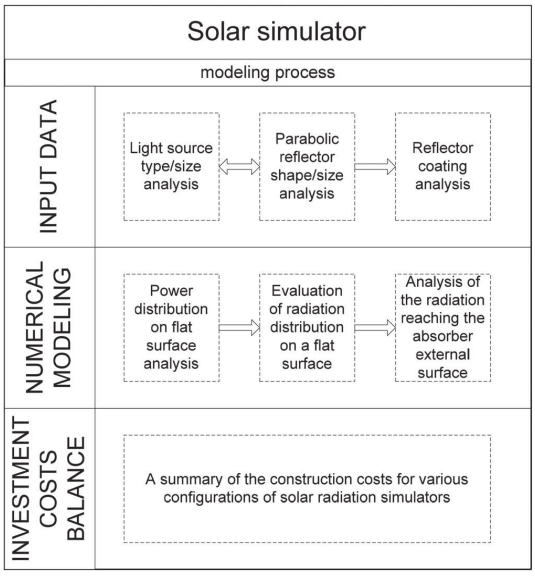

FIGURE 1 Solar simulator modeling method

The installation for testing parabolic trough collectors is planned to be constructed under the project founded by the Polish National Science Centre. The test stand's primary purpose is to assess the impact of various types of geometry on the intensification of heat absorption in a tubular pipe absorber located in the concentrators focus. Figure 2 presents the design of the experimental test stand. The pipe absorber is surrounded by a transparent glass tube. The tube is designed to reduce convective heat losses by the vacuum. The absorber is covered by selective coating to reduce the radiation loses. The length of the absorber is 1 m. The heat transfer fluid flow will be regulated by a circulating pump and measured by an ultrasonic flow meter. It is planned to install a heater at the absorber inlet. By using the electric heaters, the installation is able to simulate each additional length of the absorber being tested by preheating thermal heat transfer fluid. Consequently, the obtained results will illustrate the absorber's work on its full, appropriately assumed length. The temperatures at the inlet and outlet of the absorber will be measured. The heat exchanger will be used to collect heat from the thermal fluid. The critical aspect of the test stand is to provide heat in the radiation form. For this purpose, a solar radiation simulator will be constructed. The solar radiation simulator is the subject of research, presented in this paper.

2.1 | Solar simulator—Input data

The concept of the test stand is considering using a solar radiation simulator to obtain the conditions during the measurements as constant as possible. The system should also be able to simulate solar radiation of a range of power values. Among the most important standards defining a solar simulator's quality are the following: JIS-C8912, IEC 60904-9, and ASTM-E927-10.[27-29] There are three conditions determining solar simulators: 1-spectral mismatch to all intervals, 2-spatial nonuniformity, and 3-temporal short- and long-term instability. The simulator class is defined by three symbols among A, B, and C. The best class simulator corresponds to AAA. Symbols determining the quality of the simulator with the corresponding ranges are shown in Table 1.

2.1.1 | Selection of the light sources

A light source determines the spectral power distribution. The most common sources used to simulate solar radiation[30] are tungsten halogens, metal-halides, and xenon arc lamps.

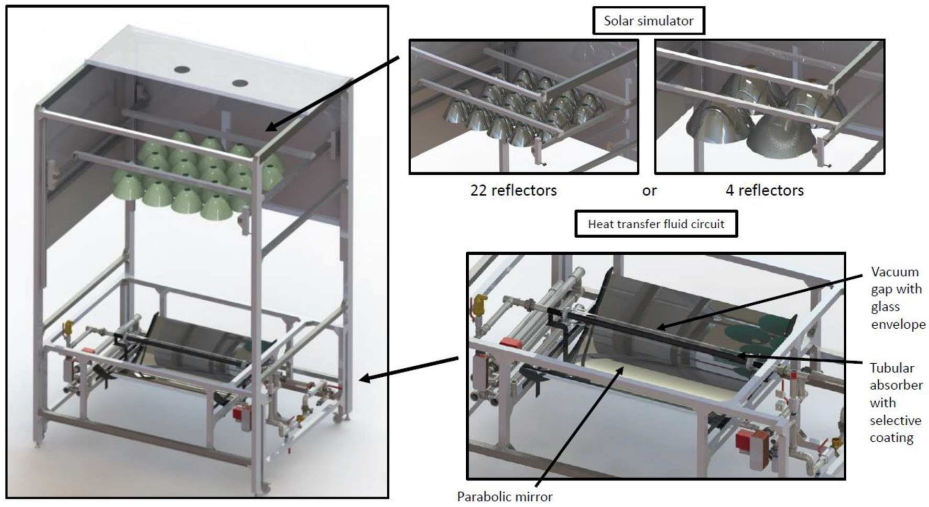

FIGURE 2 The design of the solar simulator for testing parabolic trough collectors

TABLE 1 Solar simulators classes[27-29]

Solar simulators classes	Spectral mismatch to all intervals	Spatial nonuniformity, %	Temporal instability short term, %	Temporal instability long term, %
A	0.75-1.25	2	0.5	2
B	0.6-1.4	5	2	5
C	0.4-2.0	10	10	10

Tungsten halogens are sources of a filament enclosed in a transparent container with a mixture of inert gas and halogen. They are most commonly used in multisource solar simulators due to their low color temperature of 3400 K. The color results from high proportion of infrared and lower proportion of UV, which seems to be not appropriate in the planned system. Lower color temperature, poor adaptation to the solar spectrum, and large tungsten filament size disqualify this source for design purposes.[31]

A metal-halide lamp is a mercury arc source with the addition of a metal halide. The color temperature of sources depending on the model is equal to 5000 to 6000 K, which is close to the color temperature of sun surface 5800 K.[32] The advantage of this solution is its compactness. Both connectors are placed on one side, which makes it easy to assemble and operate the device. Spectral analysis shows high compliance with the solar spectrum. Metal-halides require a suitable power supply and ignition system, making it more expensive than tungsten halogen lamps. Most metal-halide sources are not suitable for the collimation process required in the planned solar simulator. However, several MH bulbs available on the market meet the assumptions of the planned system.[21,33]

Xenon arc lamps are the most popular sources in solar radiation simulators.[30] They provide a stable spectrum, well suited to solar radiation. Source power fluctuations do not significantly affect spectral balance shifts. These sources are suitable for collimation because they produce high-intensity light beams. However, their relatively high price is significantly a disadvantage. Xenon arc lamps and special power ballasts are the most expensive among the other mentioned light sources. High xenon pressure can be also dangerous.[34] Arc lamps have a cathode and anode pins on both sides of the bulbs, which requires a special connection. With many sources placed in a row, it may be impossible to position them without significantly affecting the rays falling on the surface. Xenon lamps have a significantly short lifetime and a high price, which does not meet the assumption of constructing a low-cost solar simulator.[18,19]

A preliminary analysis was performed according to the standards JIS-C8912, IEC 60904-9, and ASTM-E927-10,[27-29] to select the right source matching the

TABLE 2 Spectral power distribution for three analyzed light sources

	Percentage of total irradiance, %		Light sources					
			Tungsten halogen[30,31]		Metal-halide[21,33]		Xenon arc lamp[18,19,30]	
Wavelength interval, nm	AM1.5 direct	AM1.5 global	Per. of energy, %	Solar simulation Class	Per. of energy, %	Solar simulation class	Per. of energy, %	Solar simulation class
400-500	16.9	18.4	3.5	—	21.7	A	13.8	A
500-600	19.7	19.9	7.7	—	18.4	A	12.7	B
600-700	18.5	18.4	12.7	B	14.1	A	12.7	B
700-800	15.2	14.9	16.2	A	10.6	B	12.7	A
800-900	12.9	12.5	19.7	B	16.4	B	15.3	A
900-1100	16.8	15.9	40.1	—	14.5	A	32.7	—

spectral power distribution to solar radiation. The results are shown in Table 2.

Tungsten halogens were rejected from further analysis because of the high infrared energy share. Preliminary analyses were made for metal-halides and xenon arc lamps.

Due to the limited availability of single sources with different nominal power, it was decided to carry out analyses for metal-halides sources with relatively low electrical power (200 W, 400 W) and xenon arc lamps of higher electric power 1600 W.

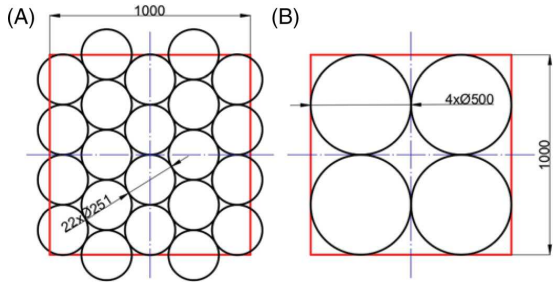

FIGURE 3 Reflector distribution cases: (A) 22 reflectors and (B) 4 reflectors

2.1.2 | Reflectors models and coatings selection

In the designed device for simulation of solar radiation, the critical aspect is the rays' angle on the surface of the parabolic mirror. The assumption for the simulator is to obtain the irradiation distribution as uniform as possible and simulation of radiation as close to direct as possible. Such conditions can be obtained for a given ratio of the size of the light source to the size of the reflector. The light sources used for numerical modeling are metal-halide and xenon discharge lamps produced in a certain series. This paper presents the most optimal solutions for the required parameters, both those that meet the initial assumption on geometry and the ratio of source-reflector size and availability. Two configurations of parabolic reflectors were considered, as shown in Figure 3. The illuminated surface is a 1-m × 1-m (1 square meter) in both cases. The first case considered using 22 parabolic reflectors with a nominal diameter of 251 mm in the 4, 5, 4, 5, 4 arrangement. In this way, the entire surface of a square meter is illuminated by incident rays. The second case is considered using only four parabolic reflectors in a two-by-two system with a 500 mm diameter. This case is a common solution presented in the literature that is used for illuminating a 1 × 1 sqr meter area but is not especially used for the research on concentrated radiation technology. However, the analyses were performed due to the relatively good availability of these devices on the market. As can be seen in Figure 3, not whole of the assumed surface can be illuminated.

Each of the analyzed reflectors is a parabolical type. This means that, in the ideal case, the rays emitted by a point source located in the focal point of the reflector should illuminate the surface with direct radiation. Reflectors models in 3D are shown in Figure 4.

According to the standards,[27-29] the spectrum's compliance reaching the surface is specified in the range 400 to 1100 nm. These standards, however, describe issues related to radiation simulation for photovoltaics research. For testing solar collectors or, as in this case, parabolic trough collectors where energy is expected in the form of transferred heat, the spectrum should be extended to 200 to 4000 nm. The software allows to choose reflectors' coatings from a

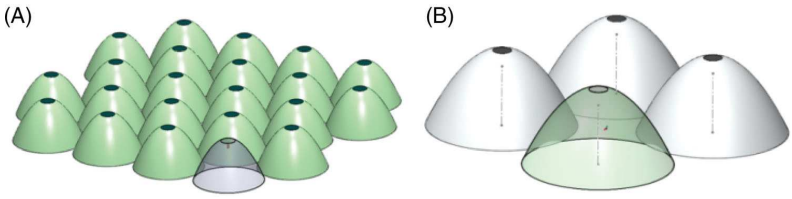

FIGURE 4 Reflector models in 3D: (A) 22 reflectors and (B) 4 reflectors (adapted from Reference 29)

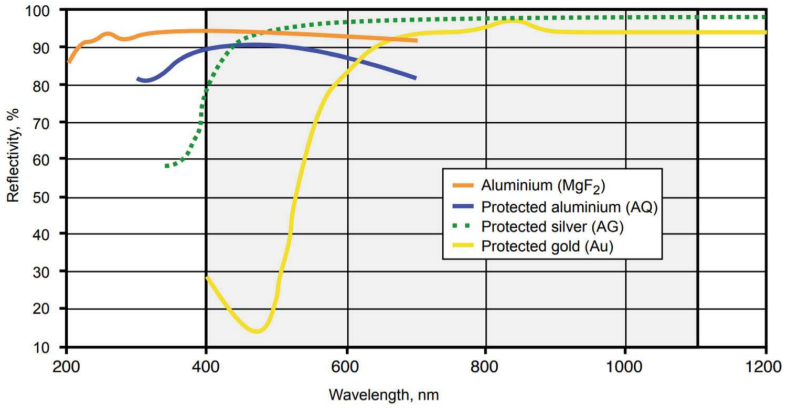

FIGURE 5 Coatings reflectivity as a function of wavelength (adapted from Reference 29)

library of coatings that can be used for surface covering.[35] The reflectivity of a given material as a function of wavelength is shown in Figure 5. Considering the ranges of information provided on the reflectivity and the spectrum emitting by solar collectors, it was decided to choose the Protected Silver (AG) coating. This coating is characterized by the highest reflectivity stability as a function of wavelength.

2.2 | Numerical optical modeling

Numerical studies were performed using the optical-engineering software APEX.[36] Based on the Monte Carlo method, numerical tests were carried out to analyze the distribution of simulated radiation on a flat surface, just above the concentrator's mirror, and then on the surface of the absorber itself. In the numerical analysis, the shape and coating of the reflector and light source as well as the position distance of the source from the flat surface above the mirror were considered. Figure 6 shows a visualization of the placement of the illuminated test surface, as well as the geometry of the concentrator at an example of 22 reflectors. The size of the test surface was 1 × 1m, and it was placed above a parabolic mirror tangent to its arms, as shown in Figure 6. The next stage of the study was to assess the energy reaching the outer surface of the absorber. For the optical analysis, a tubular absorber with a diameter of 33.7 mm and a parabolic mirror with the geometry shown in the figure were used. The absorber is placed at the focus of the concentrator.

2.2.1 | Mathematical quality estimation of the radiation field

The quality of a radiation simulator is usually determined, according to standards, by the nonuniformity index, which determines the radiation inhomogeneity of illuminated flat surface. The highest quality solar simulators have a field nonuniformity of up to 2% and are marked with A symbol. These values are determined using the Formula (1)[27-29]:

$$S_{NE} = \frac{E_{max} - E_{min}}{E_{max} + E_{min}} 100\%, \quad (1)$$

where: E_{max}—maximum value of irradiance, E_{min}—minimum value of irradiance.

Obtaining such a field results from the use of collimators, such as multistage lenses that not only collimate diffuse radiation but also establish an even distribution of power over the surface. Equation (1) finds its application in real simulator tests, where the number of measurements is relatively small, and the irradiance result is the

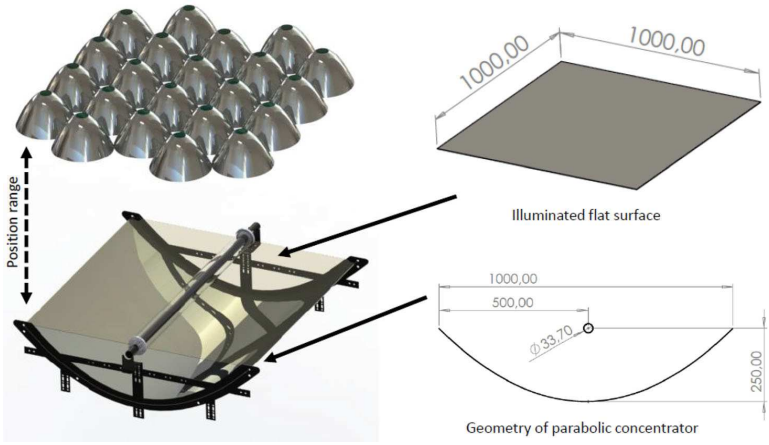

FIGURE 6 Geometry visualization for numerical modeling

average of the whole area of the measuring device, for example, pyranometer or a reference PV cell (ie, about 1-4 cm^2).

For accurate radiation distribution in the numerical modeling, the field was divided into 40 000 measurement points, each 5 × 5 mm size. Since large deviations in the numerical measurements were expected and Equation (1) only considers the highest and the lowest measured value, it was assumed that the range of energy distribution reaching the surface deviates from the assumptions in Table 1 and is not included in the ranges described by the standard A, B, C. Therefore, the evaluation index was defined for the assessment the nonuniformity of radiation. The Δ index (2) is defined as the sum of squares of differences in the expected value (average value on the surface) and the measured value at a given point divided by the sum of the average values:

$$\Delta = \frac{\sum_{i=1}^{n}(E_{av} - E_i)^2}{\sum_{i=1}^{n} E_{av}}. \quad (2)$$

The evaluation index was determined for relative values to compare both cases. Assuming the least-squares method, the value of Δ should aim toward zero.

3 | RESULTS AND DISCUSSION

The characteristics presented in Figure 7 show the radiation intensity distribution for twenty-two and four parabolic reflectors. For the 22 reflectors model, further known as case 1, 22 metal-halides of low power were used. For the four-reflector model, further, known as case 2, the modeled sources were xenon arc lamps. The exact electrical powers of the sources are described later in this article. As shown in Figure 7, total power reaching the surface for case 1 was 1081.1 W, for case 2997.0 W. A significant difference between these cases can be seen. For case 1, the field is more uniform on the analyzed surface. Only a small area is low or not illuminated. Part of the energy from the reflectors do not reach the target area of one square meter. It was important not to leave empty fields and keep the rays perpendicular to the surface. For case 2, a significant lack of energy radiation on the surface is visible. Power peaks are visible between the reflectors, resulting from the addition of irradiation from neighbor sources. Stable dispersion of energy through a large angle of the beam falls the reason. Although the center of the arc was modeled correctly in the reflector focus, the source's size strongly influenced the dispersion of energy. In both cases, the energy-emitting field's actual dimensions were assumed based on the product datasheets. However, this model can only be validated in real measurements, that are planned in future work.

A comparison of results for both cases of reflectors and the ideal case (sun), where it was assumed that the measured value is identical at each point, is summarized in Table 3. The classification $\Delta_{SUN} < \Delta_{22} < \Delta_4$ indicates the legitimacy of using case 1 with 22 reflectors. Figure 8 represents an ordered distribution of measurements according to the relative value of the radiation intensity, where one corresponds to irradiance's average value. The number of numerical results is divided almost equally into those above, and below-average value, corresponding to 1. This indicates that the median value is close to the average expected value. The curve deviation from the expected value for case 2 is more significant than for case 1. The range for case 1 is from 0.34 to 1.52, for case 2 from 0.15 to 1.85.

Figure 9 presents the comparison method between case 1 and 2 as percentage energy distribution, as a

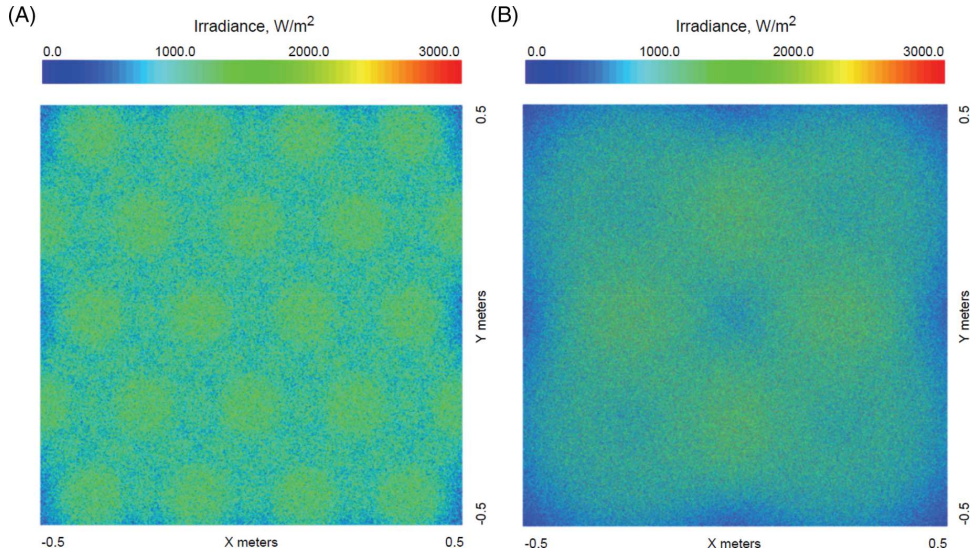

FIGURE 7 Irradiance on the one square meter surface for two cases: (A) 22 reflectors—case 1 and (B) 4 reflectors—case 2

TABLE 3 Summary of results

Case	Δ
4 reflectors	0.056
22 reflectors	0.021
Sun (ideal)	0

function of the deviation from the expected value. Since, for both cases, it is not possible to determine an equal average value on the surface, reference is made to relative values. As the power of the light sources is reduced (so-called dimming by means of power supplies), the angle of incidence of the radiation does not change, and, therefore, the percentage distribution of the radiation will be constant irrespective of the power applied to the plane surface. Therefore, the results presented below may refer to different expected values (average values on the surface), but in this case, the results are described for one of the standard conditions—1000 W/m^2. In the analysis, the average of the irradiation on a flat surface is treated as the expected value. It should be interpreted as follows. For case 1, 27.98% of the measurements taken are in the range of 0% to 5% of the expected value. For case 2, it is only 16.37%. For the expected value of 1000 W/m^2, this range corresponds to the range of 950 to 1050 W/m^2. For case 1 of 22 parabolic reflectors, the percentage of results obtained decreases as the percentage deviation increases. For case 2 of four parabolic reflectors, the

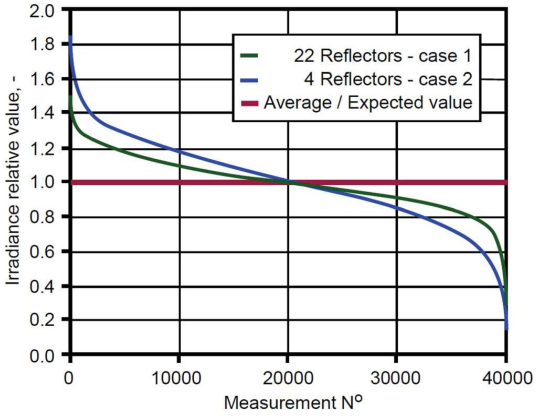

FIGURE 8 Ordered distribution of numerical results according to the relative value of the radiation intensity

highest share of measurements is in the range of 5% to 10%, that is, 1000 W/m^2 from 900 to 950 W/m^2 and 1050 to 1100 W/m^2. For the reference system, the sun, where each point should have the same value, 100% of measurements, should be in the range of 0% to 5% and in particular for 0%.

Distribution of radiation intensity appropriate for the two analyzed cases of reflectors configurations, shown in Figure 7, relates to total radiation power measured on a

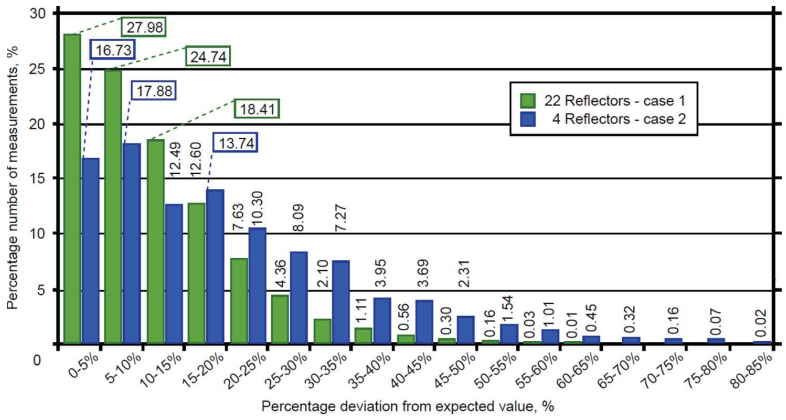

FIGURE 9 Percentage energy distribution as a function of the deviation from the expected value

surface placed 1 m from surface defined by the reflectors' focal length. Therefore, the qualitative assessment conclusions drawn based on the results presented in Table 3, Figures 8, and 9 cannot be decisive in the context of the selection of the optimal configuration of the necessary components of the simulator for parabolic concentrators testing. It would be different in case of simulators used for testing photovoltaic cells, where the angle of incidence on the working plane has less critical role. Considering requirements for the planned installation, the radiation reaching the illuminated work surface must have the character of direct radiation. Built-in simulators cannot fully reproduce solar radiation due to the low degree of concentration of sources radiation in the reflectors' focal length. Radiation distribution depends on the geometric relation of the arc of radiation source and reflector.[37] Dong et al show that this aspect is vital in radiation source modeling. Figure 10 presents examples of transverse radiation profiles for solar system simulator—parabolic trough collector: real (a) and ideal (b) in which the radiation source is focused in the focal length of the reflector. The ideal case reflects the possibility of simulating radiation if the light source were an ideal point. In such case, it could be assumed that for the appropriate shape of the reflector and the location of the light source at its focal length, the radiation would take on a direct character. Discharge lamp sources, however, are characterized by a certain arc size with the geometry of the light-emitting element. Therefore, the case described as real in terms of solar simulation device shows that not all of the radiation reflected from the parabolic mirror reaches the absorber surface.

The angle of incidence on the mirror surface has a significant impact on parabolic trough collectors' operation. For the modeled mirror geometry, an absorber with a diameter of 1 in. was assumed. An angle deviation higher

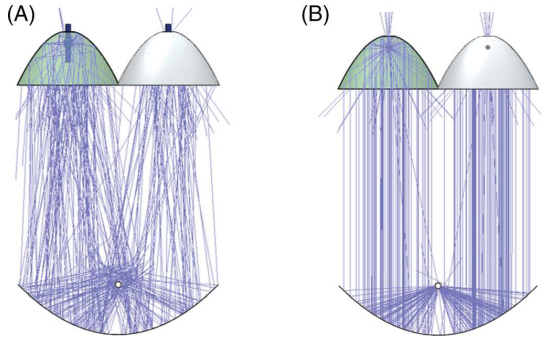

FIGURE 10 Radiation profiles for system solar simulator—parabolic trough collector; (A) real and (B) ideal, in terms of the light source modeling

than 3° caused the scattered reflected radiation and missed the pipe absorber's target. Since the use of lenses is not planned, it can be suspected that the angle of incidence may deviate from the required value. Using the APEX optical software, an analysis was performed to determine how much energy, falling on the parabolic mirror's surface, is reflected and reach the absorber external surface. In the Figure 11, second Y-axis represents the corresponding average intensity values of the concentrated radiation on the absorbers illuminated external surface, considering the constant concentration geometry factor of the parabolic mirror and the absorber of 18.25. For comparison, a system simulating the sun was modeled, where a right angle of incidence of radiation on the absorber surface was assumed. The yellow line (Figure 11) represent the results of this analysis. For modeling purposes, it was assumed that the parabolic mirror is coated with Protected Silver (AG).[35] Modeling was performed for four reflectors with

four xenon arc lamps with a nominal electric power 1600 W each. For the first case, assuming 22 reflectors, the analysis was performed for 22 metal-halides of nominal electric power 200 W each and 22 metal-halides of 400 W. Two cases were considered for metal-halides, a and b. Case a and b mean the efficiency of converting electricity into radiation at the levels of 64% and 22.6%, respectively. The different values of efficiency results from imprecise data in References 21 and spectral analyses[38] delivered to sources, which are mainly relative characteristics. A source efficiency can be determined precisely after performing the spectrometer analysis, which is planned in the tasks related to the construction of the test stand.

The slope of the radiation simulator's characteristics on relation to the slope of the characteristics representing the sun indicates higher compatibility for a system of 22 reflectors. It can be assumed that the more reflectors used to simulate radiation, the higher compatibility. The limit is the size of the sources that do not decrease proportionally to a decrease in rated power. There may be some technical problems with the construction of such a simulator. The use of four reflectors is the least favorable because only about 35% of the energy falling on the parabolic mirror's surface is reflected and reaches the absorber. This is due to the large angle of incidence on the mirror and missing the absorber after the reflection. The first case with 22 metal-halides lamps seems to be more efficient. For a maximum electric power for a system with 400 W reflectors, assuming 22.6% efficiency, the absorber surface receives 639.4 W, at a minimum of 383.9 W, respectively, less for 200 W light bulbs. According to the datasheets, the sources are dimmable down to 40%, maintaining a constant temperature color.

For each case, a distance analysis of the simulator's position relative to the absorber surface was performed. The simulator's distance from the surface of the parabolic mirror was changed from 0.3 to 1.7 m in 0.1 m intervals. For each case, as the simulator distance increases, the total power reaching the tubular absorber decreases. The ranges in which the device operation can be adjusted by changing the power and distance are shown in Figure 12(a) for efficiency of lamp 64% and (b) for 22.6%.

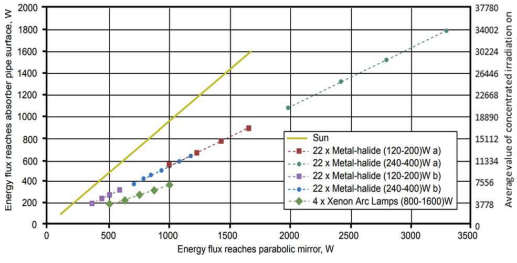

FIGURE 11 Energy flux reaches absorber pipe as function of energy flux reaches the parabolic mirror

4 | INVESTMENT COSTS BALANCE

Apart from the detailed analysis shown above, the planned costs associated with the construction of the radiation simulator were determined. The prices specify

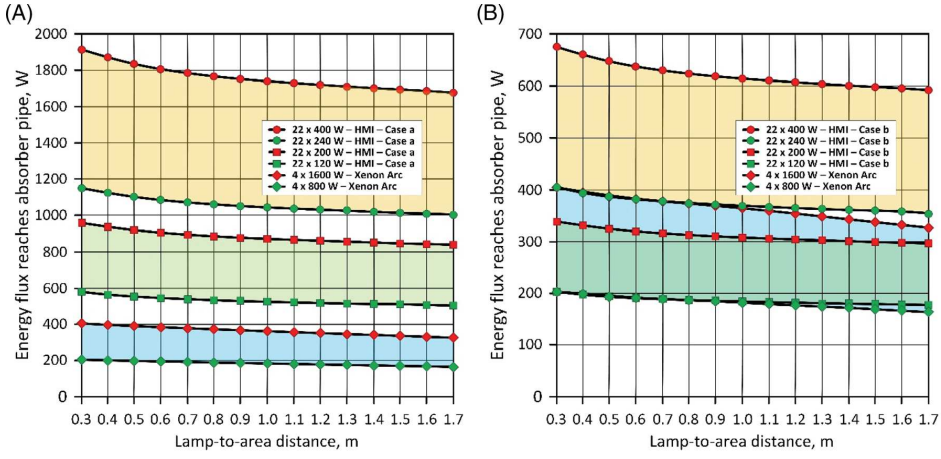

FIGURE 12 Energy flux reaches absorber pipe as a function of lamp-to-area distance: (A) 64% and (B) 22.6%

TABLE 4 Cost of materials for analyzed solar simulators models

Component(s)	Case		
	4 reflectors Cost, €	22 reflectors (200 W) Cost, €	22 reflectors (400 W) Cost, €
Light sources	6400[a]	1630[b]	1770[c]
Parabolic reflectors	2700[d]	8000[e]	8000[e]
Power supply with ignitors	18 000[f]	8600[g]	8600[g]
Cooling fans	360	360	360
Housing	270	270	270
Additional elements	360	360	360
Total	28 090	19 220	19 360

[a]4 × 1600 W xenon arc lamp.
[b]22 × 200 W metal halides lamp.
[c]22 × 400 W metal halides lamp.
[d]4 × Parabolic reflectors with diameter 500 mm.
[e]22 × Parabolic reflectors with diameter 250 mm.
[f]4 × Power supply with ignitors 1600 W.
[g]22 × Power supply with ignitors 550 W.

the range of the total cost related to the construction of the simulator. In Table 4, a list of all essential elements needed for the construction of the solar radiation simulator together with their average costs is presented. Three cases were considered: 4 reflectors with 4 Xenon Arc Lamps 1600 W, 22 reflectors with metal-halides lamps 200 W, and 22 reflectors with metal-halides lamps 400 W. The most cost-effective option is with 22 reflectors and metal-halide lamps. Moreover, there is not much difference between 200 W and 400 W lamps, which suggests choosing the option with more powerful light sources.

5 | CONCLUSIONS

The article presented a new approach for numerical modeling and assessment of a solar simulator for testing parabolic trough collectors. The use of reflectors set on a flat surface for the purpose of testing tubular absorbers was considered. Based on numerical tests indicated by the modified standards approach and the radiation on a flat surface, an analysis of the power delivered to the outer part of the absorber was performed.

Designing and manufacturing a solar radiation simulator is a complex issue. Construction of the simulator that perfectly imitates solar radiation is very challenging. This is related mainly to different, concerning solar radiation, characteristics of light sources, and optical systems (mirrors, lenses). Construction of such a simulator would also involve huge costs, especially when a large area should be illuminated. Simultaneously, depending on the purpose of using the simulator, specific requirements for the parameters of the simulated radiation can be limited. In the case of planned tests of a parabolic radiation concentrator, the most important is to obtain a light beam with the smallest possible angle of incidence and spatial nonuniformity. In the designed simulator, spectral mismatch to all intervals and temporal instability is less critical. Several types of light sources and two variants of reflectors arrangement were analyzed. Calculations and optical modeling have shown that the variant with a larger number of smaller reflectors can reproduce the more homogeneous radiation reaching the collector. The use of a higher number of smaller reflectors with metal-halide sources allows for a higher energy stream reflected from the mirror of the concentrator and reaching the absorber tube. This is mainly due to the shape of the light source with a higher degree of concentration in the reflectors' focal length. Modeling of the radiation simulator allows determining the effect of the distance change of the reflectors system from the collector, on the energy reaching the tubular absorber surface. It can be seen that by changing the headlight system's position, a relatively small change in the energy stream reaching the absorber is obtained. Depending on the analyzed case and the distance of the reflectors from the concentrator's surface, the amount of energy reaching the absorber is different; however, in the case of 22 reflectors, the assumed value of 800 W can be achieved. Therefore, other methods of regulating the intensity of radiation incident on the concentrator should also be used, for example, changing the electric power of light sources or sequentially switching off the light sources in reflectors.

Significant technical and costs advantages of the variant with 22 metal halides reflectors, compared to the variant with four reflectors with xenon arc lamps, suggest choosing this option. Due to the higher energy potential, metal-halides with a higher power (400 W) will be used in the designed test stand.

ACKNOWLEDGEMENT

The scientific work is funded by the National Science Centre within the framework of the research project no. 2018/29/B/ST8/02406.

DATA AVAILABILITY STATEMENT

The data that support the findings of this study are available from the corresponding author upon reasonable request.

ORCID

Łukasz Bartela https://orcid.org/0000-0002-1546-1550
Bartosz Stanek https://orcid.org/0000-0002-4136-4092
Daniel Węcel https://orcid.org/0000-0003-2753-9631
Anna Skorek-Osikowska https://orcid.org/0000-0003-1689-7599

REFERENCES

1. Tapetado P, Usaola J. Capacity credits of wind and solar generation: the Spanish case. *Renew Energy*. 2019;143:164-175.
2. Shubbak MH. Advances in solar photovoltaics: technology review and patent trends. *Renew Sustain Energy Rev*. 2019;115:109383.
3. Renewables 2018. Global Status Report REN21; 2018. ISBN 978-3-9818911-3-3.
4. Sanz-Casado E, Lascurain-Sánchez ML, Serrano-Lopez AE, Larsen B, Ingwersen P. Production, consumption and research on solar energy: the Spanish and German case. *Renew Energy*. 2014;68:733-744.
5. Kalogirou SA. Chapter 3: Solar energy collectors. In: Kalogirou SA, ed. *Solar Energy Engineering*. 2nd ed. Cambridge: Academic Press; 2014:142-145. https://doi.org/10.1016/B978-0-12-397270-5.00003-0.
6. Kalogirou SA. Chapter 10: Solar thermal power systems. In: Kalogirou SA, ed. *Solar Energy Engineering*. 2nd ed. Cambridge: Academic Press; 2014:541-551. https://doi.org/10.1016/B978-0-12-397270-5.00010-8.
7. Kalogirou S, Lloyd S, Ward J. Modelling, optimisation and performance evaluation of a parabolic trough solar collector steam generation system. *Solar Energy*. 1997;60(1):49-59. https://doi.org/10.1016/S0038-092X(96)00131-4.
8. Sivaram PM, Nallusamy N, Suresh M. Experimental and numerical investigation on solar parabolic trough collector integrated with thermal energy storage unit. *Int J Energy Res*. 2016;40:1564-1575. https://doi.org/10.1002/er.3544.
9. Mathioulakis E, Papanicolaou E, Belessiotis V. Optical performance and instantaneous efficiency calculation of linear Fresnel solar collectors. *Int J Energy Res*. 2018;42:1247-1261. https://doi.org/10.1002/er.3925.
10. Bartela Ł, Stanek B, Węcel D. Analysis of production of useful forms of Energy using a solar parabolic trough collectors. Proceedings of the 32nd International Conference on efficiency, cost, optimization, simulation and environmental impact of energy systems; 23–28 June 2019; Wrocław, Poland. pp. 3557-3567. ISBN 978-83-61506-51-5.
11. Al-Nimr MA, Al-Ammari WA. A novel PVT/PTC/ORC solar power system with PV totally immersed in transparent organic fluid. *Int J Energy Res*. 2019;43:4766-4782. https://doi.org/10.1002/er.4615.
12. Pehlivantürk C, Özkan O, Baker DK. Modeling and simulations of a micro solar power system. *Int J Energy Res*. 2014;38:1129-1144. https://doi.org/10.1002/er.3119.
13. Sobek S, Werle S. Solar pyrolysis of waste biomass: part 1 reactor design. *Renew Energy*. 2019;143:1939-1948.
14. Baykara SZ. Experimental solar water thermolysis. *Int J Hydrogen Energy*. 2004;29:1459-1469.
15. Pranesh V, Velraj R, Christopher S, Kumaresan V. A 50 year review of basic and applied research in compound parabolic concentrating solar thermal collector for domestic and industrial applications. *Solar Energy*. 2019;187:293-340.
16. Hamadani BH, Chua K, Roller J, et al. Towards realization of a large-area light-emitting diode-based solar simulator. *Prog. Photovolt Res Appl Ther*. 2013;21:779-789. https://doi.org/10.1002/pip.1231
17. Al-Ahmad AY, Holdsworth J, Vaughan B, et al. Modular LED arrays for large area solar simulation. *Prog Photovolt Res Appl*. 2019;27:179-189. https://doi.org/10.1002/pip.3072.
18. Sabahi H, Tofigh AA, Kakhki IM, Bungypoor-Fard H. Design, construction and performance test of an efficient large-scale solar simulator for investigation of solar thermal collectors. *Sustain Energy Technol Assess*. 2016;15:35-41.
19. Meng Q, Wang Y, Zhang L. Irradiance characteristics and optimization design of a large-scale solar simulator. *Solar Energy*. 2011;85:1758-1767.
20. Ekman BM, Brooks G, Rhamdhani MA. Development of high flux solar simulators for solar thermal research. *Solar Energy Mater Solar Cell*. 2015;141:436-446.
21. Boubault A, Yellowhair J, Ho CK. Design and characterization of a 7.2 kW solar simulator. Proceedings of the ASME 2015 power and energy conversion conference power energy; June 28, 2015-July 2, 2015; California Power Energy; San Diego. p. 49472.
22. Li L, Wang B, Pottas J, Lipiński W. Design of a compound parabolic concentrator for a multi-source high-flux solar simulator. *Solar Energy*. 2019;183:805-811.
23. Jin J, Hao Y, Jin H. A universal solar simulator for focused and quasi-collimated beams. *Appl Energy*. 2019;235:1266-1276.
24. Large Area Solar Simulators, Sciencetech-Inc. Available from http://www.sciencetech-inc.com/all-products/solarsimulators/continuous-solar/large-area-solar-simulators.html. Accessed October 25, 2019.
25. Okuhara Y, Kuroyama T, Tsutsui T, Noritake K, Aoshima T. A solar simulator for the measurement of heat collection efficiency of parabolic trough receivers. *Energy Procedia*. 2015;69:191-1920.
26. Pernpeintner J, Happich C, Lüpfert E, Schiricke B, Lichtenthäler N, Weinhausen J. Linear focus solar simulator

test bench for non-destructive optical efficiency testing of parabolic trough receivers. *Energy Procedia*. 2015;69:518-522.
27. JIS-C8912 Standard: 1998 Solar simulators for crystalline solar cells and modules. Japanese Industrial Standard, Japanese Standard Association.
28. IEC 60904–9 Standard: 2007 Photovoltaics devices–Part 9: Solar simulator performance requirements.
29. ASTM E927-19, Standard classification for solar simulators for electrical performance testing of photovoltaic devices, ASTM International; 2019; West Conshohocken, PA. Available from www.astm.org
30. Tawfik M, Tonnellier X, Sansom C. Light source selection for a solar simulator for thermal applications: a review. *Renew Sustain Energy Rev*. 2018;90:802-813.
31. Esen V, Sağlam Ş, Oral B. Light sources of solar simulators for photovoltaic devices: a review. *Renew Sustain Energy Rev*. 2017; 77:1240-1250. https://doi.org/10.1016/j.rser.2017.03.062.
32. Shu FH. *The Physical Universe: An Introduction to Astronomy*. Sausalito: University Science Books; 1982.
33. Osram. *Metal Halide Lamps Photo Optics: Technology and Application*. Osram Sylvania Inc. Available from https://www.osram.com/
34. Ma Y, Peng S, Long X, et al. Influencing factors of life of high-power linear xenon-filledflash lamp. *Qiangjiguang Yu Lizishu/High Power Laser Part Beams*. 2010;22:2483-2486. https://doi.org/10.3788/HPLPB20102210.2483.
35. Optiforms, Temecula, California, USA. Available from https://www.optiforms.com/
36. APEX. 2019. Breault Research Organization, Inc. Available from http://www.breault.com/
37. Dong X, Nathan GJ, Sun Z, Gu D, Ashman PJ. Concentric multilayer model of the arc in high intensity discharge lamps for solar simulators with experimental validation. *Solar Energy*. 2015;122:293-306.
38. Osram. *Metal Halide Lamps HMI Digital - Product Datasheet*. Osram Sylvania Inc. Available from https://www.osram.com/

How to cite this article: Bartela Ł, Stanek B, Węcel D, Skorek-Osikowska A. A solar simulator numerical modeling for heat absorption phenomenon research in a parabolic trough collector. *Int J Energy Res*. 2022;46:10074–10087. https://doi.org/10.1002/er.6585

Paper II

energies

MDPI

Article

Study of Twisted Tape Inserts Segmental Application in Low-Concentrated Solar Parabolic Trough Collectors

Bartosz Stanek, Jakub Ochmann, Daniel Węcel and Łukasz Bartela *

Department of Power Engineering and Turbomachinery, Silesian University of Technology, 44-100 Gliwice, Poland; bartosz.stanek@polsl.pl (B.S.); jakub.ochmann@polsl.pl (J.O.); daniel.wecel@polsl.pl (D.W.)
* Correspondence: lukasz.bartela@polsl.pl

Abstract: This article presents the results of an analysis of heat enhancement intensification using twisted tapes in linear absorbers for low-concentration parabolic trough collectors, a technology frequently considered as a supplementary energy source for industrial heat production. This contribution proposes a segmented application of different twisted tapes to intensify heat absorption. A 33.7 mm tubular absorber placed in the collector focal point with an aperture of 1.8 m was selected. The temperature range of the heat transfer fluid was chosen at 60–250 °C. The impact of inserts with twisted ratios of 1, 2 and 4 on system operation was analysed using the Ansys Fluent and mathematical model. The models used were validated based on experimental results from a parabolic trough collector with solar simulator test bench. The results indicated that for the range of mass flow between 0.15–0.3 kg/s, the most optimal is applying twisted ratio 1, except for the highest-temperature section. In this section, it is more optimal to use an insert with a twisted ratio 2, due to the lower need for pumping and the higher efficiency increment. The long-term analysis for the case study plant indicated that the proposed approach increased power gain by 0.27%.

Keywords: twisted tape; parabolic trough collectors; industrial heat; heat enhancement; numerical analysis

Citation: Stanek, B.; Ochmann, J.; Węcel, D.; Bartela, Ł. Study of Twisted Tape Inserts Segmental Application in Low-Concentrated Solar Parabolic Trough Collectors. *Energies* **2023**, *16*, 3716. https://doi.org/10.3390/en16093716

Academic Editor: Gianpiero Colangelo

Received: 8 March 2023
Revised: 21 April 2023
Accepted: 24 April 2023
Published: 26 April 2023

1. Introduction

Increasing the share of renewable energy in heat generation is key to minimising the carbon footprint and increasing energy independence and security. To achieve these objectives, mature installations originally designed as large-scale power generation facilities such as parabolic trough collectors are scaled down and used in distributed energy installations [1]. It is becoming increasingly common to use low-concentration parabolic trough collectors (PTC) to produce heat for a wide range of applications, primarily in areas with high solar insulation [2,3]. The potential for heat utilisation is presented in recent International Energy Agency (IEA) and International Renewable Energy Agency (IRENA) reports, where it was shown that 74% of the energy consumed by industry is in the form of heat and 52% is in the temperature range corresponding to solar installations, among other PTCs [4–6].

Heat in the temperature range up to 400 °C can be used, for example, in the food, processing and pharmaceutical industries. An example is the parabolic trough installation in Spain, where heat up to 250 °C is used for processing and preserving fruit and vegetables [7]. In Germany, the heat generated in a facility with an installed collector area of 108 m^2 is used for the manufacture of fabricated metal products [8,9]. Solar heat is used for the production of steam. The installation in Switzerland uses heat up to 190 °C in milk processing and the installation in Mexico is used for pasteurisation [8,10,11].

The determining factors for the use of such installations are primarily weather conditions and the cost and payback period of the investment. Both of these factors are strongly

connected, which is the reason why, based on the available data, it is noticeable that installations are distributed in areas with high average annual solar radiation [12]. To promote this technology to less solar-rich areas, it is necessary to improve its efficiency and reduce costs.

In the case of price reduction, the costs associated with the material depend on the market, but over the years, using full-scale solutions as an example, several studies and analyses have led to cost reductions of 68% from USD 0.340/kWh in 2010 to USD 0.108/kWh in 2020 [13]. A strong influence on the price was the structure, which must be durable enough to carry the weight of the parabolic trough collector and be able to move to follow the sun's position. Gharat et al. [14] presented the development of tracker installations and designs for PTC. For less concentrated PTCs, the technical solutions can be much simpler and still maintain a high quality of solar tracking. Despite their smaller size, optical systems where the main component is a highly reflective metal sheet can be vulnerable to wind gusts [15]. For a low-concentrated PTC with an aperture of 1 m, it was shown that the maximum angle to which the tracker can deflect without affecting the power reduction delivered to the absorber is 1.5° [16]. To prevent scattering of the concentrated radiation, Rodriguez-Sanchez et al. [17] proposed the use of a second mirror to re-concentrate the radiation on the surface of the tube if the tracking system is not accurate or is strongly susceptible to wind. Another example of cost reduction is not using vacuum covers for low-temperature installations or sections of absorbers where the temperature is low. This results in higher losses, but significantly reduces the investment and weight of the installation. Concentrating solar power (CSP) installations are optical systems which, depending on the environment in which they operate, can be affected by dust and other contaminants that settle on the surface of highly reflective elements. An example of the reduction in costs associated with periodic maintenance can be found in the solution proposed by Absolicon in its T160 product. Instead of a tubular glass envelope, it uses a simple glass plate covering the entire parabolic reflector including the absorber, which significantly improves periodic maintenance [18].

A significant proportion of the price of the absorber is represented by a highly absorptive coating, usually a selective one, which is designed to increase the absorption of radiation as well as reduce energy emission through its selective nature. Noč et al. [19] summarised a selection of developed selective coatings detailing their parameters and production technology. Zhao et al. [20] proposed the cascade arrangement of different coatings, optimising their positioning by varying their emissivity with temperature. The results showed a reduction in heat loss of 29.3% and an increase in thermal efficiency of 4.3%. Selective coatings usually require a multi-step process such as chemical vapour deposition (CVD), physical vapour deposition (PVD) or atomic layer deposition (ALD), which are expensive and require sophisticated equipment. In low-concentration PTC installations, non-selective coatings can be used in the initial low-temperature sections, but with a very high level of absorptivity, such as the Pyromark known in solar towers. For certain sections, the high absorptivity compensates for the increased emission losses and the use of a non-selective coating can reduce the investment outlay, as demonstrated in [21].

A method often investigated to increase the heat collection inside the absorber is the use of different types of inserts. Research is being conducted on fins, porous inserts, wire coils, rings, cylindrical/rods, helical axial fins and twisted tapes [22,23]. Heat transfer mediums such as molten salt, thermal oils, water, air and other gases are analysed. In general, using inserts enhances the thermal performance of parabolic trough collectors and increases pressure drop in absorbers.

The biggest challenge is proving to be the application of the various types of inserts inside the absorber and optimising their position considering all parameters. According to Allam et al. [22], fin inserts achieve an optimum thermal and hydraulic performance. Bellos et al. [24,25] also showed that fin inserts showed the highest average efficiency gain, which was 0.7% for the vacuum tube and 1.3% for the non-vacuum tube. The challenge, however, proves to be the cost of manufacturing such an absorber, where instead of a traditional mass-produced tube, the relevant components have to be specially

manufactured, which dramatically increases the required production time and requires the use of supplementary equipment. Looking globally, in this case, the required process can be much more energy-consuming than the benefits of increased heat collection.

Twisted tapes, which are characterised by a simple and fast production process, may represent an opportunity. Furthermore, twisted tapes are used in industry, so their low price can be just as significant an argument as the efficiency gains. Jaramillo et al. [26] stated that twisted tape inserts are a good passive way to augment the heat transfer in PTC. Varun et al. [27] showed a very strong research interest in twisted tape inserts for different flow conditions and configurations. Both traditional twisted tapes and twisted tapes with a wire coil, dual twisted tapes or perforated twisted tapes are analysed in [28–32]. Veera Kumar et al. [33] analysed Loose-Fit Perforated Twisted Tape and reported the peak thermal performance of 62.33%.

The majority of studies in the literature make use of certain simplifications which introduce a significant error when considering their application in linear absorbers. In numerical studies, the most common simplification is to assume a homogeneous distribution of heat flux around the absorber's circumference or to specify a homogeneous wall temperature, which completely misrepresents the heat flow in this device and also the effect of twisted tapes on its efficiency. The vast majority of the studies related to linear absorbers concern full-scale PTCs, for example with a PTR® or LS-2 absorber, where the boundary conditions differ significantly from those in a low-concentrated parabolic trough, so the correlations reported in these studies cannot be applied to the case under consideration. Furthermore, there is still a deficit of reports in the literature regarding the application of such solutions for solar loops, showing the real impact of inserts on plant operation.

Therefore, in this work, a comprehensive analysis is presented where, for a parabolic trough collector geometry compatible with an industrial system, a series of numerical tests were carried out demonstrating their real impact on linear absorber efficiency. The work also presents experimental validation based on studies obtained by using a solar radiation simulator along with a parabolic trough collector. The major novelty in this work is to study and propose a segmented arrangement of twisted tapes in linear absorbers and to determine their effect on the absorber loop, reflecting the parameters of a heat-generating plant for industrial installations.

2. Methods

This article presents a strategy for a segmental application of flow turbulence inserts in a solar absorber loop for low-concentrated parabolic trough collectors. The use of twisted tapes with different twisted ratios is aimed at intensifying heat absorption while simultaneously searching for the solution that generates the smallest pressure drop. This research is divided into 5 steps, presented in Figure 1.

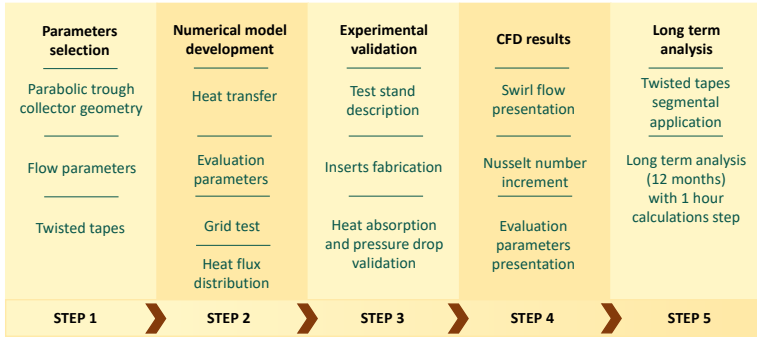

Figure 1. Methodology flow chart.

The first step is to select the right geometrical parameters of analysed technology and flow parameters as well as twisted tapes. Second is the development of a parabolic trough numerical model. Third is numerical model validation. The next step is numerical results presentation and the last one is application of these results to a mathematical model to perform a long-term analysis.

Figure 2 shows the potential application of turbulent inserts of different twisted ratios for particular segments of the absorber loop.

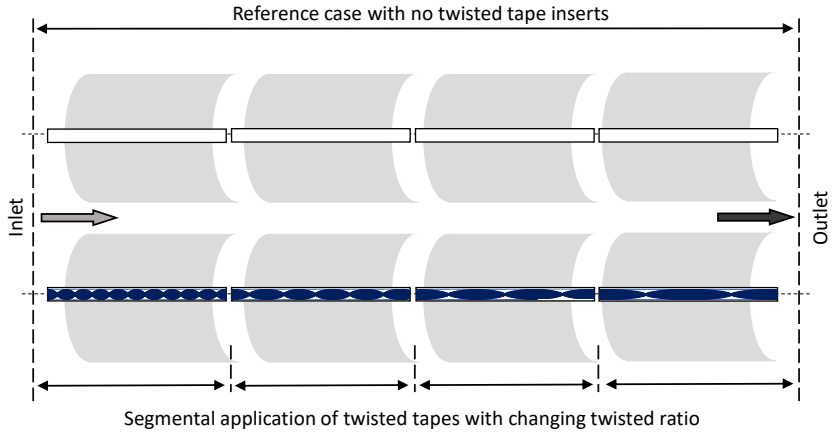

Figure 2. Strategy of twisted tape segmental application in PTC loop.

Twisted tapes are components made by twisting a flat strip, usually steel, causing a given number of turns per length. An illustrative visualisation of the twisted tape built into the linear absorber, along with the marking of the geometric characteristics, is shown in Figure 3. A twisted ratio is defined as [34]:

$$\mathrm{Tr} = \frac{H}{d_{\mathrm{abs,i}}}, \tag{1}$$

where H is the length equivalent to 180° turn and $d_{\mathrm{abs,i}}$ is the internal diameter of the absorber. In the case studied, inserts with twisted ratios of 1, 2 and 4 were considered. Parameter $2H$ defines the full rotation of the twisted tape insert. The second parameter that defines the insert is the width ratio, which is defined as [35]:

$$\mathrm{Wr} = \frac{W}{d_{\mathrm{abs,i}}}, \tag{2}$$

where W is the width of a twisted tape. One width ratio configuration of 0.9 was considered in this analysis. For each case, the thickness of the insert was 1 mm. For the purpose of the analysis, the insert was assumed to be placed directly on the axis of the absorber.

The analysis was performed for a parabolic trough collector; the geometric dimensions and optical parameters are summarised in Table 1, which reflects the parameters of the PolyTrough 1800 [36]. A linear absorber made of steel is surrounded by a glass envelope, with very low pressure close to the vacuum in between. The studies were conducted for three mass flow rates of 0.15 kg/s, 0.225 kg/s and 0.3 kg/s and five inlet temperatures of heat transfer fluid: 60 °C, 100 °C, 140 °C, 200 °C and 250 °C, which corresponds to a large percentage of installations with low-concentrated parabolic trough collectors [12]. The radiation delivered to the absorber is described in detail later in this section. The parameters of the selective coating used for the analysis correspond to the TiC-TiN/Al_2O_3 coating [37]. Therminol VP-1 was chosen as the heat transfer fluid. The selected fluid is an Eastman product, widely used in parabolic trough collector installations. The composition of the fluid is a eutectic biphenyl/diphenyl oxide mixture, where the operating temperature is

12–400 °C. Table 2 shows the parameters of Therminol VP-1 as a function of its temperature, based on the manufacturer's data [38].

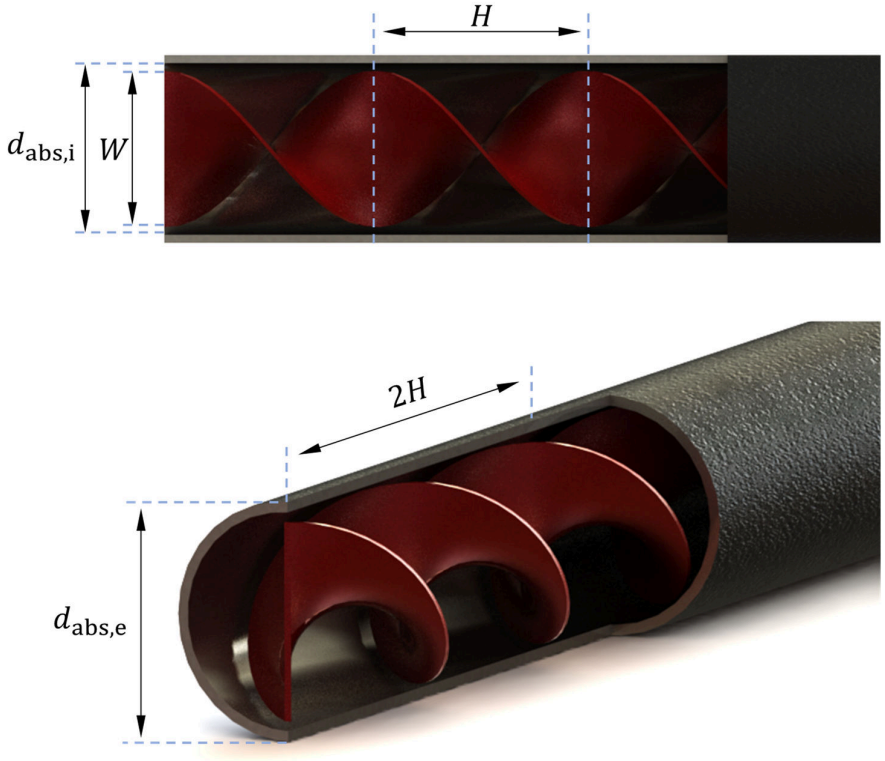

Figure 3. Linear absorber with twisted tape insert.

Table 1. Geometrical and optical parameters of analysed parabolic trough collector.

Parameter	Symbol	Value	Unit
Focal length	fl	647	mm
Aperture width	W_{ap}	1800	mm
Absorber length	L_{abs}	1000	mm
Absorber external diameter	$d_{abs,e}$	33.7	mm
Absorber internal diameter	$d_{abs,i}$	30.7	mm
Absorber wall thickness	th_{abs}	1.5	mm
Absorber thermal conductivity	λ_{abs}	15	W/mK
Glass env. external diameter	$d_{c,e}$	56	mm
Glass env. internal diameter	$d_{c,i}$	51	mm
Glass env. wall thickness	th_c	2.5	mm
Glass env. thermal conductivity	λ_c	1.1	W/mK
Transmittance of glass envelope	τ_c	0.96	-
Clean mirror reflectance	η_{ref}	0.9	-
Dirt factor	η_{dirt}	0.97	-
Absorber absorptivity	α_{abs}	0.92	-
Absorber emissivity	ε_{abs}	0.11	-

Later in this section, the heat flow in the parabolic trough collector is briefly described, compiling the main equations and evaluation parameters. The next section describes the numerical studies and the assumptions and boundary conditions. The long-term analysis

presented in the article section uses a previously developed mathematical model. A detailed description of the model and its validation has been presented in previous analyses [21].

Table 2. Heat transfer fluid parameters Therminol VP-1 [38].

Parameter	Symbol	Correlation	Unit
Specific heat	c_p	2.7137·T + 761.88	J/(kg·K)
Thermal conductivity	k	$-1.36 \cdot 10^{-4}$·T + 0.1773	W/(m·K)
Dynamic viscosity	μ	$250{,}568{,}541 \cdot T^{-4.407}$	Pa·s
Density	ρ	−0.856·T + 1316	kg/m^3

2.1. Heat Transfer in Parabolic Trough Collector

The parabolic trough collector is a device that utilises solar direct radiation. The use of a tracking system to follow the sun during the operation period is required for proper operation [39]. Direct radiation is reflected from the parabolic shape mirror and concentrated on the outer surface of the absorber tube. A linear absorber with a circular cross-section is placed in the focus of the collector. Multiplied reflected radiation results in a non-uniform distribution of radiation on its outer surface. Radiation directly delivered to the external surface from the side facing the sun also reaches the absorber. In most cases, the heat delivered in this way represents a low proportion of the total power input. Still, when analysing parabolic low-concentration devices, this heat represents a noticeable proportion and must be considered. The heat flow model and thermal resistance for the receiver cross-section are shown in Figure 4. Heat flow in the receiver assumes convection between the inner absorber wall and heat transfer fluid, conduction through the absorber, radiation loss between the external absorber surface and internal glass envelope surface, conduction through the glass envelope, convection loss between the external glass surface and ambient and radiation losses between the external glass envelope surface and sky. In the case studied an ideal vacuum was assumed between the external absorber surface and the glass envelope.

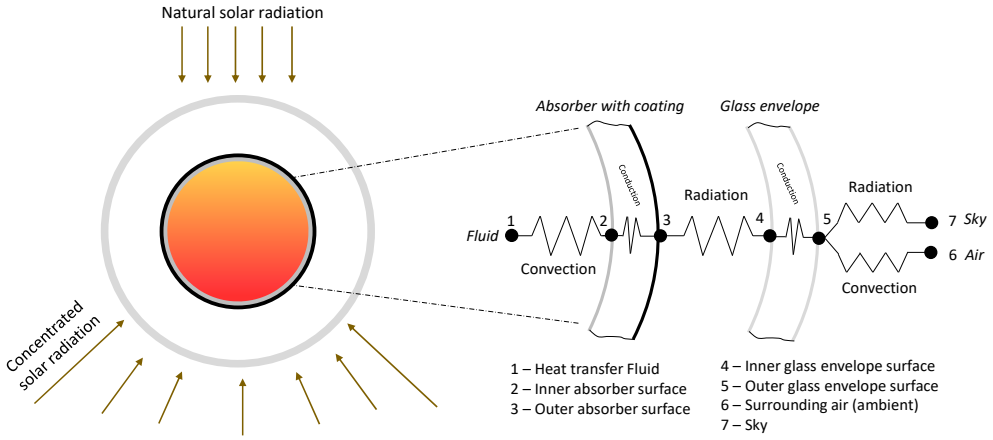

Figure 4. Heat transfer in linear absorbers.

The following equations present the main heat flow correlations of the analysed installation. The useful heat absorbed by the thermal fluid is calculated as Equation (3) according to [40]:

$$Q_u = \dot{m} \cdot c_p (T_{out} - T_{in}), \quad (3)$$

where Q_u is the useful thermal energy collected by heat transfer fluid, $\dot{m}$ is the mass flow of circulating fluid, c_p is the specific heat and $T_{out} - T_{in}$ is the difference between outlet and inlet temperature.

The heat flux can be also presented as a difference between solar energy reaching the absorber and heat losses (convection and radiation) [41].

$$Q_u = [(A_{ap} - d_{abs,e} \cdot L) \cdot G_B \cdot \eta_{opt,CSP} \cdot \cos\theta \cdot IAM] + [(d_{abs,e} \cdot L) \cdot G_B \cdot \eta_{opt,SP}] - Q_{loss}, \quad (4)$$

where A_{ap} is the aperture surface area, $d_{abs,e}$ is the absorber external diameter, G_B is the direct solar irradiance, $\eta_{opt,CSP}$ is the optical efficiency for CSP, θ is the incident angle, IAM is the incidence angle modifier, L is absorber length and $\eta_{opt,SP}$ is the optical efficiency for solar power. The equation was used as a boundary condition in a CFD simulation in the twisted tape area.

This approach separates the concentrated and non-concentrated radiation that is delivered to the absorber surface. The optical efficiency is therefore divided into two parts, relating to the corresponding path through which the radiation passes on its way from the sun to the absorber surface. A full description of our proposed model, detailing the individual components, has been presented in our previous publications and, to maintain the conciseness of the results from that study, is not repeated here [21].

Total solar energy received by a PTC installation is defined as Equation (5) [42]:

$$Q_s = A_{ap} \cdot G_B. \quad (5)$$

The efficiency of the parabolic trough should consider both the heat absorbed by the linear absorber and the power required to drive the heat transfer fluid pump. For this purpose, Equation (6) was presented as follows [25,43]:

$$\eta_{PTC} = \frac{Q_u - \frac{W_p}{\eta_{el}}}{Q_s} \quad (6)$$

where η_{PTC} is parabolic trough collector efficiency, W_p is the required pump power and η_{el} is the reference electricity production efficiency. For purposes of this analysis, the value 32.7% is selected [44].

The pumping work demand for the fluid movement is calculated as [25]:

$$W_p = \frac{\dot{m} \cdot \Delta P}{\rho} \quad (7)$$

where ΔP is pressure drop and ρ is the density of fluid.

The pressure drop can be calculated using the friction factor and Darcy–Weisbach equation:

$$\Delta P = f \cdot \frac{L}{d_{abs,\,i}} \cdot \left(\frac{1}{2} \cdot \rho \cdot u^2\right), \quad (8)$$

where f is friction factor and u is fluid velocity.

For smooth absorber the value of friction factor can be used by Petukhov's correlation [45]:

$$f = (0.79 \ln Re - 1.64)^{-2}. \quad (9)$$

The average Nusselt number is given according to Gnielinski's correlation, which is valid for low and high Reynolds numbers [46]:

$$Nu = \frac{(f/8)(Re - 1000)Pr}{1 + 12.7(f/8)^{0.5}\left(Pr^{2/3} - 1\right)}, \quad (10)$$

where Pr is Prandtl number.

For evaluation of thermal performance at constant pumping, *PEC* (performance evaluation criterion) coefficient was used [47]:

$$PEC = \frac{\left(\frac{Nu}{Nu_{\text{ref}}}\right)}{\left(\frac{f}{f_{\text{ref}}}\right)^{\frac{1}{3}}} \tag{11}$$

PEC index is a flow criterion which evaluates the heat transfer coefficient enhancement increase under the equivalent conditions of same pumping work demand.

2.2. CFD Model

Numerical calculations were performed with Ansys Fluent 19.2 using a discretised 3D domain [48]. In the case of a PTC with a twisted tape, it is not possible to apply domain optimisation techniques using, for example, the AxiSymmetric 2D feature, due to the non-axisymmetric design of the studied structure. The research was performed at a steady state and turbulent flow is modelled by the Reynold averaged Navier–Stokes (RANS) equations [49]. A pressure-based solver was used, and the governing equations of mass (12) and momentum (13) were defined as follows [50]:

$$\frac{\partial \rho}{\partial t} + \nabla \cdot \left(\rho \vec{u}\right) = 0, \tag{12}$$

$$\frac{\partial \rho U_i}{\partial t} + \frac{\partial}{\partial x_j}\left(\rho U_i U_j\right) = -\frac{\partial p}{\partial x_i} + \frac{\partial}{\partial x_j}\left[\mu_e \left(\frac{\partial U_i}{\partial x_j} + \frac{\partial U_j}{\partial x_i}\right)\right] \tag{13}$$

where μ_e is the effective viscosity defined as the sum of the molecular viscosity μ and the turbulent viscosity μ_t according to the formula:

$$\mu_e = \mu + \mu_t \tag{14}$$

CFD (computational fluid dynamics) calculations are carried out in the fluid region of the absorber, in which there is forced fluid flow between the inlet and outlet boundaries at a given mass flow rate and inlet temperature. The process of heating the fluid occurs as a result of the external heat flux, the value of which depends on the position of the wall point (x,y) in the plane normal to the inlet plane. The heat flux was implemented using the User Defined Function (UDF) [51]. The twisted tape along the entire length of the absorber is an area inert to the flowing fluid and is not involved in any heat transfer process. The energy conservation equation is defined as:

$$\frac{\partial \rho h_{tot}}{\partial t} - \frac{\partial p}{\partial t} + \frac{\partial}{\partial x_j}\left(\rho U_j h_{tot}\right) = \frac{\partial}{\partial x_j}\left(\lambda \frac{\partial T}{\partial x_j} - \frac{\mu_t}{Pr_t}\frac{\partial h}{\partial x_j}\right) + \frac{\partial}{\partial x_j}\left[U_i\left(\tau_{ij} - \rho\overline{u_i u_j}\right)\right] \tag{15}$$

Cabello et al. [52] performed an extensive analysis of different turbulence models and their impact on modelling flow and heat transfer in a PTC with a twisted tape. The authors showed that the accuracy of individual turbulence models varies with the values of Reynolds (*Re*) and Twisted ratio (*Tr*). They also proved that the k-ω SST model simulates the desired phenomena with high accuracy in the range of $Re > 17{,}000$ and $Tr \leq 4$. Due to the study of *Tr* in the range of ≤4 and the expected relatively high ranges of the *Re* number, it was decided within the scope of this article that the k-ω SST turbulence model would be used [53]. The basic equations for turbulence kinetic energy k and specific rate of dissipation ω are defined according to relations (15) and (16) [54,55]:

$$\frac{\partial \rho k}{\partial t} + \frac{\partial \rho U_j k}{\partial x_j} = G_k - \beta' \rho \omega k + \frac{\partial}{\partial x_j}\left(\left(\mu + \frac{\mu_t}{\sigma_k}\right)\frac{\partial k}{\partial x_j}\right) \tag{16}$$

$$\frac{\partial p\omega}{\partial t} + \frac{\partial pU_j\omega}{\partial x_j} = \alpha_3 \frac{\omega}{k} G_\omega - \beta\rho\omega^2 + \frac{\partial}{\partial x_j}\left(\left(\mu + \frac{\mu_t}{\sigma_\omega}\right)\frac{\partial \omega}{\partial x_j}\right) + (1 - F_1)2p\frac{1}{\sigma_{\omega 2}\omega}\frac{\partial k}{\partial x_j}\frac{\partial \omega}{\partial x_j} \quad (17)$$

The inlet boundary condition included the mass flux of the Therminol and its temperature. The mass flux $\dot{m}$ is expressed by the formula:

$$\dot{m} = \rho \cdot u \cdot A \quad (18)$$

where A is the inlet cross-sectional area. Therminol parameters were calculated from the material data shown in Table 2, which were implemented into the numerical model. The flux and inlet temperature variables for the validation of the numerical model with experimental data were implemented as external data arrays.

The computational domain was divided into subareas to optimise the numerical grid. The sub-area covering the occurrence of a twisted tape was covered by additional compaction of the elements of the numerical grid, especially around the edges of the tape. An inflation layer was generated along the entire length of the numerical model. In addition, the inlet area in front of the twisted tape was modelled to achieve fully developed fluid flow. This area was not subject to the presence of an external heat flux applied to the external surface of the model. An example of a numerical grid is presented in Figure 5.

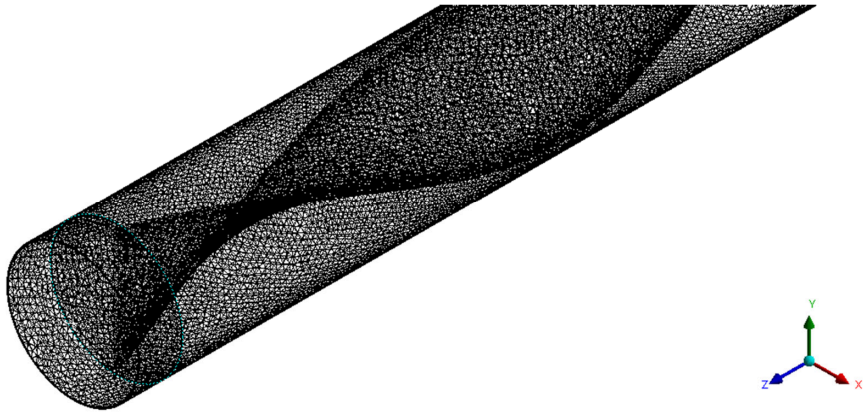

Figure 5. Sample of mesh of the absorber tube used in this study.

A grid independence test was performed, during which the degree of influence of the quality of the numerical grid on the results obtained was investigated. Table 3 presents the details of the studied numerical grids.

Table 3. Analysed numerical grids.

No.	Number of Elements	Number of Nodes
1	244,283	83,908
2	1,320,067	407,364
3	1,933,627	557,723
4	2,337,226	649,766
5	3,076,697	807,738

Figure 6 shows a comparison of the results of PTC parameter calculations with a twisted tape for different numerical grids under the same boundary conditions. The values of the Nusselt number and friction factor were determined using Equations (8) and (9).

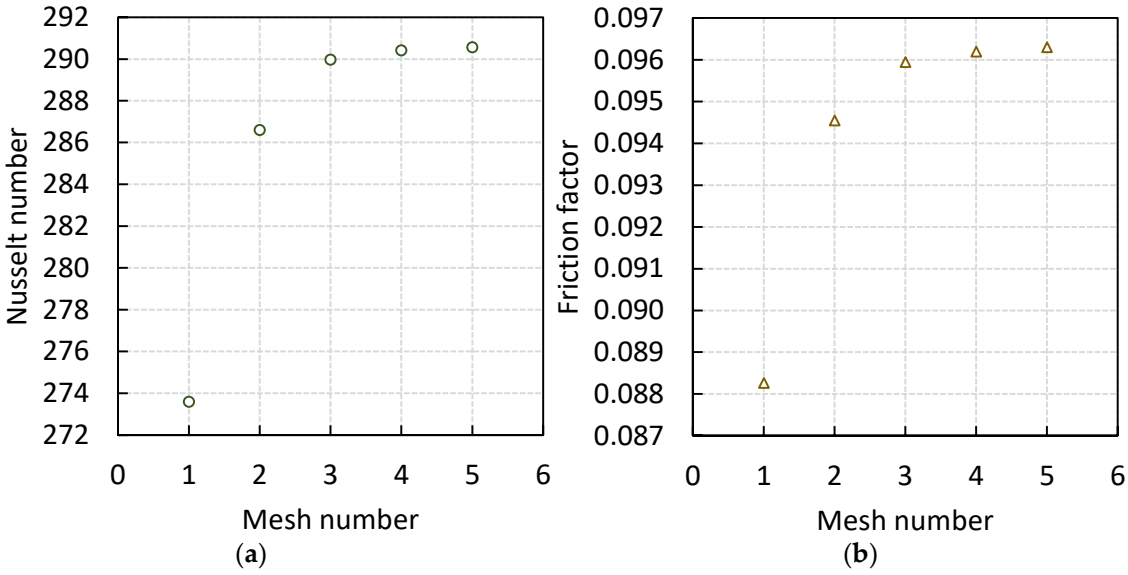

Figure 6. Mesh test for: (**a**) Nusselt number and (**b**) friction factor.

It was shown that, as the number of elements and nodes of the numerical grid increases, there is an asymptotic increase in the values of the calculated parameters. The largest deviation from the limit of the result was recorded for grid 1 (about 6% for *Nu* values). Between grids 3 and 5 there were no significant differences in the results, with a difference of about 0.2% for the *Nu* value. Both the residuals and the parameters monitored during the calculation were taken as the convergence criterion. The moment when the difference between successive results of the average temperature of the fluid at the outlet did not exceed a specific value was taken as the steady state. The same range of values is applied to the parameter of pressure drop along the length of the twisted tape in the absorber. As the number of numerical grid elements increased, the time to achieve the expected convergence of steady-state calculations noticeably increased. Therefore, it was decided that grid number 4 was optimal in terms of the accuracy of the results obtained and the time required to carry out a single series of calculations. The selected numerical grid has an average skewness value of about 0.21 with a maximum skewness not exceeding 0.5, indicating the very good quality of the numerical grid elements providing satisfactory accuracy of numerical calculations. The inflation layer cell of this mesh has a height of 0.05 mm (with a maximum of 10 inflation layer elements), and the value of the y+ parameter is ~1.6, which is the respected value for the turbulent flow model used [56]. The numerical grid was used at the stage of validation of the mathematical model with experimental data.

The heat flux supplied to the linear circular absorber was determined using the optical-engineering software APEX [57]. This numerical software allows tracking of the simulated rays and analysis of the illuminated surface, considering the individual components of the system and their optical properties [58]. The software enables the calculation of the radiation distribution and power analysis of a selected surface, including parameters such as shape, reflectivity, absorptivity, surface roughness and coating. The software adopts a Monte Carlo ray tracing method [59,60]. The tool was selected based on its commercial maturity, cooperation with Solid Works software and satisfactory accuracy. The selected ray tracing method is also frequently used in the modelling of solar radiation simulators [61–63]. In the MCRT method, the Bidirectional Reflectance Distribution Function (*BRDF*) is used to describe the reflected beam behaviour [64]. This method tracks the energy of each simulated ray and calculates the total flux as well as its distribution. The *BRDF* describes the form in

which light incident on a given surface is scattered. The BRDF function is defined as the scattered radiance per unit incident irradiance and is described by Equation (19) [65].

$$BRDF(\theta_i, \Phi_i, \theta_r, \Phi_r) = \frac{dL_r(\theta_r, \Phi_r)}{dE_i(\theta_i, \Phi_i)} \quad (19)$$

where $dL_r(\theta_r, \Phi_r)$ is the unit of radiant energy per unit of solid angle (W/m^2sr); the irradiance $dE_i(\theta_i, \Phi_i)$ is the incident power flux density per unit area (W/m^2). The angles θ_i, Φ_i, θ_r and Φ_r are the polar and azimuth incident angles and polar and azimuth reflected angles, respectively.

A numerical model of the respective solution is shown in Figure 7. The model includes a parabolic mirror with assumed reflectivity, a tubular absorber made of steel and coated with a selective coating, and a glass envelope with given transmittance. The calculations were performed by modelling direct normal radiation. Sun model was used as a radiation source, which included the solar half angle $\theta_s = 0.27°$. Figure 7a shows the radiation distribution on the outer surface of the absorber, along with the marked angle used in previously mentioned UDF. The radiation distribution is an input to the numerical model. Figure 7b shows the simulated rays and their reflection from the surface of the parabolic shape mirror. Rays number used in each model was $2 \cdot 10^8$ which provided highly accurate results which were presented in the previous publication [16].

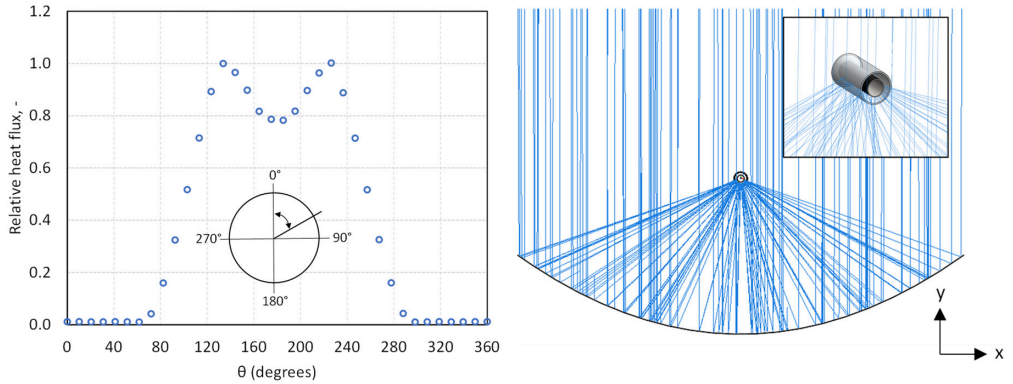

Figure 7. Concentrated irradiance on absorber pipe external surface: (**a**) relative heat flux for different position on perimeter of absorber and (**b**) visualisation of concentration process in PTC.

3. Results and Discussion

3.1. Model Validation with Experimental Research

Validation of the numerical model was carried out using the laboratory test stand shown in Figure 8. The bench consists of two main components, a solar radiation simulator and a parabolic trough collector [66]. The simulator consists of 18 metal halide lamps (HMI), 575 W each, with the possibility of reducing the power to 60% of the nominal value. The variable distance of the light source from the reflector allows for a changing character of radiation, from diffuse to direct. Furthermore, lenses are fitted to the reflectors to collimate the radiation to ensure that the rays are as similar to natural radiation. The system is air-cooled so that the impact of heat from the source on the ambient temperature can be reduced. The construction of the solar radiation simulator stand was preceded by a series of numerical analyses, based on the Monte Carlo ray tracing method and optimisation of their location [61,67]. The optical numerical model was experimentally validated and the results indicated high agreement.

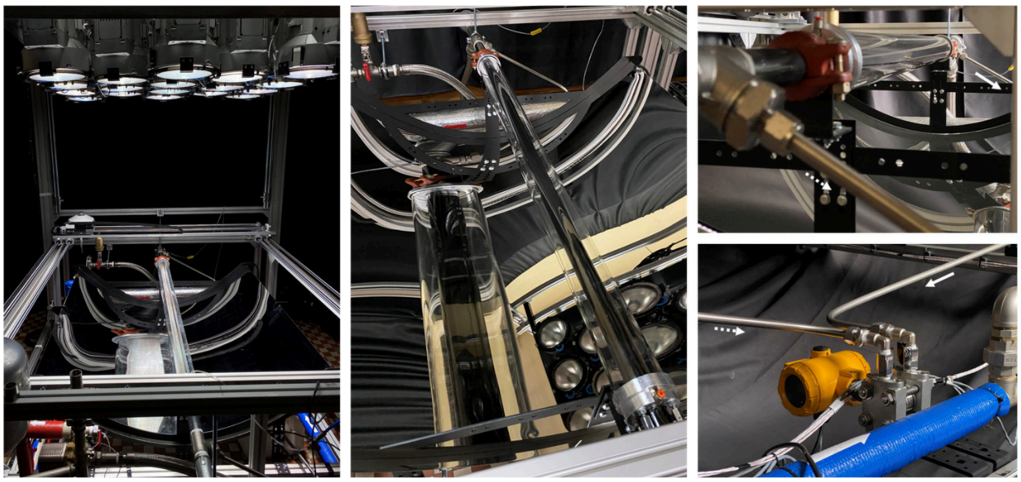

(**a**) (**b**) (**c**)

Figure 8. Experimental bench: (**a**) solar simulator and parabolic trough collector, (**b**) linear absorber placed in parabolic trough focal length, (**c**) pressure drop meter and its connections before and after linear absorber.

The second component of the stand is a parabolic trough collector with a low concentration ratio. It consists of a parabolic mirror and a linear absorber located at its focal length, which is presented in Figure 8b. The mirror with an aperture of 1 m and a length of 1 m is made of highly reflective sheet metal. The linear absorber, with an external diameter of 33.7 mm, is made of mild steel and coated with the highly-absorptive Pyromark coating, often used in various solar installations [68]. The absorber is located in a glass envelope made of borosilicate glass and connected by two brackets, at the beginning and the end of the absorber. A low pressure, close to vacuum, is maintained between the steel tube and the glass envelope to reduce heat loss. The value of the simulated radiation is measured using a pyranometer and a heat flux meter (at the focus of the parabolic mirror). The heat-transfer medium is Therminol VP-1. The quantities measured on the solar loop side are the temperature increment with K-type thermocouples, the volumetric flow and the pressure by the differential pressure sensor, shown in Figure 8c, which is crucial in assessing the use of turbulence inserts as it measures the pressure drop in the absorber pipe.

For experimental validation, tests were carried out for three cases. The first one was for the plane absorber, the second for the absorber with twisted tape where the twisted ratio was 7.6 and the third was for the absorber and twisted tape with a twisted ratio 3.8. The twisted tapes inserts were fabricated using 3D printing technology, from a PETG (polyethylene terephthalate glycol) material that had previously been selected from many others as the most durable for Therminol VP-1. However, it needs to be noted that inserts made of this material cannot be used in long-term analyses or for industrial applications. It is necessary to manufacture them in steel, but at this stage of the analysis, 3D printing, characterised by high accuracy, was used to perform fundamental tests. The inserts were printed in sections of 190 mm and then joined on a 4 mm diameter threaded rod to keep the insert stable. The total length of the twisted tape was 950 mm. Then, with the support of appropriate adapters, the insert was placed inside the absorber in such a way that it was positioned as close to the centreline as possible. The analysed inserts are shown in Figure 9.

Following an analogy with other studies using CFD presented in this article, models were made based on the geometry of the inserts used for the experimental analysis. The first parameter validated was the pressure drop as a function of flow. The pressure drop was measured using an Aplisens APR-2000 ALW (Aplisens S.A., Katowice, Poland) pressure drop sensor with a base error of 0.075% and a base range of −2.5 kPa–2.5 kPa. A Kobold

DON-215HR33H0M0 (KOBOLD Instruments, Warsaw, Poland) flow meter sensor with accuracy reported by the manufacturer 1% was used for flow measurement. The results are shown in Figure 10, where the pressure drop for the three cases is presented as a function of mass flow, determined from the volume flow from the flow meter and temperature. For all cases, the tests were carried out at constant temperatures and with the radiation simulator off. The same boundary conditions were maintained for the CFD study. Experimental measurements were made for each point separately, where a series of measurements were carried out for stable conditions. Based on the accuracy of the measuring devices, a measurement uncertainty analysis was carried out for each measurement. A-type and B-type uncertainties were determined, as well as the compound uncertainty according to the guide uncertainty measurement (GUM) [69]. The results are shown as uncertainty bars in Figure 10.

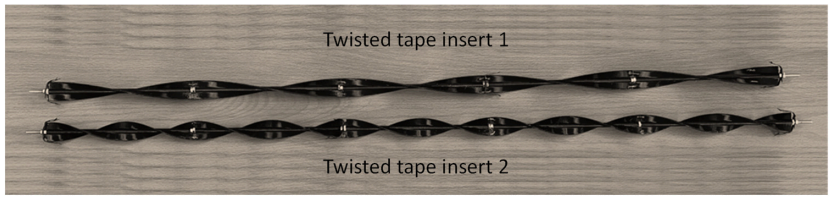

Figure 9. Twisted tape inserts used for model validation.

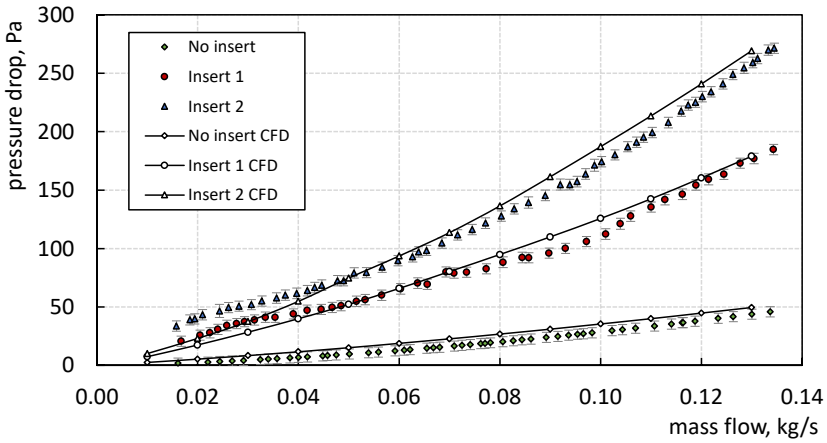

Figure 10. Experimental validation of CFD model for pressure drop as a function of mass flow.

The results obtained show a high correlation and agreement between the numerical model and the experimental tests. Despite some deviations from the curve obtained in the CFD studies, it should be noted that the shapes of the curves are consistent with the characteristics obtained in the measurement. In the numerical model, the tube joints and impulse pipe connections that occur in the actual stand were not considered. In addition, during the tests, air bubbles may have appeared in the actual bench which could have disturbed the measurement. Another factor affecting the differential pressure sensor was the vibrations accompanying the pump operation. It was noted that, for higher flows, the differential pressure sensor reacted to the vibrations accompanying the stand.

Validation of the temperature increase of the heat transfer fluid and thus the efficiency of the absorber is shown in Figure 11. Tests were carried out in two cases: (a) where an absorber without inserts was analysed and (b) an absorber with insert with Tr = 3.8. The resulting temperature values were read for steady state and each measurement point marked in chart is the average of at least 200 measurement points. For each case analysed, there is a corresponding ambient temperature value and an inlet temperature that varied

slightly. For each measured point on the experimental bench, tests were carried out using CFD for the same boundary conditions parameters. The plotting of points on the graph highlights the high accuracy of the model.

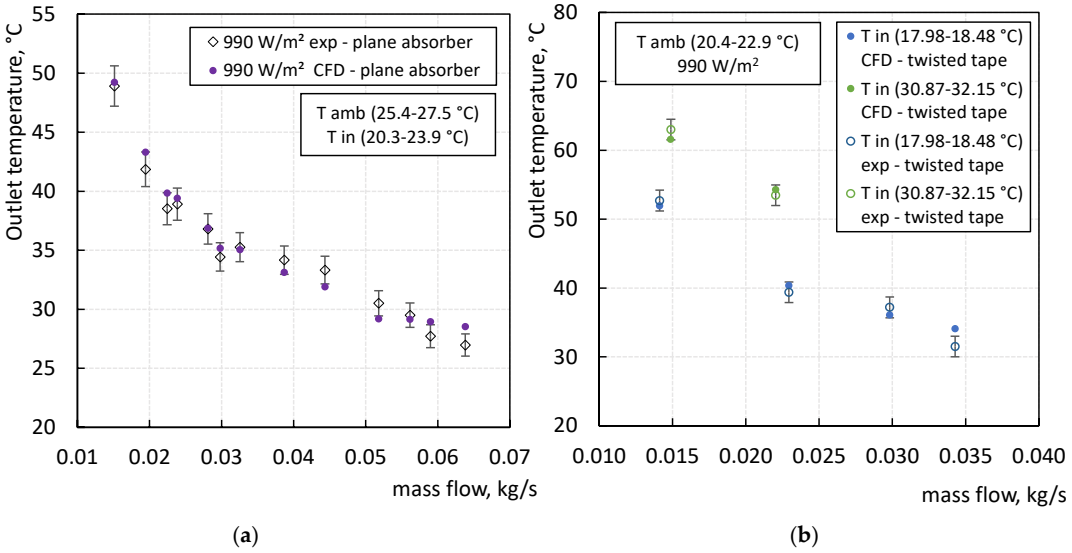

Figure 11. Experimental validation of temperature increase in a linear absorber: (**a**) validation for plane absorber and (**b**) validation for twisted tape with Tr = 3.8.

Based on the results presented, it can be concluded that the CFD model made represents the actual installation parameters well and can be used for testing twisted tapes.

3.2. CFD Analysis Results

Figure 12 presents mass flow vectors coloured by fluid temperature for four cases in equal absorber cross sections. For each, the boundary conditions are the same but differ in the twisted ratio. The figures represent the reference case without a turbulent insert (a) and three inserts with twisted ratios of 4, 2 and 1, respectively (b), (c) and (d). It can be noted that the flow vectors in the reference case are directed perpendicular to the absorber cross-section. In contrast to this case, for the inserts used, the nature of the flow changes and the vectors show fluid circulation around the absorber axis. For the reference case, it is noticeable that there is a significant non-uniform temperature distribution in the absorber due to the heat flux distribution on the absorber surface, which causes a large temperature difference and can affect material stresses and reduce durability. The swirl flow, caused by the twisted tapes, significantly reduces the temperature difference in the absorber and mixes the fluid, improving the heat transfer conditions and reducing boundary layer thickness. A noticeable trend is that the smaller the twisted ratio, i.e., the tighter the insert, the more the temperature difference in the fluid decreases.

The use of twisted tapes has a significant effect on increasing the fluid velocity in the absorber, resulting in an increase in the Reynolds number. Figure 13 shows the fluid path lines coloured by heat transfer fluid velocity. Twisted tapes cause swirl flow and extend the path of the stream in the absorber. As the twisted ratio decreases, the fluid velocity increases, which has its maximum closer to the axis of the absorber. Intense mixing of the fluid also occurs, which reduces local temperature maxima and improves heat collection.

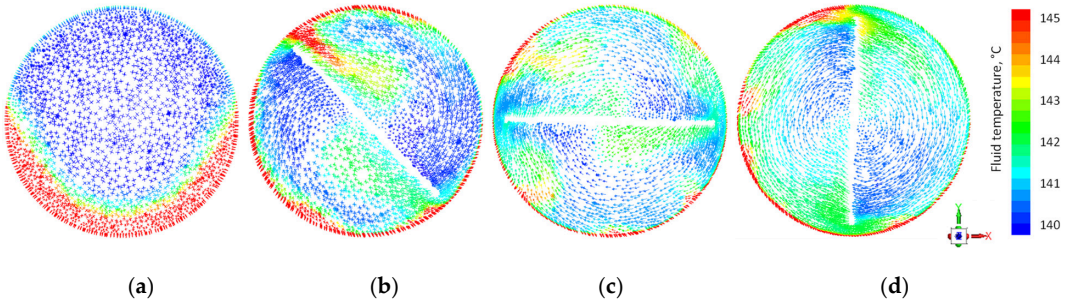

Figure 12. Mass flow vectors coloured by fluid temperature for T_{in} = 140 °C, mass flow 0.225 kg/s: (**a**) no twisted tape, (**b**) twisted ratio 4, (**c**) twisted ratio 2 and (**d**) twisted ratio 1.

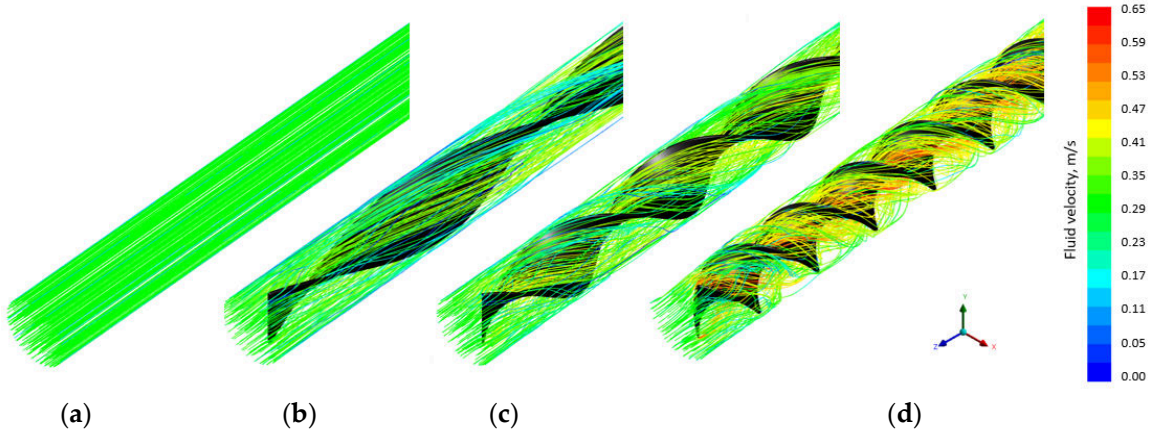

Figure 13. Fluid path lines coloured by velocity: (**a**) no twisted tape, (**b**) twisted ratio 4, (**c**) twisted ratio 2 and (**d**) twisted ratio 1.

Figure 14 illustrates an example distribution of the local Nusselt number depending on the position in the absorber tube cross-section and along its length at selected points for Tr = 1. The results of the numerical analysis indicate a large variation in the local Nusselt number which is due to the nature of the flow, the previously demonstrated velocity difference and the non-uniform distribution of radiation on the outer surface of the absorber. Figure 14a compiles the local Nusselt number for three selected cross-sectional areas, where the maximum appears in the areas between the insert and the inner wall of the absorber. The minimum can be identified closest to the twisted tape surface due to the low speed. Figure 14b plots the local Nusselt number as a function of the length of the absorber and presents the results for 4 Z-axes, where Z1 is the axis closest to the upper surface and Z2, Z3 and Z4 occur closer to the surface with concentrated heat flux. For a given axis, the maximum of the Nusselt number can be identified where the twisted tape is close to the absorber wall, which is where the most intense heat extraction occurs. The lowest heat transfer occurs at the Z1 axis, which is close to the wall on whose surface the lowest heat flux is applied. Furthermore, comparing the local Nusselt number for the Z3 and Z4 axes, there is a lack of symmetry, which is caused by the particular direction of the fluid flow in the absorber pipe, the twisted tape being twisted to the right. Therefore, as can also be seen in Figure 12, the heat absorption is higher on one side.

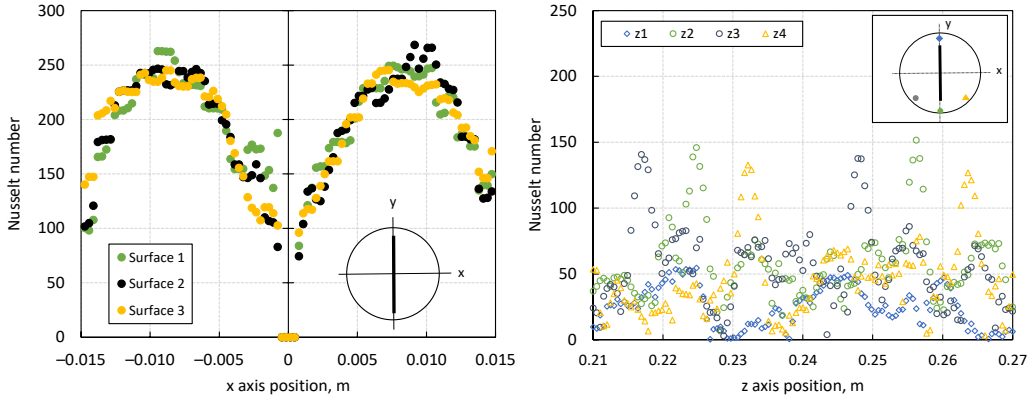

(**a**) (**b**)

Figure 14. Local Nusselt numbers for example case: (**a**) along the absorbers tube's circumference at different stream wise locations and (**b**) as a function of stream wise length along the tube.

The placement of twisted tapes inside the absorber increases the fluid velocity, resulting in improved heat extraction conditions on the one hand and increased friction and pressure drop on the other. The pressure drop generated in the system forces the circulating heat transfer fluid pump to a higher power level and this reduces the efficiency of the system. Figure 15a presents the friction factor for the reference case and different twisted tapes, as a function of the Reynolds number. An increase in this factor occurs for smaller Reynolds numbers and denser twisted tapes. For each case, the most significant decrease in friction factor occurs through turbulisation of the flow. The curves shown in Figure 15a for the individual inserts indicate a significant increase in flow resistance with a lower twisted ratio. The increase in Reynolds number relative to the reference case is shown in Figure 15b, where the Reynolds number for its equivalent for the plane absorber is compared for each twisted tape case analysed. The greatest increase is noticeable for denser inserts and higher flow parameters (higher mass flow and higher medium temperature).

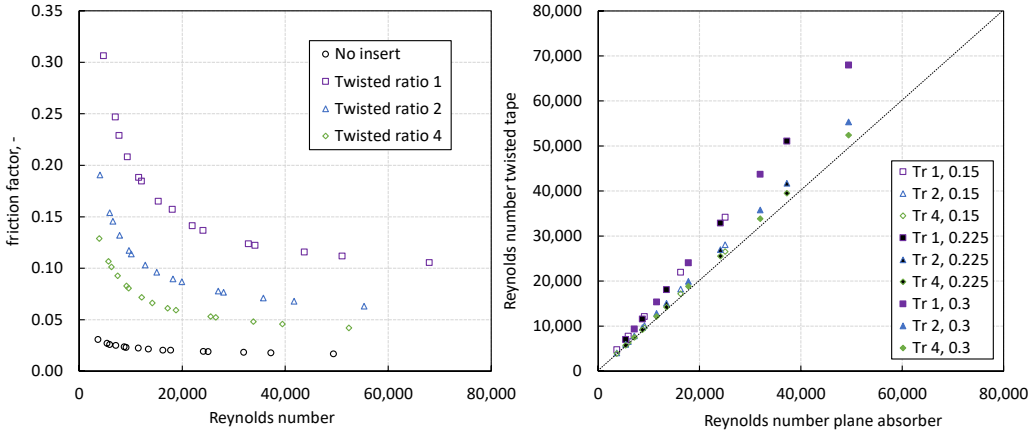

(**a**) (**b**)

Figure 15. Hydraulic flow indicators: (**a**) friction factor inside the absorber and (**b**) Reynolds number increment versus reference case.

The PEC indicator shows heat transfer enhancement if its value is greater than 1. For the analysed data set, i.e., mass flow, temperature range and twisted ratio, a positive trend in PEC growth is maintained in each case, indicating that each analysed insert results in an intensification of heat absorption by the fluid. When considering the PEC index as a function of temperature, the greatest increase occurs for the highest mass flow and inserts with a low twisted ratio. When considering the PEC index shown in Figure 16b as a function of the Reynolds number corresponding to the flow from the twisted tape, it can be seen that the given characteristic flattens out from a certain Reynolds number value. However, the most intense growth can be indicated for the range up to a Reynolds number of around 20,000.

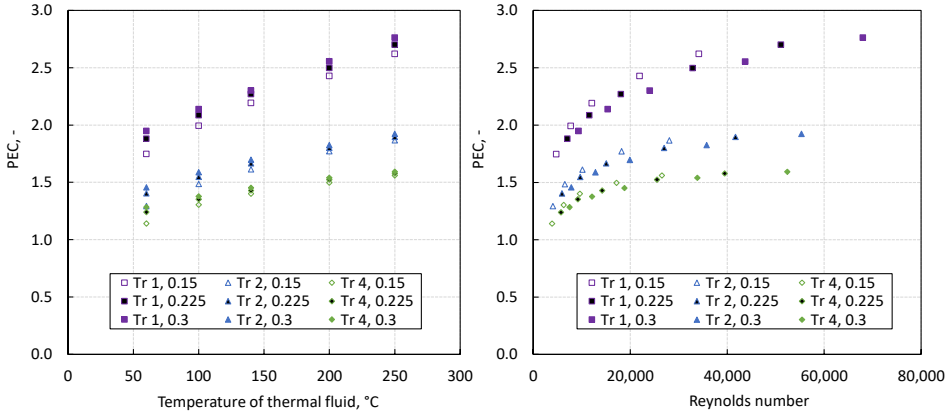

Figure 16. PEC coefficient for absorber with twisted tapes: (**a**) as a function of thermal fluid inlet temperature and (**b**) as a function of Reynolds number.

The average value of the Nusselt number as a function of the Reynolds number, for three mass flow scenarios and different absorber cases, with and without twisted tapes, is shown in Figure 17. The Nusselt number increases with an increase in the Reynolds number, which in this case is due to an increase in fluid temperature, an increase in mass flow and twisted tapes with lower twisted ratios. That emphasises the intensification of heat extraction for the entire range of boundary conditions analysed. On each characteristic, each successive point is defined by an inlet temperature, successively 60 °C, 100 °C, 140 °C, 200 °C and 250 °C. It can be seen that with twisted tapes, the Reynolds number increases for each of the corresponding points due to the increase in velocity in the absorber. The largest increase occurs for an insert with a twisted ratio of 1.

The efficiency of the parabolic trough collector (Equation (6)) as a function of Reynolds number for three analysed mass flows is presented in Figures 18–20. In this case, the increase in Reynolds number was due to a change in fluid temperature in analogy with the previously presented results. As the Reynolds number and fluid temperature increase, the efficiency decreases which is due to the higher wall temperature and greater heat loss to the ambient. The impact of twisted tapes is noticeable in each case. In overall terms, the absorber with insert with twisted ratio 1 has the largest increase in efficiency relative to the plane absorber. However, each of the cases analysed increases the efficiency of PTC because it reduced the wall temperature and intensifies the heat absorption. The largest efficiency gains are noticeable for low Reynolds number values. For higher flow rates and Reynolds numbers, the impact of twisted tapes is lower but still noticeable.

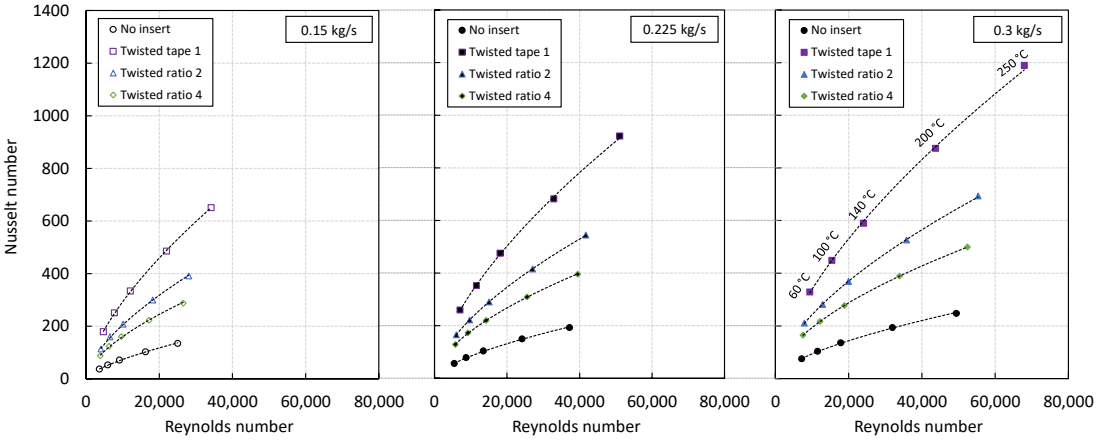

Figure 17. Nusselt number as a function of Reynolds number for mass flow: (**a**) 0.15 kg/s, (**b**) 0.225 kg/s and (**c**) 0.3 kg/s.

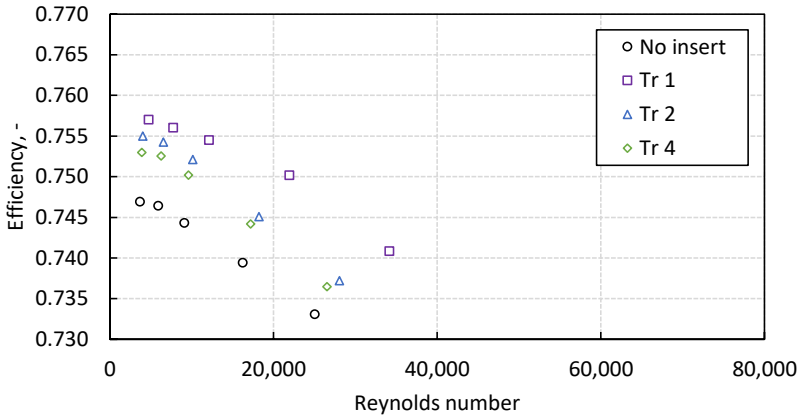

Figure 18. Parabolic trough collector efficiency comparison for mass flow 0.15 kg/s.

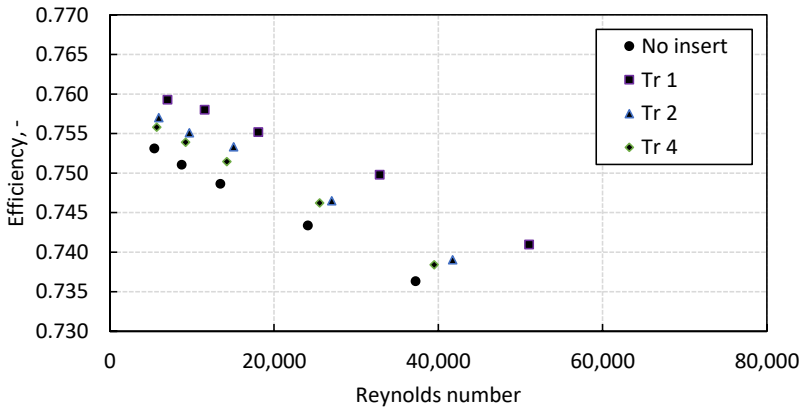

Figure 19. Parabolic trough collector efficiency comparison for mass flow 0.225 kg/s.

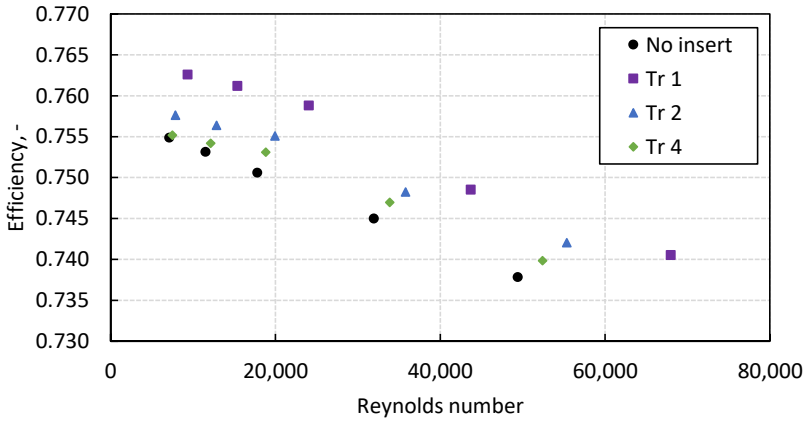

Figure 20. Parabolic trough collector efficiency comparison for mass flow 0.3 kg/s.

The efficiency value considers the additional friction created by the twisted tape placement inside the absorber. For the vast majority of cases analysed, the increase in pump power needed is lower than the benefit of increased efficiency, so for a wide range of flow parameters the most optimal is to use the densest insert with twisted ratio 1. Surface plots with isolines identifying efficiency levels for the analysed flows as a function of the temperature of heat transfer fluid and twisted ratio are presented in Figures 21–23. This estimation may allow the determination of optimum inserts with a different twisted ratio to those analysed in the numerical analysis, but their explicit determination should be pre-empted by additional numerical analysis. By analysing the efficiency of a low-concentrated parabolic trough collector system as a function of the temperature of heat transfer fluid, it is possible to identify an area where the power needed to run the pump is higher than the possible efficiency gain compared to a less dense insert. The identified area is at the end of the analysed data, for a mass flow of 0.3 kg/s and the highest heat transfer fluid temperature. In this case, it would be more optimal to use an insert with a twisted ratio of 2. It can therefore be presumed that, for potentially higher temperatures or mass flow, an increased self-requirement ratio may negatively affect the overall installation, so it may be more reasonable to use inserts with a higher twisted ratio.

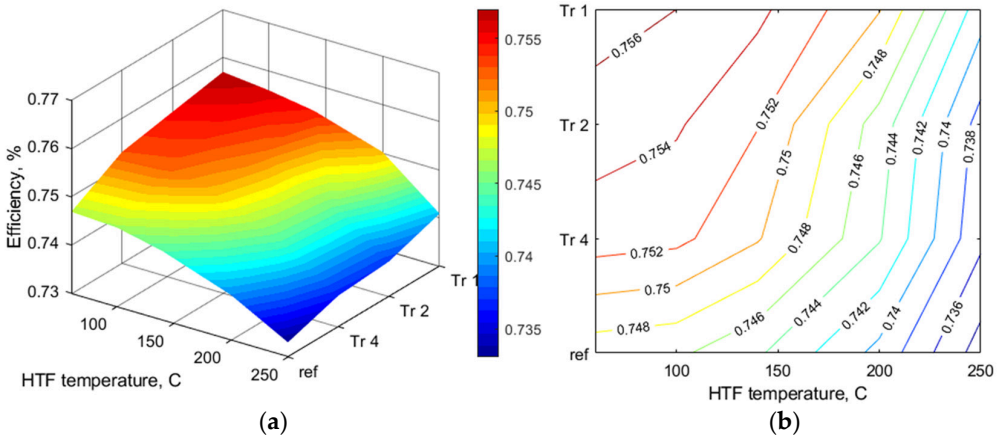

Figure 21. Efficiency comparison of parabolic trough collector as a function of heat transfer fluid for mass flow 0.15 kg/s: (**a**) efficiency surface indication and (**b**) efficiency isolines.

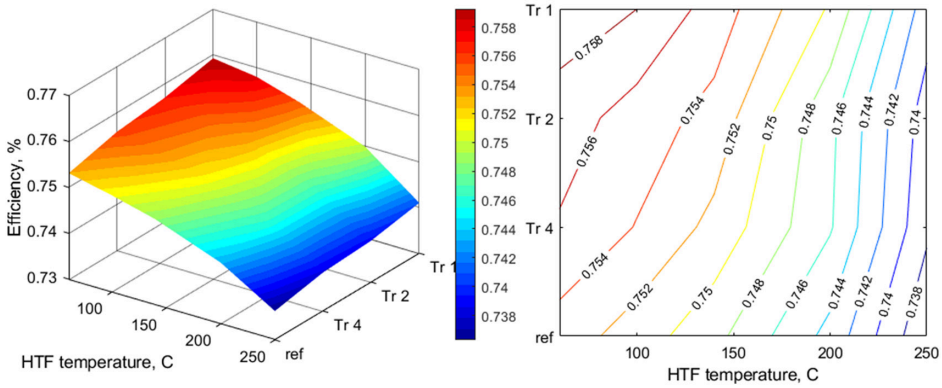

(**a**) (**b**)

Figure 22. Efficiency comparison of parabolic trough collector as a function of heat transfer fluid for mass flow 0.225 kg/s: (**a**) efficiency surface indication and (**b**) efficiency isolines.

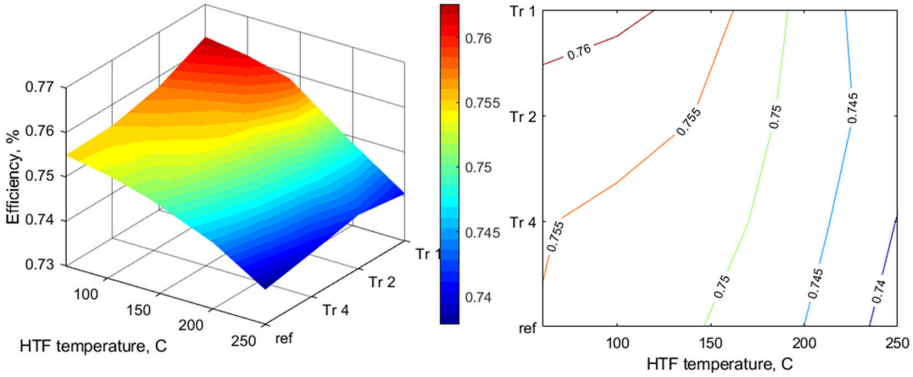

(**a**) (**b**)

Figure 23. Efficiency comparison of parabolic trough collector as a function of heat transfer fluid for mass flow 0.3 kg/s: (**a**) efficiency surface indication and (**b**) efficiency isolines.

To determine more precisely the effect of an overly dense insert on installation efficiency, the PTC efficiency was compared to the reference efficiency for the same boundary conditions for a mass flow of 0.3 kg/s in which the previously mentioned area was identified. Figure 24a,b compile this correlation as a function of temperature and the use of isolines indicates the validity of using an insert with twisted ratio 2 for temperatures greater than 190 °C.

When applying the results obtained to a solar installation, it should be pointed out that usually the mass flow in such installations is adjusted to the atmospheric conditions to achieve a certain temperature range at the outlet of the solar loop. When summarising the results for different mass flows, therefore, it is important to consider them as a comprehensive solution and to pay particular attention to the extreme results. Based on average weather data, the appropriate length of the solar loop and the conditions for adjusting the mass flow as a function of insolation can be determined. It is most desirable to operate the system for the highest designed flow rate, as this provides the highest efficiency. Therefore, for the assumed boundary conditions, flow parameters, selected fluid and geometrical dimensions, it was determined that up to a fluid temperature of 190 °C the most optimal is to use an insert with twisted ratio 1 and for higher temperatures an insert with twisted ratio 2. It should also be noted that efficiency gains relative to the reference case occur for each of the twisted tapes analysed.

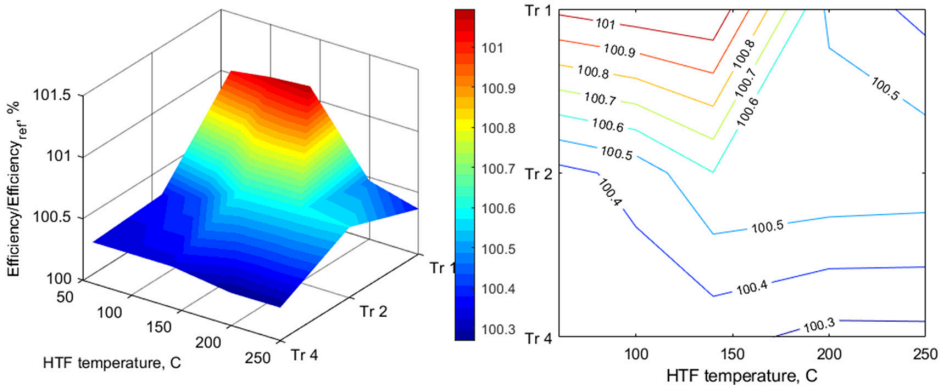

(**a**) (**b**)

Figure 24. PTC efficiency increment compared to reference efficiency: (**a**) efficiency surface indication and (**b**) efficiency isolines.

3.3. Twisted Tape Application Evaluation in Long Term Analysis

To demonstrate the impact of using twisted tapes in a solar installation, a long-term analysis was carried out and the results were compared with a reference case. A previously developed mathematical model, successfully applied in the previous analysis, was used for the study [21]. Based on the obtained Nusselt and Reynolds number increment data, relative to the reference case, a series of correlations were developed for each twisted tape and mass flow. Due to the limited range of numerical analyses, which was caused by the high computing cost and thus analysis time, it was decided that using separate correlations for each case, without estimating other mass flows, would give more reliable data. Therefore, the results of this analysis are demonstrative, presenting the potential for the use of segmental applied twisted tapes. The study analysed a case in which the installation was assumed to consist of a single solar loop, where the PTC is consistent with the geometric and optical assumptions shown in Table 1.

The solar loop consists of 90 absorbers, each 1 m long. The inlet temperature of the solar loop, as assumed in the numerical study, is 60 °C and the outlet temperature depends on the intensity of solar radiation and mass flow. Proceeding from previous assumptions, it was determined that the facility could operate in three configurations: for mass flow 0.15 kg/s for DNI (direct normal irradiance) up to 500 W/m^2, 0.225 kg/s for DNI between 500–750 W/m^2 and 0.3 kg/s for DNI > 750 W/m^2. This assumption results in a relatively constant temperature distribution along the length of the absorber. It should be noted that twisted tapes are mounted in a specific section of the absorber and, with variable input parameters, as is the case with renewable energy installations, there are different flow and heat transfer parameters in a given section.

The first iteration of the analysis was to clarify in which absorbers the inserts with twisted ratio 2 should be placed for the range from 750–1000 W/m^2, for which the mass flow is 0.3 kg/s. In the most sensitive case, the fluid temperature reached 190 °C after the 59th absorber, so it was determined that for the entire analysis, an insert with twisted ratio 1 was used for the 59 absorber sections and an insert with twisted ratio 2 was used for the remaining 31. This ratio was maintained for the rest of the analysed cases.

The study was carried out for southern Spain location, near the town of Seville (latitude 37.41, longitude −5.75), because of the high annual insolation and the many existing installations there with concentrated PTCs [12]. The results presented here can be used as a representation of the possible development path of these installations. Data on DNI, temperature and wind, as well as the position of the sun, were acquired using NSRDB: National Solar Radiation Database from NREL, with a resolution of 1 h [70]. Selected climate conditions are presented in Table 4. The study was conducted for one year, 2019.

Table 4. Selected climate condition parameters for each analysed month.

Month	Amount of Solar Energy, kWh/m^2/Month	Average Temperature, °C	Average Wind Speed, m/s
January	154.17	8.77	2.06
February	174.13	11.47	1.92
March	213.03	14.25	2.01
April	173.57	15.30	2.49
May	281.52	22.46	2.24
June	294.85	24.44	2.46
July	252.75	27.99	2.36
August	272.55	28.17	1.97
September	193.01	25.32	1.96
October	179.61	20.11	1.89
November	101.79	13.19	2.63
December	113.21	11.91	2.51

Figure 25 shows the incremental heat gain of the solar installation presented by the $\overline{\Delta\eta}$ factor, shown according to Equation (20):

$$\overline{\Delta\eta} = \frac{Q_{u,\ tape} - Q_{u,\ ref}}{Q_{u,ref}} \cdot 100\% \quad (20)$$

where Q_u is the heat gained in the installation for the case with segmental arrangement of twisted tapes and without inserts, respectively.

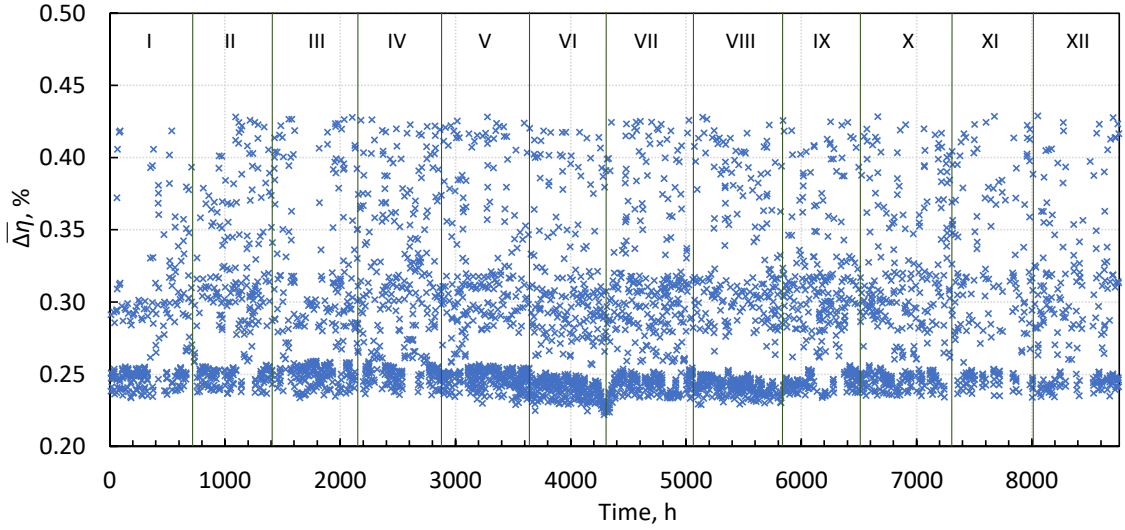

Figure 25. Heat increment coefficient during 12 months of analysis.

The graph is divided into 12 parts, reflecting the 12 months of the analysed year. In each of the analysed operating hours, as long as the plant is running, an increase in the efficiency of heat extraction is visible.

Figure 26 shows a comparison of heat production for three example days in June 2019 (1st, 2nd and 3rd). In this case, the power gain for the installation with twisted tapes is also visible. The increment in heat take-up is a maximum of 0.3 kWh for the individual hours of operation.

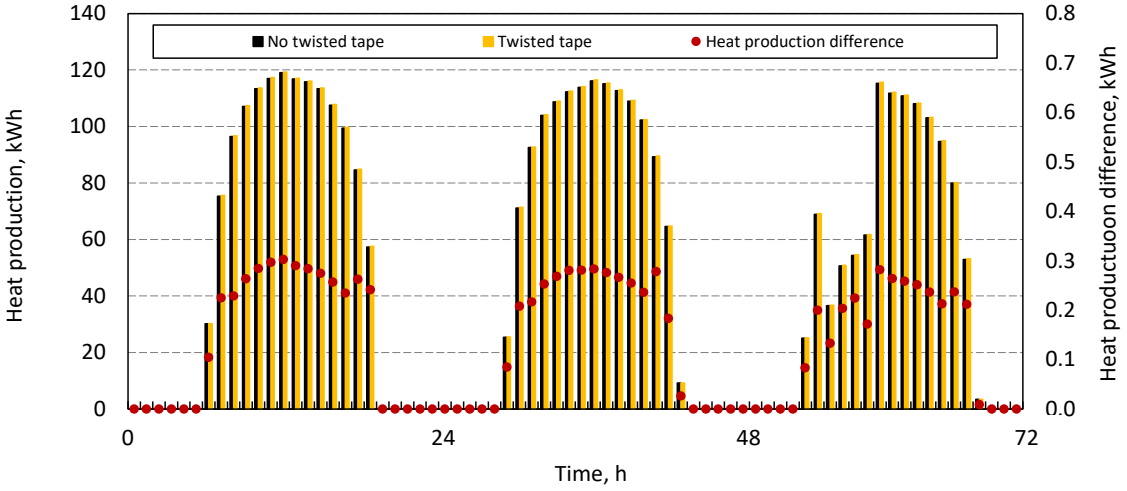

Figure 26. Heat production difference for case with twisted tapes used and without for three selected days in June.

Comparing the results in a long-term perspective, as shown in Table 5, the average increase in the heat generation was 0.27%. The highest average increase in one month was 0.29 in November and the lowest was 0.26 in January. The amount of heat generated by the solar installation increased by a total of 797.49 kWh. The highest production of heat occurred in June 36,093.89 kWh with no twisted tape and 36,188.97 with twisted tapes applied.

Table 5. Long term analysis results.

Month	Q_{ref}, kWh	$Q_{twisted\ tape}$, kWh	Q_{gain}, kWh	$\overline{\Delta\eta}$
January	18,856.45	18,906.29	49.84	0.26
February	21,269.14	21,328.36	59.21	0.28
March	26,043.76	26,114.81	71.05	0.27
April	21,187.09	21,246.75	59.67	0.28
May	34,334.51	34,427.21	92.71	0.27
June	36,093.89	36,188.16	94.27	0.26
July	30,320.91	30,403.87	82.96	0.27
August	32,821.85	32,909.64	87.79	0.27
September	23,526.48	23,591.56	65.08	0.28
October	21,943.78	22,004.65	60.87	0.28
November	12,418.88	12,454.33	35.45	0.29
December	13,756.19	13,794.78	38.59	0.28
Summary	292,572.92	293,370.41	797.49	0.27

4. Conclusions

The article presents a strategy for the application of different twisted tapes with twisted ratios of 1, 2 and 4 in the length of the solar parabolic trough collector loop. The analysis used a CFD model and a mathematical one, both of which show high agreement with the experiment. The aim of this study was to investigate the effect of twisted tapes on the operation of systems with linear absorbers in PTC solar loops, especially with low concentrated ratio. The following conclusions can be drawn.

- In terms of the parameters analysed, twisted tape inserts have a beneficial effect on the operation of PTC installations through a reduction of the temperature gradient in the tubular absorbers; the implementation of a swirl flow which minimises the boundary layer; and an increase in the velocity of the fluid which, through the nature of the flow, intensifies the collection of heat by the heat transfer fluid. The maximum PTC efficiency increment was reported as 1 percentage point.
- The densest insert analysed, with twisted ratio 1, provides the highest efficiency gain. It should be noted, however, that for the upper range of the tests carried out, i.e., mass flow of 0.3 kg/s and fluid temperatures above 190 °C, by significantly increasing the pressure drop, the increased demand for the solar plant's own needs results in a reduction in efficiency relative to insert with twisted ratio 2.
- In the search for the optimum solution, where system efficiency is maximised, it was determined that the best solution was to use an insert with a twisted ratio of 1 for the entire range except for the section where, for a mass flow of 0.3 kg/s, the fluid temperature reaches 190 °C. From this point, an insert with a twisted ratio of 2 should be used.
- The results obtained are valid for Therminol VP-1 heat transfer fluid, the geometry of a parabolic trough collector and flow parameters presented in this study.
- It is reasonable to assume that, for higher flow parameters, other inserts may prove to be optimal, so it will be necessary to extend the analyses with further assumptions to determine these parameters.
- The long-term analysis showed that by using twisted tapes in the proposed configuration, heat production increases by 0.27% which was 797.49 kWh more during 12 months of operation.
- An increase in the total pressure drop in the absorber loop will affect the need for a higher capacity pump use. Despite considering the increased pump power requirement, it is important to note the higher device price and the investment cost per twisted tape.
- The recommendation that can be drawn from these studies is, in particular, the need to consider the power gain of the pump. Additionally, based on a literature search, the authors suggest comparing the results of twisted tape applications for the same flow parameters and for the same fluid and geometry. These parameters significantly affect the obtained results. For long-term analyses, it is appropriate to consider operating parameters with a time step of one hour or less. Long-term analysis for longer periods of time, e.g., whole days, may yield uncertain results due to varying solar, temperature and wind parameters.

Author Contributions: Conceptualisation, B.S. and J.O.; methodology, B.S.; software, B.S. and J.O.; validation, B.S.; formal analysis, B.S.; investigation, B.S.; resources, B.S., J.O., D.W. and Ł.B.; data curation, B.S. and J.O.; writing—original draft preparation, B.S.; writing—review and editing, B.S., J.O., D.W. and Ł.B.; visualisation, B.S. and J.O.; supervision, D.W. and Ł.B.; project administration, Ł.B.; funding acquisition, Ł.B. All authors have read and agreed to the published version of the manuscript.

Funding: This research was funded by the National Science Centre within the framework of the research project OPUS15 No. 2018/29/B/ST8/02406.

Data Availability Statement: The data presented in this study are available on request from the corresponding author.

Acknowledgments: The work was developed within the project OPUS15, registration number 2018/29/B/ST8/02406.

Conflicts of Interest: The authors declare no conflict of interest.

Nomenclature

A	area, m^2
ALD	atomic layer deposition
BRDF	Bidirectional Reflectance Distribution Function
c_p	specific heat, J/(kg·K)
CFD	computational fluid dynamics
CSP	concentrating solar power
CVD	chemical vapour deposition
d	diameter, m
dE_i	incident power flux density per unit area, W/m^2
dL_r	unit of radiant energy per unit of solid angle, W/m^2sr
DNI	direct normal irradiance, W/m^2
f	friction factor, -
fl	focal length, m
G	irradiance, W/m^2
GUM	guide uncertainty measurement
H	twisted length, m
h	heat transfer coefficient, W/m^2K
HMI	metal halide
IAM	incidence angle modifier, -
k	thermal conductivity, W/(m·K)
k	kinetic energy
L	length, m
$\dot{m}$	mass flow, kg/s
MCRT	Monte Carlo Ray Tracing
Nu	Nusselt number, -
P	pressure, Pa
PEC	performance evaluation criterion, -
PETG	polyethylene terephthalate glycol
Pr	Prandtl number, -
PTC	parabolic trough collectors
PVD	physical vapour deposition
Q	heat flux, W
Re	Reynolds number, -
T	temperature, °C
t	time, s
th	thickness, m
Tr	twisted ratio, -
u	fluid velocity, m/s
UDF	User Defined Function
W	width, m
W_p	required pumping power, W
Wr	width ratio, -
x	x position
y	y position
Subscripts	
abs	absorber
ap	aperture
c	glass envelope
csp	concentrated solar energy
e	external
el	reference electricity production
i	internal
in	inlet
loss	energy losses
opt	optical
out	outlet

ref	reference
s	solar
sp	non-concentrated solar energy
tape	twisted tape
u	useful
Greek symbols	
α	absorptivity, -
ε	emissivity, -
η	efficiency, -
θ	incidence angle, $^{\circ}$
λ	conductivity, W/(m·K)
ρ	density, kg/m^3
μ	viscosity, Pa·s
μ_e	effective viscosity, Pa·s
μ_t	turbulent viscosity, Pa·s
τ	transmittance, -
ω	specific rate of dissipation

References

1. Weiss, W.; Spörk-Dür, M. Solar Heat Worldwide 2021. Institute of Sustainable Technologies AEE, Austria. Available online: https://www.iea-shc.org/solar-heat-worldwide-2021 (accessed on 3 June 2022).
2. POWER TROUGH 110®—Inventive Power. Available online: https://inventivepower.com.mx/english/power-trough-110/ (accessed on 1 May 2022).
3. POWER TROUGH 250®—Inventive Power. Available online: https://inventivepower.com.mx/english/power-trough-250/ (accessed on 1 May 2022).
4. Solar Heat for Industry—Solar Payback. Available online: https://www.solar-payback.com/wp-content/uploads/2017/07/Solar-Heat-for-Industry-Solar-Payback-April-2017.pdf (accessed on 3 June 2022).
5. International Renewable Energy Agency Innovation Outlook: Thermal Energy Storage. Available online: www.irena.org (accessed on 3 June 2022).
6. Kumar, L.; Hasanuzzaman, M.; Rahim, N.A. Global Advancement of Solar Thermal Energy Technologies for Industrial Process Heat and Its Future Prospects: A Review. *Energy Convers. Manag.* **2019**, *195*, 885–908. [CrossRef]
7. Rackam Solar Thermal Solutions for Industrial Process Heat. Available online: https://rackam.com/en/ (accessed on 1 June 2022).
8. Häberle, A.; Krüger, D. Concentrating Solar Technologies for Industrial Process Heat. In *Concentrating Solar Power Technology: Principles, Developments, and Applications*; Woodhead Publishing Series in Energy; Lovegrove, K., Stein, W., Eds.; Woodhead Publishing: Soston, UK, 2020; pp. 659–675. ISBN 9780128199701.
9. Reflective Surfaces—Solar—Industries—Alanod. Available online: https://alanod.com/en/industries/solar/reflective-surfaces (accessed on 2 June 2022).
10. Minder, S. Example of Concentrated Solar Systems (PTC) in the Dairy Industry in Switzerland. Available online: www.nep-solar.com (accessed on 2 June 2022).
11. IMPLEMENTED PROJECTS—Inventive Power. Available online: https://inventivepower.com.mx/english/implemented-projects/ (accessed on 2 June 2022).
12. World Map of Solar Thermal Plants | Solar Heat for Industrial Processes (SHIP) Plants Database. Available online: http://ship-plants.info/solar-thermal-plants-map?collector_type=5 (accessed on 1 June 2022).
13. Renewable Power Generation Costs in 2020. Available online: https://www.irena.org/publications/2021/Jun/Renewable-Power-Costs-in-2020 (accessed on 3 June 2022).
14. Gharat, P.V.; Bhalekar, S.S.; Dalvi, V.H.; Panse, S.V.; Deshmukh, S.P.; Joshi, J.B. Chronological Development of Innovations in Reflector Systems of Parabolic Trough Solar Collector (PTC)—A Review. *Renew. Sustain. Energy Rev.* **2021**, *145*, 111002. [CrossRef]
15. Valentín, D.; Valero, C.; Egusquiza, M.; Presas, A. Failure Investigation of a Solar Tracker Due to Wind-Induced Torsional Galloping. *Eng. Fail. Anal.* **2022**, *135*, 106137. [CrossRef]
16. Stanek, B.; Węcel, D.; Bartela, Ł.; Rulik, S. Solar Tracker Error Impact on Linear Absorbers Efficiency in Parabolic Trough Collector—Optical and Thermodynamic Study. *Renew. Energy* **2022**, *196*, 598–609. [CrossRef]
17. Rodriguez-Sanchez, D.; Rosengarten, G. Improving the Concentration Ratio of Parabolic Troughs Using a Second-Stage Flat Mirror. *Appl. Energy* **2015**, *159*, 620–632. [CrossRef]
18. T160 Solar Collector—Designed to Run Industrial Processes—Absolicon. Available online: https://www.absolicon.com/applying-absolicon/ (accessed on 2 June 2022).
19. Noč, L.; Jerman, I. Review of the Spectrally Selective (CSP) Absorber Coatings, Suitable for Use in SHIP. *Sol. Energy Mater. Sol. Cells* **2022**, *238*, 060040. [CrossRef]

20. Zhao, K.; Jin, H.; Gai, Z.; Hong, H. A Thermal Efficiency-Enhancing Strategy of Parabolic Trough Collector Systems by Cascadingly Applying Multiple Solar Selective-Absorbing Coatings. *Appl. Energy* **2022**, *309*, 118508. [CrossRef]
21. Stanek, B.; Wang, W.; Bartela, Ł. A Potential Solution in Reducing the Parabolic Trough Based Solar Industrial Process Heat System Cost by Partially Replacing Absorbers Coatings with Non-Selective Ones in Initial Loop Sections. *Appl. Energy* **2023**, *331*, 120472. [CrossRef]
22. Allam, M.; Tawfik, M.; Bekheit, M.; El-Negiry, E. Heat Transfer Enhancement in Parabolic Trough Receivers Using Inserts: A Review. *Sustain. Energy Technol. Assess.* **2021**, *48*, 101671. [CrossRef]
23. Zaboli, M.; Ajarostaghi, S.S.M.; Saedodin, S.; Pour, M.S. Thermal Performance Enhancement Using Absorber Tube with Inner Helical Axial Fins in a Parabolic Trough Solar Collector. *Appl. Sci.* **2021**, *11*, 7423. [CrossRef]
24. Bellos, E.; Tzivanidis, C.; Tsimpoukis, D. Thermal Enhancement of Parabolic Trough Collector with Internally Finned Absorbers. *Sol. Energy* **2017**, *157*, 514–531. [CrossRef]
25. Bellos, E.; Tzivanidis, C. Enhancing the Performance of Evacuated and Non-Evacuated Parabolic Trough Collectors Using Twisted Tape Inserts, Perforated Plate Inserts and Internally Finned Absorber. *Energies* **2018**, *11*, 1129. [CrossRef]
26. Jaramillo, O.A.; Borunda, M.; Velazquez-Lucho, K.M.; Robles, M. Parabolic Trough Solar Collector for Low Enthalpy Processes: An Analysis of the Efficiency Enhancement by Using Twisted Tape Inserts. *Renew. Energy* **2016**, *93*, 125–141. [CrossRef]
27. Varun; Garg, M.O.; Nautiyal, H.; Khurana, S.; Shukla, M.K. Heat Transfer Augmentation Using Twisted Tape Inserts: A Review. *Renew. Sustain. Energy Rev.* **2016**, *63*, 193–225. [CrossRef]
28. Seemawute, P.; Eiamsaard, S. Thermohydraulics of Turbulent Flow through a Round Tube by a Peripherally-Cut Twisted Tape with an Alternate Axis. *Int. Commun. Heat. Mass. Transf.* **2010**, *37*, 652–659. [CrossRef]
29. Promvonge, P. Thermal Augmentation in Circular Tube with Twisted Tape and Wire Coil Turbulators. *Energy Convers. Manag.* **2008**, *49*, 2949–2955. [CrossRef]
30. Eiamsa-ard, S.; Thianpong, C.; Eiamsa-ard, P.; Promvonge, P. Thermal Characteristics in a Heat Exchanger Tube Fitted with Dual Twisted Tape Elements in Tandem. *Int. Commun. Heat. Mass. Transf.* **2010**, *37*, 39–46. [CrossRef]
31. Bhuiya, M.M.K.; Chowdhury, M.S.U.; Saha, M.; Islam, M.T. Heat Transfer and Friction Factor Characteristics in Turbulent Flow through a Tube Fitted with Perforated Twisted Tape Inserts. *Int. Commun. Heat. Mass. Transf.* **2013**, *46*, 49–57. [CrossRef]
32. Alnaqi, A.A.; Alsarraf, J.; Al-Rashed, A.A.A.A. Hydrothermal Effects of Using Two Twisted Tape Inserts in a Parabolic Trough Solar Collector Filled with MgO-MWCNT/Thermal Oil Hybrid Nanofluid. *Sustain. Energy Technol. Assess.* **2021**, *47*, 101331. [CrossRef]
33. Veera Kumar, A.; Arjunan, T.V.; Seenivasan, D.; Venkatramanan, R.; Vijayan, S.; Matheswaran, M.M. Influence of Twisted Tape Inserts on Energy and Exergy Performance of an Evacuated Tube-Based Solar Air Collector. *Solar Energy* **2021**, *225*, 892–904. [CrossRef]
34. Hasanpour, A.; Farhadi, M.; Sedighi, K. A Review Study on Twisted Tape Inserts on Turbulent Flow Heat Exchangers: The Overall Enhancement Ratio Criteria. *Int. Commun. Heat. Mass. Transf.* **2014**, *55*, 53–62. [CrossRef]
35. Mwesigye, A.; Bello-Ochende, T.; Meyer, J.P. Heat Transfer and Entropy Generation in a Parabolic Trough Receiver with Wall-Detached Twisted Tape Inserts. *Int. J. Therm. Sci.* **2016**, *99*, 238–257. [CrossRef]
36. Ibarra, M.; Rovira, A.; Alarcón-Padilla, D.C.; Zaragoza, G.; Blanco, J. Performance of a 5 KWe Solar-Only Organic Rankine Unit Coupled to a Reverse Osmosis Plant. *Energy Procedia* **2014**, *49*, 2251–2260. [CrossRef]
37. Zhao, S.S.; Gao, X.H.; Qiu, X.L.; Yu, D.M.; Tian, G.K. A Novel TiC-TiN Based Spectrally Selective Absorbing Coating: Structure, Optical Properties and Thermal Stability. *Infrared Phys. Technol.* **2020**, *110*, 103471. [CrossRef]
38. Therminol VP-1 Heat Transfer Fluid | Therminol | Eastman. Available online: https://www.therminol.com/product/71093459 (accessed on 1 February 2022).
39. Zima, W.; Cebula, A.; Cisek, P. Mathematical Model of a Sun-Tracked Parabolic Trough Collector and Its Verification. *Energies* **2020**, *13*, 4168. [CrossRef]
40. Yilmaz, I.H.; Söylemez, M.S. Thermo-Mathematical Modeling of Parabolic Trough Collector. *Energy Convers. Manag.* **2014**, *88*, 768–784. [CrossRef]
41. Kalogirou, S.A. A Detailed Thermal Model of a Parabolic Trough Collector Receiver. *Energy* **2012**, *48*, 298–306. [CrossRef]
42. Pitz-Paal, R. Solar Energy—Concentrating Solar Power. In *Future Energy: Improved, Sustainable and Clean Options for Our Planet*; Elsevier Inc.: Amsterdam, The Netherlands, 2013; pp. 405–431, ISBN 9780080994246.
43. Kalogirou, S.A. Solar Energy Collectors. In *Solar Energy Engineering*; Elsevier: Amsterdam, The Netherlands, 2014; pp. 125–220.
44. Wirz, M.; Petit, J.; Haselbacher, A.; Steinfeld, A. Potential Improvements in the Optical and Thermal Efficiencies of Parabolic Trough Concentrators. *Solar Energy* **2014**, *107*, 398–414. [CrossRef]
45. Çengel, Y.A.; Ghajar, A.J. *Heat and Mass Transfer: Fundamentals & Applications*, 4th ed.; McGraw-Hill: New York, NY, USA, 2011.
46. Ammar, S.M.; Park, C.W. Validation of the Gnielinski Correlation for Evaluation of Heat Transfer Coefficient of Enhanced Tubes by Non-Linear Regression Model: An Experimental Study of Absorption Refrigeration System. *Int. Commun. Heat. Mass. Transf.* **2020**, *118*, 104819. [CrossRef]
47. Manglik, R. Heat Transfer Enhancement. In *Heat Transfer Handbook*; Bejan, A., Kraus, A., Eds.; John Wiley & Sons: New York, NJ, USA, 2003; pp. 1029–1130.
48. *ANSYS Fluent 19.2 User's Guide*; ANSYS, Inc.: Canonsburg, PA, USA, 2013.

49. Mor-Yossef, Y. A Stable, Positivity-Preserving Scheme for Cross-Diffusion Source Term in RANS Turbulence Models: Application to k-ω Turbulence Models. *Comput. Fluids* **2019**, *191*, 104234. [CrossRef]
50. Niu, Y.; Zhang, C.; Xu, G. A Modified Anisotropic K-ω Model for Predicting Flow and Heat Transfer in a Rotating Channel. *Int. J. Heat. Mass. Transf.* **2018**, *123*, 1–15. [CrossRef]
51. Smołka, J. User-Defined Functions Programming in Ansys Fluent. In *Undamentals of Numerical Modelling of Thermal Processes in Electric Devices and Machines*; Silesian University of Technology, Institute of Thermal Technology: Gliwice, Poland, 2019.
52. Cabello, R.; Plesu Popescu, A.E.; Bonet-Ruiz, J.; Curcó Cantarell, D.; Llorens, J. Heat Transfer in Pipes with Twisted Tapes: CFD Simulations and Validation. *Comput. Chem. Eng.* **2022**, *166*, 107961. [CrossRef]
53. Menter, F.R. Two-Equation Eddy-Viscosity Turbulence Models for Engineering Applications. *AIAA J.* **1994**, *32*, 1598–1605. [CrossRef]
54. Rahman, M.M.; Vuorinen, V.; Taghinia, J.; Larmi, M. Wall-Distance-Free Formulation for SST k-ω Model. *Eur. J. Mech.—B/Fluids* **2019**, *75*, 71–82. [CrossRef]
55. Menter, F.R.; Kuntz, M.; Langtry, R. Ten years of industrial experience with the SST turbulence model. In *Turbulence, Heat and Mass Transfer 4*; Begell House: New York, NY, USA, 2003; pp. 625–632.
56. Moshfeghi, M.; Song, Y.J.; Xie, Y.H. Effects of Near-Wall Grid Spacing on SST-K-ω Model Using NREL Phase VI Horizontal Axis Wind Turbine. *J. Wind. Eng. Ind. Aerodyn.* **2012**, *107–108*, 94–105. [CrossRef]
57. APEX. Breault Research Organization, Inc. 2019. Available online: http://www.breault.com/ (accessed on 3 February 2022).
58. Breault Research Organization. *Correlation of ASAPTM Simulation Results with Physical Components*; Breault Research Organization: Tuscon, AZ, USA, 2006.
59. Zhang, C.; Xu, G.; Quan, Y.; Li, H.; Song, G. Optical Sensitivity Analysis of Geometrical Deformation on the Parabolic Trough Solar Collector with Monte Carlo Ray-Trace Method. *Appl. Therm. Eng.* **2016**, *109*, 130–137. [CrossRef]
60. Cheng, Z.D.; He, Y.L.; Cui, F.Q.; Du, B.C.; Zheng, Z.J.; Xu, Y. Comparative and Sensitive Analysis for Parabolic Trough Solar Collectors with a Detailed Monte Carlo Ray-Tracing Optical Model. *Appl. Energy* **2014**, *115*, 559–572. [CrossRef]
61. Bartela, Ł.; Stanek, B.; Węcel, D.; Skorek-Osikowska, A. A Solar Simulator Numerical Modeling for Heat Absorption Phenomenon Research in a Parabolic Trough Collector. *Int. J. Energy Res.* **2021**, *46*, 10074–10084. [CrossRef]
62. Kong, R.; Ambrose, M.; Spanier, J. Efficient, Automated Monte Carlo Methods for Radiation Transport. *J. Comput. Phys.* **2008**, *227*, 9463–9476. [CrossRef]
63. Wang, W.; Aichmayer, L.; Garrido, J.; Laumert, B. Development of a Fresnel Lens Based High-Flux Solar Simulator. *Solar Energy* **2017**, *144*, 436–444. [CrossRef]
64. Pompea, S.M.; McCall, S.H. OPTICAL COATINGS | Optical Black Surfaces. In *Encyclopedia of Modern Optics*; Elsevier: Amsterdam, The Netherlands, 2005; pp. 349–360.
65. Martínez-Manuel, L.; Wang, W.; Laumert, B.; Peña-Cruz, M.I. Numerical Analysis on the Optical Geometrical Optimization for an Axial Type Impinging Solar Receiver. *Energy* **2021**, *216*, 119293. [CrossRef]
66. Stanek, B.; Bartela, Ł.; Węcel, D.; Rulik, S. An Experimental Study on Parabolic Trough Collector in Simulated Conditions by Metal-Halide Solar Radiation Simulator. *Arch. Thermodyn.* **2022**, *43*, 47–61. [CrossRef]
67. Stanek, B.; Bartela, Ł. Numerical and Experimental Study on 10 KWe Metal-Halide Solar Simulator for Parabolic-Trough Collector Testing, ECOS 2021 Conference Proceedings. In Proceedings of the 34th International Conference on Efficiency, Cost, Optimization, Simulation and Environmental Impact of Energy Systems (ECOS21), Taormina, Italy, 28 June–2 July 2021; pp. 1198–1209.
68. Ho, C.K.; Mahoney, A.R.; Ambrosini, A.; Bencomo, M.; Hall, A.; Lambert, T.N. Characterization of Pyromark 2500 Paint for High-Temperature Solar Receivers. *J. Sol. Energy Eng.* **2014**, *136*, 014502. [CrossRef]
69. JCGM Evaluation of Measurement Data-Guide to the Expression of Uncertainty in Measurement Évaluation Des Données de Mesure-Guide Pour L'expression de L'incertitude de Mesure. 2008. Available online: https://www.bipm.org/documents/20126/2071204/JCGM_100_2008_F.pdf/53384399-1e6d-b598-dd17-2831a6b5b812 (accessed on 6 March 2023).
70. Sengupta, M.; Xie, Y.; Lopez, A.; Habte, A.; Maclaurin, G.; Shelby, J. The National Solar Radiation Data Base (NSRDB). *Renew. Sustain. Energy Rev.* **2018**, *89*, 51–60. [CrossRef]

Paper III

Applied Energy 331 (2023) 120472

Contents lists available at ScienceDirect

Applied Energy

journal homepage: www.elsevier.com/locate/apenergy

A potential solution in reducing the parabolic trough based solar industrial process heat system cost by partially replacing absorbers coatings with non-selective ones in initial loop sections

Bartosz Stanek [a,*], Wujun Wang [b], Łukasz Bartela [a]

[a] Silesian University of Technology, Department of Power Engineering and Turbomachinery, Konarskiego 18, Gliwice, Poland
[b] KTH Royal Institute of Technology, Department of Energy Technology, Brinellvägen 68, Stockholm, Sweden

HIGHLIGHTS

- A strategy for partially replacing coating in parabolic trough loop is demonstrated.
- Low-cost coating for initial loop sections as LCOE reduction option is presented.
- A two-dimensional mathematical model of parabolic trough collectors is introduced.
- Four scenarios for solar heat industrial power installations were analysed.
- Potential for using low-cost non-selective coating was presented.

ARTICLE INFO

Keywords:
Concentrated solar power
Parabolic trough collector
Industrial process heat
Solar selective absorber coating
Cost effective absorber coating

ABSTRACT

An important step to achieve low-emission production is the integration of solar energy into industrial processes for decarbonizing the industrial sector. It is therefore necessary to attempt to minimize the cost of these solar industrial process heat systems. The article presents a strategy to reduce the investment costs and thus increase the popularity of parabolic trough collectors by partially replacing the expensive selective coating with a high absorptive, low-cost, non-selective coating in the initial sections of the solar loop where the heat transfer fluid temperature is lower. The analysis was performed for 4 case studies reflecting commercially available solutions with varying temperature ranges for different industrial applications. Calculations were performed using the two-dimensional developed mathematical model that validated with experimental data. The assumed heat transfer fluid is Therminol VP-1. The results have shown the potential of partial use of the Pyromark coating for low and medium-temperature industrial process heat systems with inlet–outlet temperature ranges of 60–120 °C and 100–200 °C. The analysis also showed that all the absorbers can be covered with a low-cost coating in the first scenario. Efficiency increases from 1.5 to 5.5 percentage points have been observed. For the second scenario, 15 of the 24 absorbers can be covered with a low-cost coating, when the installation works at a solar irradiance of 800 W/m^2. Since the results are depended on the solar irradiance and the chosen regulation strategy of the flow, the final number of absorbers possible to cover with non-selective coating requires a long-term analysis for each case examined.

1. Introduction

In 2019, the final energy consumption was reported as 418 EJ, by the International Energy Agency [1]. Global energy consumption is projected to flatten on the coming decades and grow by 14 % to 2050 [2]. According to IEA and IRENA reports, over 32 % of final energy is consumed by the industry sector, where 74 % is in the form of heat [3,4]. Fig. 1 indicates that the industry sector has the highest share of energy consumption, compared to any other sector [5]. Heat supply, which contributed>40 % of energy-related global CO_2 emissions in 2020, remains mainly dependent on fossil fuels, and renewable energies accounts for less than a quarter [6]. Therefore, the crucial step toward achieving low-carbon production system is integrating renewable

* Corresponding author.
E-mail address: bartosz.stanek@polsl.pl (B. Stanek).

https://doi.org/10.1016/j.apenergy.2022.120472
Received 19 July 2022; Received in revised form 5 November 2022; Accepted 30 November 2022
Available online 8 December 2022

Nomenclature

A	area, m^2
c	total cost, USD
C	concentration ratio, -
c_p	specific heat, J/(kg K)
d	diameter, m
f	focal length, m
g	gravitation constant, m/s^2
G_B	direct normal irradiance, W/m^2
h	heat transfer coefficient, W/m^2K
IAM	incidence angle modifier, -
k	thermal conductivity, W/mK
L	length, m
$\dot{m}$	mass flow, kg/s
N	number of sections, -
Nu	Nusselt number, -
p	price, USD/m^2
Pr	Prandtl number, -
Q	thermal flux, W
Ra	Rayleigh number, -
T	temperature, K;°C
th	thickness, mm
v	speed, m/s
W	width, m
X	number of absorbers in loop, -
Y	results to RMSD comparison, °C;W/m

Greek

α	absorptivity, -
α	thermal diffusivity, m^2/s
β	volumetric thermal expansion coefficient, 1/K
ε	emissivity, -
η	efficiency, -
θ	incident angle, °
λ	thermal conductivity, W/mK
μ	dynamic viscosity, Pa·s
ν	kinematic viscosity, m^2/s
ρ	density, kg/m^3
σ	Stefan-Boltzmann constant, W/m^2K^4
τ	transmittance, -

Subscripts

abs	absorber
amb	ambient
ap	aperture
c	cover (glass envelope)
ca	cover-air
coat	coating
cov	convection
CSP	concentration solar power
d	dirt
e	external
exp	experimental
f	fluid
i	internal
in	inlet
loss	losses
m	mirrors
m	mean (average)
num	numerical
opt	optical
out	outlet
r	receiver
rad	radiation
ref	reflectance
s	solar
sh	shadowing
sky	sky
SP	non-concentrated solar energy
track	tracking
u	useful
w	wind

Abbreviations

ALD	atomic layer deposition
CSP	concentrated solar power
CVD	chemical vapor deposition
HTF	heat transfer fluid
LCOE	levelized cost of energy
PTC	parabolic trough collector
PVD	physical vapor deposition
RMSD	root mean square deviation
SCC	selective coating
SHIP	solar heat systems for industrial process

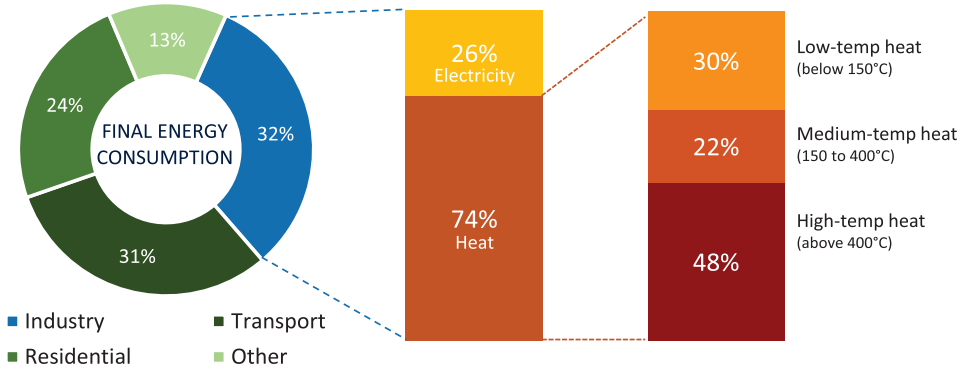

Fig. 1. Final energy consumption and heat temperature level demand based on [3–5].

energy into the industrial process heat sector.

The temperature range of the demand in the industry can be partially covered by different types of solar thermal collectors: air collectors, flat plate and evacuated tube collectors up to 100 °C and concentrating solar thermal collectors as linear Fresnel collectors and parabolic trough for temperatures up to 400 °C [7]. By the end of 2020, at least 891 solar heat systems for industrial processes (SHIP), with total collector area of 1.12 million m^2, have been installed all over the world to meet various industrial process heat requirements [8]. Selected parabolic trough collectors (PTC) based SHIP are summarized in Table 1 from the online SHIP database portal operated by AEE INTEC in Austria [9]. Usually the process heat produced in these installations is in the range of 80–250 °C. The location of SHIP plants depend on the solar irradiance. The largest share of SHIP plants is in Mexico, India and United States. Despite the lower solar radiation conditions, PTC for industrial processes can also be found in Germany and Switzerland. The heat generated is commonly used for manufacturing and fabrication processes, steam production, space cooling, drying and sterilization [9].

The weighted average levelized cost of electricity (LCOE) for concentrating solar power (CSP) plants was reduced by 68 % from USD 0.340/kWh in 2010 to USD 0.108/kWh in 2020 [28]. Although this is a significant decrease, photovoltaic panels have an even lower LCOE (USD 0.057/kWh in 2020). For PTC technology, the solar field shares approximate 39 % of the total installed costs of the whole power plant [28]. Therefore, as one of the key components in the solar field, reducing the costs of solar absorber could be an important option to reduce the costs and increase the popularity of PTC system. For the full-scale, Ultimate Trough solar field, where the aperture is reported as 7.5 m, the total installed costs were estimated at 178 USD/m^2, whereas the receiver tube cost was reported at 25 USD/m^2, which is above 14 % of total investment cost [29,30]. In the case of smaller installations such as SHIP, where the aperture is two or three times smaller than the ultimate

Table 1
SHIP installations using parabolic trough collectors technology [9].

Name	Country	Industry sector	Installed collector area, m^2	Installed thermal power, kW_{th}	Temperature range, °C	Solar thermal energy used for	Ref.
Papes Safor S.L.	Spain	Processing and preserving of fruit and vegetables	175	134	200–250	pre heating, boiler	[10]
SKF Technologies Mysore	India	Manufacture of fabricated metal products	256.4	72	130–210	heat the water for circulation through the treatment tanks	[11]
Barcel S.A DE C.V.	Mexico	Manufacture of food products	176.8	77.9	200	vegetal oil heating	[12]
Lesa Dairy	Switzerland	Manufacture of dairy products	115	67	190	milk processing	[13]
NL Industries Inc.	United States	Manufacturing	949	–	189	hectorite drying	[14]
SILAMPOS, S. A.	Portugal	Manufacture of fabricated metal products	108	67	180	process wash and drying finished product	[15,16]
Emmi Dairy Saignelégier	Switzerland	Manufacture of dairy products	627	360	140–180	steam for different dairy processes	[13,17]
Cremo SA	Switzerland	Manufacture of dairy products	581	330	125 or 170	milk processing, coffee cream production	[13,18]
Honeywell Technology Solutions	India	Manufacturing	821	574.7	165	space cooling of production hall	[19]
Bomans Lackering	Sweden	Manufacture of computer, electronic and optical products	100	40	160	hot water for chemical baths	[20]
Solar steam boiler for Procter & Gamble	China	Manufacture of chemicals and chemical products	2330	1050	160	steam generation	[21]
PSG Hospital Laundry	India	Human health and social work activities	50	35	150	drying and sterilization in laundry	[22]
Alanod Solar	Germany	Manufacture of fabricated metal products	108	75.6	143	production of saturated steam	[17,23]
Parc Solaire Alain Lemaire	Canada	Manufacture of paper and paper products	1490	800	120–140	pre heating, steam boiler	[10]
SHIP for sewage sludge drying	United States	Waste management and remediation activities	151	98	90–100	drying sewage sludge	[10]
Nestle dairy plant	Mexico	Manufacture of dairy products	224.5	126	80–95	pasteurization	[12]
Casa Armando Guillermo Prieto S.A de C.V.	Mexico	Manufacture of beverages	326.7	136.79	90	boiler preheating	[12]
COPAG	Morocco	Manufacture of dairy products	110	61	80–90	pasteurization	[10]
Laiterie Chagnon SHIP	Canada	Manufacture of dairy products	82	46	80–90	pre heating, boiler	[10]
Quesos la Ordeña	Mexico	Manufacture of food products	66	35.34	80	boiler preheating	[12]
Alimentos y Productos para Ganado Lechero	Mexico	Manufacture of prepared animal feeds	412.5	179.85	60	water heating	[12]
Woltow, Parabolic trough power plant for a fish farm	Germany	Agriculture, forestry and fishing	440	220	–	water heating	[24]
Miraah Oman	Oman	Mining and quarrying	630,000	300,000	–	enhanced oil recovery	[17,25]
Horizon Nut (project)	United States	Food products	72	50	230	drying, roasting	[26]
Frito Lay (project)	United States	Food products	5068	3548	215	general process heating	[26,27]

trough, it can be estimated that the receiver's share of the total investment is significantly higher. A significant part of the absorber's price is selective coating.

The application procedure of the solar selective coating to the absorber surface usually requires a high cost due to the multi-step processes [31]. Among the production methods of spectrally selective coating, one can distinguish: dip coating, spin coating, laser sintering, chemical vapor deposition (CVD), atomic layer deposition (ALD), physical vapor deposition (PVD), electroless plating, electroplating and lithography [32]. PVD is the most common method of selective coating manufacturing which can produce many types of coatings [33]. Usually, this process is based on multilayers applying, semiconductor–metal tandems or cermet which requires time and an expensive production line [31,32]. Commercially available selective coatings used in industrial solar power plants are characterized by high absorbance and low emissivity. Solel, a cermet-based coating, achieves an absorptivity of 0.96 and an emissivity of 0.07–0.17 for 100–400 °C [34]. PTR70 coating, also reports a high absorptivity of 0.957 [35].

Two paths can be taken to increase the attractiveness of PTC system, both for solar power plants application and industrial heat production: improve the efficiency or reduce the investment cost of installation. Many research works have been devoted to the study of parabolic trough collectors to increase their efficiency [36,37]. The optimization of parabolic mirrors and the tracker system is a frequently studied aspect [38–40]. Shaaban [41] optimized the parabolic shape and proposed the optimal solution based on wind speed effect. Tang et al. [42] proposed the secondary reflector in PTC concentrator to achieve uniform heat flux distribution. The intensification of heat transfer and efficiency improvement can also be realized by applying nanoparticles into the heat transfer fluid [43,44]. The intensification of heat absorption presented by Norouzi et al. [45,46] may also involve rotating the absorber to uniformize the heat input to its surface. Another way to increase the PTC efficiency is to use different types of inserts. Twisted tape inserts are widely studied and fins inserts are the solution which achieve an optimum thermal and hydraulic performance [47]. Efficiency improvement is also realized through the use of special coatings in various configurations. Yang et al. [48] proposed the absorber with two different coatings on the concentrated and natural radiation-absorbing side. The results reported receiver efficiency increase from 64.7 % to 68.1 %. A cascade arrangement of absorbers with different selective coatings was also considered, where Stollo et al. [49] found that LCOE could be reduced by 10.6 % and 12.3 %. Zhao et al. [50] presented the efficiency-enhancing strategy by cascade applying multiple selective coatings based on their emissivity characteristics. The results indicated a heat loss reduction by 29.3 % and a thermal efficiency enhanced by 4.3 % at 290–550 °C. However, both of these analyses were conducted for large-scale solar power plants with high concentration ratios and thermal fluid temperature levels. The high prices of the coatings, however, were not reduced in this analysis.

A possibility to reduce the investment cost could be the use of cost-effective solar absorber coatings, whose application process is extremally cheap compared to solar selective coatings. One example is the most commonly used high-temperature solar absorber coating Pyromark, which reaches an absorbance of up to 96.5 % [51,52]. Martinez et al. [53] compared the experimental results of four different low-cost, high-absorbency coatings where α was up to 95 ± 1 %. A disadvantage of these coatings, however, is their high emissivity [54].

This paper aims to present the potential for partial replacement of expensive selective coatings, with low-cost high absorption coatings in low-temperature heat transfer medium regions, which has not been proposed in the published literature to the knowledge of the authors. Such a solution can significantly affect the cost of PTC installation and reduce the required manufacturing process along with the energy required to carry it out. Thus, it could be an effective way in increasing the attractiveness of the PTC installations to produce high-temperature heat for industrial applications. The research questions that this article aims to answer are:

- Is it possible to partially replace selective coatings, with low-cost high absorbance and emissivity coatings in PTC-SHIP installations?
- For which installations and temperature range can this solution be applied?
- What parameters can influence the optimal solution?

The main contribution of this article is to propose a method to reduce the price of a PTC installation based on commercially available solutions and to demonstrate a mathematical model suitable for low concentration PTC installation.

2. Methods

In this paper, the idea for reducing installation capital costs is to partially replace expensive selective coatings with low-cost easily spray-applied coatings. Fig. 2 illustrates the concept based on a single PTC solar loop. In further sections of the solar loop, the temperature of heat transfer fluid increases, which results in higher heat losses. The following analysis is to examine how many absorbers can be replaced with a non-selective coating while maintaining the baseline efficiency. Section 2.1 describes the analysed cases in detail and section 2.2 presents the developed two-dimensional mathematical model along with experimental validation.

2.1. Model parameters

Four geometries were analyzed, referring to installations currently under operation in natural conditions. Cases 1–3 refer to SHIP installations that are designed to generate high-potential heat [9]. Cases are distinguished by the various outlet temperatures required for the industrial process and a specific concentration ratio C and geometry, along with the parameters of the commercially available collectors. The geometric concentration ratio is defined as Eq. (1) according to [55]:

$$C = \frac{W_{ap}}{\pi \bullet d_{abs,e}}, \tag{1}$$

where W_{ap} is aperture width, and $d_{abs,e}$ is external absorber diameter.

Case 4 refers to a full-size CSP power plant with a high inlet (290 °C) and outlet temperature (390 °C) in a solar loop.

The analysis was performed for 1 loop, where the total length L is comparable for cases 1–3 but not the same due to the different dimensions of the collectors (42.84 m; 44.32 m; 41.6 m). For case 4, loop length is comparable to full-scale solar power plants. Table 2 summarizes all the assumed parameters. Absorber thermal conductivity of 15 W/mK made of stainless steel 316 and borosilicate glass envelope conductivity of 1.1 W/mK were used in calculations to unify the assumptions. The assumptions regarding the optical parameters of the parabolic mirror, glass envelope, and tracking were also unified. In each case, a perfect vacuum between the glass envelope and absorber is assumed. The parameters for these data are presented in subsection 2.2.

Table 3. summarizes the absorptivity and emissivity parameters of the coatings for the various absorbers studied in this paper. For Power Trough 110, these parameters are shared by the manufacturer [56]. For Poly Trough 1800 and Power Trough 250, there is a lack of information about selective coatings applied. Then, two different coatings reported as suitable for SHIPs by Noč et al. [32] were used. The coating data for Parabolic Trough (PTR70) were obtained from an experimental study conducted and reported by The National Renewable Energy Laboratory [35].

Pyromark 2500 was selected as a cost-effective alternative coating for the first sections of the PTC loop because of its high absorptivity > 0.96 and maturity [52]. Pyromark is a silicone-based high-temperature paint, and it is most widely used as a solar absorber coating for solar

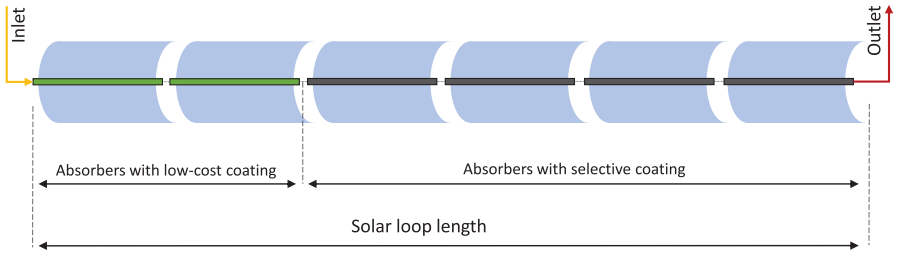

Fig. 2. Concept of reducing the investment cost by partially replacing selective coatings with cheaper alternative ones.

Table 2
Thermodynamic and geometric parameters of the analysed PTCs cases [35,56–59].

Parameter	Symbol	Unit	Case 1		Case 2	Case 3	Case 4
			Low Temp. SHIP		Mid Temp. SHIP	High Temp. SHIP	CSP power plant
			1A	1B			
Heat transfer fluid	HTF	–	Therminol VP-1	Water (2 bar)	Therminol VP-1	Therminol VP-1	Therminol VP-1
Outlet temperature	T_{out}	°C	120		200	250	390
Inlet temperature	T_{in}	°C	60		100	120	290
Collector type	–	–	Power Trough 110		PolyTrough 1800	Power Trough 250	Parabolic Trough 70
Focal Length	f	mm	341		647	929	1710
Aperture width	W_{ap}	mm	1100		1845	2500	5760
Absorber length	L_{abs}	m	3.06		5.54	4.16	4.08
Number of absorbers in loop	X	–	14		8	10	150
Total absorbers length in loop	L	m	42.84		44.32	41.6	612
Absorber external diameter	$d_{abs,e}$	mm	33.4		34	38	70
Absorber internal diameter	$d_{abs,i}$	mm	30.4		31	35	66
Absorber wall thickness	Th_{abs}	mm	1.5		1.5	1.5	2
Absorber thermal conductivity	λ_{abs}	W/mK	15		15	15	15
Glass env. external diameter	$d_{c,e}$	mm	70		56	70	120
Glass env. internal diameter	$d_{c,i}$	mm	65		51	65	115
Glass env. wall thickness	th_c	mm	2.5		2.5	2.5	2.5
Glass env. thermal conductivity	λ_c	W/mK	1.1		1.1	1.1	1.1
Concentration ratio	C	–	10.5		17.3	20.9	26.2

Table 3
Absorbers coatings and their optical parameters.

Absorber	Coating data	Absorptivity	Emissivity	Ref.
Power Trough 110	Manufacturer	0.87	0.35	[56]
PolyTrough 1800	Mo/Al_2O_3	0.9	0.08	[61]
Power Trough 250	TiC-TiN/ Al_2O_3	0.92	0.11	[62]
Parabolic Trough 70	NREL	0.957	$0.062+(2E-07)\cdot T_{abs,e}^2$	[35,63]
–	Pyromark	0.965	$-4E-13\cdot T_{abs,e}^4 + 1E-09\cdot T_{abs,e}^3 - 1E-06\cdot T_{abs,e}^2 + 0.0006\cdot T_{abs,e} + 0.7506$	[51,52]

central receivers [60] in even much higher temperatures than PTC receivers. Data for this coating were adopted from experimental studies reported in [52].

For comparative analysis, the same heat transfer fluid was selected for each scenario, the Therminol VP-1 oil. The selected fluid is an Eastman product, widely used in PTCs installations [36,64,65]. The composition of the HTF is a biphenyl/diphenyl oxide eutectic mixture where the operating temperature is 12–400 °C. Table 4 shows the parameters of Therminol VP-1 as a function of its temperature based on the manufacturer's data [66]. Case 1 calculations were performed also for pressurized water to compare the work potential. Case 1 has the lowest temperature range and for its case, pressurized water is also a commonly used medium. The pressurised water parameters were applied according to the IAPWS IF97 [67].

Table 4
Heat transfer fluid parameters Therminol VP-1 [66,68].

Parameter	Symbol	Equation	Unit
Density	ρ	$-0.856\cdot T + 1316$	kg/m^3
Specific heat	c_p	$2.137\cdot T + 761.88$	J/(kg·K)
Thermal conductivity	k	$-1.36E-04\cdot T + 0.1773$	W/(m·K)
Dynamic viscosity	μ	$250568541\cdot T^{-4.407}$	Pa·s

The main calculations were performed for the weather conditions as summarized in Table 5. The mass flow of HTF for each case was adjusted to achieve the expected temperature in the outlet.

2.2. Mathematical model

To determine the performance of parabolic trough collectors, a two-dimensional mathematical heat transfer model was developed and its fundamental parts are visualized in Fig. 3. The mathematical model

Table5
The weather and sun position data assumptions.

Parameter	Symbol	Value	Unit
Direct normal irradiance	G_B	800	W/m^2
Ambient temperature	T_{amb}	23	°C
Wind speed	v_w	2	m/s
Incident angle	θ	20	°

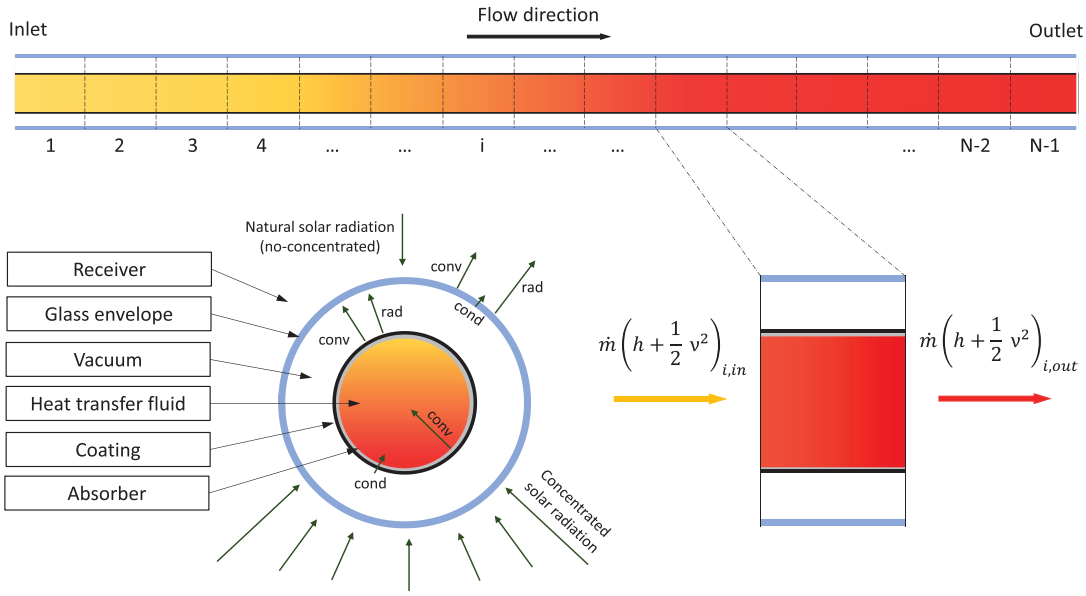

Fig. 3. Two-dimensional model of heat transfer in PTC receiver.

includes all parameters such as geometric dimensions of PTC, materials used in the installation and their properties and atmospheric conditions such as solar radiation intensity, sun position, and ambient temperature. The proposed model is based on previously developed algorithms but it is improved with several new features [69–71].

Usually, in mathematical models, the energy delivered to the absorber is only considered in concentrated radiation form. This assumption has validity for use with highly concentrated parabolic trough collectors, such as those used in industrial solar power plants. In the case of high-concentrated PTC, natural radiation, not previously concentrated but directly reaching the absorber surface from the sun direction, is only a small part of the total energy input, so its inclusion together with concentrated radiation does not introduce a large error into the calculation. Since the following analysis also considers low concentrated PTC, this aspect is included as it has a significant impact on the results. The energy delivered to the absorber tube is the sum of concentrated and non-concentrated solar energy, which is calculated separately, which is the main novelty in the following mathematical model and provides more detailed results. A further feature of the model is the identification possibility of the absorber and glass envelope average temperature in its specific section which enables the whole solar loop to be analysed in very short segments.

Each analysed receiver is divided into N sections, which increases the accuracy of the obtained results. Each case considered includes PTC components separately, such as linear absorber with particular coating, glass envelope, heat transfer fluid, parabolic mirror and its optical efficiency parameters.

Fig. 4 shows the thermal resistance model for the receiver cross-section for stable operating parameters. The heat transfer in the receiver includes: convection between the inner absorber wall and heat transfer fluid, conduction through the absorber, radiation and convection loses between the external absorber surface and internal glass

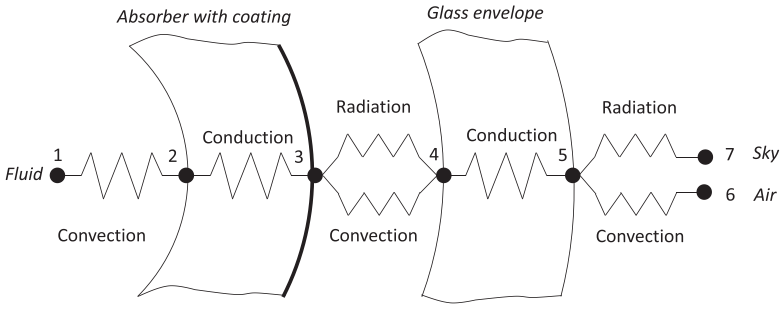

Fig. 4. Thermal resistance for the receiver cross-section.

envelope surface, conduction through the glass envelope and convection loss between the external glass surface and ambient and radiation loses between external glass envelope surface and sky. It should be emphasized that in all investigated cases, an ideal vacuum between the absorber and glass envelope was assumed, therefore convection losses were not considered in calculations, although they are also showed in Fig. 4.

All the equations used in the proposed mathematical model are presented as follows. The useful heat collected by the thermal fluid, can be calculated from the following Eq. (2) based on [70]:

$$Q_u = \dot{m} \bullet c_p \bullet (T_{out} - T_{in}), \tag{2}$$

where Q_u is the useful thermal energy in the absorber, $\dot{m}$ is the mass flow, c_p is the specific heat of the working fluid, T_{out} is the outlet temperature of the working fluid, T_{in} is the inlet temperature of the working fluid.

The useful thermal energy can also be represented by Eq. (3), which considers the optical efficiency of the radiation concentration and the thermal loses in the receiver [69]. This model divides the concentrated radiation on one part of the absorber and the natural radiation illuminating the other part as presented in Fig. 3:

$$Q_u = (Q_{u,CSP} + Q_{u,SP}) - Q_{loss} \tag{3}$$

where $Q_{u,CSP}$ is the concentrated solar energy, $Q_{u,SP}$ is the non-concentrated solar energy, Q_{loss}- energy losses. The use of such separation of the energy input to the absorber has the greatest impact on the results at low concentrated PTCs. Usually natural radiation is not considered separately in CSP systems.

Solar power from concentrated solar irradiance including the shadow of the absorber is defined as follows (4) [72]:

$$Q_{u,CSP} = (A_{ap} - d_{abs,e} \bullet L) \bullet G_B \bullet \eta_{opt,CSP} \bullet \cos\theta \bullet IAM \tag{4}$$

where, A_{ap} is the aperture surface area, $d_{r,e}$ is the absorber external diameter, G_B is the direct solar irradiance, $\eta_{opt,CSP}$ is the optical efficiency for CSP, θ is the incident angle, IAM is the incidence angle modifier. Solar power from non-concentrated radiation as follows (5):

$$Q_{u,SP} = (d_{abs,e} \bullet L) \bullet G_B \bullet \eta_{opt,SP} \tag{5}$$

where, L is absorber length, $\eta_{opt,SP}$ is the optical efficiency for SP. Since in both presented cases the solar radiation sun-to-absorber path is different, two different efficiencies have to be used (6) and (7) to calculate solar power [69]:

$$\eta_{opt,CSP} = \tau_c \bullet \alpha_{abs} \bullet \eta_{sh} \bullet \eta_{track} \bullet \eta_{ref} \bullet \eta_{d,m} \bullet \eta_{d,r} \tag{6}$$

$$\eta_{opt,SP} = \tau_c \bullet \alpha_{abs} \bullet \eta_{d,r} \tag{7}$$

Some of the above efficiencies have a fixed value, some are variable as a function of temperature. Table 6 summarizes the above coefficients, based on research conducted by the National Renewable Energy Laboratory (NREL) [73] and Kalogirou model [69] along with the assumed values.

The incidence angle modifier (IAM) is a function of incidence angle and the optical quality of the collector. It's assumed that the IAM is determined by Duffie et al. [74]:

$$IAM(\theta) = 1 - \frac{f}{L}\left(1 + \frac{W_{ap}{}^2}{48f^2}\right) tan\theta \tag{8}$$

Total solar energy received by a PTC installation is defined as Eq. (9) [75]:

$$Q_s = A_{ap} \bullet G_B. \tag{9}$$

The total efficiency of parabolic trough collector can be described as presented below [76]:

$$\eta = \frac{Q_u}{Q_s}. \tag{10}$$

Energy loss in the receiver can be defined as Eq. (11) [73]:

$$Q_{loss} = Q_{rad,5-7} + Q_{cov,5-6} \tag{11}$$

where $Q_{rad,5-7}$ is the radiation loses from external glass cover surface to sky, and $Q_{cov,5-6}$- is the convection loses from external glass cover surface to ambient. They can be calculated with the Eq. (12) and (13) [77,78]:

$$Q_{rad,5-7} = \sigma \bullet \varepsilon_c \bullet A_{c,e} \bullet \left(T_{c,e}^4 - T_{sky}^4\right) \tag{12}$$

$$Q_{cov,5-6} = A_{c,e} \bullet h_{ca} \bullet (T_{c,e} - T_{amb}) \tag{13}$$

where σ is Stefan-Boltzman constant, ε_c is the emissivity of glass cover (0.9), $T_{c,e}$ is the cover external surface temperature, T_{amb} is the ambient temperature, h_{ca} is the convection heat transfer coefficient. The sky temperature was calculated based on [79] and Köppen classification [80] and presented in following correlation:

$$T_{sky} = T_{amb} - 7. \tag{14}$$

For heat transfer convective coefficient calculation, model proposed by Forristall [81] was used:

$$h_{ca} = \frac{k_{ca}}{d_{c,e}} \bullet Nu_{d_{c,e}} \tag{15}$$

where, h_{ca} is the convection heat transfer coefficient for air at temperature of $(T_{c,e} - T_{amb})/2$, k_{ca} is the thermal conductivity of air at temperature of $(T_{c,e} - T_{amb})/2$, $Nu_{d_{c,e}}$ is the Nusselt number based on the glass envelope outer diameter.

For no wind cases, the correlation developed by Churchill and Chu [81,82] can be used:

$$Nu_{d_{c,e}} = \left\{ 0.6 + \frac{0.387 Ra_{d_{c,e}}{}^{1/6}}{\left[1 + (0.559/Pr_{ca})^{9/16}\right]^{8/27}} \right\}^2 \tag{16}$$

$$Ra_{d_{c,e}} = \frac{g \bullet \beta \bullet \left(T_{c,e} - T_{amb}\right) \bullet d_{c,e}{}^3}{(\alpha_{ca} \bullet \nu_{ca})} \tag{17}$$

where $Ra_{d_{c,e}}$ is the Rayleigh number for air based on the glass envelope outer diameter; g is the gravitational constant (9.81), m/s^2; α_{ca} is the thermal diffusivity for air at T_{ca}, ν_{ca} is the kinematic viscosity for air at T_{ca}.

For wind cases, the convection heat transfer is forced convection. The Nusselt number is estimated with Zhukauskas correlation based on [82]:

$$Nu_{d_{c,e}} = D \bullet Re_{d_{c,e}}{}^m \bullet Pr_{amb}{}^n \bullet \left(\frac{Pr_{amb}}{Pr_{ca}}\right)^{1/4} \tag{18}$$

where the equation coefficients are presented in Table 7.

Assuming that there is an ideal vacuum between the outer part of the absorber and the inner glass envelope, the sum of radiation and con-

Table 6
Model optical assumptions.

Parameter	Symbol	Value
Transmittance of glass envelope	τ_c	0.965
Absorber absorptivity	α_{abs}	f(T_{abs})
Shadowing	η_{sh}	0.99
Tracking error	η_{track}	0.994
Clean mirror reflectance	η_{ref}	0.935
Dirt on mirrors	$\eta_{d,m}$	0.96
Dirt on receiver	$\eta_{d,r}$	0.98

Table 7
Equation coefficients for Nusselt number calculation.

Re	D	m
1–40	0.75	0.4
40–1 000	0.51	0.5
1 000–200 000	0.26	0.6
200 000–1 000 000	0.076	0.7
Pr	**n**	
Pr ≤ 10	0.37	
Pr > 10	0.36	

vection losses from the glass envelope to the ambient is equal to the radiation loss between the outer part of the absorber and the inner part of the glass envelope [69]. Eq. (19) represents this correlation:

$$Q_{loss} = \frac{\sigma \bullet A_{c,e} \bullet \left(T_{abs,e}^4 - T_{c,i}^4\right)}{\frac{1}{\varepsilon_{abs}} + \frac{1-\varepsilon_c}{\varepsilon_c} \bullet \frac{A_{abs,e}}{A_{c,i}}} \tag{19}$$

where ε_{abs} is the emissivity of selective coating on absorber external surface. Thermal conductivity is calculated based on [83] for absorber (20) and glass envelope (21):

$$Q_u = \frac{2 \bullet \pi \bullet k_{abs} \bullet (T_{abs,e} - T_{abs,i})}{\ln\left(\frac{d_{abs,e}}{d_{abs,i}}\right)} \tag{20}$$

$$Q_{loss} = \frac{2 \bullet \pi \bullet k_c \bullet (T_{c,e} - T_{c,i})}{\ln\left(\frac{d_{c,e}}{d_{c,i}}\right)} \tag{21}$$

All the surfaces used in the equations are determined as follows:

$$A_i = \pi \bullet d_x \bullet L \tag{22}$$

where, d_x represents $d_{abs,i}, d_{abs,e}, d_{c,i}, and d_{c,e}$; L is the absorber length. Eq. (23) presents the method of determining the convection coefficient, where the input values are model parameters for a given absorber section [84]:

$$h = \frac{Q_u}{(\pi \bullet d_{abs,i} \bullet L) \bullet (T_{abs,i} - T_m)} \tag{23}$$

Convection coefficient is calculated for mean (average) fluid temperature [84]:

$$T_m = \frac{T_{out} + T_{in}}{2}. \tag{24}$$

In the presented model, Eq. (25) was used for laminar flow and (26) for turbulent flow due to their high conformity in the mathematical calculation of PTC systems indicated by Tzivanidis et al. [71]:

$$Nu_f = 3.66 + \frac{0.0668 \bullet Re \bullet Pr \bullet \frac{d_{abs,i}}{L}}{1 + 0.04 \bullet (Re \bullet Pr \bullet \frac{d_{abs,i}}{L})^{\frac{2}{3}}}. \tag{25}$$

$$Nu_f = 0.023 \bullet Re^{0.8} \bullet Pr^{\frac{1}{3}} \tag{26}$$

The Nusselt number can be defined according to Eq. (27), considering the convection coefficient [85]:

$$Nu_f = \frac{h \bullet d_{abs,i}}{k} \tag{27}$$

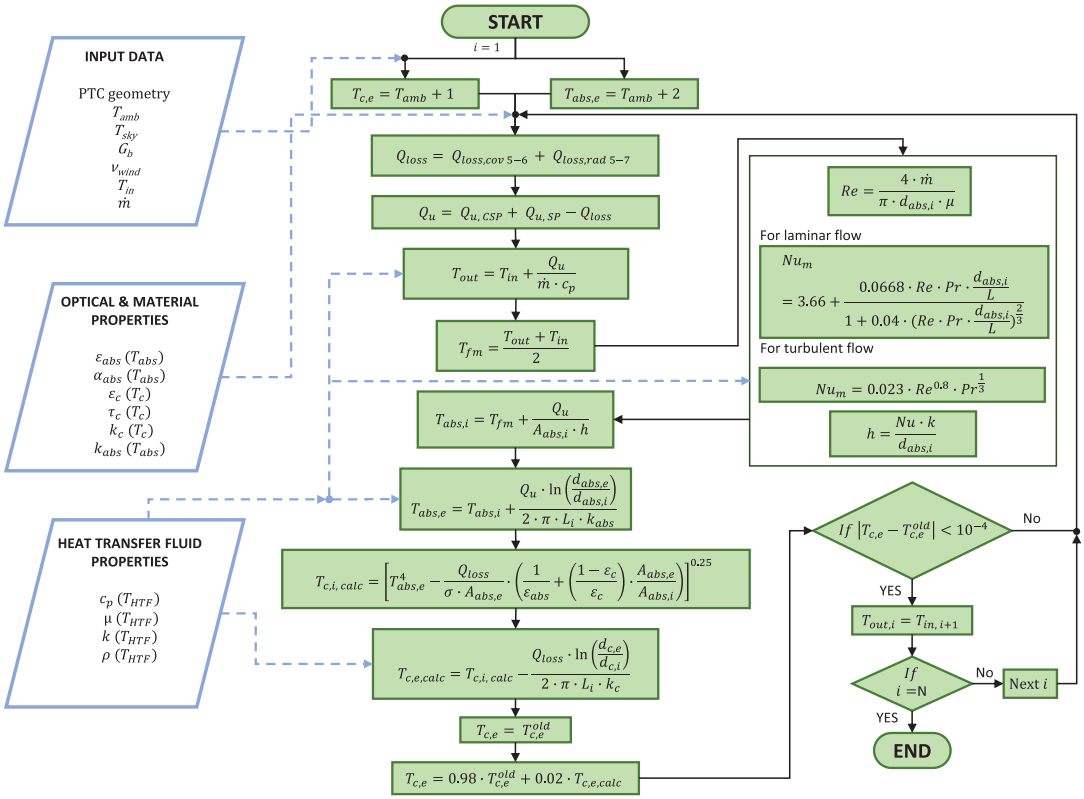

Fig. 5. Flow chart of the mathematical model.

Fig. 5 presents a flow chart visualizing the performance of the developed two-dimensional mathematical model. The calculations presented in this model are performed for each section of PTC separately. Any size of the PTC segment can be analyzed. In the blue field, boundary conditions were determined for each PTC section studied. Boundary conditions can be divided into 3 parts. Input data include geometric dimensions of the tested PTC, ambient conditions such as ambient temperature, sky temperature, irradiance, wind speed and temperature heat transfer fluid in the inlet of the loop as well as mass flow. Optical and material properties describe the performance of individual system components in terms of their optical properties. Some of these parameters are characterized by constant values, and some of them are temperature dependent. The algorithm at each step uses the appropriate value as a function of a specific temperature. It is also possible to analyze the system for varying properties as a function of solar loop length, which provides the opportunity to study different coatings for specific absorber sections. The third boundary condition is the properties of heat transfer fluid. The algorithm enables performance calculations for different mediums as a function of temperature. The corresponding application of each boundary condition is visualized in Fig. 5.

The calculations presented in the algorithm are based on the appropriately converted equations (2)–(27). The algorithm starts the calculation by assuming the first external temperature of the glass envelope wall. Then after calculating the heat losses to ambient and determining the flow parameters, the temperature outlet of heat transfer fluid is calculated. The next step is to calculate the temperature of the outer wall of the absorber and glass envelope. If the agreement is hight and the set and calculated temperatures differs less than 10^{-4}, the calculated outlet temperature of the receiver section is the inlet temperature for the next section where the calculation continues in the same way. If the temperature does not match the assumed range, the calculation is repeated for a different temperature according to the correlation shown in the algorithm. The first assumption of the absorber temperature and the glass tube temperature is only the first step in starting the calculation. Usually, the algorithm requires about 40–150 iterations per segment to achieve the required compliance, where the segment depends on the analyzed receiver length. It is usually about from a few millimetres to a few centimetres. However, the number of sections is always determined before the calculation is performed, guaranteeing high consistency and accuracy of the calculations.

2.2.1. Model validation

The mathematical model was experimentally validated based on literature data[35] The experimental study was conducted by NREL and its main objective was to determine heat loss and glass envelope temperature as a function of average absorber temperature. The PTR70 Schott, which is the receiver analysed in Case 4, was tested for model validation. The geometrical parameters of the receiver are shown in Table 2. The purpose of NREL study was to determine the emissivity of selective coating as a function of receiver temperature and calculate the heat losses. Fig. 6 presents a comparison of the results obtained from the mathematical model and NREL experiment. The test was performed indoors and an electric heater inside the receiver was used to simulate the absorber temperature. In the experimental study [35], the power of the electric heaters was varied to equalise the wall temperature along the entire length of the absorber. The temperature was measured at a dozen points along the length of the absorber and then averaged. For steady-state conditions, the temperature of the glass envelope was measured. The error associated with this measurement is shown by the error bars for the individual points in Fig. 6. Knowing the parameters of the tested absorber, the emissivity of the selective coating was determined and then the heat loss was calculated, which is marked as points in Fig. 6. For the same conditions (absorber temperature, ambient temperature and absorber parameters), the losses to ambient and the glass envelope temperature as a function of the absorber wall temperature were calculated using the developed mathematical model. These characteristics are shown as a continuous line.

The study parameters were as follows: $G_b = 0W/m^2$, $T_{amb} = T_{sky} = 24^{\circ}C$, $\nu_{wind} = 0m/s$, $\dot{m} = 0kg/s$. Heat losses and glass envelope temperature were evaluated using the root mean squared deviation (RMSD) presented as Eq. (28) based on the data from literature [86]:

$$RMSD = \sqrt{\frac{1}{n}\sum_{i=1}^{n}\left(Y_{exp,i} - Y_{num,i}\right)^2} \tag{28}$$

where n is the number of measurements, Y is results of measurement, exp is the experimental results, *num* is the numerical result from mathematical model. The relation between the RMSD values to the average results obtained was calculated as Eq. (29):

$$\sigma_{RMSD} = \frac{RMSD}{Y_{num,av}} \bullet 100\%. \tag{29}$$

The results presented in Table 8 summarizes *RMSD* and σ_{RMSD} values. Both demonstrate a high agreement between the model and the experimental data. Therefore, the results of the calculations presented in this paper can be considered as highly accurate and the determined losses reflect the real conditions.

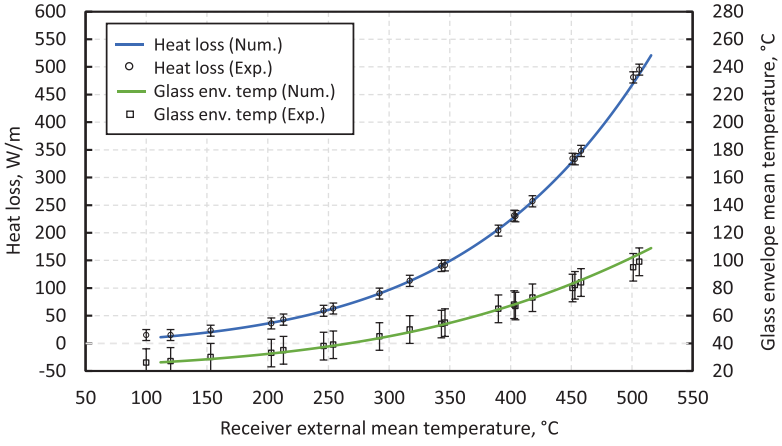

Fig. 6. Mathematical model validation based on NREL experimental results [35].

Table 8
Model validation results.

Parameter	Glass envelope temperature	Heat losses	Unit
RMSD	2.54	3.52	–
σ_{RMSD}	4.27	1.85	%

3. Results and discussion

3.1. Partially non-selective coating application potential

The PTC efficiency changes with the length of the absorber, which results from the temperature increase of the heat transfer fluid and the absorber itself. Fig. 7 compares the receiver efficiencies as a function of the medium temperature for the four previously described cases. This efficiency refers to the specific section of the absorber The mass flow for each case was adjusted to achieve the assumed outlet temperature from the solar loop. For each case, two scenarios are compared: the red line which represents the reference case that is the use of absorbers with a serially produced selective coating, and the case represented by the black line is the case that assumes the replacement of the selective coating with Pyromark 2500 over the entire length of the solar loop.

The greatest potential for cost-effective coating applications is shown in cases 1 and 2. For low-temp SHIP, an increase in total PTC loop efficiency was observed for Therminol VP-1 and pressurized water by 4.44 percentage points and 5.29 percentage points, respectively (Table 9). For this scenario, there is a visible increase in absorber efficiency along the length. Despite the higher emissivity of Pyromark relative to the base selective coating, for the temperature range of 60–120 °C, high absorption is more significant than low emissivity. It can be concluded that in case of low-concentration installations, where the temperature of the

Table 9
Summary of average solar loop efficiency after replacing selective coating to Pyromark 2500 consistent with data presented in Fig. 7.

Parameter	Case 1		Case 2*	Case 3*	Case 4*
	1A*	1B**			
η_{SCC}, %	69.36	70.05	73.85	74.61	76.44
$\eta_{PYROMARK}$, %	73.80	75.34	71.38	68.59	57.74
$\Delta\eta$, %	4.44	5.29	−2.47	−6.02	−18.71

* Therminol VP-1; ** Water

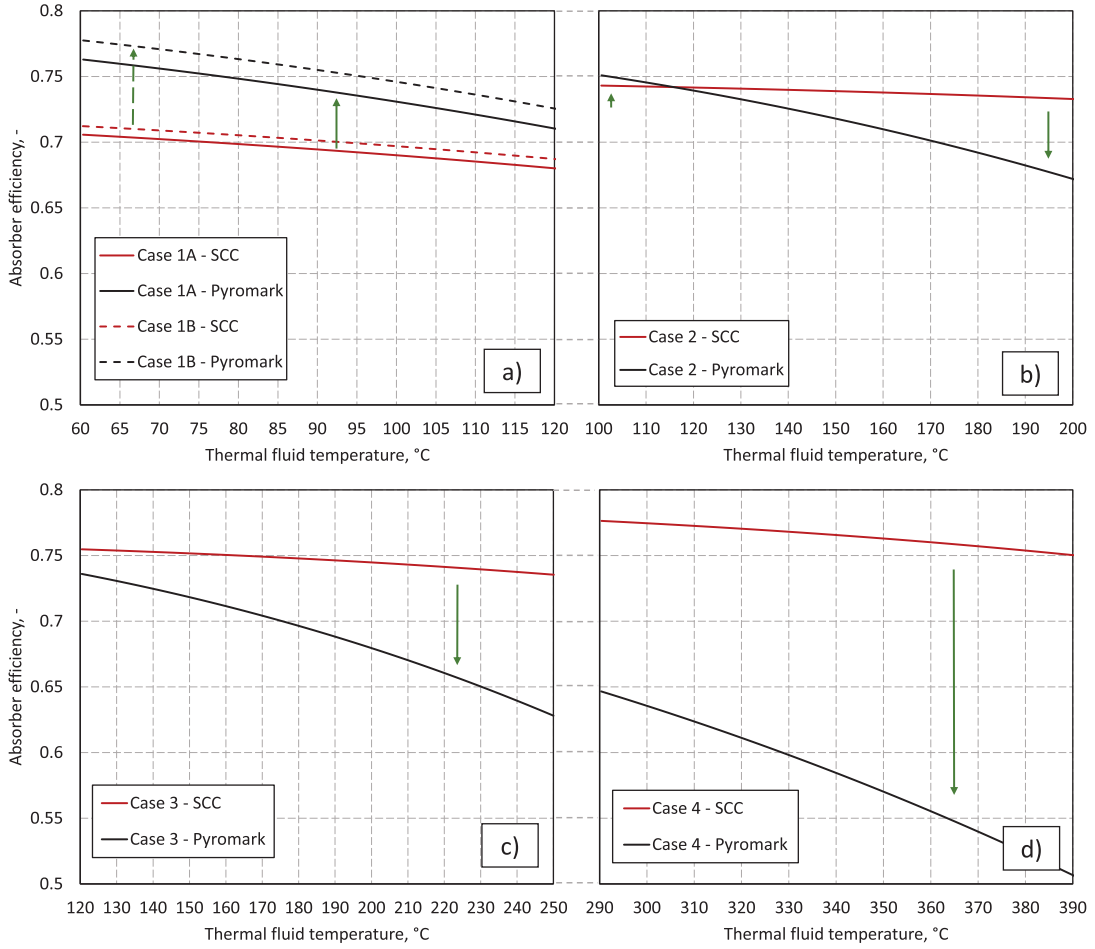

Fig. 7. Absorber efficiency as a function of heat transfer fluid temperature: a) Case 1 - low-temp. SHIP, b) Case 2 – medium temp. SHIP, c) Case 3 – high temp. SHIP, d) Case 4 – CSP power plant.

heat transfer fluid is relatively low, absorbers covered with highly absorptive coating can be used instead of selective coating. In this case, the greater potential for using water as a heat transfer fluid is also demonstrated.

For medium-temperature SHIP (case 2), the potential for the replacement of selective coatings with cheaper non-selective alternatives is characterized in the range up to about 115 °C. Above this temperature, there is a decrease in efficiency relative to the baseline curve. Total replacement of coatings with non-selective ones results in a 2.47 % decrease in loop efficiency, however, partial replacement can be beneficial.

Case 3 and case 4 represents high-temp SHIP and CSP power plant accordingly. The results show a significant decrease in average loop efficiency after replacing the coatings with non-selective ones which are caused by high losses due to the high-temperature range. For the previously assumed conditions, the decrease in efficiency of the solar loop in case 3 is 6.02 %. For the case representing a solar loop from a high-scale CSP power plant, the efficiency drops from 76.44 % to 57.44 %. Due to the lack of optimization potential, these scenarios were not considered in further work.

3.2. Results low-temperature SHIP

For the previously assumed boundary conditions, according to the results presented in Table 9, case 1 is characterized by an increase in efficiency when a high-absorptivity coating is applied to the entire length of the absorber loop. Despite the high emissivity, compared to the originally used selective coating, a significant improvement in the performance of PTC can be noted. As shown in Fig. 8, the increase in efficiency depends on solar radiation. As the solar radiation changes, the mass flow is adjusted to produce heat at the assumed potential (minimum 120 °C). For lower irradiance G_B, the solar loop efficiency decreases. For each case and irradiance, the mass flow was adjusted to achieve the minimum assumed outlet temperature (absorbers in loop with Pyromark coating = 0). For the determined mass flow, an analysis of the partial replacement of the selective coatings was carried out. The change in the solar loop outlet temperature and the mass flow values are shown in Fig. 9. For each case, T_{in} = 60 °C according to Table 2.

For case 1A, where the heat transfer fluid is Therminol VP-1 and G_B = 1000 W/m^2, the efficiency gain is almost 5 %. For G_B = 400 W/m^2 and Pyromark coating on all 14 absorbers, a slight decrease in efficiency can be noted. If the average irradiance at the location where the installation is to operate is 400 W/m^2, the use of a non-selective coating on 12 absorbers can be considered. Pressurized water, as a heat transfer fluid, is often used in low-temperature systems due to its good thermodynamic properties and cost-effectiveness. Case 1B with water as heat transfer fluid, reaches higher efficiency than Therminol VP-1 for the same temperature range. In this example, the use of high-absorptivity coating absorbers also increases the efficiency of PTC.

3.3. Results mid-temperature SHIP

As shown in Fig. 7, the case 2 shows the possibility of covering part of the absorbers with a non-selective. Fig. 10 presents the solar loop efficiency as a function of the number of Pyromark-coated absorbers. Absorber non-selective coating is considered on the initial sections of the solar loop. On the efficiency curve, two characteristic points can be distinguished. Point A, indicates the number of Pyromark coated absorbers for which the solar loop efficiency reaches its maximum. Point B is the maximum number of absorbers with Pyromark coating for which the solar loop efficiency is not lower than the base efficiency. For the assumed model input data, the results indicate that a low-cost coating can be used on 2 of the 8 absorbers in the entire loop (25 %).

The analysis also considers scenarios where 2 and 3 parallel solar loops, are connected in series. This modification affects the need for increased mass flow in the absorber tubes which changes the flow and heat transfer parameters. In this way, the lower temperature heat transfer fluid section can be extended. For a doubling of the absorber loop, Pyromark can be applied to 50 % of the absorbers. For a 3-times absorber loop length increase, 15 of the 24 absorbers can be coated with a non-selective coating. Furthermore, with the extension of the solar loop, the overall efficiency of the installation increases. For single loop, double extended and triple extended, the average reference efficiency (absorber with Pyromark = 0) is 73.85 %, 73.97 %, and 74.03 % respectively. For the most optimal non-selective coating absorbers cases (point B), it's 73.89 %, 74.06 %, and 74.08 %.

For an industrial process heat applications, the temperature levels of heat transfer fluid are usually crucial. As shown in Fig. 11, for 1 loop length, double and triple, the maximum temperature drop at the outlet of the solar loop was 2.93 °C, 1.97 °C and 1.52 °C, respectively. The outlet temperature itself is presented in Fig. 12. It is worth noting, however, that considering the desired temperature level (assumed outlet temperature minimum of 200 °C), the observed maximum temperature drop at the outlet of the absorber does not seem to be substantial, even when considering the entire absorber loop with a non-selective coating. Previously reported temperature drop corresponds to the following

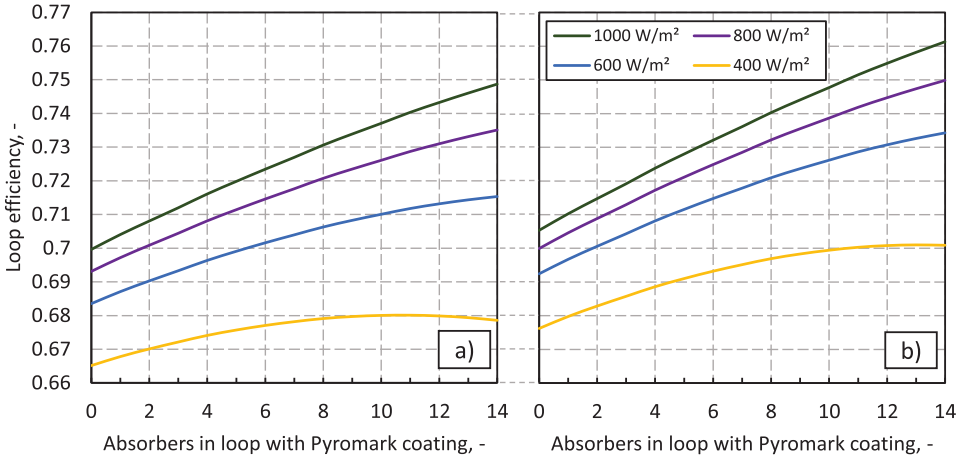

Fig. 8. Loop efficiency of low temperature SHIP installation: a) Case 1A (Therminol VP-1), b) Case 1B (Pressurized water).

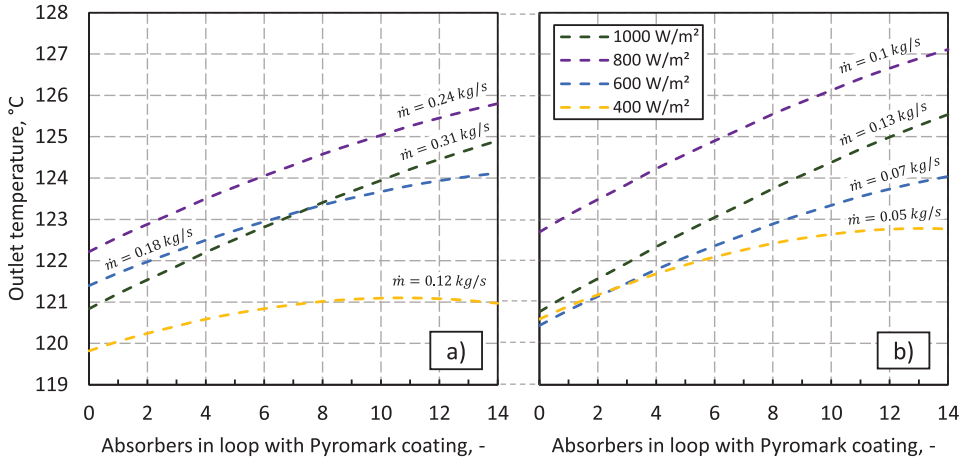

Fig. 9. Heat transfer fluid outlet temperature of low temperature SHIP installation: a) Case 1A (Therminol VP-1), b) Case 1B (Pressurized water).

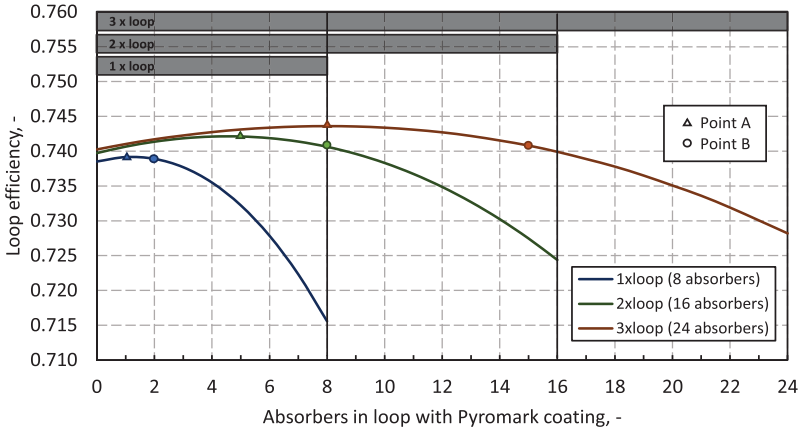

Fig. 10. Loop efficiency of medium temperature SHIP installation.

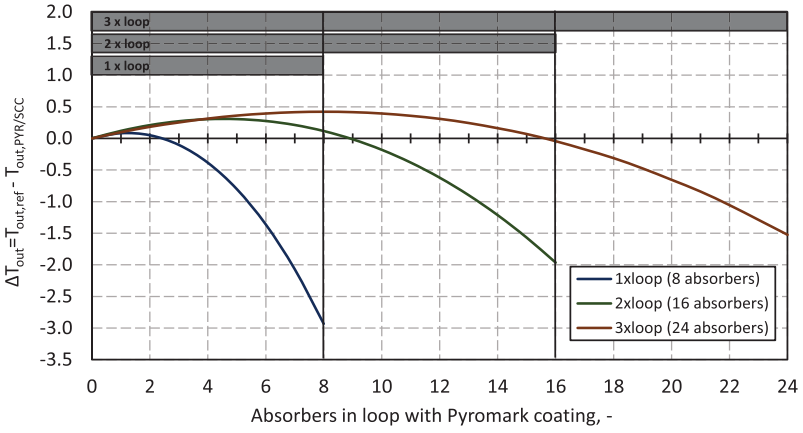

Fig. 11. Temperature drop in the solar loop outlet after changing the coating to Pyromark.

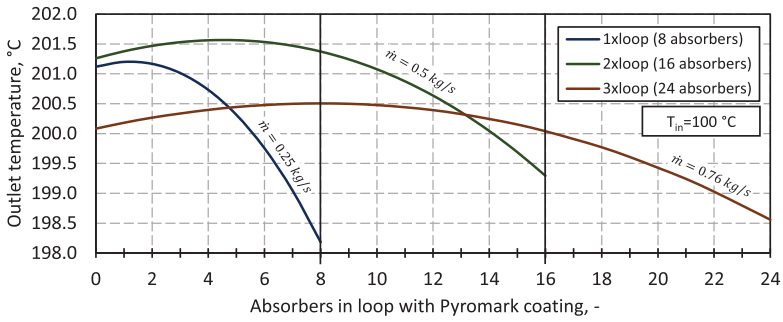

Fig. 12. Temperature in the solar loop outlet after changing the coating to Pyromark.

relative error of 1.47 %, 0.98 %, and 0.76 %. Thus, by considering the proposed strategy on temperature drop, it can be found interesting in solar heat industrial power technologies. Consideration of the validity of using non-selective coating should be conducted on a case-by-case basis. It may also be considered to extend the absorber loop by an additional length of the absorber to compensate for this loss. This case, however, strictly depends primarily on the base price of the technology and the possibility of exploitation of a larger area.

Fig. 13a represents useful energy and heat losses in the PTC loop (24 absorbers), for a different number of sections covered by Pyromark coating. Due to the high emissivity of Pyromark, total losses increase as this coating is applied to more absorber sections. However, an increase in heat collected by the heat transfer fluid resulting from the high absorptivity of this non-selective coating is also observed. This indicates that despite the increased emissivity losses, the high absorbance compensates for these losses up to a certain point. The red curve represents useful heat for the base case where only selective coatings were applied.

Fig. 13b presents the rate of solar energy utilization delivered to the external absorber surface (Q_{solar}). This characteristic tends to increase due to the larger area of the highly absorbing surface. When all absorbers are Pyromark coated, the increment of fully absorbed energy rises by 5.41 %.

The optimal number of absorbers possible to cover by cost-effective coating depends on the radiation conditions as shown in Fig. 14. As the decrease of the solar irradiance, the number of absorbers with the

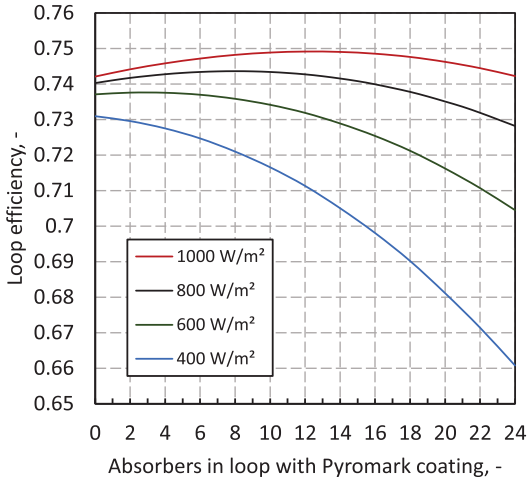

Fig. 14. Loop efficiency as a function of absorbers number with non-selective coating for different DNI in medium temp. level SHIP.

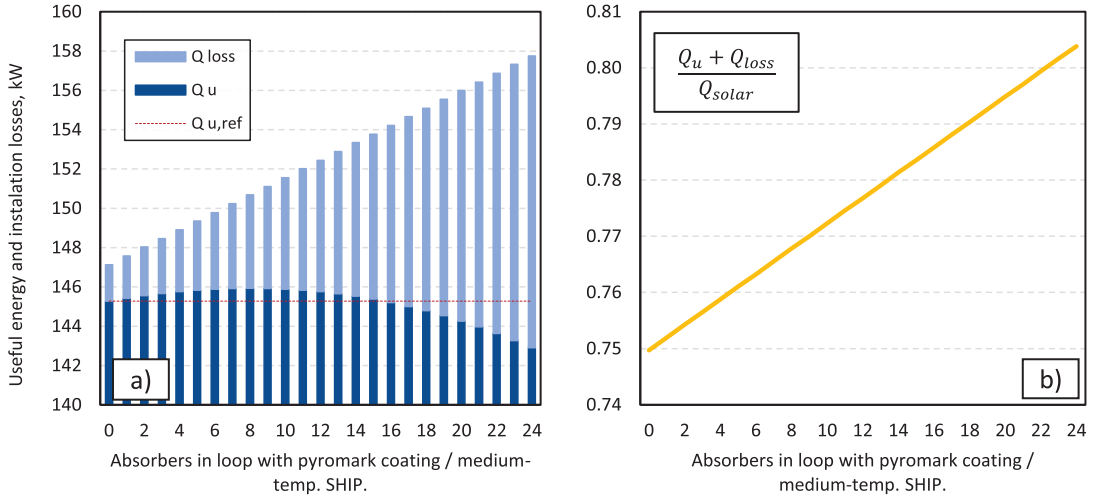

Fig. 13. A) useful energy absorbed by htf and absorber heat losses in solar loop; b) rate of solar energy utilization delivered to the external absorber surface.

possibility of non-selective coating without reducing the efficiency loop also decreases. The reason for this is the reduction of mass flow to achieve the desired outlet temperature. The weather conditions, location and position of the installation must be considered while applying the proposed method of reducing the investment cost. Long-term analysis is required for each separate location. A solution to increase the number of non-selective coated absorbers may be adding a peak heat source, which is a common technology in this type of installation.

The peak heat source reheats the medium fluid leaving the absorber loop, so the mass flow in the absorber loop does not have to be adjusted exactly to achieve a given temperature degree. Therefore, it is possible to select a mass flow that achieves the maximum efficiency for the weather conditions.

3.4. No-selective coating cost analysis

Linear absorbers in a parabolic solar concentrator system are commercial products and the prices of specific solutions strictly depend on the installation size, location and parameters. Prices for large-scale solutions are known, as cited previously in the Introduction section, whereas the receiver tube cost was reported at 25 USD/m^2 of aperture for the Ultimate Trough with aperture of 7.51 m which results in 187.5 USD per 1 m length receiver [29].

At the same time, it is not possible to scale these prices for absorbers for low-concentrated PTC for SHIP installations, due to the different production approaches, materials and methods used.

However, it can undoubtedly be argued that non-selective coating is able to reduce the cost of absorbers. As mentioned previously, the application process for selective coatings consists of a number of steps and the cost of this technology must include machinery, production time and maintenance. The PVD process is carried out in a vacuum chamber at high vacuum using a cathodic arc source [87]. PVD is characterised by a process in which the material goes from a condensed phase to a vapour phase and then back to a thin film condensed phase [88]. In the case of non-selective coatings, the coating is applied by spray painting in air and no special equipment is requires. Therefore, it can significantly reduces the price at the manufacturing stage itself.

The considered coating is a commercial product with a known price. The price for Pyromark 2500 is estimated as 12.8 USD/m^2 of covered surfaces, based on market prices (474.75 USD/Gallon) and producent covering data (400 ft^2/Gallon) [89,90]. The following equation determines the coating cost per absorber:

$$c_{coat,abs} = A_{abs,e} \bullet p_{coat} \tag{30}$$

where $c_{coat,\,abs}$ is a cost of coating on absorber surface and p is a price for coating. Table 10 represents estimated prices for coating in analysed absorbers. These data can be used for further analysis and as a reference for cost comparisons of specific coatings.

The cost associated with the purchase of the Pyromark required to cover the absorber as used in commercial receivers represents only around 1.5 % of the cost of the price of that receiver (estimation for Ultimate Trough and 70 mm OD absorber [29,89,90]). As the technology for applying selective coatings requires high investment cost and the PVD is a complex process, it is to be expected that the cost of applying the selective coating to the absorber represents a significant share of the cost of manufacturing the receiver. Knowledge of the cost structure associated with the manufacture of commercial receivers, which is a commercial secret of the companies, would make it possible to accurately determine the level of savings that would result from replacing selective coatings with non-selective ones. In addition, the use of the methodology presented in this article would allow the identification of potential heat generation cost reductions for different installations with different process requirements. Without such specific knowledge, it can be assumed that the use of non-selective coatings, especially for installations used for low-temperature heat generation, can lead to a significant reduction in installation costs and, therefore, heat generation costs.

Table 10
Non-selective coating estimated prices for analysed absorbers.

Parameter	Symbol	Unit	Case 1	Case 2
Absorber type	–	–	Power Trough 110	PolyTrough 1800
Absorber length	L_{abs}	m	3.06	5.54
Absorber external diameter	$d_{abs,e}$	mm	33.4	34
Absorber external area	$A_{abs,e}$	m^2	0.32	0.59
Coating cost per absorber	$c_{coat,\,abs}$	USD	4.11	7.57
Coating cost per 1 m absorber	$c_{coat,\,abs}$ / L_{abs}	USD/ m	1.34	1.37

4. Conclusions

In this paper, a concept of using high absorption non-selective coating to partially replace traditional solar selective coating in parabolic trough collector based, SHIP systems is presented. Four different PTC systems with varying concentration ratios, heat transfer fluid temperatures, and applications have been analysed. The developed two-dimensional mathematical model presented and used in this paper has a strong agreement with the experiment (RMSD = 2.54 and 3.52).

Based on the results obtained, the following conclusions can be drawn.

- Installations with concentration ratios of 10.5, and 17.3 where the HTF temperature ranged from 60 to 120 °C and 100–200 °C have shown the good potential of using low-cost and high absorption coatings in part of the absorbers.
- The application of the Pyromark coating in a low concentration (10.5) installation is profitable along the entire length of the solar loop. Depending on the solar irradiance, the efficiency increment is in the range of 1.5–5 percentage points for Therminol oil and 2.5–5.5 percentage points for pressurized water. In the particular cases where the installation is expected to operate in a medium–low irradiance location, 12 of the 14 absorbers in the analysed solar loop can be covered by the non-selective coating.
- The PTC system with a medium temperature range and a concentration ratio of 17.3 has also shown the possibility of optimization for absorbers where the temperature of HTF is up to 115 °C.
- Changing the connection of 3 parallel solar loops into 1 series increases the possibility of optimizing the number of absorbers. In the best optimal case (800 W/m^2), 15 of the 24 absorbers can be coated with a Pyromark instead of the reference selective coating.
- The study concluded that the proposed solution could not be applied to high-temperature SHIP installations (assumed outlet temperature 250 °C) and CSP power plants due to too high losses and lack of optimization potential.
- The no-selective coating price for absorbers was estimated as 12.8 USD/m^2, where for Power Trough 110 is. 4.11 USD and for PolyTrough 1800 7.57 USD.

This paper also demonstrates a high dependence of the application of this concept on solar conditions due to the necessity of mass flow adaptation. If a peak heat source operating with a SHIP plant is considered, the potential of the proposed solution may increase. For this solution, optimization must be performed separately for each SHIP plant under consideration, its location, weather conditions, and required process temperature parameters.

To determine the number of absorbers whose price can be significantly reduced because of the low-cost coating, a long-term analysis should be performed, which highlights opportunities for further work on

the presented solution. Reducing the investment cost can significantly affect the popularity of SHIP installations, where the market potential is very wide and will grow.

CRediT authorship contribution statement

Bartosz Stanek: Conceptualization, Methodology, Writing – original draft, Investigation, Visualization, Software, Project administration, Funding acquisition. **Wujun Wang:** Conceptualization, Methodology, Investigation, Supervision, Writing – review & editing. **Łukasz Bartela:** Writing – review & editing, Supervision, Investigation.

Declaration of Competing Interest

The authors declare that they have no known competing financial interests or personal relationships that could have appeared to influence the work reported in this paper.

Data availability

Data will be made available on request.

Acknowledgements

The scientific work is funded by the Silesian University of Technology within the framework of the research project No. 32/014/SDU/10-27-02.

Bartosz Stanek is the participant in the P4S InterPower European Social Fund program (grant POWR.03.05.00-00-Z305).

References

[1] Key World Energy Statistics 2021 - Analysis - IEA n.d. https://www.iea.org/reports/key-world-energy-statistics-2021 (accessed June 23, 2022).
[2] Global Energy Perspective 2022 | McKinsey n.d. https://www.mckinsey.com/industries/oil-and-gas/our-insights/global-energy-perspective-2022 (accessed June 23, 2022).
[3] Solar Heat for Industry - Solar Payback 2017. https://www.solar-payback.com/wp-content/uploads/2017/07/Solar-Heat-for-Industry-Solar-Payback-April-2017.pdf (accessed June 3, 2022).
[4] International Renewable Energy Agency. Innovation outlook: Thermal energy storage 2020. www.irena.org.
[5] Kumar L, Hasanuzzaman M, Rahim NA. Global advancement of solar thermal energy technologies for industrial process heat and its future prospects: A review. Energy Convers Manag 2019;195:885–908. https://doi.org/10.1016/J.ENCONMAN.2019.05.081.
[6] IEA. Renewables 2021: Analysis and forecast to 2026 2021. https://www.iea.org/reports/renewables-2021 (accessed June 3, 2022).
[7] Hess S. Solar Thermal Process Heat (SPH) Generation. Renewable Heating and Cooling: Technologies and Applications. Elsevier Inc.; 2016. p. 41–66.
[8] Weiss W, Spörk-Dür M. Solar Heat Worldwide 2021, Institute of Sustainable Technologies AEE, Austria n.d. https://www.iea-shc.org/solar-heat-worldwide-2021 (accessed June 3, 2022).
[9] World Map of Solar Thermal Plants | Solar Heat for Industrial Processes (SHIP) Plants Database n.d. http://ship-plants.info/solar-thermal-plants-map?collector_type=5 (accessed June 1, 2022).
[10] Rackam Solar thermal solutions for Industrial process heat n.d. https://rackam.com/en/ (accessed June 1, 2022).
[11] SKF Technologies (India) Pvt Ltd.| SKF | SKF n.d. https://www.skf.com/in/organisation/about-skf-india/skf-technologies-india-pvt-ltd (accessed June 1, 2022).
[12] IMPLEMENTED PROJECTS - Inventive Power n.d. https://inventivepower.com.mx/english/implemented-projects/ (accessed June 2, 2022).
[13] Minder S. Example of concentrated solar systems (PTC) in the dairy industry in Switzerland n.d. www.nep-solar.com (accessed June 2, 2022).
[14] Fernández-García A, Zarza E, Valenzuela L, Pérez M. Parabolic-trough solar collectors and their applications. Renew Sustain Energy Rev 2010;14:1695–721. https://doi.org/10.1016/J.RSER.2010.03.012.
[15] SHIP | Oncontrol n.d. https://oncontrol-tech.com/ship/ (accessed June 2, 2022).
[16] INEGI - Instituto de Ciência e Inovação em Engenharia Mecânica e Engenharia Industrial - INEGI n.d. http://www.inegi.pt/pt/ (accessed June 2, 2022).
[17] Häberle A, Krüger D. Concentrating solar technologies for industrial process heat. Concentrating Solar Power Technology: Principles. Developments, and Applications, Elsevier 2020:659–75. https://doi.org/10.1016/B978-0-12-819970-1.00011-6.
[18] Products and Equipment from NEP Solar Pty Ltd | Energy XPRT n.d. https://www.energy-xprt.com/companies/nep-solar-pty-ltd-32087/products (accessed June 2, 2022).
[19] Renewable and Energy Storage Solutions n.d. https://process.honeywell.com/us/en/industries/renewable-and-energy-storage-solutions (accessed June 2, 2022).
[20] T160 Solar collector - Designed to run industrial processes - Absolicon n.d. https://www.absolicon.com/applying-absolicon/ (accessed June 2, 2022).
[21] Solar Steam Boiler | Solar Boiler Supplier | Vicot n.d. http://newenergiescn.com/solar-steam-boiler-in-procter-and-gamble-tianjin.html (accessed June 2, 2022).
[22] CSHINDIA || HOME n.d. http://www.cshindia.in/ (accessed June 2, 2022).
[23] Reflective Surfaces - Solar - Industries - Alanod n.d. https://alanod.com/en/industries/solar/reflective-surfaces (accessed June 2, 2022).
[24] Solarlite CSP Technology GmbH - Parabolrinnenkraftwerke n.d. https://www.solarlite.de/forschung.cfm (accessed June 2, 2022).
[25] Miraah Solar Thermal Project n.d. https://www.power-technology.com/projects/miraah-solar-thermal-project/ (accessed June 2, 2022).
[26] Schoeneberger CA, McMillan CA, Kurup P, Akar S, Margolis R, Masanet E. Solar for industrial process heat: A review of technologies, analysis approaches, and potential applications in the United States. Energy 2020:206. https://doi.org/10.1016/J.ENERGY.2020.118083.
[27] Walker A, Kutscher C, Halvorsen A, McKenna C, Chambers D, May K. Design and Analysis of a Large Solar Industrial Heat Plant for Frito Lay in Modesto California. Proceedings of the Energy Sustainability Conference 2007 2009:657-62. https://doi.org/10.1115/ES2007-36050.
[28] Renewable Power Generation Costs in 2020 n.d. https://www.irena.org/publications/2021/Jun/Renewable-Power-Costs-in-2020 (accessed June 3, 2022).
[29] Kurup P, Turchi C. Parabolic Trough Collector Cost Update for the System Advisor Model (SAM) NREL 2015. https://doi.org/10.13140/RG.2.2.20792.19204.
[30] Schweitzer A, Schiel W, Birkle M, Nava P, Riffelmann KJ, Wohlfahrt A, et al. ULTIMATE TROUGH® - Fabrication, Erection and Commissioning of the World's Largest Parabolic Trough Collector. Energy Procedia 2014;49:1848–57. https://doi.org/10.1016/J.EGYPRO.2014.03.196.
[31] Ding Z, Qi C, Wang Y, Tu J, Wang C, Du X. Spectrally selective absorption coatings and their applications: A review. Sustain Energy Technol Assess 2022;52:102031. https://doi.org/10.1016/J.SETA.2022.102031.
[32] Noč L, Jerman I. Review of the spectrally selective (CSP) absorber coatings, suitable for use in SHIP. Sol Energy Mater Sol Cells 2022:238. https://doi.org/10.1016/J.SOLMAT.2022.111625.
[33] Weinstein LA, Loomis J, Bhatia B, Bierman DM, Wang EN, Chen G. Concentrating Solar Power. Chem Rev 2015;115:12797–838. https://doi.org/10.1021/ACS.CHEMREV.5B00397/ASSET/IMAGES/LARGE/CR-2015-00397F_0024.JPEG.
[34] Kennedy CE, Price H. PROGRESS IN DEVELOPMENT OF HIGH-TEMPERATURE SOLAR-SELECTIVE COATING, ISEC2005-76039, 2005.
[35] Burkholder F, Kutscher C. Heat Loss Testing of Schott's 2008 PTR70 Parabolic Trough Receiver. 2008.
[36] Manikandan GK, Iniyan S, Goic R. Enhancing the optical and thermal efficiency of a parabolic trough collector – A review. Appl Energy 2019;235:1524–40. https://doi.org/10.1016/J.APENERGY.2018.11.048.
[37] Abdulhamed AJ, Adam NM, Ab-Kadir MZA, Hairuddin AA. Review of solar parabolic-trough collector geometrical and thermal analyses, performance, and applications. Renew Sustain Energy Rev 2018;91:822–31. https://doi.org/10.1016/J.RSER.2018.04.085.
[38] Wu CH, Wang HC, Chang HY. Dual-axis solar tracker with satellite compass and inclinometer for automatic positioning and tracking. Energy Sustain Dev 2022;66:308–18. https://doi.org/10.1016/J.ESD.2021.12.013.
[39] Sallaberry F, Pujol-Nadal R, Larcher M, Rittmann-Frank MH. Direct tracking error characterization on a single-axis solar tracker. Energy Convers Manag 2015;105:1281–90. https://doi.org/10.1016/j.enconman.2015.08.081.
[40] Lee CY, Chou PC, Chiang CM, Lin CF. Sun Tracking Systems: A Review. Sensors 2009, Vol 9, Pages 3875-3890 2009;9:3875–90. https://doi.org/10.3390/S90503875.
[41] Shaaban S. Enhancement of the solar trough collector efficiency by optimizing the reflecting mirror profile. Renew Energy 2021;176:40–9. https://doi.org/10.1016/J.RENENE.2021.05.040.
[42] Tang XY, Yang WW, Yang Y, Jiao YH, Zhang T. A design method for optimizing the secondary reflector of a parabolic trough solar concentrator to achieve uniform heat flux distribution. Energy 2021;229:120749. https://doi.org/10.1016/J.ENERGY.2021.120749.
[43] Bindu M v., Joselin Herbert GM. A review on application of nanomaterials in heat transfer fluid for parabolic trough concentrator. Mater Today Proc 2021;46:7651–60. https://doi.org/10.1016/J.MATPR.2021.01.957.
[44] Tiwar AK, Kumar V, Said Z, Paliwal HK. A review on the application of hybrid nanofluids for parabolic trough collector: Recent progress and outlook. J Clean Prod 2021;292:126031. https://doi.org/10.1016/J.JCLEPRO.2021.126031.
[45] Norouzi AM, Siavashi M, Ahmadi R, Tahmasbi M. Experimental study of a parabolic trough solar collector with rotating absorber tube. Renew Energy 2021;168:734–49. https://doi.org/10.1016/J.RENENE.2020.12.088.
[46] Norouzi AM, Siavashi M, Khaliji Oskouei MH. Efficiency enhancement of the parabolic trough solar collector using the rotating absorber tube and nanoparticles. Renew Energy 2020;145:569–84. https://doi.org/10.1016/J.RENENE.2019.06.027.
[47] Allam M, Tawfik M, Bekheit M, El-Negiry E. Heat transfer enhancement in parabolic trough receivers using inserts: A review. Sustainable Energy Technol Assess 2021;48:101671. https://doi.org/10.1016/J.SETA.2021.101671.

[48] Yang H, Wang Q, Huang X, Li J, Pei G. Performance study and comparative analysis of traditional and double-selective-coated parabolic trough receivers. Energy 2018;145:206–16. https://doi.org/10.1016/J.ENERGY.2017.12.126.
[49] Stollo A, Chiarappa T, D'Angelo A, Maccari A, Matino F. LCOE reduction for parabolic trough CSP: Innovative solar receiver with improved performance at medium temperature, 2016, p. 030034. https://doi.org/10.1063/1.4949086.
[50] Zhao K, Jin H, Gai Z, Hong H. A thermal efficiency-enhancing strategy of parabolic trough collector systems by cascadingly applying multiple solar selective-absorbing coatings. Appl Energy 2022;309:118508. https://doi.org/10.1016/J.APENERGY.2021.118508.
[51] Garrido J, Aichmayer L, Abou-Taouk A, Laumert B. Experimental and numerical performance analyses of Dish-Stirling cavity receivers: Radiative property study and design. Energy 2019;169:478–88. https://doi.org/10.1016/j.energy.2018.12.033.
[52] Ho CK, Mahoney AR, Ambrosini A, Bencomo M, Hall A, Lambert TN. Characterization of Pyromark 2500 Paint for High-Temperature Solar Receivers. J Sol Energy Eng 2014:136. https://doi.org/10.1115/1.4024031.
[53] Martínez-Manuel L, González-Canché NG, López-Sosa LB, Carrillo JG, Wang W, Pineda-Arellano CA, et al. A comprehensive analysis of the optical and thermal performance of solar absorber coatings under concentrated flux conditions. Sol Energy 2022;239:319–36. https://doi.org/10.1016/J.SOLENER.2022.05.015.
[54] Boubault A, Ho CK, Hall A, Lambert TN, Ambrosini A. Durability of solar absorber coatings and their cost-effectiveness. Sol Energy Mater Sol Cells 2017;166:176–84. https://doi.org/10.1016/J.SOLMAT.2017.03.010.
[55] Moya EZ. Parabolic-trough concentrating solar power systems. Concentrating Solar Power Technology, Elsevier; 2021, p. 219–66. https://doi.org/10.1016/B978-0-12-819970-1.00009-8.
[56] POWER TROUGH 110® - Inventive Power n.d. https://inventivepower.com.mx/english/power-trough-110/ (accessed May 1, 2022).
[57] Ibarra M, Rovira A, Alarcón-Padilla DC, Zaragoza G, Blanco J. Performance of a 5 kWe Solar-only Organic Rankine Unit Coupled to a Reverse Osmosis Plant. Energy Procedia 2014;49:2251–60. https://doi.org/10.1016/J.EGYPRO.2014.03.238.
[58] POWER TROUGH 250® - Inventive Power n.d. https://inventivepower.com.mx/english/power-trough-250/ (accessed May 1, 2022).
[59] Bishoyi D, Sudhakar K. Modeling and performance simulation of 100 MW PTC based solar thermal power plant in Udaipur India. Case Stud Therm Eng 2017;10:216–26. https://doi.org/10.1016/J.CSITE.2017.05.005.
[60] Trevisan S, Wang W, Laumert B. A high-temperature thermal stability and optical property study of inorganic coatings on ceramic particles for potential thermal energy storage applications. Sol Energy Mater Sol Cells 2022;239:111679. https://doi.org/10.1016/J.SOLMAT.2022.111679.
[61] Lu JZ, Chen BH, Jin LH, Fang Z, Liu G, Gao XH. Thermal stability investigation of the SS/MO/Al2O3 spectrally selective solar absorber coatings. Https://DoiOrg/101080/026708442018153708 3 2018;35:565–72. https://doi.org/10.1080/02670844.2018.1537083.
[62] Zhao SS, Gao XH, Qiu XL, Yu DM, Tian GK. A novel TiC-TiN based spectrally selective absorbing coating: Structure, optical properties and thermal stability. Infrared Phys Technol 2020;110:103471. https://doi.org/10.1016/J.INFRARED.2020.103471.
[63] HCE Tubes - Rioglass n.d. https://www.rioglass.com/our-products/hce-tubes.html (accessed May 1, 2022).
[64] Nawsud ZA, Altouni A, Akhijahani HS, Kargarsharifabad H. A comprehensive review on the use of nano-fluids and nano-PCM in parabolic trough solar collectors (PTC). Sustainable Energy Technol Assess 2022;51:101889. https://doi.org/10.1016/J.SETA.2021.101889.
[65] Bellos E, Tzivanidis C. A detailed exergetic analysis of parabolic trough collectors. Energy Convers Manag 2017;149:275–92. https://doi.org/10.1016/J.ENCONMAN.2017.07.035.
[66] Therminol VP-1 Heat Transfer Fluid | Therminol | Eastman n.d. https://www.therminol.com/product/71093459 (accessed February 2, 2022).
[67] IAPWS Industrial Formulation 1997 for the Thermodynamic Properties of Water and Steam. International Steam Tables, Berlin, Heidelberg: Springer Berlin Heidelberg; 2008, p. 7–150. https://doi.org/10.1007/978-3-540-74234-0_3.
[68] Stanek B, Grzywnowicz K, Bartela Ł, Węcel D, Uchman W. A system analysis of hybrid solar PTC-CPV absorber operation. Renew Energy 2021;174:635–53. https://doi.org/10.1016/J.RENENE.2021.04.110.
[69] Kalogirou SA. A detailed thermal model of a parabolic trough collector receiver. Energy 2012;48:298–306. https://doi.org/10.1016/J.ENERGY.2012.06.023.
[70] Yilmaz IH, Söylemez MS. Thermo-mathematical modeling of parabolic trough collector. Energy Convers Manag 2014;88:768–84. https://doi.org/10.1016/J.ENCONMAN.2014.09.031.
[71] Tzivanidis C, Bellos E, Korres D, Antonopoulos KA, Mitsopoulos G. Thermal and optical efficiency investigation of a parabolic trough collector. Case Stud Therm Eng 2015;6:226–37. https://doi.org/10.1016/J.CSITE.2015.10.005.
[72] Mansour K, Boudries R, Dizene R. Optical, 2D thermal modeling and exergy analysis applied for performance prediction of a solar PTC. Sol Energy 2018;174:1169–84. https://doi.org/10.1016/J.SOLENER.2018.09.040.
[73] Dudley VE; KGJ; MA; MTR; MCW. Test Results: SEGS LS-2 Solar Collector. SAND94-1884. Albuquerque: 1994.
[74] Duffie J, Beckerman W. Solar Engineering of Thermal Processes. Fourth Edition. New Jersey: John Wiley & Sons, Inc; 2013.
[75] Pitz-Paal R. Solar Energy - Concentrating Solar Power. Future Energy: Improved, Sustainable and Clean Options for our Planet, Elsevier Inc.; 2013, p. 405–31. https://doi.org/10.1016/B978-0-08-099424-6.00019-3.
[76] Kalogirou SA. Solar Energy Collectors. Solar Energy Engineering, Elsevier 2014:125–220. https://doi.org/10.1016/B978-0-12-397270-5.00003-0.
[77] Ganji DD, Sabzehmeidani Y, Radiation SA, Transfer H. Nonlinear Systems in Heat Transfer. Elsevier; 2018. p. 105–51.
[78] Lovegrove K, Pye J. Fundamental principles of concentrating solar power systems. Concentrating Solar Power Technology, Elsevier; 2021, p. 19–71. https://doi.org/10.1016/B978-0-12-819970-1.00013-X.
[79] Evangelisti L, Guattari C, Asdrubali F. On the sky temperature models and their influence on buildings energy performance: A critical review. Energy Build 2019;183:607–25. https://doi.org/10.1016/J.ENBUILD.2018.11.037.
[80] Köppen climate classification - Hans Chen n.d. http://hanschen.org/koppen (accessed April 27, 2022).
[81] Forristall R. Heat Transfer Analysis and Modeling of a Parabolic Trough Solar Receiver Implemented in Engineering Equation Solver 2003.
[82] Incropera FDD. Fundamentals of Heat and Mass Transfer. Third Edition. New York: John Wiley and Sons; 1990.
[83] Balmer RT. The First Law of Thermodynamics and Energy Transport Mechanisms. Modern Eng Thermodyn 2011:99–146. https://doi.org/10.1016/B978-0-12-374996-3.00004-X.
[84] Bellos E, Tzivanidis C, Antonopoulos KA. A detailed working fluid investigation for solar parabolic trough collectors. Appl Therm Eng 2017;114:374–86. https://doi.org/10.1016/J.APPLTHERMALENG.2016.11.201.
[85] Nagy E. Membrane Contactors. Basic Equations of Mass Transport Through a Membrane Layer, Elsevier; 2019, p. 337–45. https://doi.org/10.1016/B978-0-12-813722-2.00011-X.
[86] Piñeiro G, Perelman S, Guerschman JP, Paruelo JM. How to evaluate models: Observed vs. predicted or predicted vs. observed? Ecol Modell 2008;216:316–22. https://doi.org/10.1016/J.ECOLMODEL.2008.05.006.
[87] Shang SM, Zeng W. Conductive nanofibres and nanocoatings for smart textiles. Multidisciplinary Know-How for Smart-Textiles Developers 2013:92–128. https://doi.org/10.1533/9780857093530.1.92.
[88] Rane AV, Kanny K, Abitha VK, Thomas S, Thomas S. Methods for Synthesis of Nanoparticles and Fabrication of Nanocomposites. Synthesis of Inorganic Nanomaterials: Advances and Key Technologies 2018:121–39. https://doi.org/10.1016/B978-0-08-101975-7.00005-1.
[89] Pyromark High Temperature Paint – markal.com n.d. https://markal.com/products/pyromark-high-temperature-paint?variant=9204789116975 (accessed August 9, 2022).
[90] PK2500FBLK - TDS - Pyromark Series 2500 TDS - Pyromark Product Image n.d. https://www.datasheetarchive.com/whats_new/d484cb021dbf4938e9c08d1d515c4609.html (accessed August 9, 2022).

Paper IV

Renewable Energy 196 (2022) 598–609

Contents lists available at ScienceDirect

Renewable Energy

journal homepage: www.elsevier.com/locate/renene

Solar tracker error impact on linear absorbers efficiency in parabolic trough collector – Optical and thermodynamic study

Bartosz Stanek *, Daniel Węcel , Łukasz Bartela , Sebastian Rulik

Silesian University of Technology, Department of Power Engineering and Turbomachinery, Konarskiego 18, 44-100, Gliwice, Poland

ARTICLE INFO

Article history:
Received 26 March 2022
Received in revised form
17 June 2022
Accepted 4 July 2022
Available online 8 July 2022

Keywords:
Parabolic trough collectors
Concentrated solar energy
Solar tracking error
Renewable energy sources

ABSTRACT

The parabolic-trough solar concentrating systems are often considered element of heat generation systems from renewable energy sources. It is important to use appropriate optical systems and solar trackers because parabolic trough collectors utilize only direct solar radiation. The paper presents the results of an analysis of the effect of solar tracker error on the optical and thermodynamic efficiency of linear absorbers. The results are presented for low concentrated geometry, popular among scientific institutions, consistent with the existing facility operating under natural conditions. Two diameters of the linear receiver were considered in the analysis: 33.7 mm and 21.3 mm. The research was carried out in optical engineering software based on the Monte Carlo ray-tracing method. Thermodynamic analysis was performed based on the mathematical model of the radiation absorption phenomenon by heat transfer fluid. The maximum angle error of the solar tracker for the tested geometry, not significantly affecting the performance of the linear absorber for a diameter of 33.7 mm is 1.5°, and for 21.3 mm is 0.9°. The reduction in efficiency for 2° error is 4.7% points, and 42.5% points respectively. The analysis also presents the results of the radiation distribution on the surface of the absorber tube.

1. Introduction

Parabolic trough collectors are a mature solar concentration technology, capable of producing high-temperature heat [1]. The principle of their operation is the concentration of direct radiation on the surface of the linear absorber. The concentrated radiation is absorbed by the heat transfer fluid circulating inside the tubular receiver. As the technology utilises direct radiation, it is necessary to use a high-precision solar tracking device.

A PTC installation is an optical system in which various issues can affect its operation, e.g. tracking error, no-ideal reflected mirror surface, dusty glass envelope surface, wind affect on the installation stability, the tracking mechanism usage and the accuracy of the positioning sensor. Investigation of the solar radiation quantity reaching the absorber in a parabolic trough concentrator system can be carried out by analytical calculations [2–4], numerical modelling [5] or by conducting measurements, e.g. photogrammetric [6–8]. Different types of optical errors can be identified during such tests. The mentioned optical errors result from the design, manufacturing of the reflector and absorber and from errors in the solar tracking system [9,10].

Assuming that the reflector and absorber are manufactured correctly, it should be noted that during operation, PTC may deform due to the heating of the construction and some stresses caused by weather conditions (wind, rain, snow) [11]. The correct positioning of the solar tracker is based on the measurement of the current position of the sun or the solar calendar. Both methods can lead to some errors [12,13].

It should be highlighted, that the tracking error is directly linked to the costs of the solar tracking system. The cost of these devices increases with their accuracy. However, many studies are being conducted to improve the efficiency of solar tracking and reduce the cost [11]. Wu et al. [14] introduced dual-axis tracker with inclinometer for automatic positioning with open-loop GPS tracking system. Fuentes-Morales et al. [15] and Lee et al. [16] highlighted the importance of control algorithms to improve the tracking systems.

Errors in the optical system can be reduced but cannot be completely eliminated, so many studies are usually limited to determining the sensitivity of the PTC to errors from the optical efficiencies point of view of the, the local concentration ratio (LCR), and consequently the heat loss in the PTC absorber [17].

* Corresponding author.
E-mail address: bartosz.stanek@polsl.pl (B. Stanek).

https://doi.org/10.1016/j.renene.2022.07.021

The geometry of the PTC with circular receiver causes not uniform distribution of the sun's rays focused on the absorber [18], but the errors in the optical system may also increase the maximum differences in the values of the local concentration ratio [19,20], indicating that the absorber may occur local overheating, which may shorten the lifetime of the receiver. The most frequent errors are: mirror shape error (not ideal parabola), slope error (e.g. surface undulations), receiver deviation error (longitudinal circular axis of the receiver is not at the focal line), reflection error (imperfect reflection of the mirror), tracking error (optical axis of the mirror is not centred on the solar disk), frame deformation (effect of wind on the structure and surface of the PTC) [21].

Many studies are being carried out to increase the optical efficiency of PTCs. Kaluba et al. [22] introduced the hot mirror coating onto the absorber glass envelope to reduce the energy losses. Dahlioui et al. [23] developed the anti-soiling coating on the solar mirrors which increased the cleanliness. Valentin et al. [24] analysed the wind affect on solar trackers. Pawar et al. [25] proposed the proteus ISI 7.6 software for tracking device to enhancement the performance of dual axis solar tracker.

Numerical, optical methods enable very precise determination of the circumferential distribution of radiation energy flux reaching the absorber. It is possible to test many cases under idealized conditions considering only one, selected type of error. In numerical modelling of CSP installations, the Monte Carlo raytracing technique is commonly used [3,26]. Zou et al. [27] performed an theoretical analysis and discussed the effect of geometric parameters based on Monte Carlo ray tracing method. Cheng et al. [28] also used the MCRM to design more effective PTC.

Many papers can be found in the literature that analyse the optics of parabolic trough collectors and the errors that can occur within them [29]. However, these are mainly analyses made for commercial size installations, which are mostly used in solar power plants. Solar tracking errors are not so visible in this case, as the results usually refer to long-term performance. In this aspect, each scale of geometry must be considered individually.

In research institutions, low concentrated parabolic trough collectors [30–33] are commonly used. Low concentration parabolic trough collectors are also use in SHIP installations to produce high temperature heat for industrial processes [34–36]. The small size also allows consideration of a 2-axis solar tracker installation [37]. Although the temperature range of the heat transfer medium and the power is lower, such a geometry allows comparative analyses of the different types of absorbers being developed [38]. However, to obtain high-quality results, it is essential to consider the application of solar tracking, and include the influence of imperfections and errors on the results.

As there is still a lack of information in the literature of the subject about different types of errors and requirements of solar trackers for low concentration geometries, the following analysis has been performed to fill this gap. The motivation for the analysis was to determine the impact of the solar tracking error on the existing research installation, including the optical efficiency, thermal efficiency and concentrated radiation distribution on the absorber surface calculations.

The main questions this article answers are: what is the maximum tracker error that does not affect installation operation? How does a positioning error affect the installation thermal efficiency? How does the positioning error affect the radiation distribution on the absorber surface?

The contribution of this paper is to provide researchers data on the methodology of tracking error estimation, highlight the tracking error affect on efficiency and to emphasize the validity of using a proper tracking system. The paper shows a highly significant dependence between imperfections in solar tracking systems and obtained results which emphasize the necessity of performing such analysis.

2. Methods

The analysis of the impact of the solar tracker position error on the performance characteristics of the concentrator is presented based on a test facility of parabolic trough collector with low concentration ratio operating at the Silesia University of Technology, located in the south of Poland. The installation shown in Fig. 1 consists of 3 parabolic trough collectors, each with a length of 1.5 m and an aperture width of 1 m, which can work both in parallel and in series. The PTCs are installed on a 2-axis solar tracker. The solar tracker operates with two actuators, one for each axis. The installation allows tracking the sun in 2 ways: using a position sensor or on a sun position database.

The purpose of the analysis is to determine the sensitivity of an installation of a specific geometry to solar tracking system error. The analysis based on numerical calculations was performed in optical software APEX where the boundary conditions for thermodynamic model were evaluated. APEX software is based on the Monte Carlo ray-tracing method, common in CSP installation research. In the analysis, the concentrated solar power supplied to the absorber surface as a function of the system position error was determined.

Then, the mathematical model was used for calculating the efficiency of analysed installation. The methodology of each study is presented in the following subsections. The information on solar radiation and parabolic trough collectors geometry, crucial for the analysis, is presented in section 2.1.

2.1. Solar radiation

The global solar irradiance I_β reaching the surface at any angle β to the horizontal surface is the sum of three radiation components: direct $I_{B\beta}$, diffuse $I_{D\beta}$ and reflected $I_{R\beta}$ (*1*), [39].

$$I_\beta = I_{B\beta} + I_{D\beta} + I_{R\beta} \tag{1}$$

Considering solar radiation concentrators, only radiation whose rays are parallel to the optical axis of the focusing system should be taken into account. Because the absorber is not a point heat receiver, some deviations from the above assumption are allowed. In practice, the diffuse radiation rays propagate in all directions, so the concentrating optical system does not focus this radiation on the absorber, regardless of the position of the system. It can be assumed that the diffuse solar irradiance incident on the absorber surface, corresponds to the value of this radiation on the horizontal plane, regardless of the position of the optical system. The above assumption is correct for the model of isotropic sky radiation, which is true for low global irradiance reaching the horizontal plane $I_{ch} \leq 800$ W/m^2 [40]. In Poland, such an assumption does not cause significant errors, due to relatively short periods of higher radiation occurrence, which takes up to 5% of the time between sunrise and sunset, based on data provided by Photovoltaic Geographical Information System [41] and the website of the Ministry of Investment and Development, presenting Typical meteorological years and statistical climatic data for energy calculations of buildings [42]. The reflected radiation also spreads in many directions, although in some cases this radiation may constitute a significant part of the global radiation, e.g. when rays reflected from the water surface or the glass facade of a building reach the receiver. The rays of the reflected radiation are not parallel to the direct rays, therefore this radiation can be ignored when analysing the operation of the solar concentrators per year,

Fig. 1. Parabolic trough collector test facility with 2-axis solar tracker.

especially when concentrating optical system is tracking the sun's movement.

Direct radiation is a component of global radiation that reaches a given surface directly from the sun, without any refractions. Since the sun is not really a radiation point source, not all direct rays reaching a given focusing system parallel to its optical axis. It can be assumed that all the focused direct rays will reach the absorber, by selecting the appropriate proportions of the absorber dimensions to the parameters of concentrating system. The concentration discrepancies of the sun's rays result from the so-called the half angle θ_s, due to the distance between the Earth and the Sun R and the Sun's radius r (Fig. 2).

During the year, the distance between the Earth and the Sun varies within a range: 147.1 × 10^6 km (January 3) to 152.1 × 10^6 km (July 4) [43]. Assuming a constant radius of the sun, the half-angle varies during the year with the range $\theta_s = 0.266 \pm 0.004°$. Usually, the half angle is given for the average distance between the Earth and the Sun, which is $\theta_s = 0.267° = 16'$.

2.2. PTC geometry

The geometry of parabolic concentrators enables the rays to be concentrated in the focal point, but only if the optical axis of the concentrator is parallel to the incident rays. The parabola is described by the equation (2), [44]:

$$x^2 = 4fy, \tag{2}$$

where f is the focal length.

In the case of a circular absorber, its center should be at the mirror focus. PTCs are performed with various parameters defined by: aperture width (W), focal length (f), height of the reflector/mirror (h), which can be determined from geometric dependencies in Eq. (3), [45,46]:

$$h = \frac{W^2}{16f}. \tag{3}$$

Instead of the height of the reflector, the rim angle (φ) is also given, which defines the "flatness" of the shape of a finite parabola. Rim angle can be calculated from Eq. (4), according to Ref. [45]:

$$\varphi_r = \tan^{-1}\left[\frac{8\left(f/W\right)}{16\left(f/W\right)^2 - 1}\right] = \sin^{-1}\left(\frac{W}{2 \cdot r_r}\right), \tag{4}$$

where, r_r – maximum mirror radius.

A schematic of the investigated installation of parabolic trough collector is shown in Fig. 3. The characteristic parameters and values describing its geometry are marked in the figure. The solar-half angle and θ_x and θ_z angles of the solar tracker position error are also marked. Since the system under study has 2-axis solar tracker, and according to Refs. [47,48], θ_z up to 15° does not significantly affect losses and solar radiation distribution, the analysis presented here focuses on the effect of angle θ_x on the system operation. The installation dimensions for all cases are summarised in Table 1. The individual cases differ in the size of the absorber, hence the concentration ratio of PTC, and the use or lack of a glass tubular envelope.

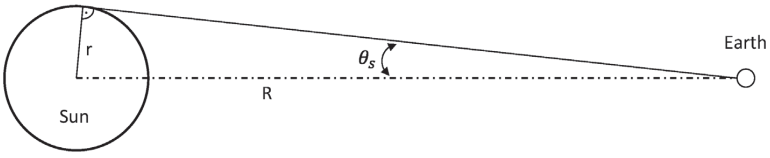

Fig. 2. Suns half-angle presented as a Sun-Earth (concentrator) position.

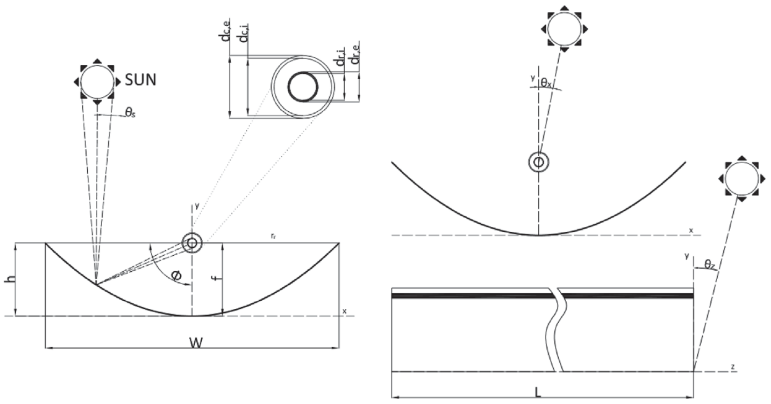

Fig. 3. Geometry of parabolic trough collector.

2.3. Optical analysis

Modeling the influence of solar tracker errors was performed using the optical-engineering software APEX [49]. This numerical tool enables tracking of the simulated rays, analysis of the illuminated surface considering the influence of individual optical elements and their properties in complex 3D geometries. Considering the shape, reflectivity, coatings of individual elements of the system, the software enables calculating distribution and power analysis on selected surfaces [50]. The software uses the Monte Carlo ray-tracking method, which is a mature, well known method for CSP and CPV system analysis [51–53]. Moreover the APEX software has been extensively used in author's previous work for optimization the solar simulation for PTC testing [54]. The results presented in authors another previous work [55], where the APEX software was used, indicated high compliance of the numerical data with experimental ones, where simulated radiation in designed solar simulator was measured. Therefore the numerical results obtained in following analysis are considered highly reliable. Selection of the software was supported with its commercial maturity, ease implementation and satisfactory accuracy [56]. The embedded method is also reliable for complicated radiation simulations which was reported in other researchers papers [54,57–59].

In the MCRT method, the Bidirectional Reflectance Distribution Function (BRDF) is used to describe the reflected beam behaviour [60]. This method allows to tracks the energy of each simulated ray and calculate the total flux and its distribution. The BRDF function describes the form at which the incident light over a surface is scattered. The BRDF function graphically presented in Fig. 4 is defined as the scattered radiance per unit incident irradiance, and is described by Eq. (5) [61]:

$$BRDF(\theta_i, \Phi_i, \theta_r, \Phi_r) = \frac{dL_r(\theta_r, \Phi_r)}{dE_i(\theta_i, \Phi_i)} \quad (5)$$

where, $dL_r(\theta_r, \Phi_r)$ is the unit of radiant energy per unit of solid angle (W/m^{2}sr); the irradiance $dE_i(\theta_i, \Phi_i)$ is the incident power flux density per unit area (W/m^2). The angles $\theta_i, \Phi_i, \theta_r, \Phi_r$ are the polar and azimuth incident angles and polar and azimuth reflected angles, respectively.

A model of the analysed device is presented in Fig. 5. The model consisted of a parabolic mirror and tubular absorber placed in a glass vacuum tube (glass envelope for case 1 and 3). Table 1, presents the dimensions of the analysed system along with the optical properties assumed in the analysis.

A parabolic mirror with the dimensions specified in Table 1 is characterised by the surface of reflectivity equal to 0.9. The absorber covered with a selective coating with the absorption 0.96 is placed in the focal point of the mirror, the emissivity of the selective coating is 0.1. The parameters of the analysed coating are according to the data for four layer coating W/CrAlSiN$_x$/CrAlSiO$_y$N$_x$/SiAlO$_x$ reported by Al-Rjoub et al. [62] The absorber is surrounded by a borosilicate tubular envelope whose function is to minimise convection losses. The refractive index of the glass tube with respect to vacuum is 1.5163.

The calculations were performed by modeling direct normal

Table 1
PTC dimensions and optical model parameters.

Parameter	Symbol	Case 1	Case 2	Case 3	Case 4	Unit
Receiver internal diameter	$d_{r,i}$	29.7	29.7	17.3	17.3	mm
Receiver external diameter	$d_{r,e}$	33.7	33.7	21.3	21.3	mm
Glass cover internal diameter	$d_{c,i}$	63.6	-	63.6	-	mm
Glass cover external diameter	$d_{c,e}$	70	-	70	-	mm
Width	W	1				m
Length	L	1.5				m
Focal length	f	0.25				m
Receiver emissivity	ε_r	0.1				-
Glass cover emissivity	ε_c	0.88				-
Glass cover transmittance	τ	0.95				-
Receiver absorptivity	α	0.96				-
Parabolic mirror reflectivity	ζ	0.9				-

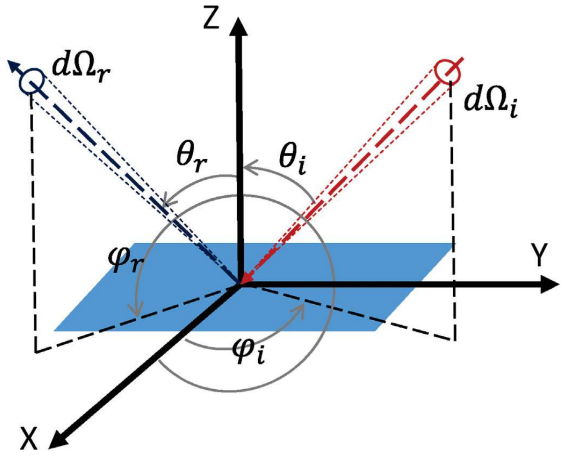

Fig. 4. Graphically presentation of Bidirectional reflectance Distribution Function (BRDF) of the incident ray on the surface.

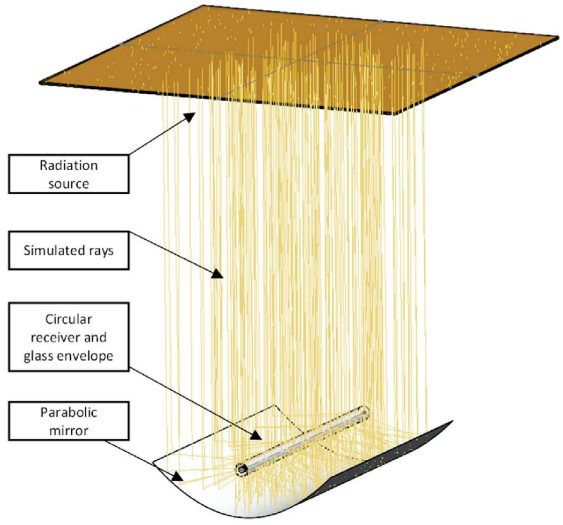

Fig. 5. Numerical investigation model in optical engineering software.

radiation. Sun model was used as a radiation source, which included the solar half angle $\theta_s = 0.27°$. The simulations were carried out by changing the value of the radiation flux emitted by the source in the range of 200–1000 W/m^2 and changing the angle of the optical axis of the mirror, relative to the theoretical line connecting the center of the light source with the center of the absorber (the so-called incidence angle θ_x) from 0° to 6°. This angle was changed by rotating the concentrator around the absorber longitudinal axis.

Based on the simulation, total solar power on absorber external surface and distribution of solar irradiance on outer absorber circumference were determined. Solar power absorbed by the external surface of the receiver can be presented as Eq. (6) based on [63]:

$$Q_{r,e} = \eta_{opt} \cdot A_a \cdot I_B \tag{6}$$

where, η_{opt}-optical efficiency, A_a- aperture surface area, m^2; I_B-direct solar irradiance, W/m^2.

The optical efficiency is the product of the individual optical parameters of the system components (7) [64]:

$$\eta_{opt} = (\alpha \cdot \tau \cdot \zeta) \cdot u_{\theta x} \tag{7}$$

where: α - receiver absorptivity; τ - transmittance of glass envelope; ζ- parabolic mirror reflectivity, $u_{\theta x}$- coefficient resulting from the tracking error (for $\theta_x = 0°$, $u_{\theta x} = 1$).

The dimensions of the PTC allows to determine an important parameter, the concentration factor C. This parameter describes the radiation concentration process. In other words the concentration ratio is the coefficient by which the incident energy flux I_B is optically enhanced on the receiving surface.

Based on the geometrical dimensions of the mirror and the absorber, a geometric concentration ratio can be determined as C_g in Eq. (8). This parameter is usually indicated when describing PTC systems [65]:

$$C_g = \frac{A_a}{A_{r,e}}, \tag{8}$$

where: $A_{r,e}$ – external area of the receiver.

In the case of a cylindrical absorber, the concentration factor is calculated for the entire surface area of the absorber (irrespective of the part of the absorber on which the concentrated radiation falls) and not only for its diameter. The solar radiation is not uniformly distributed on the absorber surface [9] moreover, the optical system has some imperfections, so other coefficients are provided [66]. Based on the radiant flux values incident on the mirror surface I_B and the average value of the radiant flux over the receiver, the optical concentration ratio C_{opt} (or flux concentration ratio) can be determined as Eq. (9) according to Ref. [67]:

$$C_{opt} = \frac{\frac{1}{A_{r,e}} \int I_{lr} d_{r,e} A_{r,e}}{I_B}, \tag{9}$$

where: I_{lr} – local radiant flux on the receiver.

2.4. Thermodynamic analysis

The equations presented in the following section of the paper are intended to determine the effect of the tracker error of a parabolic solar concentrator on its global efficiency characteristics. The tracking error has a direct effect on the partial under-radiation of concentrated solar radiation to the absorber surface, which leads, to a smaller temperature rise in the analysed linear absorber. The calculations were performed using a developed calculation algorithm, based on [63,64,68].

The useful heat collected by the thermal fluid, which can later be used in heating or other technological processes, can be calculated from the following Eq. (10) as suggested in Ref. [69]:

$$Q_u = \dot{m} \cdot c_p \cdot (T_{out} - T_{in}), \tag{10}$$

where, Q_u- useful thermal energy in the absorber, W; $\dot{m}$ – mass flow, kg/s; c_p- specific heat, J/kg K; T_{out} – outlet temperature of the circulating medium, K; T_{in}- inlet temperature of the circulating medium, K.

The useful thermal energy can also be represented by Eq. (11),

which considers the optical efficiency of the radiation concentration and the effect of solar tracker error [64]:

$$Q_u = \eta_{opt} \cdot A_a \cdot I_B - Q_{loss} \tag{11}$$

where: Q_{loss}- energy losses, W.

The solar energy fed into the parabolic trough collector system is described by Eq. (12) based on [70]:

$$Q_s = A_a \cdot I_B. \tag{12}$$

According to Kalogirou [46], the efficiency of parabolic trough collector is defined as the ratio of useful thermal energy to solar energy (13):

$$\eta = \frac{Q_u}{Q_s}. \tag{13}$$

System losses can be described by both equations (14) and (15) according to Refs. [45,71]:

$$Q_{loss} = \sigma \cdot \varepsilon_c \cdot A_{c,e} \cdot \left(T_c^4 - T_{amb}^4\right) + A_{c,e} \cdot h_{ca} \cdot (T_c - T_{amb}) \tag{14}$$

$$Q_{loss} = \frac{\sigma \cdot A_{c,e} \cdot \left(T_r^4 - T_c^4\right)}{\frac{1}{\varepsilon_r} + \frac{1-\varepsilon_c}{\varepsilon_c} \cdot \frac{A_{r,e}}{A_{c,i}}} \tag{15}$$

where: σ- Stefan-Boltzman constant, W/m^2 K^4; ε_c- emissivity of glass cover; ε_r- emissivity of selective coating on receiver external surface; T_c- mean cover temperature, K; T_{amb}- ambient temperature, K; T_r- mean receiver temperature, K; h_{ca}- heat transfer coefficient, W/(m^2 K).

The given temperatures are average values for the individual absorber surfaces. These surfaces are determined as follows:

$$A_i = \pi \cdot d_i \cdot L \tag{16}$$

where, d_i- $d_{r,i}$, $d_{r,e}$, $d_{c,i}$, $d_{c,e}$; L-absorber length, m.

Eqs. (14) and (15) refer to cases 1 and 3, where the glass tube forms a vacuum envelope around the tubular receiver. In this cases, the total losses are considered as the sum of the convective losses from the surface of the glass tube to the ambient and the radiation losses of the glass tube to the ambient. Another approach to this issue is presented in eq. (15) where losses are defined as radiation losses from the surface of the tubular receiver to the glass envelope. By using a glass envelope and vacuum, convection losses from the surface of the tubular receiver are eliminated.

In Cases 2 and 4, the installation did not include a glass vacuum cover, the effect of its absence was investigated. Therefore, Eq. (17) for these cases is as follows [45,71]:

$$Q_{loss} = \sigma \cdot \varepsilon_r \cdot A_{r,e} \cdot \left(T_r^4 - T_{amb}^4\right) + A_{r,e} \cdot h_{ra} \cdot (T_r - T_{amb}) \tag{17}$$

The heat transfer coefficient from the receiver inner wall to the fluid is an important parameter in calculating the device efficiency. Two correlations of the Nusselt number were used in the mathematical model [68,72]. Eq. (18) was used for a laminar flow:

$$Nu_f = 3.66 + \frac{0.0668 \cdot Re \cdot Pr \cdot \frac{d_{r,i}}{L}}{1 + 0.04 \cdot \left(Re \cdot Pr \cdot \frac{d_{r,i}}{L}\right)^{\frac{2}{3}}}. \tag{18}$$

For turbulent flow, Eq. (19) was used:

$$Nu_f = 0.023 \cdot Re^{0.8} \cdot Pr^{\frac{1}{3}} \tag{19}$$

The validity of using these two correlations is suggested by Tzivanidis et al. [68], highlighting the high compliance with the real model.

The Nusselt number can be defined according to Eq. (20), considering the convection coefficient [73]:

$$Nu_f = \frac{h \cdot d_{r,i}}{k} \tag{20}$$

where, h- convection coefficient; W/m^{2}K; k-thermal conductivity, W/m K.

Eq. (21) shows the method of determining the convection coefficient, where the input values are parameters extracted from the model for a given absorber section [74].

$$h = \frac{Q_u}{(\pi \cdot d_{r,i} \cdot L) \cdot (T_r - T_m)} \tag{21}$$

The calculation of the convection coefficient uses the average temperature of the fluid [74]:

$$T_m = \frac{T_{out} + T_{in}}{2}. \tag{22}$$

The analyses were carried out for thermal oil Therminol VP-1 [75]. It is a heat transfer medium with highly efficient heat transfer properties used in large scale solar power plants [74,76] and in the installation shown in Fig. 1. The characteristic parameters of the fluid as a function of temperature, are summarised in Table 2.

To determine global characteristics for the technology analysed, wide-parametric analyses were carried out for the variables shown in Tab. 3.

3. Results and discussion

The following section presents the results of the performed analyses. The results of the optical analysis carried out in numerical software are presented in first section. The next section presents the results of the thermodynamic analysis of the parabolic trough collector. The final chapter is devoted to a discussion of the radiation distribution on the linear absorber.

3.1. Optical results

3.1.1. Study of ray quantity dependence

For the MCRT method, high accuracy can be obtained with high rays number. To increase the accuracy of the results and optimize the computational cost, the analysis of rays number was performed. Fig. 6a presents the ray-tracing results for the selected absorber section. Under ideal conditions, the intensity of radiation concentrated on the absorber length, assuming a single reference point on the circumference, should be constant. Relative intensity dependence analysis for rays from 20 million to 300 million was performed.

The results indicated that the best case is the use of 300 million rays. Considering 300 Mrays as a reference case, the relative error for the 120 million rays case was a maximum of 1.21%, as shown in Fig. 6b. Therefore, the 120 million rays option was considered to be optimal in terms of performance and computational cost. Results presented in the analysis were performed using 120 million rays.

3.1.2. MCRT results

Based on the simulation, a set of light rays were obtained. The distribution of rays in the cross-section of PTC for selected three tracking error is shown in the Fig. 7. Distribution is presented for case 1.

Table 2
Therminol VP-1 thermal fluid parameters [75].

Parameter	Symbol	Value	Unit
Max. temp. for industrial applications	T_{max}	400	°C
Density	ρ	−0.856 T + 1316	kg/m^3
Specific heat	c_p	2.7137 T + 761.88	J/(kg·K)
Thermal conductivity	k	−1.36E-04 T + 0.1773	W/(m·K)
Dynamic viscosity	μ	250568541 T ^ (−4.407)	Pa·s
Characterization:	mixture of biphenyl and diphenyl oxides		

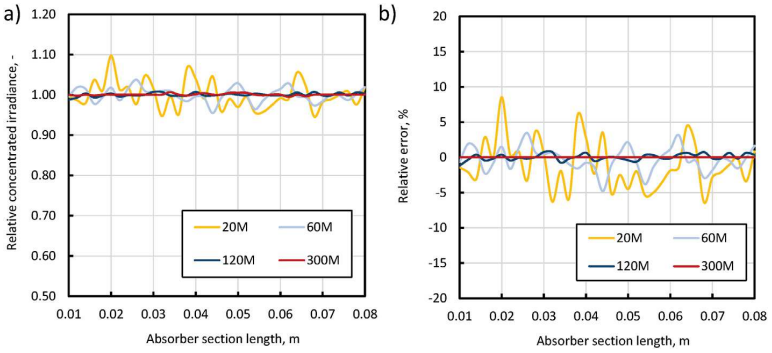

Fig. 6. Determination of the number of used rays in MCRT: a) rays presented between 20 Mrays to 300 Mrays, b) relative error with respect of the best estimate 300 Mrays.

For reference case ($\theta_x = 0°$), the radiation distribution is uniform about the y axis. A larger tracker error, and thus a higher angle θ_x, affects the concentration of radiation on one side of the absorber. Part of the radiation is scattered enough that it does not focus on the surface of the tubular receiver. Increasing the incident angle (tracking deviation) to value of 4° causes that almost all rays pass the absorber. The tubular glass envelope with assumed refractive index and material parameters has a low impact on the overall distribution of the simulated rays.

The total solar power on receiver external surface ($Q_{r,e}$) was calculated for the entire length (L = 1.5 m) of absorber. Figs. 8 and 9 presents the results of the analysis. A small increase in the amount of energy reaching the absorber was obtained for smaller diameter of the absorber. However, a much greater sensitivity to the incidence angle was observed. For an absorber with a diameter of 33.7 mm (Case 1 and 2), the change of the angle θ_x to approx. 2° does not cause any significant changes in energy reaching the absorber, and the ability of the optical system to concentrate occurs up to an angle of 4°.

In the case of an absorber with an outer diameter of 21.3 mm (Case 3 and 4), the energy flux incident on the absorber does not change to the angle of 1°, and the concentration is up to the angle of 2.5°. Reducing the diameter of the absorber pipe allows to increase the concentration ratio, but at the same time causes greater sensitivity to any concentration errors. An absorber with smaller diameter, for a perfectly positioned concentrator, receive a slightly larger total solar power on its surface, which is related to a smaller shading of the mirror by the absorber.

For case 1 and 2, after reaching the 4° of solar tracker error, the only radiation that reaches the absorber is non-concentrated radiation - reaching directly the absorber without any reflection or multiplication. For case 2 and 3, this value of tracker error is 2.5°.

Because the tubular glass envelope is not 100% transparent and the light rays refract on its surfaces, the energy reaching the absorber in the case 2 and 4 is over 10% higher than in the case with the glass tube. In practice, the glass cover is an essential part of the

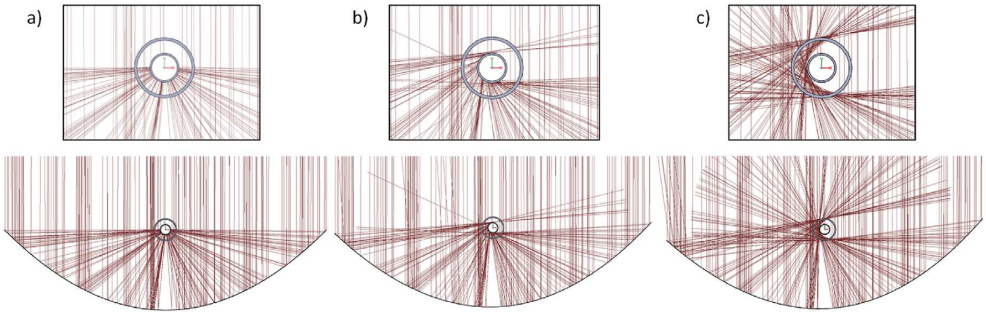

Fig. 7. Solar radiation path for selected tracker error presented in the cross-section: a) $\theta_x = 0°$, b) $\theta_x = 2°$, c) $\theta_x = 4°$.

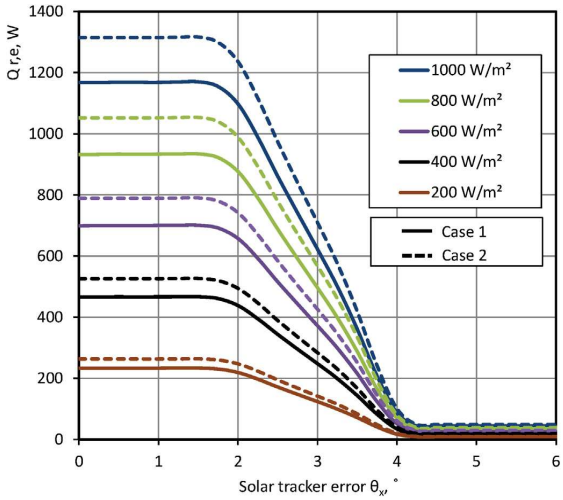

Fig. 8. Solar radiation supplied to the linear absorber including the PTC optical efficiency as a function of solar tracker error for case 1 and 2.

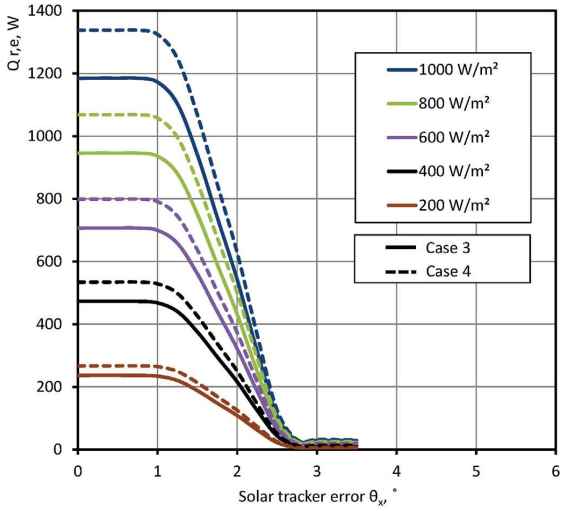

Fig. 9. Solar radiation supplied to the linear absorber including the PTC optical efficiency as a function of solar tracker error for case 3 and 4.

PTC used to limit convective heat losses, which is presented in thermodynamic analysis results. The results of optical concentration ratio calculations are presented in Table 4.

3.2. Thermodynamic results

The results of the thermodynamic analysis are presented in Figs. 10 and 11, separately for both geometries of the analysed absorbers. The efficiency profiles are presented as a function of $(T_{in}-T_{amb})/I_B = (\Delta T/I_B)$, as polynomials of 2nd degree. The input parameters for the analysis performed were the results of optical modelling. For each case, multi-parametric analyses were performed for the same data set, shown in Table 3. In fact, the temperature dependence of heat losses in quite complex, therefore, these results should be considered as trend lines in various conditions. These profiles can also be used for long term and system analyses.

Table 3
Assumption for wide range thermodynamic analysis.

Parameter	Symbol	Value	Unit
Irradiance	I_B	100–1000	W/m^2
Mass flow	$\dot{m}$	0.01-0.15	kg/s
Ambient temperature	T_{amb}	250–310	K
Inlet temperature	T_{in}	315–600	K
Convection coefficient	h_{ca}/h_{ra}	10	W/(m^{2}K)

As $\Delta T/I_B$ increases, the total efficiency of the absorbers decreases due to higher losses from the system. It should be noted, however, that the efficiency of the absorber drops significantly in the absence of a vacuum shield, which highlights the need for using one.

For a value of $\Delta T/I_B$, close to zero, the efficiency in case 2 is about 0.3% points higher than for the case with the glass cover applied. This is the only case where case 2 has a higher efficiency than case 1, due to the very low radiation and convection losses in the system and the lack of loss due to the transmissivity of the glass tube. The efficiency for the glass envelope cases is significantly higher.

For reference value of $\theta_x = 0°$, the efficiency for case 1 is in the range 78-67%. The maximum reduction in efficiency is therefore 11 pp. For the same example, but without the use of a vacuum shield, the efficiency range is between 81% and 18%. The reduction in efficiency in this case is 63 pp.

The impact of the tracking system error was determined for all cases. For case 1 and case 2, an error of 1° does not significantly affect the global performance of the absorber. With an error of $\theta_x = 2°$, the reduction in efficiency averages 4.7% points. For an error of $\theta_x = 3°$, the reduction is 36.2 pp. The error $\theta_x = 4°$ is a 99.8% reduction in efficiency relative to the reference case.

It is also worth noting that the error of the tracking system reduces the application spectrum of the parabolic concentrator in some cases. This means that heat loss to the environment is almost 100% of the energy input to the receiver surface. For an error $\theta_x = 4°$ for case 1, for a value $\Delta T/I_B > 0.36$, the device efficiency is 0%. For the same error and case 2, the operating range as a function of $\Delta T/I_B$ is only 0.06.

For cases 3 and 4, where a smaller diameter absorber is used, a lower decrease in efficiency can be observed for the entire spectrum of application of the device (the slope of the curve is lower than for the larger diameter receiver). For the reference condition $\theta_x = 0°$, where a vacuum cover is used, the efficiency is in the range 79%–72%. This means that despite the higher degree of concentration, the reduction of the absorber's surface area, i.e. the loss-emitting surface area, has a positive effect on its efficiency. What is strongly noticeable, is that a small tracker error highly affects the efficiency of the absorber. The error $\theta_x = 1°$, which did not affect the operation of the device in case 1 and case 2, in these cases leads to a reduction in efficiency of almost 1 pp, and $\theta_x = 2°$, 42.5% points.

3.3. Radiation distribution

For proper analysis of heat transfer along the entire length of the absorber, it is advisable to determine the radiation distribution over its entire surface. It is assumed that the distribution will be identical along the longitudinal axis of the PTC. All calculations were made with the assumption of a two-axis tracking system, therefore the axis of the optical system is always oriented towards the sun. During the simulation, only the influence of errors in the position of the solar tracker in relation to the longitudinal axis of the PTC was

Table 4
The results of optical concentration ratio calculations.

θx, °	Case 1		Case 2		Case 3		Case 4	
	C_{opt}, -	$C_{opt,\theta x}/C_{opt,\theta x=0}$	C_{opt}, -	$C_{opt,\theta x}/C_{opt,\theta x=0}$	C_{opt}, -	$C_{opt,\theta x}/C_{opt,\theta x=0}$	C_{opt}, -	$C_{opt,\theta x}/C_{opt,\theta x=0}$
0.0	7.36	1.00	8.28	1.00	11.81	1.00	13.33	1.00
0.5	7.36	1.00	8.28	1.00	11.81	1.00	13.33	1.00
1.0	7.36	1.00	8.28	1.00	11.68	0.99	11.68	0.88
1.5	7.36	1.00	8.28	1.00	9.38	0.79	9.38	0.70
2.0	6.91	0.94	7.79	0.94	5.40	0.46	6.25	0.47
2.5	5.43	0.74	6.14	0.74	1.08	0.09	1.08	0.08
3.0	3.92	0.53	4.47	0.54	0.28	0.02	0.28	0.02
3.5	2.27	0.31	2.64	0.32	0.27	0.02	0.27	0.02
4.0	0.55	0.07	0.64	0.08	0.27	0.02	0.27	0.02
4.5	0.28	0.04	0.31	0.04	0.27	0.02	0.27	0.02

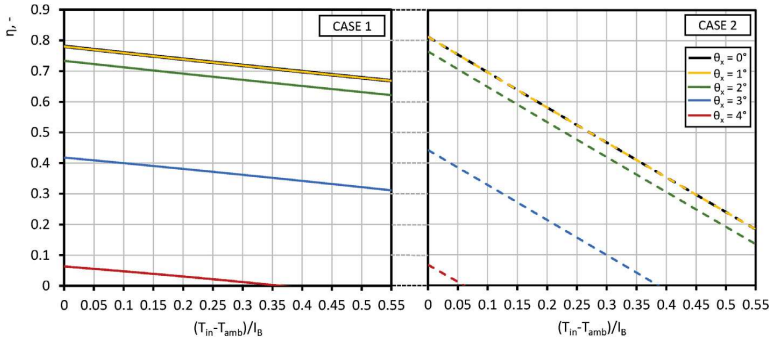

Fig. 10. Parabolic trough collector efficiency calculated for wide multi-parametric analyses, case 1 and 2.

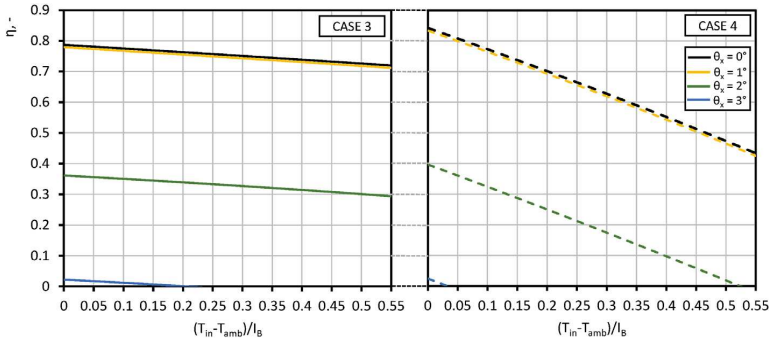

Fig. 11. Parabolic trough collector efficiency calculated for wide multi-parametric analyses, case 3 and 4.

analysed. As research shows, the change of the sun position in relation to the transverse direction of the mirror, i.e. the change of the incidence angle θ_z value within the range of 15°, does not cause significant changes in the radiation distribution on the absorber surface [47,48]. Therefore, modeling with the variable angle θ_z was not performed. The results of the distribution of solar irradiance on outer circumference of the absorber were presented in the Fig. 12. The calculations were set for the value of the incident angle at which the rays are still concentrated on the absorber surface. All charts were created for solar irradiance 1000 W/m^2. Fig. 12 also shows the description of the angles around the circumference of the absorber.

For each of the analysed cases, at an incident angle different than 0°, the distribution of solar irradiance on outer circumference of the absorber is non-uniform. It is caused by focusing the rays only on a part of the absorber, shading of the mirror part by the absorber and the non-parallelism of the sun's rays. The symmetry in distribution of solar irradiance is only visible for the no solar tracker error. Increasing the incident angle θ_x changes the concentrated flux distribution and results in obtaining much higher local values of concentrated energy flux. With a higher solar tracker error, the total solar power on absorber decreases significantly and the area of the absorber to which the concentrated flux reaches is reduced. The presented distributions confirm the greater sensitivity of the system with a smaller absorber diameter to solar tracker error. There are also greater differences in the local values of

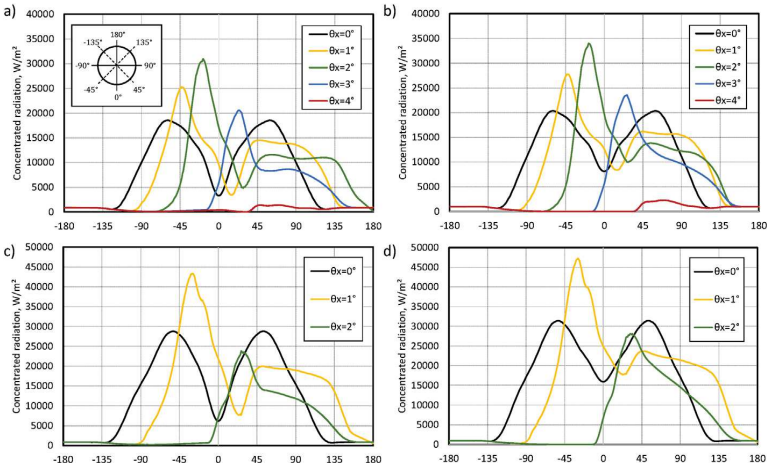

Fig. 12. Radiation distribution on the absorber external surface for selected solar tracker error (I_B = 1000 W/m^2): a) Case 1, b) Case 2, c) Case 3, d) Case 4.

concentrated energy flux for a system with a higher concentration ratio.

4. Conclusion

The paper presents the optical and thermodynamic calculation results of the small parabolic trough collector of geometry consistent with operating PTC installation. The optical-engineering software used allowed to determine the ray propagation paths and analysis of the illuminated surface considering the influence of individual optical elements and their properties.

The maximum angle error of the solar tracker for the tested geometry, not significantly affecting the performance of the linear absorber for a diameter of 33.7 mm is 1.5°, for 21.3 mm is 0.9°. It was found that increasing the concentration ratio by reducing the absorber diameter causes increasing the sensitivity of the system to optical errors. For 33.7 mm absorber diameter, 3° tracking error causes decrease in concentration ratio from 7.36 to 3.92. For smaller absorber diameter, reduction from 11.81 to 5.4 is calculated for 2° error. The maximum tracking error for 33.7 mm and 21.3 mm diameter in this geometry is 4.5 and 2.7 respectively. For higher values the solar radiation is not concentrated on the absorber.

The use of a glass cover reduces the energy value reaching the absorber surface due to the transmittance of light rays, but also glass envelope of this size did not affect the distribution of concentrated energy flux significantly. The results show a strong decrease in absorber efficiency in the absence of the glass envelope with the vacuum barrier. For $(T_{in}-T_{amb})/I_b$ = 0.15 and 33.7 mm absorber the decrease in efficiency for vacuum and co-vacuum case was 10%. For 21.3 mm, the efficiency decrease from 77% to 73%.

In analysed parabolic trough collectors with larger solar tracking error, the greater differences in the values of concentrated energy flux reaching the absorber surface can be noticed, which may cause greater temperature gradients in the absorber and worse heat transfer to the fluid but also cause a high stresses in absorber material. For 1000 W/m^2 and 2° tracking error, the maximum value of concentrated irradiance for 33.7 mm increase from 17 500W/m^2 to almost 32 000 W/m^2. For 21.3 mm absorber the irradiance increase from 20 000 W/m^2 to 34 000 W/m^2.

The results underline the need for a highly accurate solar tracker system even for low concentration solar technologies.

CRediT authorship contribution statement

Bartosz Stanek: Conceptualization, Methodology, Writing – original draft, Investigation, Visualization, Software. **Daniel Węcel:** Writing – original draft, Conceptualization, Investigation, Methodology. **Łukasz Bartela:** Project administration, Funding acquisition, Writing – review & editing, Resources, Supervision. **Sebastian Rulik:** Investigation, Writing – review & editing.

Declaration of competing interest

The authors declare that they have no known competing financial interests or personal relationships that could have appeared to influence the work reported in this paper.

Acknowledgements

The scientific work is funded by the National Science Centre within the framework of the research project No. 2018/29/B/ST8/02406.

NOMENCLATURE

A	area, m^2
C	concentration ratio
c_p	specific heat, J/(kg K)
d	diameter, m; mm
f	focal length, m
h	height, m
h_{ca}/h_{ra}	heat transfer coefficient, W/(m^2 K)
I	irradiance, W/m^2
k	thermal conductivity, (W/m K)
L	length, m
Nu	Nusselt number
Pr	Prandtl number
Q	power, W
r	sun radius, km
R	Sun - Earth distance, km
Re	Reynolds number
r_r	maximum mirror radius, m
T	temperature, K

W	width, m
u	tracking error coefficient
$\dot{m}$	mass flow, kg/s
α	absorptivity,
ε	emissivity,
ζ	reflectivity,
μ	dynamic viscosity, Pa·s
ρ	density, kg/m^3
τ	transmittance,
ϕ_r	rim angle
η	efficiency,
σ	Stefan-Boltzman constant, (5.67 × 10− 8 W/m^{2}K^4)
θ	angle, °

Subscripts

A	aperture
amb	ambient
B	beam (direct)
C	glass cover
ca	cover to ambient
D	diffuse
e	external
f	fluid
g	geometric
i	internal
in	inlet
loss	losses
lr	local radiant
m	mean
opt	optical
out	outlet
R	reflected
r	receiver
ra	receiver to ambient
S	sun/solar
u	useful
x	x axis/position
y	y axis/position
z	z axis/position

Abbreviations

CSP	Concentration solar power
PTC	Parabolic trough collector
SHIP	Solar heat industrial process

References

[1] S.A. Kalogirou, Solar thermal power systems, in: Solar Energy Engineering, Elsevier, 2014, pp. 541–581, https://doi.org/10.1016/B978-0-12-397270-5.00010-8.
[2] J. Song, K. Tong, L. Li, G. Luo, L. Yang, J. Zhao, A tool for fast flux distribution calculation of parabolic trough solar concentrators, Sol. Energy 173 (2018) 291–303, https://doi.org/10.1016/j.solener.2018.07.068.
[3] Z.D. Cheng, Y.L. He, F.Q. Cui, B.C. Du, Z.J. Zheng, Y. Xu, Comparative and sensitive analysis for parabolic trough solar collectors with a detailed Monte Carlo ray-tracing optical model, Appl. Energy 115 (2014) 559–572, https://doi.org/10.1016/j.apenergy.2013.11.001.
[4] M. Eck, W.-D. Steinmann, J. Rheinländer, Maximum temperature difference in horizontal and tilted absorber pipes with direct steam generation, Energy 29 (2004) 665–676, https://doi.org/10.1016/S0360-5442(03)00175-0.
[5] B. Schiricke, R. Pitz-Paal, E. Lüpfert, K. Pottler, M. Pfänder, K.-J. Riffelmann, A. Neumann, Experimental verification of optical modeling of parabolic trough collectors by flux measurement, J. Sol. Energy Eng. 131 (2009), https://doi.org/10.1115/1.3027507.
[6] C.A. Arancibia-Bulnes, M.I. Peña-Cruz, A. Mutuberría, R. Díaz-Uribe, M. Sánchez-González, A survey of methods for the evaluation of reflective solar concentrator optics, Renew. Sustain. Energy Rev. 69 (2017) 673–684, https://doi.org/10.1016/j.rser.2016.11.048.
[7] K. Pottler, E. Lüpfert, G.H.G. Johnston, M.R. Shortis, Photogrammetry: a powerful tool for geometric analysis of solar concentrators and their components, J. Sol. Energy Eng. 127 (2005) 94–101, https://doi.org/10.1115/1.1824109.
[8] G. Burgess, M.R. Shortis, A. Kearton, K. Garzoli, Photogrammetry for dish concentrator construction. https://www.researchgate.net/publication/228544335, 2009.
[9] J. Song, W. Wang, Y. Niu, J. Wang, H. Yu, A note of optical error diagnosis of parabolic trough concentrator based on flux image, Sol. Energy 197 (2020) 359–362, https://doi.org/10.1016/j.solener.2020.01.024.
[10] T. Fend, K. Wenzel, Optical flux measurements in the focal area of a parabolic trough concentrator, 09, J. Phys. IV (1999), https://doi.org/10.1051/jp4:1999396. Pr3-605-Pr3-609.
[11] P.v. Gharat, S.S. Bhalekar, V.H. Dalvi, S.v. Panse, S.P. Deshmukh, J.B. Joshi, Chronological development of innovations in reflector systems of parabolic trough solar collector (PTC) - a review, Renew. Sustain. Energy Rev. 145 (2021), 111002, https://doi.org/10.1016/j.rser.2021.111002.
[12] F. Sallaberry, R. Pujol, B. Perers, Optical losses due to tracking Misaligment on linear concentrating solar thermal collectors, in: Proceedings of EuroSun2016, International Solar Energy Society, Freiburg, Germany, 2016, pp. 1–12, https://doi.org/10.18086/eurosun.2016.07.10.
[13] F. Sallaberry, R. Pujol-Nadal, M. Larcher, M.H. Rittmann-Frank, Direct tracking error characterization on a single-axis solar tracker, Energy Convers. Manag. 105 (2015) 1281–1290, https://doi.org/10.1016/j.enconman.2015.08.081.
[14] C.H. Wu, H.C. Wang, H.Y. Chang, Dual-axis solar tracker with satellite compass and inclinometer for automatic positioning and tracking, Energy Sustain. Dev. 66 (2022) 308–318, https://doi.org/10.1016/J.ESD.2021.12.013.
[15] R.F. Fuentes-Morales, A. Diaz-Ponce, M.I. Peña-Cruz, P.M. Rodrigo, L.M. Valentín-Coronado, F. Martell-Chavez, C.A. Pineda-Arellano, Control algorithms applied to active solar tracking systems: a review, Sol. Energy 212 (2020) 203–219, https://doi.org/10.1016/J.SOLENER.2020.10.071.
[16] C.Y. Lee, P.C. Chou, C.M. Chiang, C.F. Lin, Sun tracking systems: a review, Sensors 9 (2009) 3875–3890, https://doi.org/10.3390/S90503875, 9 (2009) 3875–3890.
[17] B. Yang, S. Liu, R. Zhang, X. Yu, Influence of reflector installation errors on optical-thermal performance of parabolic trough collectors based on a MCRT - FVM coupled model, Renew. Energy 185 (2022) 1006–1017, https://doi.org/10.1016/j.renene.2021.12.102.
[18] S. Khanna, S.B. Kedare, S. Singh, Analytical expression for circumferential and axial distribution of absorbed flux on a bent absorber tube of solar parabolic trough concentrator, Sol. Energy 92 (2013) 26–40, https://doi.org/10.1016/j.solener.2013.02.020.
[19] Y.-L. He, J. Xiao, Z.-D. Cheng, Y.-B. Tao, A MCRT and FVM coupled simulation method for energy conversion process in parabolic trough solar collector, Renew. Energy 36 (2011) 976–985, https://doi.org/10.1016/j.renene.2010.07.017.
[20] S.M. Jeter, Calculation of the concentrated flux density distribution in parabolic trough collectors by a semifinite formulation, Sol. Energy 37 (1986) 335–345, https://doi.org/10.1016/0038-092X(86)90130-1.
[21] P.D. Tagle-Salazar, K.D.P. Nigam, C.I. Rivera-Solorio, Parabolic trough solar collectors: a general overview of technology, industrial applications, energy market, modeling, and standards, Green Process. Synth. 9 (2020) 595–649, https://doi.org/10.1515/gps-2020-0059.
[22] V.S. Kaluba, K. Mohamad, P. Ferrer, Experimental and simulated performance of hot mirror coatings in a parabolic trough receiver, Appl. Energy 257 (2020), 114020, https://doi.org/10.1016/J.APENERGY.2019.114020.
[23] D. Dahlioui, J. Wette, A. Fernández-García, H. Bouzekri, I. Azpitarte, Performance assessment of the anti-soiling coating on solar mirrors soiling in the arid climate of Ouarzazate-Morocco, Sol. Energy 241 (2022) 13–23, https://doi.org/10.1016/J.SOLENER.2022.05.063.
[24] D. Valentín, C. Valero, M. Egusquiza, A. Presas, Failure investigation of a solar tracker due to wind-induced torsional galloping, Eng. Fail. Anal. 135 (2022), 106137, https://doi.org/10.1016/J.ENGFAILANAL.2022.106137.
[25] P. Pawar, P. Pawale, T. Nagthane, M. Thakre, N. Jangale, Performance enhancement of dual axis solar tracker system for solar panels using proteus ISIS 7.6 software package, Global Transit. Proc. 2 (2021) 455–460, https://doi.org/10.1016/J.GLTP.2021.08.049.
[26] H. Hoseinzadeh, A. Kasaeian, M. Behshad Shafii, Geometric optimization of parabolic trough solar collector based on the local concentration ratio using the Monte Carlo method, Energy Convers. Manag. 175 (2018) 278–287, https://doi.org/10.1016/j.enconman.2018.09.001.
[27] B. Zou, J. Dong, Y. Yao, Y. Jiang, A detailed study on the optical performance of parabolic trough solar collectors with Monte Carlo Ray Tracing method based on theoretical analysis, Sol. Energy 147 (2017) 189–201, https://doi.org/10.1016/J.SOLENER.2017.01.055.
[28] Z.D. Cheng, Y.L. He, K. Wang, B.C. Du, F.Q. Cui, A detailed parameter study on the comprehensive characteristics and performance of a parabolic trough solar collector system, Appl. Therm. Eng. 63 (2014) 278–289, https://doi.org/10.1016/J.APPLTHERMALENG.2013.11.011.
[29] B. Yang, S. Liu, R. Zhang, X. Yu, Influence of reflector installation errors on optical-thermal performance of parabolic trough collectors based on a MCRT - FVM coupled model, Renew. Energy 185 (2022) 1006–1017, https://doi.org/10.1016/J.RENENE.2021.12.102.
[30] S. Akbarzadeh, M.S. Valipour, Energy and exergy analysis of a parabolic trough collector using helically corrugated absorber tube, Renew. Energy 155 (2020) 735–747, https://doi.org/10.1016/j.renene.2020.03.127.
[31] P.P. Dutta, S.S. Begum, H. Jangid, A.P. Goswami, T. Doley, M. Bardalai,

P.P. Dutta, Modeling and performance evaluation of a small solar parabolic trough collector (PTC) for possible purification of drained water, Mater. Today Proc. 47 (2021) 4226–4234, https://doi.org/10.1016/j.matpr.2021.04.489.
[32] Q.F. Chen, Z.X. Yuan, Z.Q. Guo, Y. Zhao, Practical performance of a small PTC solar heating system in winter, Sol. Energy 179 (2019) 119–127, https://doi.org/10.1016/j.solener.2018.12.061.
[33] M. Halimi, A. el Amrani, C. Messaoudi, New experimental investigation of the circumferential temperature uniformity for a PTC absorber, Energy 234 (2021), 121288, https://doi.org/10.1016/j.energy.2021.121288.
[34] L. Noč, I. Jerman, Review of the spectrally selective (CSP) absorber coatings, suitable for use in SHIP, Sol. Energy Mater. Sol. Cell. (2022) 238, https://doi.org/10.1016/J.SOLMAT.2022.111625.
[35] C.A. Schoeneberger, C.A. McMillan, P. Kurup, S. Akar, R. Margolis, E. Masanet, Solar for industrial process heat: a review of technologies, analysis approaches, and potential applications in the United States, Energy (2020) 206, https://doi.org/10.1016/J.ENERGY.2020.118083.
[36] A. Häberle, D. Krüger, Concentrating solar technologies for industrial process heat, in: Concentrating Solar Power Technology: Principles, Developments, and Applications, Elsevier, 2020, pp. 659–675, https://doi.org/10.1016/B978-0-12-819970-1.00011-6.
[37] G.C. Bakos, Design and construction of a two-axis Sun tracking system for parabolic trough collector (PTC) efficiency improvement, Renew. Energy 31 (2006) 2411–2421, https://doi.org/10.1016/j.renene.2005.11.008.
[38] B. Stanek, K. Grzywnowicz, Ł. Bartela, D. Węcel, W. Uchman, A system analysis of hybrid solar PTC-CPV absorber operation, Renew. Energy 174 (2021) 635–653, https://doi.org/10.1016/j.renene.2021.04.110.
[39] J. Reca-Cardeña, R. López-Luque, Design principles of photovoltaic irrigation systems, in: Advances in Renewable Energies and Power Technologies, Elsevier, 2018, pp. 295–333, https://doi.org/10.1016/B978-0-12-812959-3.00009-5.
[40] T. Chmielniak, Technologie Energetyczne, Wydawnictwo Naukowo-Techniczne, Warszawa, 2008.
[41] B. Cattaneo, PVGIS Photovoltaic Geographical Information System, EU Science Hub - European Commission, 2018. https://ec.europa.eu/jrc/en/pvgis. (Accessed 7 July 2021).
[42] Dane do obliczeń energetycznych budynków - Ministerstwo Inwestycji i Rozwoju (n.d.), https://www.gov.pl/web/archiwum-inwestycje-rozwoj/dane-do-obliczen-energetycznych-budynkow. (Accessed 13 June 2022).
[43] S.A. Kalogirou, Low concentration ratio solar collectors, in: Comprehensive Renewable Energy, Elsevier, 2012, pp. 149–163, https://doi.org/10.1016/B978-0-08-087872-0.00305-X.
[44] S.M. Blinder, Analytic geometry, in: Guide to Essential Math, Elsevier, 2013, pp. 67–77, https://doi.org/10.1016/B978-0-12-407163-6.00005-9.
[45] K. Lovegrove, J. Pye, Fundamental principles of concentrating solar power systems, in: Concentrating Solar Power Technology, Elsevier, 2021, pp. 19–71, https://doi.org/10.1016/B978-0-12-819970-1.00013-X.
[46] S.A. Kalogirou, Solar energy collectors, in: Solar Energy Engineering, Elsevier, 2014, pp. 125–220, https://doi.org/10.1016/B978-0-12-397270-5.00003-0.
[47] A. Malan, K. Ravi Kumar, A comprehensive review on optical analysis of parabolic trough solar collector, Sustain. Energy Technol. Assessments 46 (2021), 101305, https://doi.org/10.1016/j.seta.2021.101305.
[48] K.-J. Riffelmann, A. Neumann, S. Ulmer, Performance enhancement of parabolic trough collectors by solar flux measurement in the focal region, Sol. Energy 80 (2006) 1303–1313, https://doi.org/10.1016/j.solener.2005.09.001.
[49] APEX, Breault Research Organization, Inc, 2019 (n.d.), http://www.breault.com/. (Accessed 3 February 2022).
[50] Breault Research Organization, Correlation of ASAP™ Simulation Results with Physical Components, Tuscon, 2006.
[51] M. Shadmehri, H. Narei, R. Ghasempour, M.B. Shafii, Numerical simulation of a concentrating photovoltaic-thermal solar system combined with thermo-electric modules by coupling Finite Volume and Monte Carlo Ray-Tracing methods, Energy Convers. Manag. 172 (2018) 343–356, https://doi.org/10.1016/J.ENCONMAN.2018.07.034.
[52] C. Zhang, G. Xu, Y. Quan, H. Li, G. Song, Optical sensitivity analysis of geometrical deformation on the parabolic trough solar collector with Monte Carlo Ray-Trace method, Appl. Therm. Eng. 109 (2016) 130–137, https://doi.org/10.1016/J.APPLTHERMALENG.2016.08.058.
[53] X. Duan, C. He, X. Lin, Y. Zhao, J. Feng, Quasi-Monte Carlo ray tracing algorithm for radiative flux distribution simulation, Sol. Energy 211 (2020) 167–182, https://doi.org/10.1016/J.SOLENER.2020.09.061.
[54] Ł. Bartela, B. Stanek, D. Węcel, A. Skorek-Osikowska, A solar simulator numerical modeling for heat absorption phenomenon research in a parabolic trough collector, Int. J. Energy Res. (2021), https://doi.org/10.1002/er.6585.
[55] B. Stanek, Ł. Bartela, Numerical and experimental study on 10 kWe metal-halide solar simulator for parabolic-trough collector testing, ECOS 2021 Conference Proceedings, in: 34th International Conference on Efficiency, Cost, Optimization, Simulation and Environmental Impact of Energy Systems (ECOS21), Taormina, 2021, pp. 1198–1209.
[56] Y.F. Lin, C. Zheng, X.D. Zheng, X.P. Wang, X. Liu, Simulation of conoscopic interference in uniaxial crystal using optical software-advanced system analysis program, Guangdian Gongcheng/Opto-Electronic Eng. 39 (2012) 98–103, https://doi.org/10.3969/J.ISSN.1003-501X.2012.02.019.
[57] R. Kong, M. Ambrose, J. Spanier, Efficient, automated Monte Carlo methods for radiation transport, J. Comput. Phys. 227 (2008) 9463–9476, https://doi.org/10.1016/j.jcp.2008.06.037.
[58] W. Wang, L. Aichmayer, J. Garrido, B. Laumert, Development of a Fresnel lens based high-flux solar simulator, Sol. Energy 144 (2017) 436–444, https://doi.org/10.1016/j.solener.2017.01.050.
[59] L. Martínez-Manuel, W. Wang, M.I. Peña-Cruz, Optimization of the radiative flux uniformity of a modular solar simulator to improve solar technology qualification testing, Sustain. Energy Technol. Assessments 47 (2021), 101372, https://doi.org/10.1016/j.seta.2021.101372.
[60] S.M. Pompea, S.H. McCall, OPTICAL COATINGS | optical black surfaces, in: Encyclopedia of Modern Optics, Elsevier, 2005, pp. 349–360, https://doi.org/10.1016/B0-12-369395-0/00872-1.
[61] L. Martínez-Manuel, W. Wang, B. Laumert, M.I. Peña-Cruz, Numerical analysis on the optical geometrical optimization for an axial type impinging solar receiver, Energy 216 (2021), https://doi.org/10.1016/J.ENERGY.2020.119293, 119293.
[62] A. Al-Rjoub, L. Rebouta, P. Costa, N.P. Barradas, E. Alves, P.J. Ferreira, K. Abderrafi, A. Matilainen, K. Pischow, A design of selective solar absorber for high temperature applications, Sol. Energy 172 (2018) 177–183, https://doi.org/10.1016/J.SOLENER.2018.04.052.
[63] K. Mansour, R. Boudries, R. Dizene, Optical, 2D thermal modeling and exergy analysis applied for performance prediction of a solar PTC, Sol. Energy 174 (2018) 1169–1184, https://doi.org/10.1016/j.solener.2018.09.040.
[64] S.A. Kalogirou, A detailed thermal model of a parabolic trough collector receiver, Energy 48 (2012) 298–306, https://doi.org/10.1016/j.energy.2012.06.023.
[65] E.Z. Moya, Parabolic-trough concentrating solar power systems, in: Concentrating Solar Power Technology, Elsevier, 2021, pp. 219–266, https://doi.org/10.1016/B978-0-12-819970-1.00009-8.
[66] M.A. Hassan, An Optimized Optical Model of Parabolic Trough Solar Collector Using MCRT Method, Giza, Egypt, 2015.
[67] H. Zheng, Solar energy utilization and its collection devices, in: Solar Energy Desalination Technology, Elsevier, 2017, pp. 47–171, https://doi.org/10.1016/B978-0-12-805411-6.00002-6.
[68] C. Tzivanidis, E. Bellos, D. Korres, K.A. Antonopoulos, G. Mitsopoulos, Thermal and optical efficiency investigation of a parabolic trough collector, Case Stud. Therm. Eng. 6 (2015) 226–237, https://doi.org/10.1016/j.csite.2015.10.005.
[69] I.H. Yilmaz, M.S. Söylemez, Thermo-mathematical modeling of parabolic trough collector, Energy Convers. Manag. 88 (2014) 768–784, https://doi.org/10.1016/J.ENCONMAN.2014.09.031.
[70] R. Pitz-Paal, Solar energy - concentrating solar power, in: Future Energy: Improved, Sustainable and Clean Options for Our Planet, Elsevier Inc., 2013, pp. 405–431, https://doi.org/10.1016/B978-0-08-099424-6.00019-3.
[71] D.D. Ganji, Y. Sabzehmeidani, A. Sedighiamiri, Radiation heat transfer, in: Nonlinear Systems in Heat Transfer, Elsevier, 2018, pp. 105–151, https://doi.org/10.1016/B978-0-12-812024-8.00003-5.
[72] U. Roy, P.K. Roy, Advances in heat intensification techniques in shell and tube heat exchanger, advanced analytic and control techniques for thermal systems with heat exchangers. https://doi.org/10.1016/B978-0-12-819422-5.00007-4, 2020, 197-207.
[73] E. Nagy, Membrane contactors, in: Basic Equations of Mass Transport through a Membrane Layer, Elsevier, 2019, pp. 337–345, https://doi.org/10.1016/B978-0-12-813722-2.00011-X.
[74] E. Bellos, C. Tzivanidis, K.A. Antonopoulos, A detailed working fluid investigation for solar parabolic trough collectors, Appl. Therm. Eng. 114 (2017) 374–386, https://doi.org/10.1016/j.applthermaleng.2016.11.201.
[75] Therminol VP-1 heat transfer fluid | Therminol | Eastman (n.d.), https://www.therminol.com/product/71093459. (Accessed 1 February 2022).
[76] W. Fuqiang, C. Ziming, T. Jianyu, Y. Yuan, S. Yong, L. Linhua, Progress in concentrated solar power technology with parabolic trough collector system: a comprehensive review, Renew. Sustain. Energy Rev. 79 (2017) 1314–1328, https://doi.org/10.1016/j.rser.2017.05.174.